A SHIFTING HYDROLOGICAL REGIME:
A FIELD INVESTIGATION OF SNOWMELT RUNOFF PROCESSES AND THEIR CONNECTION TO SUMMER BASEFLOW
SUNSHINE COAST, B.C.

by

Mathieu Beaulieu

B.Sc., Université du Québec à Montréal, 2006

A THESIS SUBMITTED IN PARTIAL FULFILLMENT OF
THE REQUIREMENTS FOR THE DEGREE OF

MASTER OF SCIENCE

in

The Faculty of Graduate Studies

(Resource Management and Environmental Studies)

THE UNIVERSITY OF BRITISH COLUMBIA

(Vancouver)

February 2011

Abstract

The annual hydrographs in British Columbia rivers are either characterized by glacial, nival, pluvial or "hybrid" (both pluvial and nival) sources of runoff. Climate change scenarios for the 2050s indicate that snow-water-equivalent (SWE) will diminish by 50 to 80% in lower snowfed-dominated basins in the South Coastal region compared to historical values. This could trigger a shift from a hybrid to a pluvial regime for many creeks, including streams used as primary water supply such as Chapman Creek on the Sunshine Coast. It has been suggested in previous studies that this change in runoff regime will negatively impact summer low flows due to an earlier onset of snowmelt and a prolonged summer recession period. However, the connection between groundwater recharge during snowmelt and late-summer water yield remains unclear. A local headwater catchment (Stephen's Creek) was instrumented and monitored from the fall of 2008 to the fall of 2009. A two- and a three-component isotopic hydrograph separation (2-, 3-IHS) method was developed by adapting the runoff-corrected model (runCE) to a semi-distributed environment in order to account for spatial variability in snowmelt and in isotopic release from the snowpack. IHSs results show that event water (snowmelt) and soil water composed most of the streamflow both at the headwater site (66 ± 19%) and at the mouth (62 ± 23%) during the peak of the freshet, while the contribution of event water to streamflow was significantly different in July (34 ± 11 % at the headwater site vs. 7 ± 4% at the mouth). Hydrometric, isotopic and geochemical data suggest that saturated throughflow was the predominant flow-path taken by melt water during freshet. Preliminary streamflow recession analysis revealed that the snowmelt-recharged headwater catchment can support a steadier summer baseflow than Robert's Creek – a much larger, but rainfed-dominated watershed. It is concluded that the large input of melt water during the spring was sufficient to "over-turn" the shallow subsurface reservoir of the headwater catchment and recharge deeper flow-paths at a rate that can not be matched by rainfed-dominated systems. The results are of interest to water resource planning in the South Coastal region.

Table of Contents

List of Tables

List of Figures

Acknowledgments

I have been very fortunate to be supported by extraordinarily kind, smart and benevolent people during the course of this long-lasting endeavor. First, I would like to thank my main supervisor, Dr. Hans Schreier, for his unwavering trust, accessibility and his support to an ambitious project, despite all the unknowns and the challenges we faced during the initial phase. I would also like to thank my co-supervisor Dr. Gunilla Oberg, as well as Jacquie Belize and Laura Grant for stimulating discussions during the planning phase of the project. Thank you to my committee members (Hans, Gunilla and Dan Moore) for your helpful and timely comments during the drafting stage of this thesis.

I want to extend my gratitude to Kevin Davie and Al Jenkins for all of our reconnaissance trips in the area. Thank you to Dion Whyte, Bryan Shoji and Beth Brooks from the SCRD for having provided logistic and technical support during the instrumentation phase of the project and during the summer of 2009.

This thesis would not have been possible without the invaluable help of my dedicated friends who volunteered their precious time to assist me build the hydrometric instruments and collect data – often for many days and under adverse meteorological conditions. My warmest thanks to:

-Adam Brioux	-Christine Chevalier	-Julie Kyliko	-Nicolas Sirois
-Aio Häberli	-David Atlee	-Kirsten Kleint	-Patricia Keen
-Alex Bogdan	-Eike Birgteneiger	-Laura DeVries	-Peter Leverman
-Andrew Balakshin	-Elizabeth Irvine	-Laura Grant	-Tom-Pierre Frappé-S.
-Carole Dubois	-François Mettra	-Maria Staudinger	
-Christian Evans	-Gabriel Gerber	-Martine Raté-Boulianne	

Special thanks go to Jakob Schekler and Dr. Georg Jost who kindly provided much needed help and advice regarding simulation models. I would also like to acknowledge the support of the SWEL members, in particular Dr. Les Lavkulich for fascinating discussions about silicon and Trudy Naugler for her patience. Warm thanks to Brian Carson and all the family for their great hospitality, passionate discussions, for looking after me and more generally for introducing Laura and I to the “gods’ country” lifestyle. Thank you Lianne for editing my thesis – I’m aware it wasn’t all that easy at times. I gratefully acknowledge the financial support of the Natural Sciences and Engineering

Council and the Canadian Water Resources Association. Finally, thanks to my family and my friends for moral support. I dedicate this thesis to you.

1 Introduction

1.1 The Complexity of the Hydrologic Cycle in Forested Environments: “Blue”, “Green” and “White” Waters

The water cycle is rather complex because of its many storage components, all of which have distinct residence-time distributions with very different orders of magnitude between and within reservoirs. Furthermore, the ease with which water exists in its three different phases (gas, liquid and solid) on earth greatly increases this complexity by maximizing the interactions and possible flow-paths in-between those reservoirs. Ultimately, the purpose of hydrological investigation is to come up with a general unifying law overriding microscale heterogeneities that would numerically describe these interactions in any watershed. This would enable us to make accurate quantitative predictions of flows, nutrient export, sediment transport and contaminant faith (McDonnell *et al.*, 2007; Sivapalan, 2003; Dooge, 1986).

The three overarching hydrological processes in a forest are the “blue”, the “green” and the “white” water flow (as defined in Jewitt, 2006; and Savenije, 2004). Blue water is the amount of rainfall or snowmelt that runs off the surface and through the subsurface and delivers water to streams and lakes and recharges groundwater. Its residence time can vary from minutes to hundreds of years (e.g., saturated overland flow vs deep groundwater flowpaths) and it encompasses many runoff-generating processes (Figure 1.1) including rainfall, throughfall, stemflow, throughflow, snowmelt, overland flow, and a variety of subsurface flowpath such as lateral flow (or rapid subsurface runoff – mainly as macropore flow), vertical flow (recharge – mainly as matrix flow), interflow (or perched/transient aquifer discharge/saturated throughflow) and groundwater flow (also referred to as piston flow or delayed subsurface runoff). In-depth descriptions of those many terms can be found in most hydrology textbooks (e.g. Hewlett, 1982 and Dingman, 2008). The prevalence of some of these processes varies greatly between different environmental settings and/or under different initial conditions, hence the difficulty of predicting streamflow using a fully deterministic approach.

Green water is the amount of rainfall or snowmelt that participates in biomass production and consists of soil-moisture uptake below the root zone and air-moisture exchange at the stomatal level. Evaporation from free-water surfaces, soil-moisture or interception from vegetation is classified as white water because it is considered "unproductive" since it does not participate in either runoff or biomass growth. Green water's residence time ranges from hours to months, while white water's residence time is even shorter, with a lifespan of minutes to days. It is worthwhile to understand the differences between those water flows. For the most part, hydrological models focus on blue water because it is often the final product of interest for resource extraction or flood forecasting. However, green and white waters can represent a substantial percentage of a catchment's water balance – especially in semi-arid and arid climates, but even in a maritime climate. Calder (1990) reported that evaporation from interception can amounts to 40–50% of the annual rainfall in an upland forested catchment in Britain (cited from Savenije, 2004). Although blue water's runoff-processes are regulated by water inputs and large spatial variability in the hydraulic characteristics and antecedent soil moisture conditions of the catchment, green and white water's flow are highly variable temporally and can have distinct but ever-changing behaviour seasonally, daily and even hourly in correlation to air temperature, air moisture content and solar radiation.

1.2 Research Rationale

1.2.1 Water resources

The increased societal demand for water and increased climatic variability are crucial water-resource-management issues. The latter is challenging to address because water-scarce periods and unusual storm events are difficult to predict.

Mounting evidence derived from historic trends and climate models for the Pacific Northwest's coastal region suggests that streams that have been historically classified as hybrid (i.e. annual water yield dominated by autumnal rain events and spring freshet) will eventually shift to a pluvial regime (i.e. dominated by fall and winter rain events) within upcoming decades (Rodenhuis *et al.*, 2007). The monthly distribution of precipitation is not expected to change, meaning that summer baseflow conditions will likely prevail for a much longer period during the summer (Leith and Whitfield, 1998). However, given the current state of the research, it is yet unclear to what extent the late summer streamflow discharge will be affected by this shift in hydrological regime. Historically, the vast majority of the research done in experimental hydrology is aimed at understanding runoff processes contributing to stream peak-flows during storm or snowmelt events (see benchmark papers compiled by K.J. Beven, 2006). At the other end of the "response-time spectrum" are studies oriented towards multi-event, annual or even decadal time scale (e.g. Hamlet and Lettenmaier, 1999; Scibek and Allen, 2006).

Figure 1.1 The hydrologic cycle typical of a British Columbian coastal ecosystem

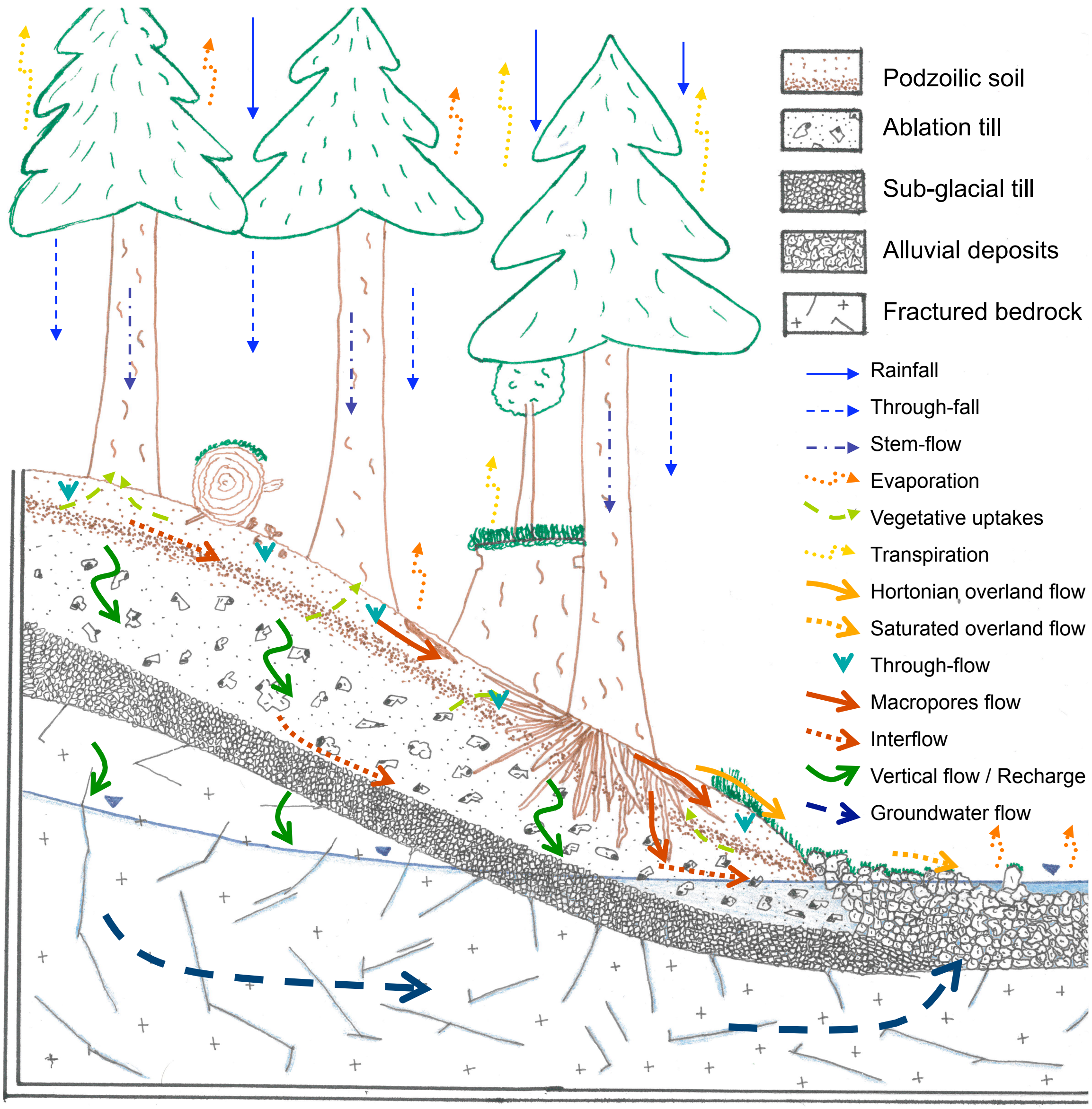

Authors of climate-change-oriented literature regarding water resources in British Columbia and the Western U.S. all agree that low flows during late summer will *likely* worsen in watersheds that have been historically known to have a pronounced snowmelt component (see section 2.2). Logically, as the snow melts earlier, the recession periods after the spring freshet will increase steadily, resulting in less water in the late summer. However, annual groundwater recharge may also be diminished due to the disappearance of prolonged snowmelt inputs and long-term groundwater yield might be affected. Currently, emerging research focusing on the modeling of water residence-time distribution will probably factor in this inter-annual response-function (Sayama & McDonnell, 2009). Nevertheless, the possibility that groundwater recharge might be affected by shifting hydrological regimes is an under-investigated topic in the current body of literature. Most studies regarding the predicted impact of climate change on groundwater systems are limited to model simulations (Moore *et al.*, 2007). Trends in groundwater-levels that could be attributed to climate change and their possible relationship to summer low flows are difficult to detect in B.C. because few groundwater wells monitor aquifers unaffected by human activity (e.g., groundwater withdrawals, widespread impervious surfaces, engineered land drainage), and only a fraction of these are located in stream-gauged basins with long-term records (Moore *et al.*, 2007). Few authors have studied the historic and projected impact of climate change on late summer low flows in British Columbia (see sections 2.3 and 2.4).

Scibek *et al.* (2007) have demonstrated that streams in large valleys in B.C.'s cordillera are sustained in the summer by extensive alluvial aquifers that are recharged from the stream during freshet (reported in Moore *et al.*, 2007). However, field-based studies that specifically investigate snowmelt flow-path and the transition from freshet conditions to late summer baseflow are still greatly needed, especially in coastal areas.

1.2.2 Solutes and nutrients

Water is essential for life, and it is also the transport medium of essential nutrients in both terrestrial and aquatic environment. Some solutes are considered more conservative than others – their concentrations vary along the flow path mainly due to dilution processes. Many other solutes of interest for their nutritional value, such as carbon, nitrate or phosphate, are reactive and can gain or lose in concentration simply by interacting with their bio-geophysical environment. A systematic change in the distribution of the annual runoff could affect the fluxes of the key nutrients to the aquatic ecosystems. The transport of solute is intrinsically linked with the timing of the fixation/ionization at the source (e.g., in the bioactive layer of the soil for nitrate/nitrite) and the moment of mobilization, which is regulated by the soil moisture content, the seasonality of runoff events and the water residence-time distribution in the catchment. Some hypotheses have been derived from theory and experimental studies to show how the nitrogen and carbon cycles is impacted by these processes (Luo *et al.*, 2004; Shaver *et al.*, 2000; Ineson *et al.*, 1998). However, it is yet unclear in what direction and to what extent climate change could affect the terrestrial nutrient budget as a whole. Shifts in the hydrological regimes will most likely impact the fluxes of both conservative and reactive solutes because the timing of mobilization will change. On the B.C. coast, streams draining forested ecosystems in granitic environments are known to be depleted in solutes, particularly in nutrients (e.g. nitrate concentrations are usually under 0.05 ppm). Some major nutrient exports occur during high-flows after periods characterized by low precipitation and high biological activity, such as the first autumn storm when most of the excess nutrient from decomposition and dry deposition is “flushed” as throughflow. This nutrient spike can also be observed during spring freshet in coastal climate, as the biological production of nutrient doesn’t necessarily stop over the winter while most of the precipitation occurs as snow at higher elevation. Land use changes like forest harvesting have also resulted in short term nutrient flushes (Reynolds and Edwards, 1995). A change in runoff regime could impact the nitrate export dynamic during the spring, which could have consequences on the lower trophic levels of the food chain during the later spring and summer months.

1.3 Research Question and Objectives

Bearing in mind this reflection and the climate-change projections for southwestern B.C., the following research question was formulated:

"Does the shift from a hydrid to a pluvial hydrological regime, caused by climate change, have the potential to negatively impact late summer water yield and change the timing of nutrient export in rivers located in B.C.'s south coast?"

In order to address this question, three research objectives were set:

(1) Investigate melt-water flow path and evaluate whether the runoff mechanisms at play are significantly different than what is expected during rainfall events by performing two- and three-component isotopic hydrograph separations during spring freshet, and into the summer low flow period.
(2) Define the main mechanisms controlling nutrient export to streamflow during the freshet and the summer low flow.
(3) Compare the streamflow recession behaviour of a snowfed headwater catchment and an adjacent rainfed watershed by using existing recession models.

The overall goal of this research is to contribute to a better understanding of hydrological processes in B.C.'s coastal environment and facilitate an informed dialogue on how climate change may impact groundwater recharge and late summer water yield.

2 Research Context and Literature Review

2.1 British Columbia's Surface Water

Climate change has emerged as a global concern for water resources sustainability (Nijssen *et al.,* 2001; Huntington, 2006), and a priority for water resource managers from Western U.S. to southern British Columbia (Markoff and Cullen, 2007; Snover *et al.*, 2003; Thompson, 2007). In these regions, the hydrological regime of streams that are not fed by glaciers is largely dominated by autumn peak-flows induced by heavy rainfalls and spring freshet forced by snowmelt from higher elevation catchments. These systems, when driven by these two major hydrological responses, are known as "hybrids" watersheds (Eaton and Moore, 2010). The spring freshet is without any doubt the most important period of the year from a water-resource perspective. Where climate and terrain allow its formation, a deep snowpack acts as a major reservoir for the summer as it slowly releases melt-water to the soil, which generates stream-flow response and groundwater recharge. Once the snow has completely melted (by mid-summer), the hydrograph recedes and the streams enters a baseflow phase dominated by groundwater inputs, which typically lasts about two months. Despite the ability of the air masses to generate considerable snowfall during the winter, the temperatures are mild and an increase of only a few degrees Celsius could compromise the very existence of this reservoir at lower elevations where the snow usually accumulates on topographical plateaux (Mote *et al.*, 2005). Baseflow conditions would commence earlier in the summer and the seasonal groundwater recharge flux occurring as a result of daily snowmelt input would also be heavily reduced, which would compromise delayed-runoff to the stream during the later summer – especially if potential summer evapotranspiration is expected to rise due to climate warming (McCarty *et al.*, 2001). Where artificial storage capacity is not sufficient, this shift in streamflow regime will most likely worsen an already precarious situation during the late summer for many coastal communities, especially for those facing important population growth.

2.2 Regional Context

2.2.1 Sunshine Coast's regional hydrology

The site where the empirical data collection was conducted is located in the Sunshine Coast, which is one of the British Columbian regions that are expected to be the most impacted by the negative effect of climate change on snowpack's snow-water-equivalent (Rodenhuis *et al.*, 2007). Most of the major streams are flowing from an elevated physiographic ensemble, the Tetrahedron plateau (900 to 1700 m of elevation) directly to the sea. Those watersheds are characterized by thin soils, impervious granitic bedrock and steep slopes, and receive a large volume of precipitation. As a result, the basins typically have a steep gradient, a small area, and are very responsive to rainfall or snowmelt inputs.

The majority of the population living in the lower Sunshine Coast (around 25,000 residents) is supplied with treated water through a regional aqueduct system distributing water mainly originating from Chapman Creek and, to a lesser extent, the Town of Gibsons' aquifer (see localization map, Figure 3.1). With a basin area of 7315 ha, an elevated headwater plateau that usually receives an impressive amount of snow over the winter, and two major lakes with a total storage capacity of 1.77 $\times 10^6$ m^3 (Triton, 2006), Chapman Creek is the most important hydrological system in the region, and therefore the most reliable source of water for the communities.

The annual hydrograph of Chapman Creek (Figure 2.1a) displays a typical hybrid response characterized by "flashy" peak-flow events during the fall and snowmelt pulses in the spring, which is consistent with its geographic and climatic settings. Similarly, streams draining lower-elevation basins (e.g. Roberts Creek - Figure 2.1b, a few kilometers away from Chapman Creek) show a quite different hydrograph more typical of a pluvial regime, with only one prolonged high-flow season over the winter, an early and modest spring freshet, and a longer dry season over the summer. These two different hydrological regimes are good illustrations of the potential sensitivity of coastal systems to climate change, since the major difference between the two neighbouring streams, all other things being equal, is a much deeper snowpack for Chapman Creek due to different basin elevation.

Figure 2.1 (A) Chapman Creek 1959-1970 and **(B)** Roberts Creek 1959-2007 annual hydrographs. The dark lines are median flows and the dashed lines are the 1st and 3rd quartiles, respectively. The Chapman Creek data is limited to 1959-1970 since a dam was built in the headwaters in 1971 to augment the storage capacity of Chapman Lake. Note that the hydrometric monitoring station for Chapman Creek was located below the municipal water intake.
Source : Environment Canada, Hydat databases (2009)

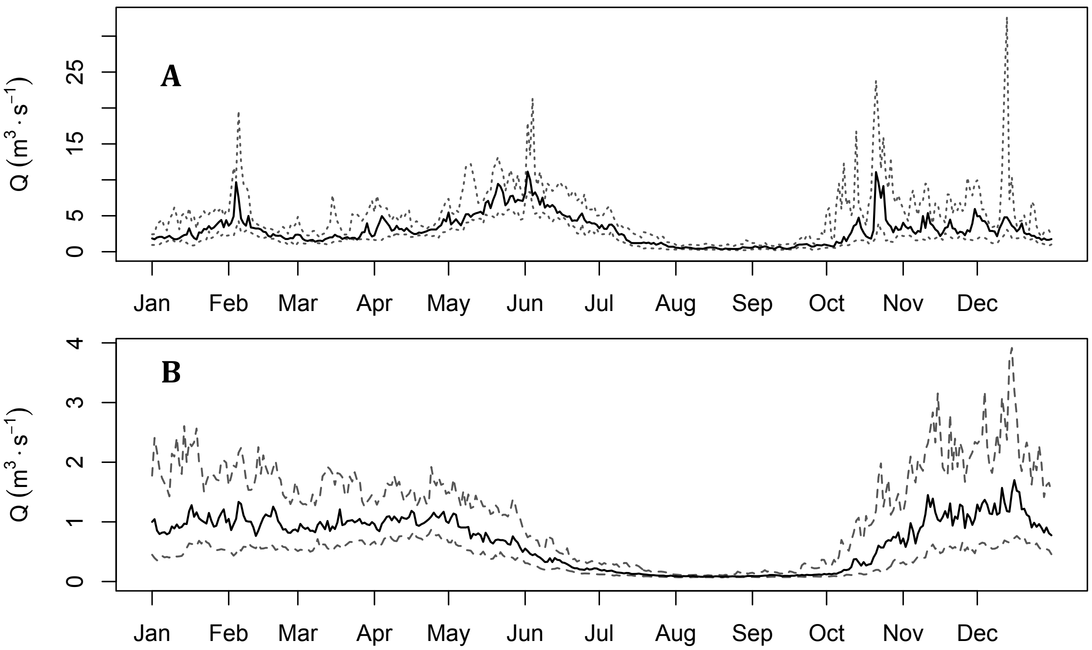

2.2.2 Surface water resources and growth projections for the Sunshine Coast

The Chapman Creek system provides nearly 90% of the drinking water consumed by Sunshine Coast users (Trition, 2006). The SCRD is licensed to withdraw over 1 $x10^{10}$ litres of water per year from Chapman Creek for waterworks purposes. The withdraws do not have to be evenly distributed during the year and the daily limits authorized by licenses are sometimes more than what the creek can yield during summer low flows (B.C. Ministry of Environment, 2009). This flexibility allows the SCRD to satisfy the high demand during summertime, but raises concerns about the management of the allocation, since it is left to the exploiter to decide the volume of water to be yielded downstream of the water intake (Figure 2.2). The fact that a fish hatchery operates down-streams of the water intake in combination with the absence of clear regulations or bylaws regarding minimum requirements has been a source of tensions between the

SCRD and the Department of Fisheries and Ocean (DFO) for many years (Triton, 2006). When it is judged that Chapman Creek's stream-flow is insufficient to supply both the treated-water demand and the ecosystemic allocation, stream-water from Gray Creek watershed (Figure 3.1), an adjacent basin of similar catchment area, is withdrawn and fed to the distribution system. The total organic carbon (TOC) concentration of Gray Creek is typically quite high, which has raised concerns among the public (Carson, 2008, personal communication). High organic matter content in combination with chlorine treatment, which is the disinfection method used, is known to potentially cause carcinogenic chlorination by-products in the distribution system (Reckhow and Singer, 1990; Doyle *et al.*, 1997). The SCRD has the option to exploit Gray's surface water more often in the future if water demand rises and if summer low flows diminishes.

Figure 2.2 (A): Water withdrawals on Chapman creek. **(B):** Average stream-flow for Chapman (1959-1970) compared to the average monthly withdrawals (1999-2008). The black line represents mean streamflow, the red dashed line represents minimum flow, and the blue line represents monthly withdrawals. Note that streamflow and water-use data in (B) are not extracted from the same period, therefore this figure should be interpreted with caution. Sources: A: SCRD (2009), B: Environment Canada (2009) and SCRD (2009)

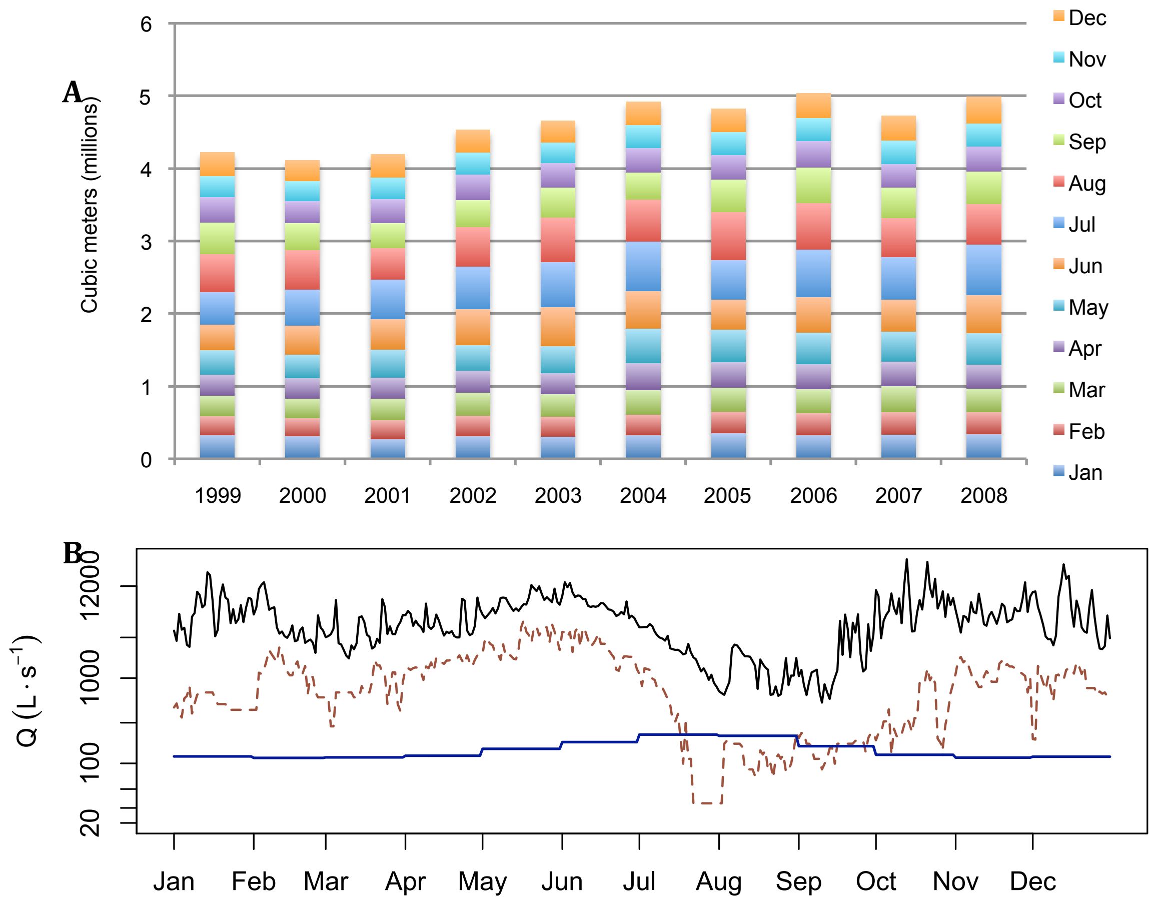

The precariousness of their summer water supply has motivated the SCRD to increase the storage capacity of their main watershed. In 1971, a dam was built at the outlet of Chapman Lake to increase its reservoir volume in order to supply summer water demand. Edwards Lake naturally discharges into Gray Creek but the outflow was diverted towards Chapman Lake, significantly increasing the storage capacity and catchment area of the Chapman Creek watershed. Weirs control the levels of the lakes so that water can be released when needed in periods of low flow. Please note that the flow data shown in Figure 2.2b are prior to the construction of the dam on Chapman Lake.

The SCRD (2008) is expecting a 25% population growth by 2036, which suggests a rapidly growing demand for potable water in the upcoming decades. However, forecasting water demand based only on population growth is difficult, since communities are increasingly adopting best-management practices that greatly reduce the amount of water used per capita. Neale (2005) demonstrated that water conservation efforts are yielding positive results in communities that have enforced aggressive measures, such as water metering with increased block rate structures (32% savings) or mandatory installation of highly efficient fixtures and appliances (40% savings in indoor uses only). In 2004, the SCRD implemented water conservation programs regarding bathroom appliances. Encouraging figures show that the overall demand for treated water has been more or less stable since 2004 (Figure 2.2a) despite an 8.4% population growth from 2001 to 2006 (SCRD, 2008).

2.3 Climate Change and Projected Impact on Streamflow

The Fourth Assessment Report of the International Panel on Climate Change asserts that "warming of the climate system is now unequivocal" (Solomon *et al.*, 2007). It is suggested that emissions reduction efforts should be coupled with adaptation strategies to respond to the projected impacts of climate change at the regional level. The integrated effects of climate change and land use change on the water cycle is indisputably one of the key research area in need of more attention.

Local researchers in British Columbia have modelled the climate of the province for the next 50 years using the output of several global circulation (climate) models (GCMs) calibrated for different emission scenarios (Wang *et al.*, 2006). The Pacific Climate Impacts Consortium (PCIC) used the Canadian Regional Climate Model version 4.1.1 (CRCM4) developed by the Ouranos consortium (Cayan & Laprise, 1999) to build regional predictions for the 2050s (2041-2070). Among their results, the winter temperature along the southern coastal area of British Columbia is expected to rise by 2°C to 4°C while no significant variations are expected in precipitation (Rodenhuis *et al.*, 2007). Consequently, snow-water-equivalent (SWE) values are supposed to drop by 40% to 80% in comparison with historic averages in those areas. The absolute decrease in SWE is expected to be the greatest at high-elevation sites along the southern coast. At those locations, declines could be greater than 1000 kg/m^2 (or -1000 mm SWE) (Rodenhuis *et al.*, 2007), which more or less represents the mean SWE value from 1993 to 2002 for Chapman Creek at 1022 m of elevation (BC Ministry of Environment, 2009b – see Figure 3.4).

American studies focusing on the "Pacific Northwest", an international geographic ensemble that includes the American states of Washington, Oregon, western Montana, Idaho and southern British Columbia in Canada, show similar results (McCabe & Wolock, 1999; Mote, 2003). Analyses of historic meteorological data show how the rising temperature over the last 50 years has impacted April 1st SWE values. The most impacted regions are the Cascades and the Coast Range, where the decrease in SWE is often greater than 40%. Linear regression of the trend in April 1st SWE plotted against elevation shows an average decrease of 25% in SWE at 1700 m and of 50% at 1000 m (Mote, 2003). Simulations using various general-circulation models predict a decrease in SWE values of as much as 50 to 70% for the 2041-2070 period in the Pacific Northwest region (McCabe & Wolock, 1999).

The long-term variation in SWE proposed by the studies mentioned above is apparently not attributable to a decrease in precipitation, but more to an increase in minimum temperatures during the winter. Knowles (2006) documented the variation of the ratio of snowfall-water-equivalent (SFE) to total winter precipitation for approximately the same 50-year period (1949-2004). He showed that wet-days minimum temperatures have risen during winter and in the early spring across all of the western U.S. This warming induced an increase in the rain fraction during precipitation events. The variation in total precipitation was of lesser importance than the variation in SFE, enhancing the primacy of thermal dependency over the amount of precipitation during winters in the coastal regions (Hamlet *et al.,* 2005).

Determining a clear climate-change signal in streamflow is not an easy task, mainly because watersheds share diverse physiographic characteristics that evolve at different scales (e.g., soil, superficial deposits, bedrock, vegetation, lake, glacier), all of which have non-negligible influences on the water cycle. These characteristics create a range of antecedent conditions, so that every stream responds differently to rain or snowmelt events. However, regional trends – more likely to be driven by climatic fluctuations – can be detected. Historic records show a significant advance in the timing of spring peak flow over the past 40–50 years across Canada (Zhang *et al.* 2001) and in the western U.S.. The strongest trend is exhibited in the Pacific Northwest region at lower and middle altitudes, where the winter temperatures are close to the melting point. In the Coast Range, the present-day spring peak-flow occurs more than 15 days earlier than it did in 1950. In basins located at less than el. 2500m, a 10-to-20-days shift in the timing of peak flow is common. During this 50-year period, the total annual discharge has been relatively constant, confirming the redistribution of annual streamflow in between seasons due to the dominant role of temperature on the hydrological regime of the region (Regonda *et al.*, 2005; Barnett *et al.*, 2005). The Pacific Decadal Oscillation (PDO) warm phase has had a certain influence on these records, but the centurial trend shows that warming cannot only be explained by the PDO, suggesting the early sign of an overarching warming signal detectable in hydrological systems (Stewart *et al.*, 2005).

Historic trends also show that low flows in southern British Columbian streams are the most impacted in the country by climate warming; the mean minimum daily streamflow has significantly declined over the past 40 years. The increasing mean annual temperature is believed to be the main climatic variable driving this process. As the climate warms, the resulting increase in spring rainfall may accentuate direct runoff and accelerate snowmelt (Zhang *et al.*, 2001). Leith and Whitfield (1998) also found statistically significant decreases in late summer and early fall low flows and an earlier onset of spring snowmelt in six watersheds in B.C.'s interior. In coastal systems, summer low flows have mainly decreased in hybrid systems (Whitfield, 2001; reported by Moore *et al.*, 2007). This is interpreted as being the result of an earlier onset of snowmelt and an extended streamflow recession period in the summer. This interpretation was challenged by Moore *et al.* (2007), who also found decreasing discharges for the month of September in most of the unglacierized basins studied, while no trends were observed for August. However, the controlling factor explaining the decrease in September streamflow is primarily the decrease in September precipitation, as opposed to lagged variables such as winter precipitation.

Based on multiple linear regressions from historic data in 38 forested watersheds spread across eastern Canada and eastern U.S., Huntington (2003) found that every °C increase in mean annual temperature (MAT) would force an increase of 28 mm in potential evapotranspiration (PotEVP). Consequently, a hypothetical increase of 3°C over the next century could trigger a decrease in annual runoff of 11–13% (85 ± 30 mm, 95% confidence limits), assuming that the observed empirical relationship between MAT and PotEVP remains linear.

An earlier spring runoff and an increase in PotEVP, with little or no change in precipitation, would negatively impact the summer soil-moisture content and reduce soil-water contributions to streamflow and, by extension, to groundwater recharge. However, even if the impact of evapotranspiration on the low flows can sometimes be observed and validated in historic trends, they remain difficult to model deterministically because PotEVP is mostly driven by wind speed, long-wave radiations and vegetative demand (length of the growing season), all of which will likely change with a warmer climate (Hamlet & Lettenmaier, 1999). The associated uncertainties due to the local scale at which these processes operate make analyzing the results of the low flow simulations a delicate task.

2.4 Groundwater Recharge in a Mountainous Catchment: a Review

2.4.1 Evapotranspiration as a potential factor affecting groundwater recharge

As mentioned in section 1.2.1, the detection and projection of climate change impact on annual groundwater recharge is hindered by the poor state of groundwater monitoring in B.C. Nevertheless, a few simulations are available for some regions. For instance, surface water/groundwater modelling of the Grand Forks aquifer under climate change scenarios show that an advance timing of snowmelt leads to a decrease in late summer groundwater discharge in the Kettle River (Allen *et al.*, 2004).

In coastal environments at lower elevation, climate change is projected to cause a shift in the hydrological regime from hybrid to pluvial. However, at the “runoff processes” scale in unsaturated environments, not much evidence in the literature suggests that snowmelt events recharge aquifers differently than rainfall events. To the best of my knowledge, only a few authors address the issue. Krabbenhoft *et al.* (1990) estimated groundwater–surface water interactions in Wisconsin’s lake-dominated system over a two-year monitoring period. The authors concluded that the significant difference in $\delta^{18}O$ isotopic signatures (-0.6‰) they found between average precipitation and groundwater was attributable to the "selective" recharge of spring snowmelt over summer rain events. Arguably, one important variable that could impact the recharge flux between rain and snowmelt events is evapotranspiration (EVPT), which would suggest that a greater proportion of soil water not contributing to runoff preferentially migrates toward the aquifer during snowmelt episodes because of minimal vegetative uptakes and virtually no soil-moisture evaporative fluxes. However, the synchronicity between the growing season and both the rainfall and snowmelt dominated periods in southwestern British Columbia is not optimal, which suggests that EVTP won't have a significant impact on soil-moisture content in both cases.

This logical connection between the growing season and EVTP seems to be challenged by evidence presented by some authors that shows that at least two coniferous species investigated in Europe (Engelmann spruce and Norway spruce) uptake a significant amount of soil-water during the dormant season (snow-covered conditions for the Engelmann Spruce) from late autumn to early spring (Boyce and Lucero, 1999; Schume *et al.*, 2004) compared to deciduous trees, which suggests that we can't rule out EVPT during the winter, as has been generally accepted. On the other hand, early spring soil-water deficits occur only in the topmost-hydraulically-conductive soil layers for the Norway spruce (Schume *et al.*, 2004) and are minimal compared to summer soil-water deficits recorded in the same monitored stand.

It seems reasonable to assume that seasonal soil-water uptake patterns for western hemlock and western red cedar mixed forests at higher elevations are similar to the Norway spruce because the root density also decreases with depth (Wang *et al.*, 2002), limiting the capacity of the trees to uptake gravitational water during the dormant season. In fact, biomass and soil-water isotopic evidence in a study by Brooks *et al.* (2010) support this line of reasoning by showing that vegetative demand preferentially uptakes **immobile** water present in the very small pores and on grain surfaces, and very little interactions occur between this pool and the one contributing to runoff (**mobile** water). Very small pores and grain surfaces have a high soil-water tension during the dry season and, in our Mediterranean-like climate, are usually the first sites to be replenished during the "wetting-up" period (i.e., first rainfalls after the dry season that usually produce very little runoff response). This immobilized water would be enough to supply the vegetative demand for the remaining of the growing season. The term *immobile water* refers to the water that is not likely to be "flushed" and replaced by subsequent rainfall or melt-water input because of the tight bonding attraction existing between the water molecule and the grain. These results also demonstrate that vegetation is not likely to interact with mobile soil-water originating from precipitation/snowmelt events producing runoff response (lateral flow), and by extension recharge (vertical flow).

This recent study suggests that in Mediterranean climates (i.e. hot and dry summers coupled with cool and wet winters), it is reasonable to assume that the potential impact of EVPT on lateral or vertical flow during the dormant season (which coincides with the most hydrologically active season) could be disregarded, which goes against the more universal and traditional understanding of a causal relationship between through-fall, soil-water and recharge (Huntington, 2003).

2.4.2 Flow-path as a potential factor affecting groundwater recharge

Another possible factor that could conceivably affect groundwater recharge between rainfall and snowmelt events is a variation in the runoff flow-path. Runoff is a complex phenomenon that depends on a variety of physical characteristics specific to each catchment (e.g., soil depth and compaction, hydraulic conductivity, geology, vegetation type and structure, structural and superficial geology, elevation, aspect), meteorological variables (e.g., intensity of rainfall/snowmelt, wind speed, air temperature, radiation budget) and an array of antecedent soil-moisture, soil-frost and snowpack conditions. Not many authors address the role that unsaturated runoff flowpaths play on groundwater recharge (Zentner *et al.*, 2000), as it is usually assumed that the volume and timing of groundwater recharge is directly related to stream discharge peaks (Halford and Mayer, 2000) – an assumption yet to be challenged in hydrology.

Snowmelt events are usually more regularly distributed over time than rainfall events. Once the snowpack is ripened (ice grain matrix saturated with water), melt-water output usually occurs proportionally to the energy input from different sources, as expressed in equation 4.1 from Male and Gray (1981):

$$\mathbf{Q_m = Q_{sn} + Q_{ln} + Q_h + Q_e + Q_g + Q_p - dU / dt} \qquad \textbf{(eq 2.1)}$$

where Q_m is the energy flux available for melt, Q_{sn} is the net short-wave radiation flux absorbed by the snow, Q_{ln} is the net long-wave radiation flux at the snow-air interface, Q_h is the convective or sensible heat flux from the air, Q_e is the flux of latent heat (evaporation, sublimation, condensation) at the snow-air interface, Q_g is the flux of heat from the snow-ground interface by conduction, Q_p is the flux of heat from rain throughout the snowpack and dU/dt: rate of change of internal (or stored) energy per unit area of snowcover. In the spring, these variables are usually maximized during daytime, which explains why melt-water output from the snowpack follows a more-or-less sinusoidal pattern.

These daily snowmelt events consistently create high antecedent soil-moisture conditions for the snowmelt event on the following day, which increase the soil's hydraulic conductivity and consequently favour rapid subsurface runoff. In B.C.'s coastal climate, rainfall events differ from snowmelt events in that they can usually deliver a much larger instantaneous volume of water, but also as the antecedent soil-moisture conditions are presumably more variable due to the sporadic nature of rainfall events compared to spring snowmelt. This hydrological behaviour can easily be visualized as the *soil-moisture memory*, which is the capacity of the soil to "remember" wet (or dry) conditions caused by accentuated and prolonged water inputs (or deficits) long after the originating conditions have been forgotten by the atmosphere. The dissipation of that memory may take weeks to months (Koster and Suarez, 2001). Constant elevated soil-moisture content before, during and long after the snowmelt season arguably creates favorable conditions for an extended groundwater recharge flux to occur, as opposed to smaller intermittent recharge fluxes during the rainfall dominated season, which is usually triggered when the antecedent soil-moisture condition is at its lowest in the year.

The *flow-path* concept can be interpreted as the sum of all the hydrological responses operating at different time scales (e.g., evaporation, overland flow, macropore flow, interflow, piston or matrix flow, groundwater recharge) that the "event" water follows (new water input – can be either rain, melt-water, or both). Following the mass-balance principle, the total volume of event water must always be accounted for by those fluxes, but their relative contributions largely depend on antecedent conditions and water input intensity. Based on this premise, the hypothesis formulated above would suggest that a significant difference of the recharge flux between snowmelt- and rainfall-dominated periods would inevitably change the relative contribution of event water to other fluxes composing the flow-path, namely the ones contributing to stream response.

Recharge-flow is largely dependent on the capacity of the overlying mediums to allow through-flow to drain further down towards the aquifer. Hardened iron-pan in podzolic soils and the underlying sub-glacial till have a low saturated hydraulic conductivity. Those layers usually follow the topography and can act as aquitards by producing short-lived perched or transient aquifers when the inflow exceeds the infiltration capacity, resulting in a fast delivery of water to streamflow as interflow during storm/snowmelt events (Hutchinson and Moore, 2000). Of course, the response is especially quick in mountainous catchments and is a prevalent runoff response in the study area as demonstrated by Kim (2001 – unpublished) and Kim *et al.* (2004) at the hillslope scale. Despite the high volume of water input during rainstorms or snowmelt, those shallow flow-impeding layers can theoretically limit groundwater recharge by deviating vertical flow laterally towards the channel. Laudon *et al.* (2004) presented evidence derived from isotopic and hydrometric measurements from a boreal catchment in Sweden of similar geology and pedology that deeper flowpaths (90cm and deeper) were not hydrologically connected during snowmelt and therefore did not contribute to stream runoff, even though pre-event water largely dominated the hydrograph. Since the isotopic signature of deeper groundwater and the soil moisture of deeper unsaturated layers did not appreciably change during active snowmelt, one can interpret those results as evidence of delayed and slow groundwater recharge more likely controlled by constant soil moisture content than by the intensity of water-input.

Subsurface runoff through preferential pathways, such as macropores and root channel, greatly contributes to streamflow in steep landscapes (McDonnell, 1990) and has been identified as an important runoff generation mechanism in coastal British Columbia (Anderson, 2008 – unpublished).

2.5 Nitrate Export During Snowmelt

Nitrate is an essential nutrient for terrestrial and aquatic ecosystems. Traditionally, nitrate (NO_3-) is formed as a result of biologically driven soil processes – mainly through the biodegradation of ammonium (NH_4+). This bacteria-driven process, known as nitrification, usually operates all year round – as long as the soil's temperature stays above 0°C. The accumulation of nitrate in the soil takes place when the vegetative demand cannot meet the production of NO_3-. Some of it is taken up by denitrifying bacteria and transformed into various forms of atmospheric nitrogen (N_2, N_2O_2, etc…), but a large portion is transported to water bodies.

In B.C.'s coastal environment, the terrestrial vegetation goes dormant for a few weeks at most at lower elevations – maintaining a quasi-constant demand for nitrate all year round. However, bacterial activity diminishes during the winter due to the colder environment. The resulting depletion of NO3- in the soil logically explains why it occurs naturally at very low concentrations in coastal streams. However, the seasonality of vegetative growth at higher elevations presumably favours the accumulation of soil nitrate in the winter – which could be mobilized during snowmelt and likely lessen the downstream nutrient deficiency in the summer through hyporheic storage and release. Even if headwater systems are not the dominant ecosystem area-wise, they represent 60–80% of the stream network in forested environments (Benda *et al.*, 2005). Those streams are necessary vehicles for nutrient transport to downstream reaches (interpreted from Gomi *et al.*, 2002) and could theoretically be a significant source of dissolved N species after spring freshet at high elevations.

Two main hydrological mechanisms are believed to drive nitrate export to streamflow: the draining and the flushing mechanisms. The draining mechanism is the "traditional" hypothesis, which states that nitrate percolates to the aquifer and is eventually delivered at a somewhat constant rate through groundwater discharge to the channel (Allan, 1995; Peterson *et al.*, 2001). The flushing mechanism, proposed by Hornberger *et al.* (1994) and experimentally confirmed again by Creed *et al.* (1996), explains the variability in NO_3- concentration as a function of soil saturation deficit. The nitrate accumulates in the soil when the soil saturation deficit is high (assuming low vegetative uptake), whereas an important increase in soil moisture would hydrologically connect the hillslopes, creating a saturated subsurface flow path that "flushes" the nitrate in the soil's upper layers directly into the stream. According to this hypothesis, the nitrate concentration peaks during the rising limb of the hydrograph and diminishes quickly prior to the peak-flow because nitrate is quickly exhausted due to its high mobility. The initial conditions necessary to the flushing mechanism are optimal prior to snowmelt, thus it is expected to be the prevalent form of nitrate transport during spring freshet.

3 Study Area

3.1 Location

The study was conducted in one of the main headwater tributaries of Stephens Creek, a mountainous stream flowing from the west face of Mount Elphinstone and down through the municipality of Roberts Creek, a town located about 25 km northwest of Vancouver, British Columbia (Figure 3.1). Stephen's Creek is a local stream adjacent to Chapman Creek and was chosen because winter access to the headwaters of Chapman is logistically too challenging.

The research catchment comprises 718 ha ranging in elevation from 670 m at the catchment outlet to 1,170 m at the most eastern divide point, but about 70% of the catchment area is above 1000 m (Figure 3.2). The lower part of the catchment is generally WSW facing and the upper part has a pronounced symmetric mountain-valley shape with two dominant aspects, SSW and WNW. The slope shows a rapid increase from 15° at the outlet to 25° over most of the catchment area, and then decreases rapidly to about 0-5° approaching the catchment divide on both aspects.

3.2 Climate

A Mediterranean-like climate (*Csb* in the Köppen system – Peel *et al.*, 2007) dominates over this part of British Columbia, which is distinguished by a contrasted annual signal in precipitations, oscillating between relatively dry conditions in the summer (~50 mm per month) to very humid in the winter (~200 mm per month – see Figure 3.3). This climatic pattern is driven by global-scale atmospheric circulation mechanisms that cause relatively warm oceanic air masses with considerable water holding capacity to penetrate inland. Moreover, the mountainous physiography of the region provokes orographic precipitation along the coastline, a phenomenon that is clearly visible from the isohyet contour map built by Danard (1980) and reported by Chapman (1991). Based on multi-annual precipitation data from multiple

weather stations and snow courses, his interpolated results show that the Tetrahedron plateau, an area ranging in elevation from 900 m to 1700 m located only 20 km north of Gibsons, receives annually about twice the volume of precipitation (2750 – 3000 mm) than adjacent areas located at sea level. The inequity of the temporal distribution of precipitation is evident from the climatic averages at Gibsons Gower Point (no. 1043152), located 9 km south of the research catchment (Figure 3.3 - Environment Canada - 2009), which shows that the six-month period from October to March receives about 72% of the annual precipitation.

Figure 3.1 Localization maps of the study area

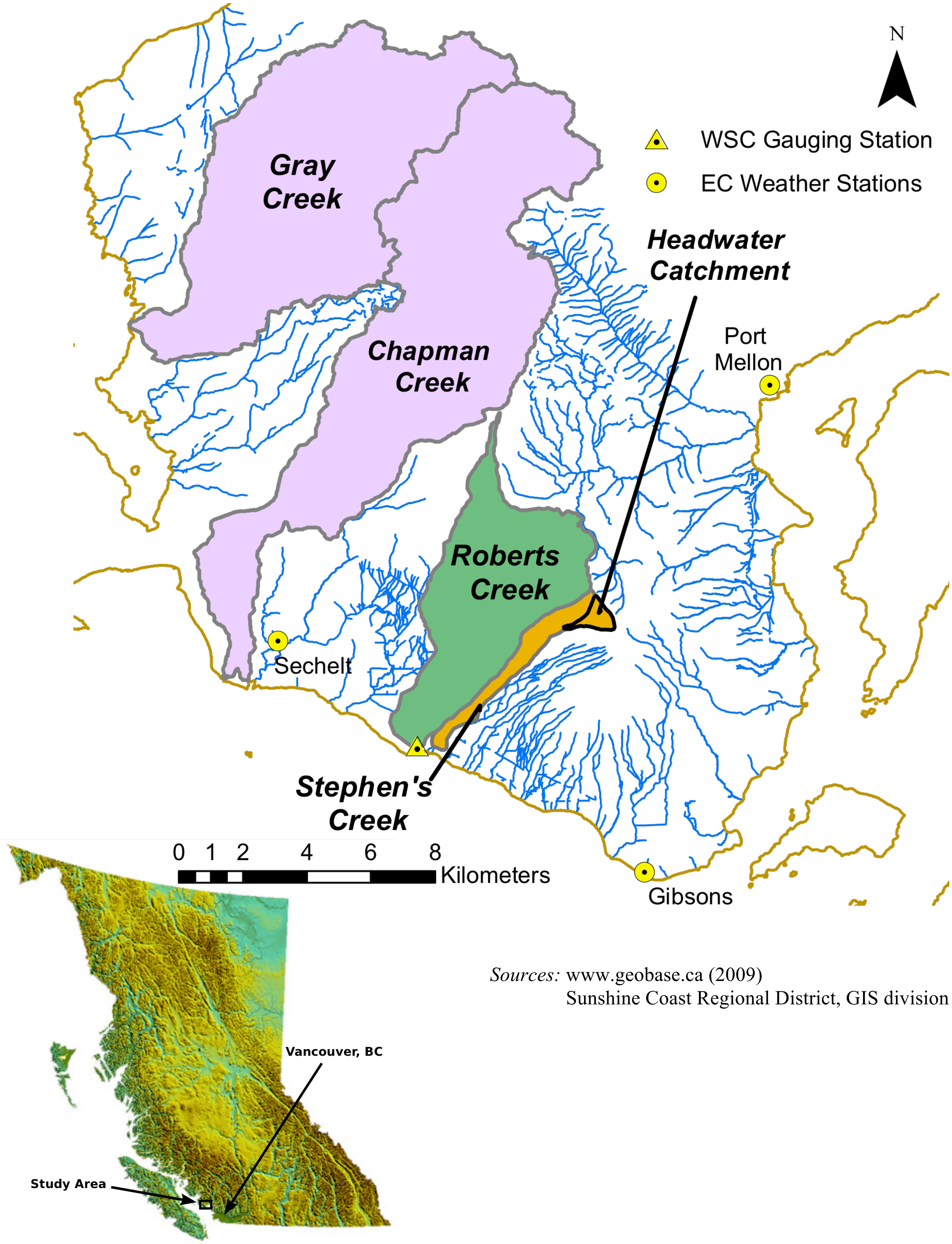

Sources: www.geobase.ca (2009)
Sunshine Coast Regional District, GIS division (2007)

Figure 3.2 Elevation distribution of Stephen's Creek research catchment. Localization of snow lysimeters and snow courses are for further references

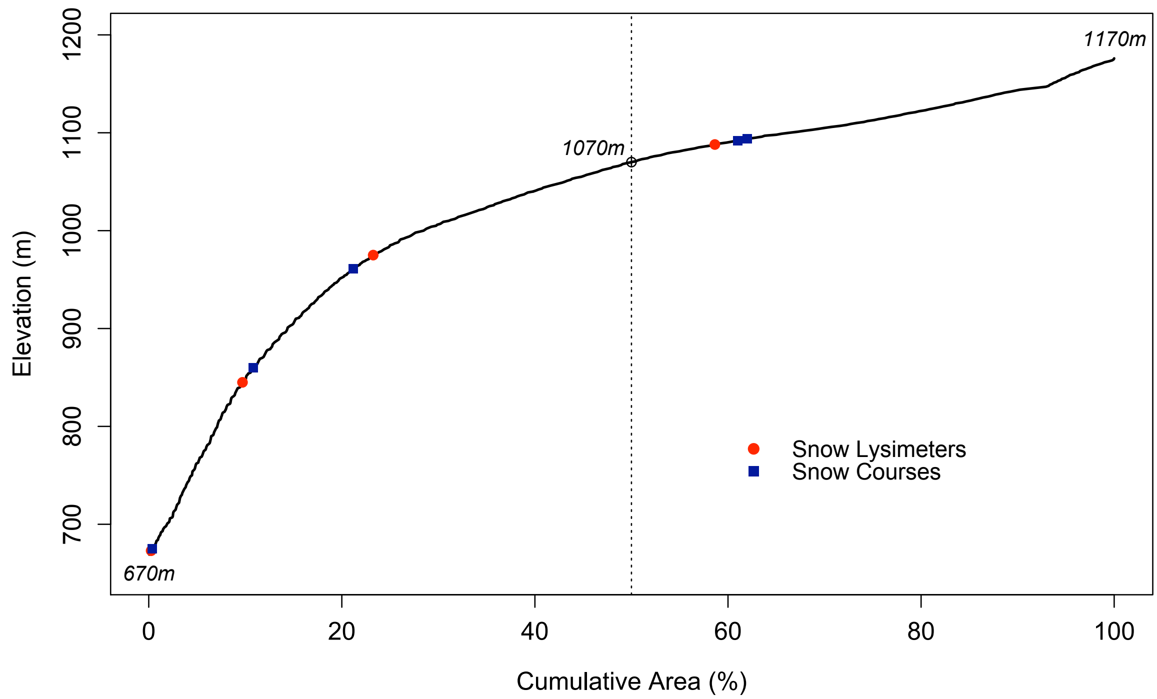

Figure 3.3 Monthly climatic averages for Gibsons Gower Point (elevation 34m) from 1970 to 2000. The vertical bars represent precipitation, the black line indicates daily mean temperature and the dashed lines represent daily minimum-maximum temperatures

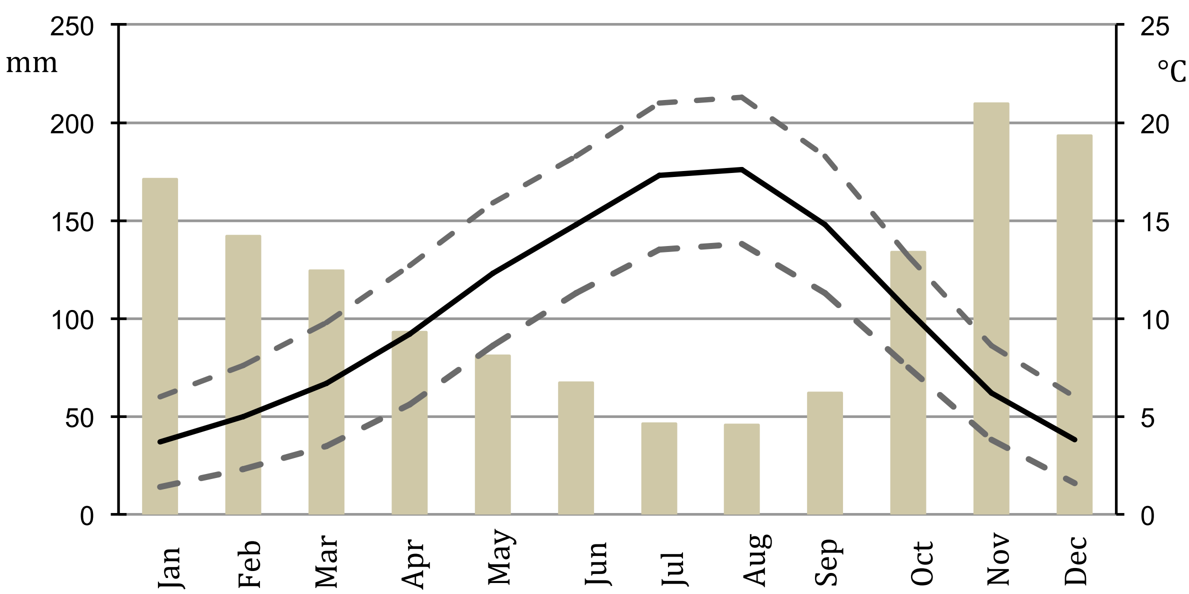

Figure 3.4 Snow-Water Equivalent in the Chapman Creek watershed (elevation 1022 m) from 1993 to 2002 (BC Ministry of Environment, 2009).

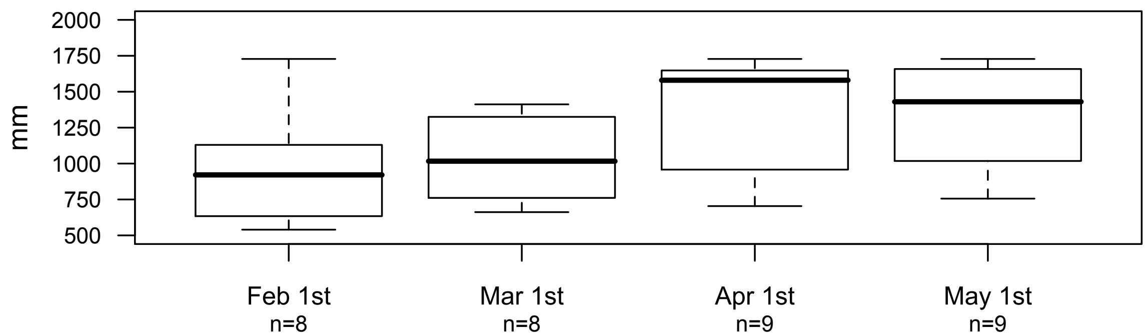

The temperature regime is generally dominated by continentality, but the extremes are heavily dampened by maritime influence (Baker & Nyberg, 1974). Therefore, almost all the precipitation occurs as rainfall at lower elevations all year around. However, the temperature gradient explained by elevation gain causes the average winter temperature to drop below the freezing point, enabling heavy snowfall and, therefore, seasonal snow cover at elevation above ~ 600 – 700 m (Carson, personal communication, 2008). Snow-course data collected in collaboration with the BC Ministry of Environment (2009) in the Chapman Creek watershed (Tetrahedron plateau, Figure 3.4) between 1993 and 2002 show the capacity of air masses to generate extensive snowpack over the winter, but a more meaningful observation would be the highly variable snow conditions illustrated by the large gap between the maximum and minimum values. Climate data would enable us to investigate whether precipitation or temperature dominantly explains this variation, but unfortunately none of these variables is recorded at high elevation in the region. Also, note that SWE values remain practically unchanged during the month of April, suggesting that a negative trend in the snowpack mass balance (snowmelt) on the Tetrahedron plateau is not likely to occur before the 1st of May.

3.3 Geology

The regional geological setting of the Lower Sunshine Coast is dominated by quartz diorite and granodiorite plutonic complex, an intrusive crystalline bedrock formed during the Late Jurassic to Early Cretaceous that is very resistant to erosion and weathering (Friedman *et al.*, 1990). However, a metavolcanic formation from the Bowen Island

Group underlies the research catchment. It is an older bedrock formed during Early to Middle Jurassic based on U-Pb dating conducted by Friedman *et al.* (1990) on the North summit of Mount Elphinstone, only 600 m north of the catchment area. These authors describe the lithology of the area as being "strongly foliated fine-grained amphibolites interlayered with green chlorite schist and local exposures of pale grey, white and green fine-grained schistose felsic metavolcanic rocks" (Friedman *et al.*, 1990). Excavated soil pits and visual inspection of bedrock blasts along the side of the forest roads show evidence of fractures ranging in size from micro to mesoscale features. Roots frequently penetrate the bedrock, which can be easily broken into pieces by a geological hammer or a shovel—demonstrating a poor resistance to physical stress, and consequently a propensity to chemical weathering because of increased mineral surface area. Numerous dikes cutting through a larger ensemble at many locations across the catchment confirm that the genesis of the formation is metavolcanism. Because the rock is generally highly chemically altered, no crystalline features or layering are apparent and no primary minerals could be identified visually. However, every rock sample collected in 4 soil pits and along the stream channel showed evidence of fracture plans and further visual inspections uncovered the presence of pyrite (FeS_2) as a secondary mineral in abundant quantity within those fracture plans (Leslie, 2008 – personal communication). A significant amount of iron in the bedrock has implications for the dissolved chemical load of the groundwater. The rate of dissolution for Fe-containing mineral is expected to occur faster then its Ca or Mg equivalent (Brantley & Chen, 1995), largely because iron hydroxide precipitation contributes to acidity in the system, therefore accelerating the pH-controlled dissolution reaction.

3.4 Geomorphology and Stratigraphy

Mount Elphinstone has three distinctive summits called the North, West and East summits. The North and West summits are plateau shaped, suggesting that the mountain was completely covered by an ice sheet during the last Pleistocene glacial maximum. Two north-facing glacial cirques isolate the East summit from the geomorphic ensemble. At the regional level, many streams occupy glacial-carved valley bottoms, flowing over various till substrates at higher elevation and reorganizing glacial outwash deposits at lower elevation. Initial reconnaissance of the research catchment revealed that channels flow mainly over glacial till and alluvial deposits, but bedrock channel sections are frequent—especially at higher elevation. A highly compacted sub-glacial till of an unknown thickness was identified in the stratigraphic sequence along the forest road 500 m south-west of the catchment outlet at a depth of about 1.5m from the surface. Many sub-metric boulders, presumably morainal deposits, are surfacing at lower elevation in the catchment. At higher elevation, a soil pit excavated on the southwest facing aspect (1080 m) showed no signs of ablation till or sub-glacial till.

3.5 Soils

Four soil pits were excavated at different elevations across the catchment (670 m, 835 m, 975 m and 1080 m) to qualitatively characterize soil profiles and to install snow lysimeters. The soil on the hillslopes is deeper than 130 cm at lower elevation and about 70 cm deep close to the catchment divide at higher elevation. Based on the Canadian system of soil classification (Soil Classification Working Group, 1998), the dominant soil type occurring in the catchment was identified as Ferro-Humic Podzol. The litter-organic horizon was uneven in thickness and composition, but usually 5 to 10 cm thick and mainly composed of decaying needles. The A horizon showed evidence of many dead root channels and other macropores, suggesting a pre-disposition for bypass flow. Decaying woody debris of metric dimensions was also observed in this layer. A 3 to 4 cm-thick eluvial horizon (Ae) and a clearly illuvial B horizon enriched with amorphous organic matter complexes (imogolite) and oxidized iron suggest a strong great leaching capacity of the soils. The presence of cemented layer—a hardened Fe_2O_3-enriched pan (reported thickness of 5 to 20 cm in the literature)—at the C horizon contact zone strengthens the conclusion of high leaching rates. The literature reports that the hydraulic characteristics of these layers are similar to sub-glacial till (Jugen & Lewis, 2007). This cemented layer was reached at decreasing depth with elevation, varying from 1.3 m at 670 m to 95 cm at 980 m. No cemented layer was found in the soil pit located at 1080 m. Since it is nearly impossible to dig through the cemented layer with the usual field tools, the thickness of the C horizon at most locations could not be assessed. The soil landscapes at higher elevation show significant pockets of organic soils, mainly on the northern summit.

3.6 Vegetation

The research catchment is located in the transitional area from the Coastal Western Hemlock to the Mountain Hemlock biogeoclimatic ecosystem subzones (Ministry of Forests and Range, 2008). The two prevalent tree species present at lower elevation are the western hemlock *(Tsuga heterophylla)* and the western red cedar *(Thuja plicata)*. The riparian areas at lower elevation are mainly colonized by alder *(Alnus sp.)* stands, while the higher elevation areas are mainly populated by mountain hemlock *(Tsuga mertensiana)* and coast douglas-fir *(Pseudotsuga menziesii*) with a dense understory dominated by berry-prolific species. Most of the forest in the catchment area has been logged in blocks between 1930 and 1960 (SCRD, 2008). Two significant old growth stands exist, one at mid elevation and the other one at higher elevation on the northwest facing aspect. Because of the high forest productivity in the region, the second growth can be considered mature at lower elevations, while in-situ mensuration measurements show a generally immature forest in the more recently logged blocks (40 years ago) and those above 900 m.

The catchment area was divided into five vegetation ensembles representing different forest covers: Coastal Western Hemlock (CWH) old growth; CWH second growth (older re-growth and younger re-growth); Mountain Hemlock (MH) old growth; and MH second growth (Figure 3.6). A summary of the mensuration measurements can be found in table 3.1, the method is described in section 4.9.

Figure 3.6 Forest cover classification in Stephens Creek research catchment

Source: Sunshine Coast Regional District, GIS division (2007)
Ministry of Forest and Range (2008)

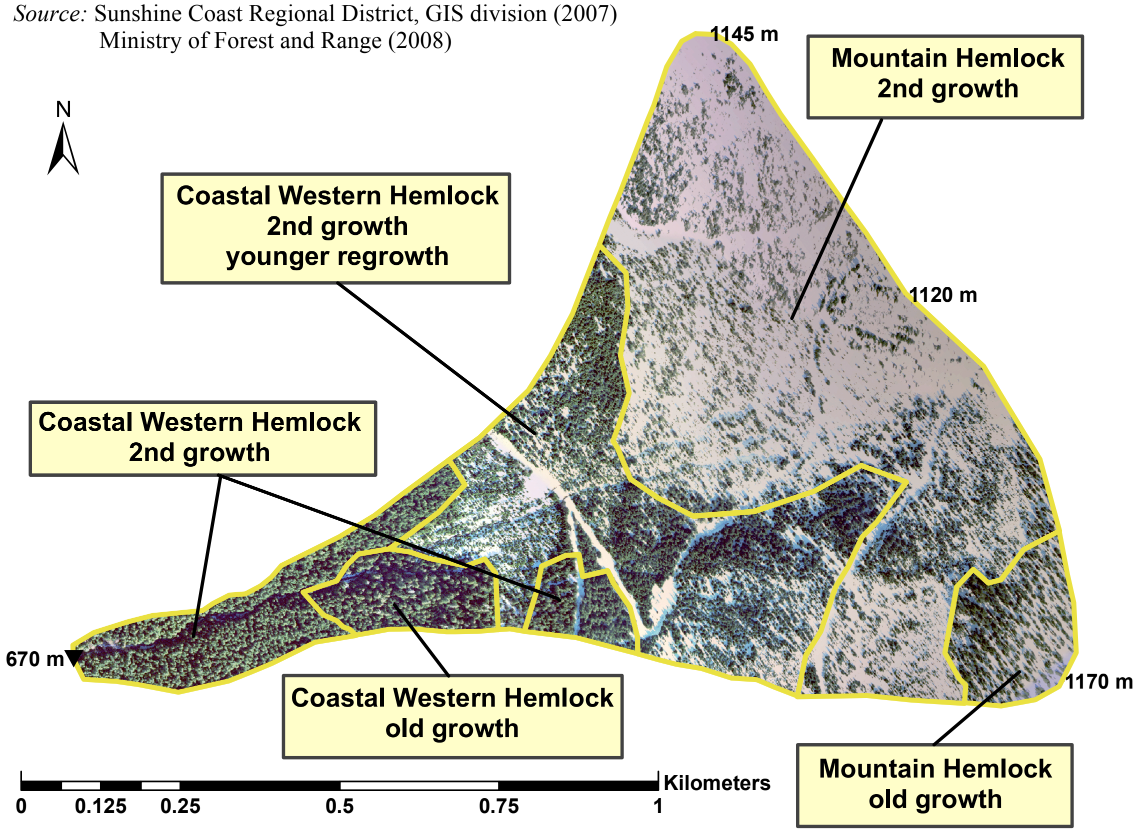

Table 3.1 In-situ forest mensuration measurements for dominant forest covers

Forest cover	Sample size (n)	DBH (cm)	Tree height (m)	Crown dominance[1] (%)	Density (trees per ha)	Canopy closure (%)
CWH old growth	6	82	37	45	1952	70
CWH sec. growth	20	44	29	48	3337	75
CWH sec. growth (younger)	14	24	14	71	5125	85
MH old growth	6	72	34	46	1363	65
MH sec. growth	12	33	9	88	955	10

1 – (Crown's height / Tree height) ratio

3.7 Hydrology and Water Quality

The gauging station defining the outlet of the catchment was built on a third-order stream, based on the Horton-Strahler stream hierarchy classification system (Horton, 1945). The streamflow data collected on site showed that the stream supported flow in late summer 2008 and 2009. A combination of steep slope gradient from the outlet to the divide, which averages 30%, and a generally shallow soil overlaying impervious layers, create the ideal settings for rapid runoff response to rainfall and snowmelt episodes. GIS analysis showed that the total drainage density of the network, including perennial and ephemeral channels, approaches 5.8 km per square kilometer, which also gives a good indication of the great dynamicity of the hydrological response. A major debris jam was observed at about 25 m downstream of the catchment outlet but at no other locations within the catchment area. Preferential flow were also observed during rainfall and snowmelt events at some locations along the sides of channels and forest access trails.

In these pristine environments, total dissolved solids (TDS) load in the water is a good indication of mineral chemical weathering. It can be approximated by electrical conductivity measurements and deviations from background can be used to quantify the contribution from another source with a much lower TDS load, such as channel precipitation or rapid through-flow (Moore *et al.*, 2008). The average electrical conductivity value for Stephens Creek during baseflow-dominated periods is 32.5 $\mu s\ cm^{-1} \pm 11.4$ (n = 7). This is interpreted as water that has a very low ionic charge and is evidence of a poorly buffered system, which makes it prone to periods of acidification.

4 Field Monitoring and Laboratory Methods

4.1 Streamflow Monitoring

The research catchment has been equipped with a limited number of hydrometric instruments. A sharp-crested 100° V-notch weir was installed at the outlet to monitor streamflow (Figure 4.1). The material used to build the weir plate is 1.9 cm-thick fir plywood, supported by spruce boards (2.5 cm x 15.2 cm). The weir plate and the supportive boards are bolted into an underlying wooden structure (1.8 m x 3.7 m) buried 40 cm under the streambed. The walls of the detention pond were built with burlap sacs filled with gravel and sand deposits found on-site. The streambed, the inside walls and the weir plate were covered with a thick polyethylene plastic to minimize water leakage from the detention pond. The maximum measuring head of the weir is 81 cm, and at no moment during the monitoring period did the discharge exceed the capacity.

Given the short duration of the monitoring period (from September 2008 to November 2009), the recorded water level was referenced to the bottom of the v-notch; no permanent datum was established using benchmarks. The stage was recorded every 15 minutes by an Odyssey capacitance water level probe (ODYWL20), housed in a perforated PVC pipe and deployed in the detention pond 1.8m away from the weir plate. The stage recorder was backed up by another probe of the same model in case of failure. Both probes were installed at the end of August 2008, maintained and reset in May 2009 and removed in November 2009. No biofilms were detected on the probes and a limited amount of sedimentation was observed at the bottom of both pipes, but not extending above the plane created by the bottom of the v-notch.

The size of the weir is too large to satisfy the assumptions of the contracted or the partially contracted v-notch weir equation (Corbett *et al.*, 1943). The stage discharge relationship was calibrated using salt tracing, a volumetric-velocity method that evaluates the variation of the stream water ionic charge through electrical conductivity measurements after the injection of a given mass of salt. The procedure chosen was dilute slug injection with NaCl. The salt solutions were mixed on-site using stream water about an hour prior to the injections in order to allow full dissolution of the salt. The injection solutions were poured into the weir's waterfall and electrical conductivity (EC) readings were recorded about 20m downstream of the weir. No secondary EC probe were available to assess if complete mixing occurred, but it is fair to assume so since the injection was done in highly turbulent water. The channel was slightly modified before the first salt injection was performed to guarantee that stream water would not flow into a side channel at high discharge and bypass the EC recording station. The calibration corrections were achieved in the field as described by Moore (2005) for every observation.

Water temperature was recorded every 10 minutes in the detention pond using an Onset light-temperature logger (UA-002-64).

Figure 4.1 Gauging station during different streamflow conditions

4.2 Precipitation and Air Temperature

Rainfall was monitored by the use of two Onset tipping buckets rain gauges (5 mL RG3-M), one at the weir (670 m) and one close to the summit of the catchment (1080 m). The rain gauges were mounted on 2m posts and secured to the ground with steel cables. A few alder trees around the rain gauge deployed at lower elevation had to be logged to ensure a minimal canopy opening (60°). The rain gauge at higher elevation has a 45° canopy opening around it, satisfying the standard for rainfall measurements (Dingman, 2008). It was assumed that this difference in canopy opening did not significantly impact

Figure 4.2 Stephens Creek research catchment

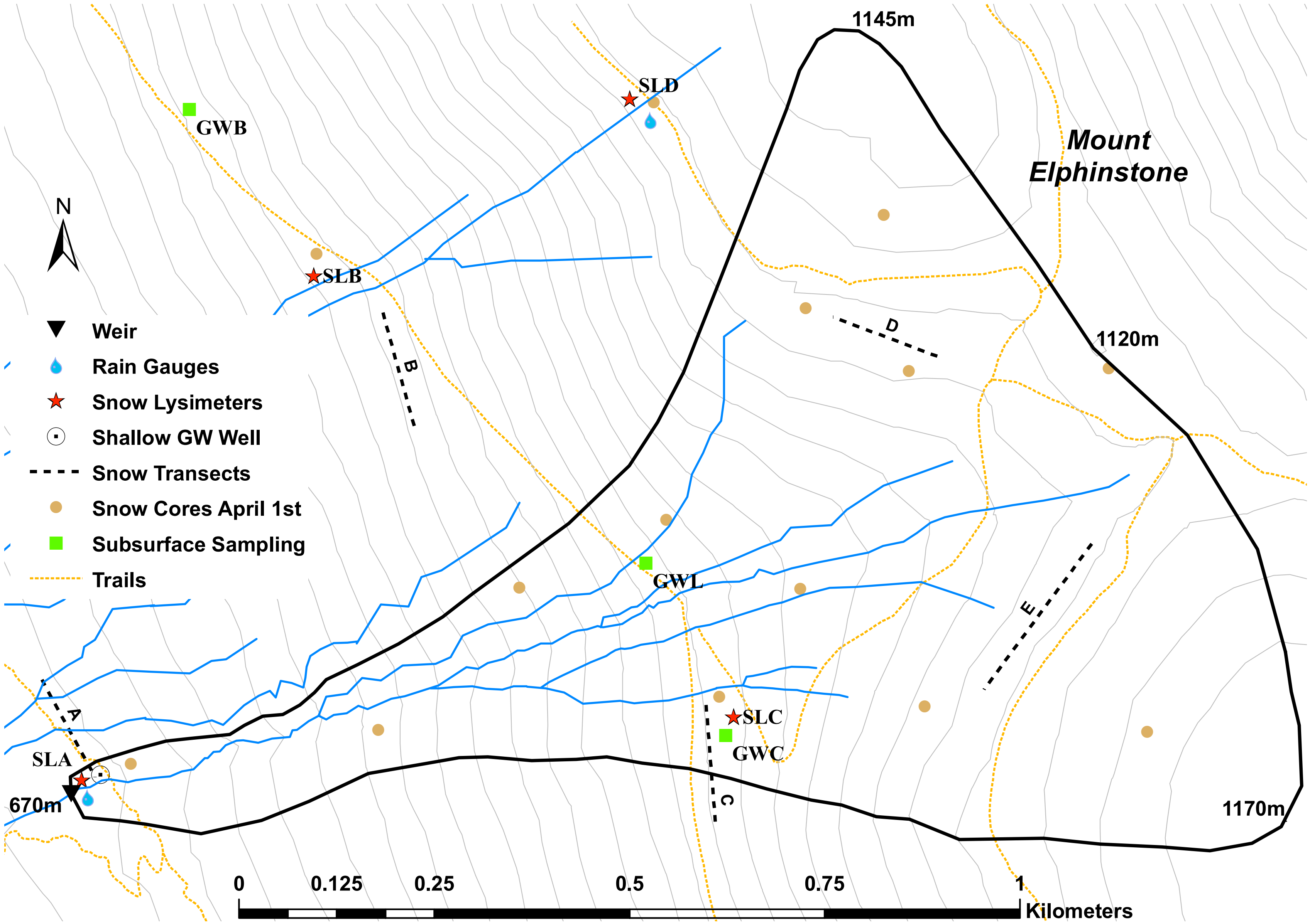

the rainfall catch when computing precipitation lapse rate. The rain gauges were occasionally adjusted and cleared from snow. The gauges could only be used to measure rainfall intensity and not total precipitation since they were not equipped with heating devices. The rainfall measurements at higher elevation were however discarded from Decembre 15th to April 15th due to consecutive failures of the tie-downs and the data logger. The measurements at lower elevation were also discarded for the same time interval because of inaccurate readings due to ice and wildlife damage.

Air temperature was recorded hourly at an elevation of 980 m under forest canopy with an Onset event-temperature logger (UA-003-64) and a six-plate Onset radiation shield (RS1).

4.3 Shallow Groundwater

A piezometer was installed in August 2008 at an elevation of 673 m, 15 m away from the stream channel in a hillslope's hollow filled with sandy deposits. The water level was recorded every 15 minutes by an Odyssey capacitance water level probe (ODYWL20), housed in a perforated PVC pipe and covered with geo-textile. The datum of the piezometer was buried 85 cm underground and elevated at about 150 cm relative to the streambed. Three other piezometers were installed at higher elevation, but were destroyed under the weight of the snowpack. The piezometer was removed in November 2010.

4.4 Snowmelt

A total of four snowmelt lysimeters (SLs) with a 6 m x 1 m catchment area were constructed on site to directly monitor water leaving the snowpack (Figure 4.4). The catchment surface was a thick polyethylene plastic (i.e. industrial-rated vapour barrier available in construction supply stores) with a steady slope angle ranging from 10° to 15°, depending on the terrain where the SL was installed. It is framed by spruce boards (2.5 cm x 15.2 cm), which were dug halfway into the soil. This was assumed sufficient to minimize lower boundary influences or capillary pressure gradients. An ABS piping apparatus drained the melt and rain water from the lowermost corner into a cooler containing the tipping bucket flow gauge device (Unidata 6506G, maximum recording capacity of 3 L per minute) buried 80 cm to 100 cm deep into the hillslope. The draining pipes were reinforced with a wooden frame in order to support the load of the snowpack and isolated with thick layers of foam polystyrene. No evidence of freezing were ever detected in the drains or in the flow gauges. The snowpack water output intensity values were recorded with Onset event-temperature loggers (UA-003-64) and the data were offloaded weekly during the snowmelt period.

Figure 4.4 Snow lysimeter installation

The four snow lysimeters were deployed at different elevations (670 m, 835 m, 975 m and 1080 m) and under a similar west-facing aspect. Due to access constraints, two SLs had to be deployed about 500 m north of the catchment. SLA and SLB were installed under a second growth (older re-growth) western coastal hemlock (WCH) forest cover, SLC under a second growth (younger re-growth) WCH forest cover, and SLD under an open canopy of second growth Mountain Hemlock.

The data loggers were activated prior to the main snowmelt season on March 28th. Connection failures occurred at SLD and no data were recorded from April 1st to April 10th. The time series was filled with linear regression using SLB as predictor values.

4.5 Snow Course

Four 150 m snow transects were sampled weekly at different elevation (674 m, 860 m, 958 m and 1085 m) for snow depth (every 5 m) and snow density (every 10 m) to monitor snow-water equivalent (SWE) evolution from April 4th until full snowpack disappearance. Snow depth was measured with a standard aluminum probe (G3 320cm pro-tech probe) with a precision of 0.5 cm and the Federal sampler was used to assess snow density. No strong relationships were found between snow depth and snow density during the early season (R^2 = 0.57). Therefore, only the snow depth measurement points paired with snow density observations were used to compute SWE. A single SWE value for each transect was obtained by averaging the 15 observations. This method is detailed by Goodison *et al.* (1981).

A different data collection procedure was used for the fifth transect on the northwest facing aspect of the catchment at higher elevation (1090 m). Because the April 1st snowpack was generally too deep at this location to be measured with a snow depth probe, 15 snow wires made with a UV-resistant braided fishing line were deployed just above the snow surface between two adjacent trees over a distance ranging from 3 m to 15 m (Figure 4.5). The snow wires were spread over a distance of 200 m under similar aspect, forest cover and elevation. Although the snow wire technique is usually used to calculate daily ablation rate (Murray and Buttle, 2003; Mielko and Woo, 2006) and is vulnerable to damage, a careful installation and monitoring make it effective to measure snow depth where the usual probe fails to reach the ground.

The distances from the wire to the snow surface were measured weekly at marked locations: every 50 cm for wires under 7 m in length, every meter for longer wires, and at least a meter away from both trees in all cases in order to minimize local influence. The snow-depth values were computed by subtracting the wire-to-snowpack distances from the wire-to-ground distance measured at the end of the snowmelt season. A weekly averaged snow depth value was computed for every snow wire.

Figure 4.5 Snow wire measurement

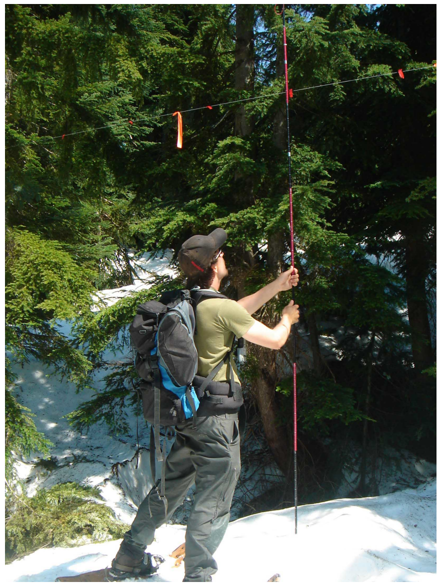

A single snow-density measurement was taken at every snow wire for each sampling occasion. During the first three weeks of observations, the measurements were taken in tree depressions using the federal sampler. Subsequent observations were conducted in undisturbed areas within a meter of each snow wire. A single weekly SWE value was calculated by averaging the SWE values obtained from the 15 snow wires.

4.6 Water Sampling Program

4.6.1 Stream water

Stream water was sampled at three different locations along Stephen's Creek (Figure 3.1): at the outlet of the headwater catchment (STH – 670 m), at the mouth (STM – 26 m) and about halfway in between those two points (STL – 308 m). Samples were collected for isotopic determination and metals analysis at STH and STM and for nutrient concentrations at all three points. Samples were collected daily from April 1st to May 19th, every two days from May 20th to June 19th, and weekly during baseflow conditions from June 20th to September 25th. The *in-situ* treatment for water samples is detailed in section 4.8.

4.6.2 Snowmelt

Many authors have shown that the fractionation process occurring during snowmelt causes a gradual enrichment in snowmelt isotopic composition (Stichler, 1987, Taylor *et al.*, 2001; Unnikrishna *et al.* 2002). The latter made a significant contribution to the hydrograph-separation science in snowmelt-dominated environments by demonstrating that snowmelt isotopic signatures can vary considerably within a single snowmelt episode ($\delta^{18}O$ = 2.95‰). This result alone indicates that frequent snowmelt sampling is required in order to capture most of the temporal variability of the snowmelt signature and build an appropriate input function. Following this recommendation, snowmelt samples were collected on a daily basis in the afternoon from the tipping bucket flow gauge outflow of every snowmelt lysimeter. Unfortunately, last-minute logistical constraints with the flow gauge containers made the collection of daily composite samples impossible. Therefore, every sample is considered a "snapshot" of the isotopic signature at time of collection.

4.6.3 Soil water and groundwater

Saturated soil water through-flow (saturated flow over a cemented soil horizon) was collected from two soil profiles (labeled GWC and GWL in Figure 4.1) during the period extending from April 25th to June 14th. Shallow groundwater was sampled from April 25th to May 13th from a spring flowing out of the mineral soil – bedrock interface in a section of blasted bedrock alongside the forest access trail (GWB). Deeper groundwater samples were collected at two locations (Figure 3.1): a perennial spring (GWE) situated approx. 6 km south of the research catchment (27 m), and a municipal well in the Town of Gibsons (GWG) located 8 km southeast of the research catchment (20 m). Those deeper groundwater sources were sampled from April 1st to August 21st. In all cases, grab samples were collected at weekly to bi-weekly intervals from April 25th to June 14th, and monthly in the summer for the deeper groundwater sources. All soil water and groundwater samples were analyzed for isotopic determination, metals and nutrients.

4.6.4 Snow core samples

A total of 15 integrated snow-depth samples were taken on March 31st and April 1st across the catchment to determine the initial isotopic and chemical signatures of the snowpack prior to snowmelt initiation. The snow cores were extracted using the Federal sampler, stored in polyethylene bags, and wrapped in a white plastic tarp in order to prevent freeze/thaw during transport. The snow cores were fully melted in a controlled environment at temperatures oscillating between 2°C to 5°C, as prescribed by Cooper (1998), in order to prevent evaporative isotopic enrichment as much as possible. The melt water was subsequently sampled for isotopic determination, metals and nutrients.

4.7 *In-Situ* Samples Treatment

Samples for isotopic determination were collected in 20 mL borosilicate scintillation vials and capped with cone-shaped lids to prevent air bubbles from being trapped with the water samples. They were kept in a dark and cool (3ºC) environment until analysis. Samples for metals analysis were filtered using a 60 mL syringe and 0.45 μm pore-size filter membrane, collected in 120 mL acid-washed polyethylene bottles and acidified in the field under pH 2.0 with a 5 molar solution of nitric acid, trace metal grade. Samples were kept dark and refrigerated at 3°C until being concentrated (see Section 4.9.2). Samples for nutrient analysis were also filtered in the field with a 0.45 μm pore-size filter membrane and stored in 30 mL acid washed polyethylene bottles. They were frozen a few hours after collection to prevent de-nitrification and were thawed just before analysis. Blank samples were taken about twice a week from April 1st to June 19th and received identical sampling and storage treatments.

4.8 Laboratory Samples Preparation and Analysis

4.8.1 Isotopic analysis

All samples for isotopic determination ($\delta^{18}O$ and $\delta^{2}H$) were analyzed at the University of Calgary's Isotope Science Lab by laser spectroscopy (LS). As opposed to conventional isotope ratio mass spectroscopy (IRMS) techniques, the LS technique does not involve converting or equilibrating the H_2O molecules with other gases (CO, H_2, H_2/CO_2). The molecule is vaporized and both water isotopes (^{18}O and ^{2}H) are simultaneously analyzed using a gas analyzer based on off-axis integrated cavity output spectroscopy technology. A thorough quality assessment of this method is provided by Lis *et al.* (2008) and their results show that the long-term instrumental accuracy is comparable or better to the standard IRMS techniques if routine data-normalization procedures are conducted.

The instrument used was a Los Gatos Research (LGR) model DLT-100. All values are expressed in per mil (‰) deviation from the Vienna Standard Mean Ocean Water (VSMOW) and are calculated as demonstrated in equation 4.1:

$$\delta^{18}O_{sample} = \frac{\frac{(^{18}O_{sample})}{(^{16}O_{sample})} - \frac{(^{18}O_{VSMOW})}{(^{16}O_{VSMOW})}}{\frac{(^{18}O_{VSMOW})}{(^{16}O_{VSMOW})}} \quad \textbf{(eq. 4.1)}$$

where ^{18}O and ^{16}O are respectively the heavy and common isotopes for oxygen. Most continental and atmospheric waters are depleted in ^{18}O relative to VSMOW and will show negative $\delta^{18}O$ values. The smaller the value, the more depleted it is in heavy isotopes—the "lighter" the water. The opposite terms "enriched" or "heavy" waters are widely used in the literature to qualify waters closer to VSMOW. The delta deuterium values ($\delta^{2}H$) were also calculated using Equation 4.1 by substituting ^{18}O and ^{16}O with ^{2}H and ^{1}H respectively.

A Local Meteoric Water Line (LMWL) was built as a tool for quality control assessment to evaluate if evaporative fractionation processes have significantly altered water sample composition during storage and transport.

Quality control (QC) procedures were performed and two error terms were computed. The QC analytical standard is an "internal" error term calculated by the laboratory and it represents the standard deviation from the mean for 35 runs of the W-31 QC standard. The second error term is the replicate analytical error and represent the average of the standard deviation values from 33 sample replicates hidden in the sample. All error terms are expressed in Table 4.1.

Table 4.1 Analytical Errors for Isotopic Determination

	QC analytical standard (‰; n=35)	Replicates analytical error (‰; n=33)
$\delta^{18}O$	-19.37 ± 0.1	0.06
$\delta^{2}H$	-149.37 ± 0.83	0.38

4.8.2 Metals analysis

Stream water samples were suspected to have a very low concentration in metals. In order to ensure detection, all samples and field blanks were concentrated on a 4:1 ratio using an evaporative technique. First, 100 mL of each water sample were measured with a graduated borosilicate cylinder and poured into polyethylene beakers. The beakers were then plunged 0.5 cm deep in a sand bath and reduced down to a volume of around 5-10 mL using a hot plate placed in a negatively pressurized fume hood at a temperature not exceeding 60°C. The water temperature was monitored with a mercury thermometer immersed in a polyethylene beaker filled with de-ionized water. The concentrates were diluted with a 3% HNO_3 solution and made up to 25 mL using borosilicate volumetric flasks. The samples were then poured into 30 mL polyethylene bottles, refrigerated and analyzed within a week. All laboratory dishes were acid washed prior to utilization. This sample-concentration technique has been tested by Thompson *et al.* (1982) with de-ionized H_2O samples and their results demonstrated that the technique successfully improves detection limits by the equivalent concentration ratio while not compromising full recovery of elements. In order to verify those conclusions, un-concentrated groundwater and soil water samples, which were expected to have metal concentrations above detection limits, were compared to their concentrated counterparts to see if significant errors were induced from this process. These plots can be found in appendix A.

The water was analyzed for elemental concentrations of Mg, Na, K, Ca, Fe, Al and Si using a Vista CCD simultaneous Inductively Coupled Plasma Atomic Emission Spectroscopy technique (ICP-AES) at the Department of Earth and Ocean Sciences, University of British Columbia. The details concerning ICP-AES analytical procedures can be found in appendix B.

Two error terms were also computed for this analysis. The QC analytical error represents the standard deviation from the mean for every metal analyzed in the quality-control standard (22 replicates). The second error term, which represents analytical error, is computed as the average of the 15 standard deviation values from 15 sample replicates. Both error terms are expressed as percentages relative to the mean. They are listed in Table 4.2, along with the detection limits established by the manufacturer and the detection limits corrected for the concentration procedure. The sample analytical error will be the one used for further analysis because it is assumed that it also encompasses errors associated with the concentration process.

4.8.3 Nutrient analysis

Nutrients were analysed by the use of a Lachat Instruments QuickChem FIA+ 8000 at the Faculty of Land and Food Systems, University of British Columbia. The samples were analysed for ammonia, nitrate/nitrite and orthophosphate. Chloride was also analysed through the same instrument as part of the analytical routine. The details regarding the colorimetric methods are summarized in appendix C.

Table 4.3 provides a summary of the methods used, the detection limits (Lachat Instruments) and the lowest calibration standard. Absolute values below the lowest standards were not interpreted. As with the ICP-AES analysis, two error terms were computed: the QC analytical errors and the replicate analytical errors.

Table 4.2 Detection Limits and Analytical Errors for ICP-AES Analysis

Elements	Number of spectral line(s) used	Detection Limits (ppm)	Quality Control Standard (ppm)	QC Analytical Errors [1] (%)	Adjusted Detection Limits [2] (ppm)	Replicate Analytical Errors [3] (%)
Al	2	0.05	1	3.5	0.013	5.7
Ca	2	0.1	10	3.6	0.025	4.6
Fe	2	0.05	1	4	0.013	5.1
K	1	0.5	9.5	4	0.125	12.6
Mg	2	0.01	10	3.9	0.003	4.4
Na	2	0.25	10	3.4	0.063	4.3
Si	3	0.15	10	3.3	0.038	4.5

1 – Based on standard deviations from the quality control standard (n=22)
2 – Adjusted for the concentration process (1:4)
3 – Based on standard deviations from sample replicates (n=15)

Table 4.3 Detection Limits and Analytical Errors for Lachat Methods

Analyte	QuickChem Method #	Detection Limits (ppm)	Lowest Calibration Standard (ppm)	Quality Control Standard (ppm)	QC Analytical Errors[1] (%)	Replicate Analytical Errors [2] (%)
NH_3^+	10-107-06-2-A	0.005	0.1	0.5	2.42	NA
NO_3^- / NO_2^-	12-107-04-1-B	0.025	0.05	1	1.09	5.37
PO_4^{3-}	10-115-01-1-A	0.01	0.02	0.5	0.24	NA
Cl^-	10-117-07-1-A	0.5	6	6	0.75	1.79

1 – Based on standard deviations from the quality control standard (n=27)
2 – Based on standard deviations from sample replicates (NO_3^- / NO_2^-: n=12; Cl^-: n=22). Not enough replicates were above detection limits to compute error terms for NH_3^+ and PO_4^{3-}

4.9 Mapping and Spatial Statistics for Vegetation Cover

The general topographic maps describing the study area were prepared using arcGIS® software, version 9.3, based on the 1 : 50 000 topographic base-layers (92G05) issued by Natural Resources Canada (NRCAN, 2007).

The catchment's hydrographic network was mapped using orthophotos and complemented with field surveys. During the process, no distinctions were made between perennial and ephemeral channels. Because of temporal variations due to antecedent moisture conditions, a significant error could have arisen from mapping the uppermost limits of first-order channels; therefore, they should be interpreted with caution. The catchment's divide delineation was based on the resulting hydrographic mapping and on a digital elevation model acquired from Geobase.ca (NRCAN, spatial resolution: 0.75 x 0.75 arc-seconds).

Orthophotos of the region were graciously provided by the Sunshine Coast Regional District – GIS division and were used to delineate forest blocks in the catchment. Field biometric measurements characterizing the five forest ensembles (Table 3.1) are based on non-neighbour individual trees from the dominant canopy cover, which were measured using a measurement tape and a Suunto® PM-5/360 PC clinometer. The canopy closure term is an approximation from field observations.

5 Analysis

5.1 Generalities about Hydrograph Separations

The four research objectives largely rely on the hydrograph separation results. These techniques have a long history in the realm of hydrology. The first hydrograph separations prior to the 1970s were done graphically by manually dividing the baseflow component from the event flow component. Although many techniques exist as to "how" to draw the line (e.g., linear vs non-linear), the dividing line generally starts at the onset of the rising limb of the hydrograph and ends somewhere close to the middle-end of the recession limb based on empirical methods (see Brodie and Hostetler for details, 2005). Dingman (2008) describes these methods as being "convenient fiction" since no data other than discharge are necessary to produce the results, which generally supports the Hortonian construct, widely accepted at the time, that storm water is mainly composed of event water.

5.1.1 Two-component isotopic hydrograph separation (2-IHS)

The rapid development of isotopic analytical instrumentations during the 1970s and its "democratization" during the 1990s allowed the improvement of the method by introducing a mass balance approach for water isotopic signatures instead of solute concentrations (equation 5.1). The isotopic composition of water mixes conservatively, meaning that the streamflow composition is a mixture of water from pre-defined end-members (Kendall and Caldwell, 1998). The present study attempts a two-component isotopic hydrograph separation (2-IHS), separating the input of "new" water (i.e., snowmelt) in the stream from the "old" water previously stored in the catchment,

$$Q_sC_s = Q_eC_e + Q_pC_p \qquad \textbf{(eq. 5.1)}$$

where *Q* stands for flux of water, *C* for isotopic concentration and the subscripts *s*, *e* and *p* for streamflow, event and prevent components respectively. The information needed to solve for both components is the specific discharge of the stream, the flux of event water (rainfall or snowmelt) and the isotopic concentration of both components and stream water at time *t*. Equation 5.1 can be re-arranged for the following:

$$f_{p(t)} = \frac{\delta^{18}O_{s(t)} - \delta^{18}O_e}{\delta^{18}O_{p(t)} - \delta^{18}O_e} \qquad \textbf{(eq. 5.2)}$$

which solves for the fraction of pre-event water present in the stream. The oxygen-18/oxygen-16 isotopic system was chosen as a passive tracer in equation 5.2. The deuterium/hydrogen isotopic system also fractionates conservatively and may be used as a tracer. Both isotopic system fractionate colinearly, meaning that they basically provide the same information concerning the origin of water not subject to intensive evaporation (e.g. geothermal waters, lake water in the summer). The data required to solve equation 5.2 seems minimal, but 2-IHS techniques involve a number of assumptions that can be fairly difficult to meet (from Buttle, 1998):

(1) There is a significant difference between the isotopic content of the event and pre-event components;

(2) The isotope signature of event water is constant in space and time, or any variations can be accounted for;

(3) The isotope signature of pre-event water is constant in space and time, or any variations can be accounted for;

(4) Contributions of water from the vadose zone to stormflow must be negligible, or the isotopic content of soil water must be similar to that of groundwater and other tracers should be used to separate those two components; and

(5) Contributions to streamflow from surface storages (i.e., lakes) are negligible.

To assess the validity of these conditions, IHS is sampling intensive and often carried out at a catchment scale. Even though the technique solves for the temporal sources of runoff, the IHS used alone only offers an insight – not an assessment – about the flow paths that the event water took to reach the stream channel – which is crucial information to most solute/contaminant studies.

5.1.2 Three-component isotopic hydrograph separation (3-IHS)

A more thorough approach is to include geographical variation in the separation. For instance, a three-component separation (3-IHS) partitions the streamflow using two tracers: usually an isotopic tracer (δD or $\delta^{18}O$) for the time-source component (event vs pre-event water) and a geochemical tracer, such as [Si] or [Cl], for the geographical component (shallow vs deep flow-paths). By combining temporal and geographical partitioning, 3-IHS gives a better appraisal of the dominant hydrological processes operating in a watershed during storm or snowmelt events. It has been used successfully in numerous studies (DeWalle *et al.*,1988; Wels *et al.*, 1991 and Hinton *et al.*, 1994) and the findings usually confirm that old water dominates the hydrograph. The flow-path taken by this old water (shallow vs deep) is variable under different antecedent conditions and rainfall events, just as we expect the runoff mechanisms to be variable under different scenarios. The mass balance equation that describe the model is similar to the 2-IHS, but more complex. The present study will attempt to separate old groundwater (till and bedrock), old soil water and new snowpack drainage water; therefore,

$$Q_tC_t = Q_{gw}C_{gw} + Q_{sl}C_{sl} + Q_{sn}C_{sn} \qquad \textbf{(eq. 5.3)}$$

where the subscripts *t*, *gw*, *sl* and *sn* refers to stream water, groundwater, soil water and snowpack drainage water respectively. Re-organising equation 5.3 makes it possible to solve for the fraction of snowpack drainage water (eq. 5.4) and subsequently for the fraction of soil water (eq. 5.5) and the fraction of groundwater (eq. 5.6) – from Hinton *et al.* (1994):

$$\frac{Q_{sn}}{Q_t} = \frac{\left[(C_t^{Si} - C_{sl}^{Si}) \cdot (C_{gw}^{i} - C_{sl}^{i}) - (C_t^{i} - C_{sl}^{i}) \cdot (C_{gw}^{Si} - C_{sl}^{Si})\right]}{\left[(C_{sn}^{Si} - C_{sl}^{Si}) \cdot (C_{gw}^{i} - C_{sl}^{i}) - (C_{sn}^{i} - C_{sl}^{i}) \cdot (C_{gw}^{Si} - C_{sl}^{Si})\right]} \qquad \textbf{(eq. 5.4)}$$

$$\frac{Q_{sl}}{Q_t} = \left(\frac{C_t^{t} - C_{gw}^{t}}{C_{sl}^{t} - C_{gw}^{t}}\right) - \frac{Q_{sn}}{Q_t} \cdot \left(\frac{C_{sn}^{t} - C_{gw}^{t}}{C_{sl}^{t} - C_{gw}^{t}}\right) \qquad \textbf{(eq. 5.5)}$$

$$\frac{Q_{gw}}{Q_t} = \left(\frac{C_t^{t} - C_{sl}^{t}}{C_{gw}^{t} - C_{sl}^{t}}\right) - \frac{Q_{sn}}{Q_t} \cdot \left(\frac{C_{sn}^{t} - C_{sl}^{t}}{C_{gw}^{t} - C_{sl}^{t}}\right) \qquad \textbf{(eq. 5.6)}$$

where *i* and *Si* represent the isotopic tracer (here $\delta^{18}O$) and the concentration in Silicon. Equations 5.5 and 5.6 can be applied with either tracer (*t*) – as long as the groundwater and the soil water concentrations are different for the selected tracer.

Just as its 2-IHS counterpart, a number of assumptions need to be respected for 3-IHS (from Hinton *et al.*, 1994):

(1) The concentration of each component must be distinct from the other two components for one or both of the tracers;

(2) The concentrations of the components cannot be colinear for the two tracers;

(3) The average concentration of each component must remain constant for the duration of the event;

(4) There are only three components (based on the concentration of the two tracers) contributing to stream discharge; and

(5) The tracers must mix conservatively.

One of the most violated assumptions in 2-IHS is that soil water (or vadose water) often has a significantly different isotopic signature than groundwater and contributes to streamflow in most watersheds (Buttle, 1994). This problem is usually addressed by using a 3-IHS model. However, this method is more sampling intensive than the 2-IHS since a third component must be characterized,.

5.1.3 Applying IHS to a snowmelt dominated environment

IHS during snowmelt events has been used for several decades, starting from the original work of Dinçer *et al.* (1970) in the Modry Dul watershed in northern Czechoslovakia. Very special considerations inherent to the relation between the snowpack and its meltwater have to be acknowledged before undertaking an IHS study in a snowmelt-dominated environment. The isotopic composition of the snowpack's depth profile is heterogeneous during the accumulation phase since it is reflective of the isotopic composition of individual snowfall events (Dinçer *et al.* 1970; Stichler *et al.* 1987; Unnikrishna *et al.* 2002). After the snowpack has become isothermal in the late winter;

snow metamorphism, snowmelt infiltration and rain events typically homogenize the isotopic composition of the snowpack's profile. Based on nival studies, the melt water is initially depleted in heavy isotopes due to fractionation processes occurring in the snowpack during the melting phase (Stichler, 1987; Taylor *et al.*, 2001; Unnikrishna *et al.* 2002). Later in the season, the melting of the mature snowpack – combined with rain events – give rise to an enriched snowmelt signal. Thus, a proper temporal characterization of the event water reservoir is essential in order to account for the dynamicity of the snowpack drainage isotopic signature

The use of IHS to characterize the spring freshet is certainly more challenging if the fundamental assumptions of the technique are to be respected. Several IHS catchment studies have used snow cores to define the event water signature and separate the hydrograph between "old" and "new" water (Dinçer *et al.*1970, Cooper, 1998). However, large temporal variations are inevitably missed when using this method. The preferred technique for characterizing event water is to use a snowmelt (pan) lysimeter (Hooper and Shoemaker, 1986; Moore, 1989; Laudon, 2002), from which the user can sample the snowpack drainage water (melt water and rainfall). This method does away with the need to sample rainfall separately and rely on equations (or assumptions) concerning snowpack fractionation.

5.1.4 Literature review on IHS methods during snowmelt

Even if the total volume of melt water is often greater than the total volume of stream water discharged during the spring freshet, IHS studies undertaken during snowmelt episodes in forested environments routinely report the preponderance of the pre-event water fraction in stream water – which is also the case for most IHSs performed during rainfall events. In fact, Buttle (1994) published an exhaustive review on IHS, which reports that the average pre-event fraction during snowmelt in streams from forested environments (μ = 0.58, σ = 0.18, n= 32) is significantly lower than the pre-event contribution observed during rainfall events (μ = 0.77, σ = 0.17, n= 32) at a level of α = 0.05. As Buttle points out, this could be due to soil frost impeding infiltration of snowmelt runoff and consequently creating Hortonian overland flow, or due to saturated overland flow since some studies (Bengtsson, 1985; McDonnell and Taylor, 1987) have found that near-stream saturated areas are often at their greatest during snowmelt. This interpretation seem to contradict a conclusion put forward by Krabbenhoft *et al.* (1990), which is, incidentally, also the main hypothesis of this study; that snowmelt events preferentially contribute to groundwater recharge.

The first critique regarding the application of this method for snowmelt events is that snowmelt water is too temporally variable to be used as event water if those errors are not quantified and accounted for in some way. First of all, the widespread utilization of snowmelt lysimeters to define C_e as opposed to snow core samples greatly reduces the temporal uncertainty related to snowmelt isotopic signature. These multiple samples obtained from the lysimeters are commonly weighted by volume of output and averaged over the whole melt period to characterise C_e as a single value for every time step (as proposed by Mast *et al.*, 1995). Even though this technique accounts for fractionation driven by melt, it is arguably as biased as the snow core approach since it accounts for event water at time t that has not yet melted (or rainfall that has not yet precipitated). Similarly, the use of the current melt water sampled at time t as C_e for the same time step is also physically incorrect because it does not allow the necessary travel time for the event water to reach the stream. Laudon (2002) developed a simple volume-weighted average model which transfers the current melt water isotopic flux into a well-mixed subsurface event water reservoir. This "reservoir" is a figure of speech since it does not represent a volume of water, but rather the signature of event water (e.i. the delayed signature of melt water). Its function is to buffers the "noise" of the isotopic signature of melt water and delay the general event water signal (as opposed to a volume of water) composing the streamflow. This empirical method indirectly corrects for the transit time between the melting of snow and its arrival to the stream. It was preferred for the present study and will be presented in more detail later in this chapter.

Another common criticism of IHS concerns the spatial variability of snowmelt. Moore (1989) failed to reject the null hypothesis stating that no significant differences exist between the outflow concentration from eight snow lysimeters at a 95% level of confidence (p = 0.057 for D and p = 0.595 for ^{18}O). Furthermore, evidence presented by Laudon (2007) also supports a spatially uniform snowpack from a study conducted in a 67km^2 basin in Sweden where the standard deviation for $\delta^{18}O$ was only 0.4‰ (n= 40 snowcores). Melt water collected from nine snow lysimeters under three different types of vegetation also showed very little spatial variability with a standard deviation of only 0.1‰ in the volume weighted average value between the three sites. However, it should be said that both studies were undertaken in catchments characterised by a small elevation gradient (30 m over 0.051 km^2 for Moore and 239 m over 67 km^2 for Laudon), which undoubtedly creates favourable conditions for the development of an isotopically homogeneous snowpack.

Another critique formulated by the detractors of the IHS during snowmelt concerns the spatial variability of pre-event water and is, in my opinion, still unresolved. Most studies use pre-event baseflow concentrations as an integrated signature of the pre-event reservoir likely to contribute to stormflow (Sklash, 1990). However, as pointed out by Buttle (1994) in his review of the subject, one study found different values for baseflow at different points along the river, while others found profound spatial variation in the isotopic signature of soil water at the hillslope scale and varying signatures between shallow and deep groundwater. These spatial heterogeneities, some of which could be attributed to spatial variation in groundwater residence time due to geologic complexities (Bonell *et al.*, 1998) and some of which could be attributed to infiltration of enriched water from a wetland or lake, reflect the complexities underlying hydrological processes. Simple spatially lumped mixing models, such as IHS, with all their constitutive assumptions must be recognize for what they are: black-box approaches; whose results must be interpreted accordingly. Keeping in mind these words of caution, pre-event baseflow is still seen as a reliable source to characterize C_p in recent studies (Joerin *et al.*, 2002; Laudon *et al.*, 2007).

5.2 Manipulation and Computation of Hydrometric and Climatic Data

This section describes how the raw data collected in the field (see chapter 4) or obtained from monitoring agencies were manipulated and/or transformed to fit the data requirements of the snow-water-equivalent model and the hydrograph separation model.

5.2.1 Water level and discharge for Stephen's Creek at the weir *(Q_{weir})*

The water level and discharge measurements at the weir were collected as per section 4.1. The water level (WL) time series was complete from the installation (Oct. 2008) to the removal (Nov. 2009) of the gauging station and no data were estimated. Freezing occurred on several occasions from mid-December to late February. Water level was not estimated and the data are deemed unreliable between these two dates. The difference in the raw values from the two WL sensors was within the expected sensor drift error during the ice-free period. For consistency, only the data from the main sensor was used. Two linear sensor reset corrections were applied to the data: a +16 mm correction from October 2008 to May 2009 and a +13 mm correction from May to November 2009.

A segmented non-linear stage-discharge relationship was computed at the weir (Figure 5.1) using recorded water-level data and discharge measurements following standard procedures used by the Water Survey of Canada and the USGS (Rantz, 1982). All discharge measurements plotted within 8% of the curve at low flows ($Stage_t < 14.3$cm) and 3% at higher flows. The 15 minutes "raw" discharge time series (volume · s^{-1}) was truncated and than aggregated to the hour/day and divided by the catchment area (71.2 ha) to produce hourly/daily specific discharge data (length · $time^{-1}$). Therefore, both time series are "forecasts," meaning that the discharge value at time *t* represents the stream flow condition between time *t* and *t+1*. The hydrograph for the full monitoring period and *R* codes are available in appendix D and E.

Figure 5.1 Stage Discharge relationship for Stephens Creek at the weir (670m el.)

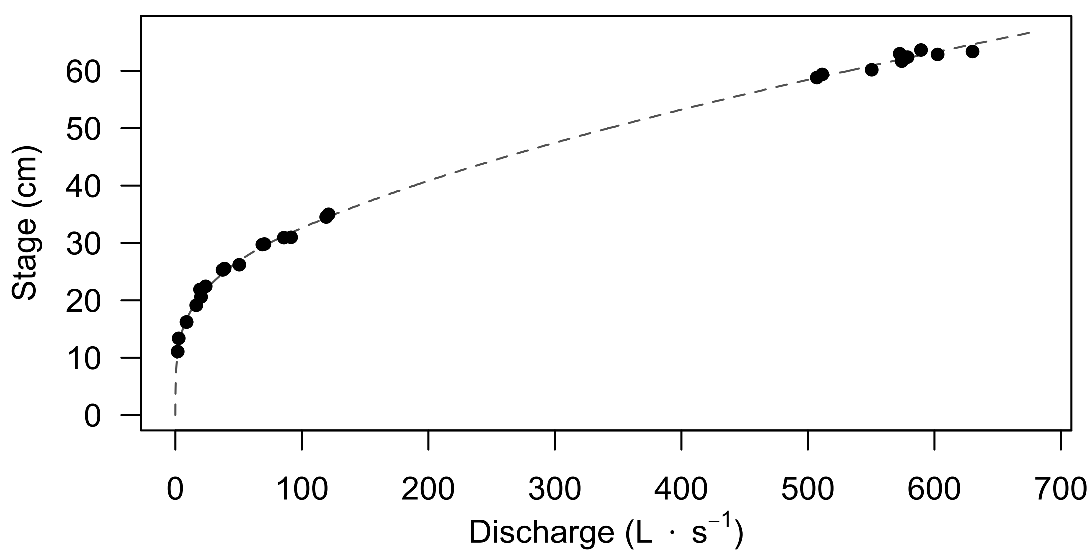

5.2.2 Discharge for Stephen's Creek at the mouth *(Q_{St})*

Water level monitoring and discharge measurements were not conducted at this site due to logistic constraints. Discharge was estimated using the specific discharge from the headwater monitoring site (weir) and the Water Survey of Canada (Environment Canada, 2010b) monitoring station (08GA046 – Roberts Creek at the mouth) in the adjacent watershed. Apart from sharing the same climatic regime, both watersheds are almost identical in terms of land use, forest cover, slope and aspect (Figure 5.2). The main difference between those two watersheds lies above 700 m of elevation, where the morphology of Stephen's Creek watershed is convex, allowing for greater snow accumulation (Figure 5.3).

Given the striking similarity between the daily hydrographs for Roberts Creek and Stephen's Creek at the weir daily, discharge for Stephen's Creek at the mouth was estimated using equation 5.7 and 5.8:

$$Q_{low(t)} = \frac{Q_{RC(t)} - \left(Q_{weir(t)} \cdot f_{subalpine(RC)}\right)}{f_{low(RC)}} \quad \textbf{(eq. 5.7)}$$

$$Q_{St(t)} = \left(Q_{low(t)} \cdot f_{low(St)}\right) + \left(Q_{weir(t)} \cdot f_{subalpine(St)}\right) \quad \textbf{(eq. 5.8)}$$

where Q_{RC} stands for specific discharge at Roberts Creek, f_{low} and $f_{subalpine}$ are the fractions of lower elevation and subalpine areas respectively, the subscripts *RC* and *St* identify Roberts Creek and Stephen's Creek watersheds, Q_{low} is for specific discharge for areas under 850 m of elevation, Q_{St} is for specific discharge at Stephen's Creek at the mouth and Q_{weir} is for specific discharge at Stephen's Creek at the weir. Based on GIS analysis, the "lower elevation" fraction (f_{low}) is 0.89 for Roberts Creek and 0.77 for Stephen's Creek.

The discharge at the mouth can be estimated by assuming the following:

1) The only physical parameter that could explain a significant difference in specific discharge between Roberts Creek and Stephen's Creek at the mouth is elevation.

2) The specific contribution to the streamflow for areas under 850 m (Q_{low}) is the same for both watersheds,
3) The specific discharge data at the weir (Q_{weir}) is representative of the subalpine contribution (areas above 850 m) for both watersheds.

The threshold value of 850 m of elevation was arbitrarily chosen to divide the subalpine areas based on snow surveys from the research catchment. The snowpack below 850 m disappears early in the snowmelt period. Moreover, the area lying within 670 – 850 m of elevation represents only 10% of the research catchment (Figure 3.2). Thus, it is fair to assume that Q_{weir} is representative of the area above 850 m (assumption 3).

5.2.3 Precipitation data

The rainfall time series from the research catchment is discontinuous. It extends from August 25th to December 14th, 2008, and again from April 15th to November 15th, 2009. The raw data was truncated to the hour and aggregated hourly and daily in order to produce a "forecast" dataset as explained in section 5.2.1. The daily precipitation data for the missing period were estimated using a nearby Environment Canada weather station (# 1043152 Gibsons Gower Point; Environment Canada, 2010a) located 9 km south of the catchment at 34 m (Figure 3.1), by developing a mean precipitation lapse rate (linear) during periods with complete records between the catchment and the weather station. The days with air temperature below 1.5°C at either site were discarded from the lapse rate calculation. Hourly precipitation data were estimated from April 1st to April 15th for the location of both tipping buckets (RGW – 670 m and RGE – 1080 m) in the catchment by redistributing the daily estimation previously performed proportionally to the hourly snowpack drainage output recorded at SLA. This method assumes a ripe snowpack and a relatively short response time to rainfall events, which is considered a fair assumption since the snow depth at SLA was 40 cm at most during that period.

Figure 5.2 Distribution of aspect for terrain above 850m el.

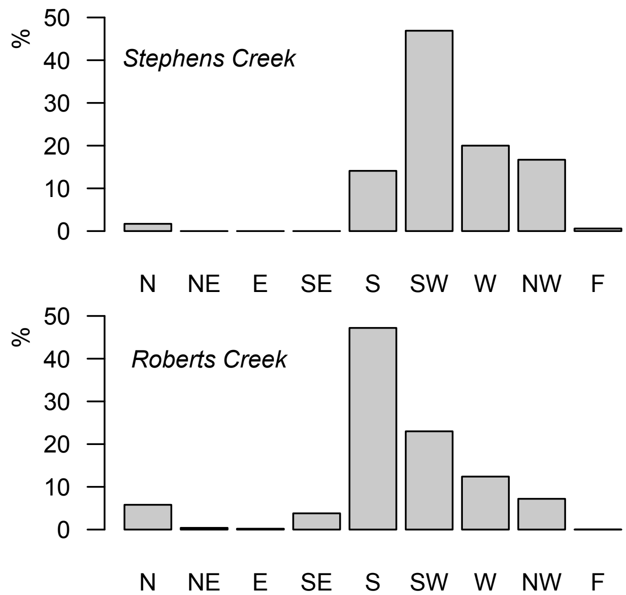

Figure 5.3 (a) Hypsometric curves of Stephen's Creek and Roberts Creek watershed; **(b)** Subalpine terrain only

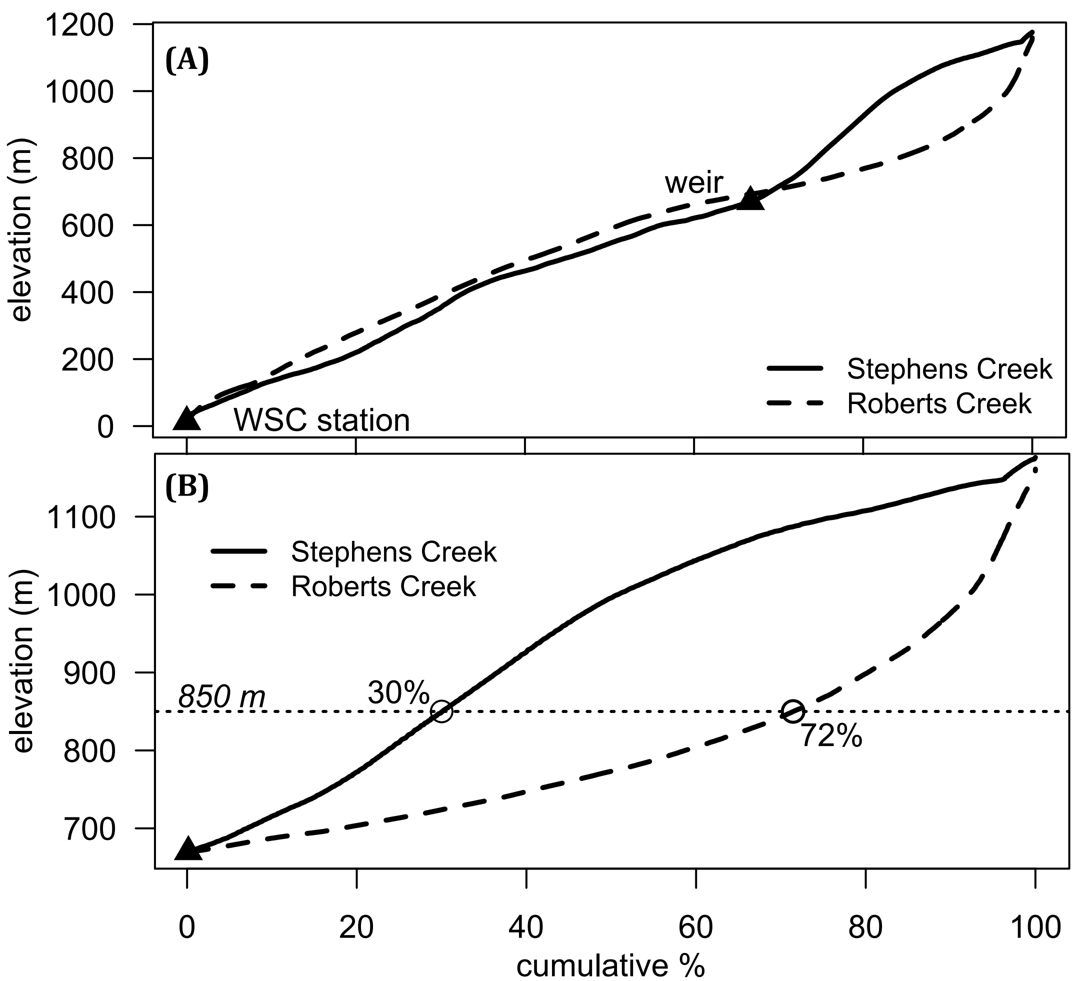

As a requirement for snowmelt modelling (section 5.3), an hourly dynamic precipitation lapse rate was developed between the two tipping buckets from April 15th to July 31st by damping the large variations due to orographic and advective processes using a seven day moving average (Jost, personal communication). The mean lapse rate was used to fill in the period from April 1st to April 22nd. A quality control simulation was performed and the simulated rainfall at RGW (670 m) was overestimated by only 5% using rainfall data at RGE (1080 m).

Throughfall from April 1st to July 31st was modelled for forested areas using the canopy interception algorithms built in the snow-water-equivalent YAM model (Jost, in prep.) which will be presented in section 5.3.

5.2.4 Temperature data

Air temperature (T_a) was recorded continuously at 975 m from August 25th 2008 to November 15th 2009. The raw data was truncated and averaged hourly.

An hourly dynamic lapse rate was calculated by averaging the lapse rate obtained from two Environment Canada weather stations (#1047172 Sechelt and #1046332 Port Mellon; Environment Canada, 2010a) located in opposite directions from the catchment but at similar distances (10.8km and 9.8km respectively; see Figure 3.1).

Water temperature (T_w) was collected continuously at the weir from October 1st 2008 to November 15th 2009. The raw data were truncated and averaged hourly.

5.2.5 Snowpack drainage data

Various data logger and/or tipping bucket issues were experienced with the snowmelt lysimeters during the winter. Therefore, the snowpack drainage data are deemed unreliable before April 1st. The drainage outflow from the four snow lysimeters was recorded continuously for SLA and SLB from April 1st until the complete disappearance of the snowpack. Two missing periods were reported for SLC, from April 11th to April 13th and from May 10th to May 12th, which coincide with large rain events. The tipping bucket was likely submerged by the water table on both occasions since it was discovered on May 10th that the pipe draining the instrument's enclosure was clogged with litter. A longer missing period was also experienced for SLD between April 1st and April 14th due to data logger failure. The missing periods were estimated by subtracting the throughfall precipitation corrected for elevation from the drainage output at SLB, SLC and SLD and by feeding those results into a linear regression model for neighbouring lysimeters during days at either end of the missing periods. The throughfall values were subsequently added to the simulated snowmelt output.

5.2.6 Antecedent condition indexes

Antecedent soil moisture condition is one of the main factors controlling hydrological connectivity of hillslopes and explaining the variability of rainfall/snowmelt runoff responses for a given watershed (Grayson *et al.*, 1997). While no quantitative soil moisture parameters were monitored for this study, the need for indexes as surrogates to represent antecedent soil moisture conditions was acknowledged. First, a lumped antecedent rainfall and melt index (ARMI) formulation was elaborated for the spring and summer of 2009 based on the antecedent rainfall index reported by Viessman *et al.* (1989) and used by McHale *et al.* (2002):

$$\mathrm{ARMI_i} = \mathrm{K}(\mathrm{ARMI_{i-1}}) + (\mathrm{R_i} + \mathrm{M_i}) \quad , \qquad \mathrm{ARMI_i} = \frac{\mathrm{ARMI_i}}{\mathrm{ARMI_{max}}} \qquad \textbf{(eq. 5.9)}$$

where $ARMI_i$ is a variable ranging from 0 to 1 for the period of interest, R_i represents daily throughfall at the i^{th} time based on a semi-distributed grid to be presented in section 5.3, M_i represents snowmelt as modelled by YAM (section 5.3) and where K is a depletion factor typically ranging from 0.85 to 0.98. K was set to 0.9 for this study as reported by McHale *et al.* (2002) for a similar subsurface environment. From inspection of equation 5.9, it is apparent that the antecedent soil moisture condition is presumed at its highest for the period of interest when $ARMI_i$ equals one.

Simple antecedent discharge indexes were also computed for Stephens Creek at the weir: a seven-day standard moving average was performed along with a daily peak-to-trough ratio for instantaneous discharges.

5.2.7 Weekly hydrologic budget

The water-balance approach as reported by Dingman (2008) was selected to estimate the weekly changes in sub-surface storage during the spring and summer of 2009. Because Stephen's Creek's headwater is a montane catchment well delimited by its steep topography, the groundwater inflow-outflow and surface storage contributions were considered insignificant.

$$\Delta S_i = R_i + M_i - (Q_i + ET_i) \qquad \textbf{(eq.5.10)}$$

where i is a weekly time-step and ET_i is evapotranspiration restricted to snowpack sublimation, soil water evaporation and canopy transpiration as simulated using the Shuttleworth-Wallace (1985) method built-in as subroutines in the lumped Brook90 hydrologic model version 4.4 (Federer, 2003) – similarly to the work done by McHale *et al.* (2002). Canopy interception was ignored since it is already accounted for by throughfall calculations (section 5.3.2). The information regarding rooting structure, necessary in Brook90, was obtained from the work done by Wang *et al.* (2002) at the UBC research forest and in the Capilano watershed since the climate, soil type, forest cover and tree essence distribution are assumed similar to the research area based on the site description provided by the authors and their geographic proximity (< 50 km). The Brook90 simulation was developed using streamflow, rainfall and air temperature data collected in the research catchment. The precipitation dataset from the catchment only covers a fraction of the streamflow monitoring records at the weir. The missing periods were filled using the daily precipitation data from Gibsons Gower Point weather station (#1043152; Environment Canada, 2010a), corrected for elevation using the averaged rainfall lapse rate as explained in section 5.2.3. The model was calibrated using the observed discharge at the weir and the parameters were adjusted by maximizing the efficiency function (R_{eff}) presented in equation 5.11:

$$R_{eff} = 1 - \frac{\left[\sum_{i=1}^{n} (Q_{obs} - Q_{sim})^2\right]}{\left[\sum_{i=1}^{n} (Q_{obs} - \overline{Q_{sim}})^2\right]} \qquad \textbf{(eq. 5.11)}$$

where Q_{obs} and Q_{sim} are the observed and simulated discharges at time step i, respectively.

5.3 Snow Water Equivalent Model (YAM)

This section describes the snow water equivalent routine of a semi-distributed temperature-index model that was used to simulate the daily variations in SWE values for the research catchment. A modelling platform (YAM) for snowmelt-dominated environments was developed by Dr. Georg Jost, a post-doctoral fellow at the department of geography, University of British Columbia. This modelling tool has the advantage of requiring a minimal amount of parameters and climatic variables (i.e., no measured radiative terms). The climatic variables necessary for the simulation are: hourly precipitation, hourly air temperature, precipitation lapse rate and air temperature lapse rate. The static variables needed for each modelling cell are: geographical coordinates, aspect, slope, fraction of crown closure, tree density, average diameter at breast height (DBH), average height of crown, average height of stem and initial SWE value on April 1st.

At the time of drafting of this thesis, this model has yet to be presented in a scientific publication since the runoff response routine is under development. The information given from section 5.3.2 to 5.3.4 is an adaptation of the manuscript provided to me by Dr. Jost and will eventually be made available in its original format in Jost *et al.* (in prep.).

5.3.1 Classification of the catchment area in sub-zones

The headwater catchment was subdivided into 22 cells, each one displaying uniform physical characteristics. The criteria for subdivision are the main factors influencing the distribution of snow accumulation and melt in coastal watersheds: elevation, forest structure, aspect and slope. The interpretation of a recent orthophoto paired with a DEM helped to delineate the cells (section 4.10). The canvas used to establish the boundaries are shown in Figure 5.4.

The biometric measurements describing the forest structure were collected in the field for the majority of cells as described in section 4.10. I assumed similar forest structure for the cells where the measurements were not made to a selection of neighbouring cells based on the orthophoto and general knowledge of the area. The table describing the forest structure for individual cells can be found in appendix F.

Figure 5.4 Development of the semi-distributed modeling space based on the main variables controlling snow accumulation/ablation dynamic

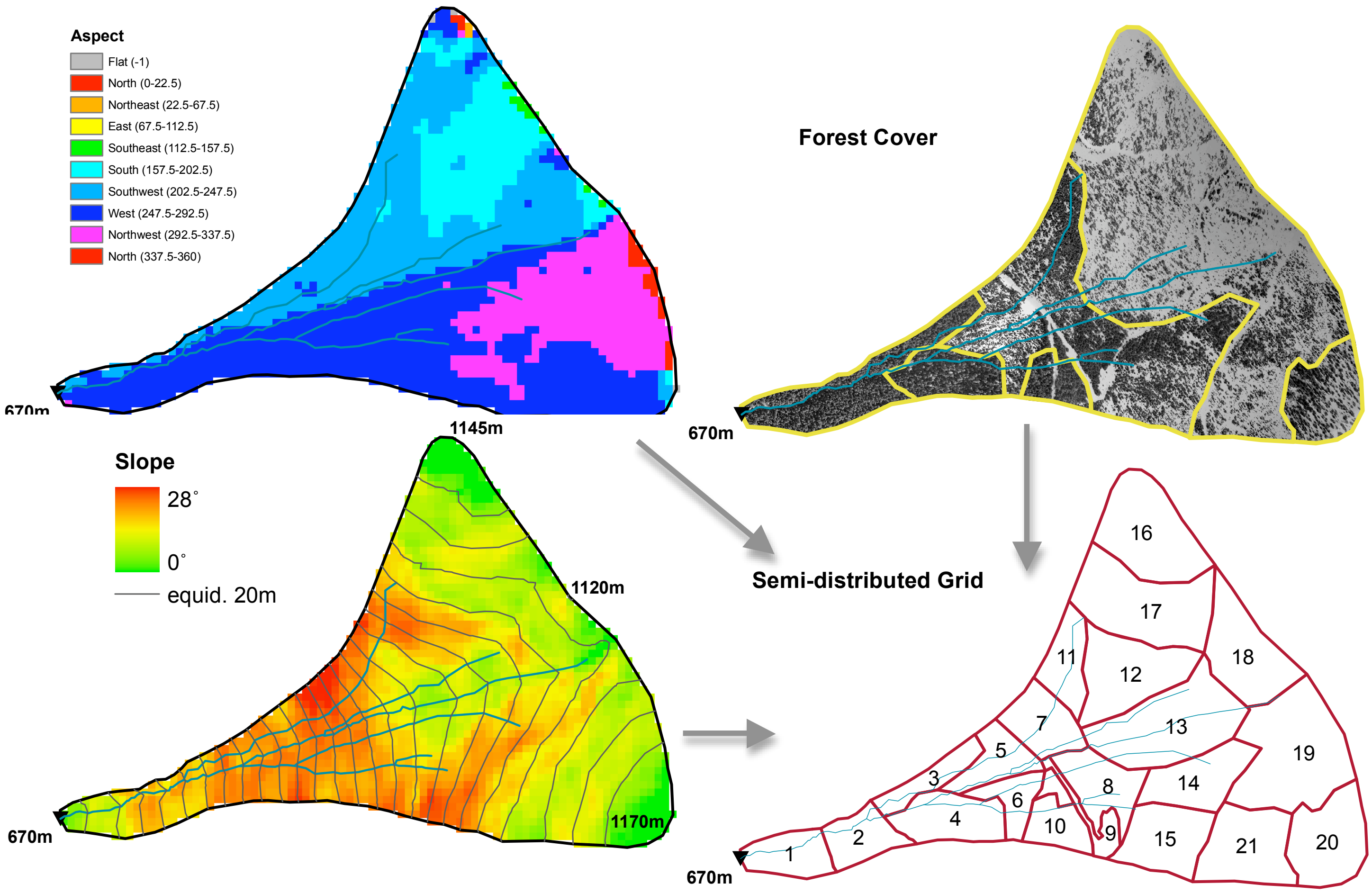

5.3.2 Canopy interception

The calculation of interception does not require extensive calculation of potential and actual evaporation (sublimation). The Rutter model (Rutter *et al.*, 1971) given in Dingman (2008) inspired the simple approach used by the YAM model to maximize the storage capacity of the canopy. The canopy water balance is given (Eq. 5.12):

$$\frac{dS_i}{dt} = I - E_i \qquad \textbf{(eq. 5.12)}$$

where S_i is the interception storage, I is the net interception rate (i.e., the amount of water or snow that can leave the canopy only via evaporation/sublimation), and E_i is the interception's evaporation/sublimation. Note that I excludes all structural unloading of snow from branches and meltwater drip. I is a function of a constant catch rate C_F and fraction of forest cover F:

$$I = C_F * F \quad \textbf{(eq. 5.13)}$$

In this study, C_F was set to 0.7. The maximum interception capacities for rain and snow I_{max} are linear functions of a maximum interception capacity M_F for a fully closed canopy (F = 1) and the fraction of forest cover F:

$$I_{\max} = M_F * F \quad \textbf{(eq. 5.14)}$$

M_F was set equal to 8.0 mm for snow and 4.0 mm for rain. With F between 0.7 – 0.8, this gives maximum snow interception capacities between 5.6 - 6.4 mm. I assumed E_i to be constant over time and different for rain or snow. Interception evaporation for rain was set to 1.0 mm/day and sublimation from intercepted snow was set to 0.5 mm/day. Given a forest canopy that reached I_{max} equal to 6.0 mm, with a sublimation rate of 0.5 mm it would take 12 days for the snow stored in the canopy to sublimate entirely.

5.3.3 Snowpack

The snowpack is represented as a two-layer environment by YAM – a surface and a deep layer. The deep layer builds up once the surface layer has reached 100 mm SWE. The model tracks SWE, cold content and snow liquid water storage for both layers. The liquid water holding capacity for both layers is assumed to be constant at 5% of SWE. New inputs (rain or snow water equivalent – depending on T_a) are added to the surface layer. Energy inputs from rain and snow are added to the snowpack as described in section 5.3.4. It is assumed that energy exchange with the atmosphere only occurs at the surface layer. The surface and deep layer only exchange liquid water, which is then refrozen in the deep layer (and thereby decreasing its cold content). Snowpack outflow starts when the deep layer has reached its liquid water holding capacity (or in cases with SWE < 100 mm when the surface layer has reached its liquid water holding capacity). Formulating a cold content helps to better predict the onset of snow melt, but the estimation of snow temperatures, which is necessary to approximate energy gradients between the snow and the atmosphere, is difficult for temperature index based models. Because YAM estimates snow temperature based on a single cold content value, the two-layer conceptualization provides a more realistic estimate of the snow temperature, since it is calculated from the cold content of two "snowpacks" instead of one. This formulation is essential for estimating a reasonable snow temperature value when the snowpack becomes isothermal, especially with a high SWE value and when the energy input is low (higher cold content) such as on a north-facing aspect. The tracking of cold content in the surface layer of a two-layer snowpack ensures that gradients between the atmosphere and the snowpack in the case of positive energy input are less variable in space and that cold contents at various aspects and elevations decrease at a similar rate.

5.3.4 Energy input to the snowpack

The hourly energy input to the snowpack is calculated on an algorithm that is based on the temperature index approach. This algorithm is only one of the many different temperature index based formulations that have been reported in literature.

The formulation that was selected includes a simple solar angle of incidence to calculate potential clearsky radiation. Hock (1999) extended the classical temperature index algorithm by incorporating potential direct solar radiation to account for aspect and slope effects on snowpack energy input, M:

$$M = \begin{cases} (m_f + c_f \times Rad) \times T_{air} & : \quad T_{air} > 0 \\ (m_f + c_f \times Rad) \times (T_{air} - T_{snow}) & : \quad T_{air} < 0 \wedge T_{air} > T_{snow} \\ (m_f - c_f \times Rad) \times (T_{air} - T_{snow}) & : \quad T_{air} < 0 \wedge T_{air} < T_{snow} \end{cases} \qquad \textbf{(eq. 5.15)}$$

where m_f is an empirical base melt factor, c_f is a radiation factor, and Q is the potential direct solar radiation. The potential direct solar radiation Q is calculated using standard methods given in Iqbal (1983). For details see Hock (1999). One reason for the lower energy input under forest cover compared to open areas is the lower incoming shortwave radiation under forest canopies. Hence, differences between forests and open areas should not only be modelled within the base melt factor but also with the potential direct solar radiation (Q in equation 5.16). Federer (1971) showed that the direct solar radiation at the forest floor, Q_f, can be predicted by a two-layer representation of the canopy – the crown space and the stem space:

$$Q_f = Q \times t_c \times t_s \qquad \textbf{(eq. 5.16)}$$

where t_c is the crown space transmissivity and t_s is the stem space transmissivity. The direct beam transmissivity of the crown space is given by

$$t_c = \exp(-\alpha \times l_c) \qquad \textbf{(eq. 5.17)}$$

where α is an empirically defined absorption coefficient for the crown space and l_c is the path length direct beam radiation through the crown space. Rowland and Moore (1992) adapted equations originally proposed by Federer (1971) to account for slope and aspect. For sloping forested surfaces, l_c, can be calculated as

$$l_c = h_c \times \cos\beta / \cos i \qquad \textbf{(eq. 5.18)}$$

where h_c is the height of the crown space, β is the slope inclination, and i is the angle of incidence between the normal to the slope and the solar beam. The direct beam transmissivity of the stemspace, l_c, for sloping surfaces can be calculated as (Federer, 1971):

$$t_s = \exp(-n \times A_s) \qquad \textbf{(eq. 5.19)}$$

where n is the stand density (stems m $^{-2}$) and A_s is the area of shadow cast by a single tree , which for a sloping surface is given by (Rowland and Moore, 1992):

$$A_s = D \times h_s \times \sin\theta / \cos i \qquad \textbf{(eq. 5.20)}$$

where D is the diameter of stems (m), h_s is the height of the stemspace, and θ is the solar zenith angle.

5.3.5 Computation of the daily snowpack drainage output

Since the precipitation data for the catchment were judged unreliable during the winter, the YAM simulation was made possible by giving an initial SWE value to each cell. Those values were linearly interpolated using elevation as a predictor based on the March 30th measurements at the snow transects. When the cell's SWE value had to be extrapolated, the results were adjusted in regards to discrete snow density and snow depth measurements taken during the snow core sampling campaign on April 1st.

The model was calibrated to daily time step using snow course measurements. An arbitrary cold content value was given to higher elevation cells based on the initial drainage output from the snow lysimeters (SLs). Unfortunately, the results have not yet been calibrated to the hour using the SL data, but efforts are made to model snowpack drainage output intensity for future publication.

The daily snowpack drainage output for each cell was computed by adding the precipitation throughfall values lapsed for elevation to the negative rate of change in SWE modelled by YAM. A daily area weighted average was calculated for the purpose of the hydrograph separation. See appendix G for computational codes.

5.4 Snowmelt Isotopic Determination Across Space

The second assumption of the IHS method states that the event water isotopic signal has to be constant in time and in space. This assumption is somewhat flexible if those variations can be well represented with a high level of confidence (Joerin *et al.,* 2002). Based upon many other IHS studies undertaken during snowmelt, the temporal isotopic signature is expected to vary as explained in section 5.1.3. This temporal variation was accounted for by using the runCE model (Laudon, 2002), which is presented in the next section (5.5). However, contrary to most published IHS work, a spatial relationship in the melt water signature based on elevation is expected in the present study. Fractionation processes linearly deplete the water vapour in ^{18}O and ^{2}H with increasing distance from the oceanic source: higher in altitude, higher in latitude (seasonal effect) and deeper into the continent. In IHS studies, pronounced seasonal variations are beneficial because they allow a big contrast between event and pre-event water. This is why most studies (rainfall or snowmelt) are conducted in the mid to upper hemispheres (Buttle, 1994). The altitude fractionation is not desirable because it adds a trend to the isotopic signature of event water as a function of the elevation range of the catchment, which violates the spatial uniformity assumption. The sampling design addresses the possibility of spatial variation in snowpack drainage output by deploying the SLs at four locations, covering most of the elevation range of the research catchment. Empirical statistical techniques were used to model the daily isotopic signature for each cell. These daily isotopic values were subsequently paired with the daily snowpack drainage output as modelled by YAM to provide an accurate melt-water input at the catchment scale for the hydrograph separation (runCE model, see section 5.5).

5.4.1 Daily linear regressions

The snowmelt isotopic signature was sampled during 49 days: daily at the beginning of the snowmelt and every two to three days towards the end; the time series was interpolated to daily increments. The $\delta^{18}O$ signature of individual cells was modelled with daily linear regression using mean elevation as a predictor and with varying degrees of freedom – depending whether three or all four SLs were used to compute the relationship. Elevation is used as a surrogate to explain the variability of fractionation processes in the snowpack, which are caused by energy input such as air temperature and diffused latent heat form the re-freezing of melt and/or rain water. The predicted values were discarded when the coefficient of determination (R^2) was less than 0.75. The data were interpolated for the cells located between SLC and SLD for the days when only those last two SLs were snow covered. By definition, no coefficients of determination were available for the days with only two samples. Even though the difference in $\delta^{18}O$ is minimal between SLC and SLD during the second half of the snowmelt, the interpolated results are kept if the samples are clearly showing a consistent relationship with elevation.

5.4.2 Averaging protocol

The SL values were averaged using different empirical methods when the linear relationship was rejected. For instance, when the isotopic signatures of the bottom three lysimeters (SLA, SLB and SLC) clustered around the same value, the cells located between SLA and SLC were given their averaged value and the upper cells were given the SLD value. Or, when no clustering or relationship with elevation was observed, the mean value from all SLs was given to every cell. The use of this “case by case” procedure is highly empirical, but is defendable given the complexity of the physical processes governing an open isotopic system. For instance, the discrepancies due to melt at lower elevation only or rain-on-snow events cannot be accurately modelled without an extensive sampling design. This method attempts to capture the dominant spatial signal explained by the fractionation of snowfall precipitation with elevation. Discrepancies in this signal during snowmelt are acknowledged and cannot necessarily be dismissed as white noise by simply averaging the SLs values all together when reasonable doubts exist about the presence of other variable(s), which may or may not be colinear with elevation, influencing the spatial distribution of melt water $\delta^{18}O$.

5.4.3 Isotopic mass balance assessment

The means of verifying the isotopic predictions for every cell are limited, but an attempt was made to determine if the snow core isotopic concentrations varied spatially in accordance with the regression model. The daily isotopic signature was converted to a flux by multiplying it by the daily ΔSWE modelled by YAM (equation 5.21):

$$\text{Mass Balance}_j = \frac{\left(\sum_{i=1}^{t} M_{j(i)} \cdot \delta^{18}O_{j(i)}\right) - \left(SWE_{j(1)} \cdot \delta^{18}O_{j(sc)}\right)}{\left(SWE_{j(1)} \cdot \delta^{18}O_{j(sc)}\right)} \cdot 100 \qquad \textbf{(eq. 5.21)}$$

where the mass balance for the j^{th} cell is given as a percentage, where M is the daily ΔSWE given by YAM, where $SWE_{j(1)}$ is the initial SWE value as modelled by YAM and where the subscript sc refers to snow core values. Rainfall precipitation was left out of the term M since it cannot be accounted for using the initial snowpack sampling. Snow core isotopic composition taken within the j^{th} cell on April 1st was attributed to the said cell, while neighboring snow core isotopic values were averaged for the few cells that were not sampled.

It is acknowledged that this mass balance equation assumes a closed system from April 1st to the disappearance of the snowpack; therefore, an isotopic imbalance is expected since this condition is not representative of the dynamics of the environment. This calculation was first applied to the measured values at the SLs to estimate the impact of the snowmelt fractionation process and added rainfall on the $\delta^{18}O$ snowpack mass balance. A negative closure error value can be interpreted as an isotopic enrichment of the snowpack drainage-water compared to its initial snowpack value, and inversely. This initial assessment at the SLs allows defining the natural "imbalance" of the open system by evaluating the uncertainty created by the spatial regression models. This calculation was subsequently applied to the results obtained from the regression models to assess if the closing errors were comparable to the ones obtained at the SLs.

5.5 Modelling the Event Water Lagged Response

The quantitative consideration of the time lag for the event water to reach the channel has always been a challenge to address with IHS methods. Joerin *et al.* (2002) have used an "influence function" inspired from the unit-hydrograph concept to account for the transit time of event water in the basin during a rainfall event in Switzerland. Laudon *et al.* (2002) developed a volumetric-corrected approach during snowmelt events that computes the event water signature by correcting for the weighted isotopic signature of the cumulative amount of snowmelt (depth) that has left the snowpack at time *t* but has not yet been discharged to the stream. These methods are known as triangular weighting functions (Weiler *et al.*, 2003); they are similar to transfer functions, except that they transfer the isotopic signature of the snow rather than its volume. Their simplicity embeds assumptions such as uniform flow velocities, a well-mixed event water reservoir and similar drainage structures.

A more comprehensive approach would be to use transfer functions representing a combination of hydraulic and tracer responses to rainfall/snowmelt events like the TRANSEP model developed by Weiler *et al.* (2003). The hydraulic response function of this model is based on the instantaneous unit-hydrograph approach (Dooge, 1959), a simple lumped rainfall-runoff model still frequently used by water resources/flood engineers. TRANSEP offers clear benefits compared to the traditional 2-IHS by coupling the invaluable "molecular" information gained from the hydrograph separation into a hydraulically coherent response scheme. The model derives transfer functions for runoff, event and pre-event water, capitalizing on the temporal variation of the event water signal and enabling the interpretation of runoff generation processes (Weiler, 2003).

Despite all the promising advantages offered by TRANSEP, the model runCE developed by Hjalmar Laudon (2002) was chosen for the purpose of this work because of its simplicity and because it was initially developed for snowmelt events. TRANSEP has not yet been used during snowmelt, probably because the event water contribution is derived from an algorithm calculating effective rainfall based on an antecedent rainfall index that may not be applicable for snowmelt events.

5.5.1 The runoff corrected event water approach (*runCE*)

The runCE model delays the isotopic signal of the accumulated melt water transiting in the catchment through a weighting equation, which is presented by Laudon (2002) as:

$$\delta^{18}O_{e(t)} = \frac{\left(\sum_{i=1}^{t} M_{(i)}\, \delta^{18}O_{m(i)} - \sum_{i=1}^{t} E_{(i)}\, \delta^{18}O_{e(i)} \right)}{\left(\sum_{i=1}^{t} M_{(i)} - \sum_{i=1}^{t} E_{(i)} \right)} \qquad \textbf{(eq. 5.22)}$$

where $M_{(i)}$ is the incrementally collected melt and rain water depth (see section 5.3.5), $E_{(i)}$ is the incrementally calculated event water discharged to the stream and where the subscripts e and m stands for event and melt water respectively. The value for $E_{(i)}$ is determined from the fraction of event water in the stream (equation 5.2). Since both $E_{(i)}$

and $\delta^{18}O_{e(i)}$ depend on the calculated runCE $\delta^{18}O_{e(t)}$, equation (5.22) must be solved iteratively for each time step (day). This simulation is initiated by setting $\delta^{18}O_{e(i)}$ equal to $\delta^{18}O_{e(t-1)}$. The optimization can be achieved by minimizing the difference in the sum of squared errors between $\delta^{18}O_{e(t)}$ and $\delta^{18}O_{e(i)}$ at every time step. For this application, the stopping criterion was reached when the root means square (RMS) got below $1e^{-8}$. Jakob Schelker (2008) graciously provided the computational codes and an example of their application in the *R* modelling environment is attached in appendix H.

5.5.2 Uncertainty calculation

Because of the heterogeneities of the system, uncertainties in the separation are inevitable. Earlier studies did not compute uncertainty, which led to a false impression of "absoluteness" of the results. Further research has questioned the validity of IHS because the assumptions had to be systematically violated (or ignored) in order to come up with a quantitative value. The method evolved and hydrologists started to routinely associate errors terms with the signature of their components. Computing the uncertainty still enables the researcher to come up with a quantitative answer, but it formally acknowledges this "gray" area peculiar to this method and empowers hydrologists to embrace with an appropriate level of confidence the interpretative strength of tracer-based information (McDonnell *et al.*, 2007).

For this study, the commonly used first order propagation of uncertainty adapted by Genereux (1998) for 2-IHS models was used to compute the uncertainty of the separation:

$$W_p(t) = \left\{ \left[\frac{(\delta^{18}O_{e(t)} - \delta^{18}O_{s(t)})}{(\delta^{18}O_{p(t)} - \delta^{18}O_{e(t)})^2} \cdot W_{\delta^{18}O_p} \right]^2 + \left[\frac{(\delta^{18}O_{s(t)} - \delta^{18}O_{p(t)})}{(\delta^{18}O_{p(t)} - \delta^{18}O_{e(t)})^2} \cdot W_{\delta^{18}O_e} \right]^2 + \left[\frac{1}{(\delta^{18}O_{p(t)} - \delta^{18}O_{e(t)})} \cdot W_{\delta^{18}O_s} \right]^2 \right\}^{1/2} \quad \textbf{(eq. 5.23)}$$

where $W_p(t)$ is the total uncertainty calculated for the separation, $W_{\delta 18O}$ is the uncertainty specific to each component and where the subscripts *e*, *p* and *s* refers to event, pre-event and stream waters. As Genereux (1998) himself points out, it is obvious from the equation that a large difference in concentration between the components is beneficial to the separation. Also, $W_p(t)$ is larger when the most uncertain component makes up more than half of the stream discharge.

This method is somewhat flexible because it gives the user the choice of uncertainty to propagate. For this study, I chose to propagate the analytical uncertainty (0.1‰, Table 4.1) for stream water and pre-event water. The error propagated from the event water signature is the largest because of the spatial variation observed in the catchment. Because the temporal variation in the snowpack drainage signature is intrinsically accounted by *runCE*, I only propagated the unexplained variance for elevation gain as expressed by the residual standard errors for the daily regressions (section 5.4).

5.5.3 The *runCE* – three-component approach

A three-component hydrograph separation (3-IHS) method was performed as proposed by Hinton *et al.* (1994) to partition streamflow based on geographical sources of runoff: old groundwater, old soil water and new snowpack drainage water (see section 5.1.2). Soil water was characterized with biweekly samples from three different saturated throughflow resurgence points in the research area (GWB, GWL, GWC – Figure 3.1) from the end of April until the end of May 2009. Like many studies aiming at differentiating soil water from groundwater, silicon was used as a secondary tracer since it is not present in precipitation (Hinton *et al.*, 1994; Laudon and Slaymaker, 1997 and Hoeg *et al.* (2000). The snowpack drainage output signature modelled by the runCE simulation was reused in the three-component separation model. Computational codes for the 3-IHS are found in appendix I.

5.6 Streamflow Recession Modelling

Interesting information can be extracted from the recession limbs of the hydrograph, such as insights on the storage capacity of the catchment and drainage characteristics of empirically defined geographical or temporal flow-components (e.g., upslope vs riparian storage or storm seepage vs baseflow – Barnes, 1939; Hall, 1968; Anderson and Burt, 1980; Griffiths and Clausen, 1997; Moore, 1997). Recession analysis was also proven useful to forecast and estimate storage requirements to augment low flows (Bako and Owoade, 1988; Kachroo, 1992). Recession constants of multiple rivers can also be compared to weight the influence of a given variable on streamflow yield, such as: bedrock and sedimentary substrate, soil types, climatic factors, land use and vegetation (Knisel, 1963; Tallaksen, 1995).

Recession analysis aims at solving the storage-outflow relationship of a watershed. Usually, the goal is to override temporal variations initiated by antecedent moisture conditions by developing a “master” recession curve. This is achieved by applying a recession model representative of the runoff mechanisms of the watershed to multiple recession segments and by optimizing the model’s coefficients through a calibration of the predicted discharges to the observed values. This approach allows inter-basin comparisons regardless of climatic variables and constitutes the basic approach for low flow forecasting – although evapotranspiration must be accounted for *a posteriori* for the later example. If the purpose of the study is to address seasonal variations in streamflow recession for a given river or to compare recession limbs between small watersheds under the same meteorological regime, it is relevant for the recession characteristics of the hydrograph to be analyzed and interpreted segment by segment (Tallaksen, 1989).

Many methods and mathematical expressions describing recession characteristics of rivers have been developed during the last century, starting with the pioneer work of Boussinesq in 1877 (see review by Tallaksen, 1995). Early studies utilized this linear expression to define streamflow recession as a function of singular storage depletion:

$$Q_t = Q_0 k^t \qquad \textbf{(eq. 5.24)}$$

where Q_t is the flow at time t, Q_0 is the flow at $t = 0$ and where k^t is the recession constant at time t and take on values between [0:1]; commonly $k > 0.7$ for what is interpreted as the baseflow recession limb. A simple alternative to equation 5.24 is found in equation 5.25, which is still the most widely used expression in recession analysis today (from Tallaksen, 1995) despite the fact that recession limbs behave non-linearly most of the time.

$$Q_t = Q_0 e^{-\phi t} \qquad \textbf{(eq. 5.25)}$$

where ϕ is a recession constant and t is the time step since the beginning of the recession.
Moore (1997) derived master recession curves from three commonly used models (linear – eq. 5.25, power-law – eq. 5.26 and exponential reservoirs) and a dual linear reservoirs model (eq. 5.27 presents the serial reservoirs variation) and compared the predicted results to the observed discharges from a small forested catchment in southwestern British Columbia.

$$Q_t = Q_0(1+\mu t)^p \ , \quad p = \frac{\beta}{1-\beta} \ , \quad \mu = \alpha^{\frac{1}{\beta}} \cdot (\beta - 1) \cdot Q_0^{\frac{\beta-1}{\beta}} \qquad \textbf{(eq. 5.26)}$$

$$Q_t = Q_0 e^{-\phi_2 t} + \frac{\phi_2 Q_1}{\phi_2 - \phi_1} \cdot \left(e^{-\phi_1 t} - e^{-\phi_2 t}\right) \qquad \textbf{(eq. 5.27)}$$

where ϕ_1 and ϕ_2 are the master recession parameters for the upslope and footslope zones as described by Moore (1997), α and β are master storage outflow parameters, and where Q_0 and Q_2 are parameters representing outflow for an initial volume of water in the reservoir(s) and must be determined for each recession segment. All the parameters are solved by nonlinear iterative algorithm calibration.
Moore (1997) reported that the dual reservoirs model was substantially more accurate than the three single reservoir models and was judged consistent with the runoff-generating mechanisms of catchments with shallow soil over an impervious substrate. The heterogeneities in the initial distribution of water amongst reservoirs, defined as the upslope and footslope zones of the catchment, were interpreted as being the main physical reason explaining the non-linearity observed in the recession limbs.
For comparability, the master recession parameters ϕ_1 and ϕ_2 for dual-linear reservoirs can be transformed with the following equation (5.28) in order to obtain constants within the range usually reported in the literature (0.5-1.0):

$$k_{(1,2)} = \exp\left(-\phi_{(1,2)}\right) \qquad \textbf{(eq. 5.28)}$$

The present study used the linear, power-law and dual-linear reservoirs models as proposed by Moore (1997) to compute master recession curves and compare the summer baseflow recession characteristics of the Stephen's Creek headwater catchment and Roberts Creek watersheds. Segmented linear recession curves are computed – along with "baseflow-only" segmented linear recession curves determined by graphical interpretation. Given the proximity of the two gauging stations, the watersheds are assumed to share the same geological, pedological and vegetative characteristics. Evidence supporting this claim comes from reconnaissance field visits to the Chapman Creek and Gray Creek watersheds (Figure 3.1) during the summer of 2008, where throughflow and imogolite complexes spilling over impervious glacial till were observed at various locations (from ~50 m to 900 m) on the sides of forest access roads and creeks at about 1 m below the soil's surface – similar to what was observed in the research catchment. Climatic variables are also assumed to be similar, although the difference in elevation affects air temperature and to some extent evapotranspiration. The main identifiable difference between both watersheds is that the Stephen's Creek runoff regime is dominated by a much larger snowmelt component during the spring as opposed to Roberts Creek, which is mainly rainfall dominated over the winter. Therefore, it is proposed that significant and recurring differences in their recession constants is attributed to their contrasting runoff regimes.

The calibration of the master curve recession models was done iteratively by minimizing a loss function using Powell's method as described by Press *et al.* (1986) and adapted by Moore (1997):

$$\varepsilon_r = \sqrt{\frac{1}{n_r}\sum_{j=1}^{n_r}\left[\frac{1}{n_j}\sum_{i=1}^{n_j} r_{ji}^2\right]} \qquad \textbf{(eq. 5.29)}$$

where r_{ji} is the difference between predicted and observed discharge for the i^{th} time in the j^{th} recession segment, as a fraction of the observed discharge; n_j is the number of observation in the j^{th} recession segment and n_r is the number of recession segments used to compute the master recession curve. Moore (1997) presented an alternative loss function based on the absolute difference between predicted and observed discharges.

The later was shown to be more effective in simulating stormflow outflow, whereas the loss function selected for this study is more accurate for low flows.

The segmented linear recession curve parameters in the present study were optimized using the nonlinear least-square algorithm (Newton's method). For details see Gallant (1975).

The same number of recession segments was defined for both watersheds. Either snowmelt or rainfall periods preceded the recession limbs. In all cases, the recession modelling was initiated from the day after the peakflow occurred until the day preceding the start of the subsequent rainfall event. Computation codes for recession analysis can be found in appendix J.

6 Results

6.1 Hydrometric Data

6.1.1 Precipitation and snowmelt

A total of 1375 ± 151 mm of precipitation fell from October 18th, 2008 to October 17th, 2009 at 975 m, based on the 30-day moving-average static precipitation lapse rate over the winter and the 7-day moving-average dynamic lapse rate during the rainfall monitoring period (see Table 6.1 for lapse rate figures—the reported error is the one from the static lapse rate). Most precipitation occurred between December 1st, 2008 and March 31st, 2009, creating a snowpack on April 1st ranging from 212 ± 54 mm SWE at the lowest measurement transect to 1052 ± 78 mm at the highest, northwest- facing transect.

Table 6.1 Summary of precipitation lapse rate[1] based on hourly rainfall data at RGW and RGE[2] for the rainfall monitoring period (May 2nd to October 17th 2009)

M.A.[3] method	Summary (static lapse rate)				Observed rainfall (mm)		Prediction at RGW		% error *(Selected L.R.)*	
	μ	**σ**	**max**	**min**	**RGE**	**RGW**	**Dyn.[4]**	**Static[4]**	**Dyn.**	**Static**
24 hrs	-3.66E-05	1.17E-03	1.83E-03	-1.07E-02	540.7	465.9	492.9	548.9	5.8	17.8
7 days	1.46E-04	8.58E-04	1.22E-03	-1.07E-02	490.6	411.3	430.1	461.2	***(4.6)***	12.1
14 days	1.68E-04	5.70E-04	6.80E-04	-5.25E-03	469.9	386.6	415.6	437.6	7.5	13.2
30 days	2.12E-04	1.81E-04	4.91E-04	-6.70E-04	435.6	357.9	391.6	397.7	9.4	***(11.1)***

1- Lapse rate expressed as: " ((RGE – RGW) / Δelevation) / RGE "
2- RGW and RGE elevations: 670m and 1080m ASL respectively
3- Moving-average
4- Dynamic and static lapse rates

Snowpack drainage output observations show the onset of snowmelt occurring around April 5th for the lower snow lysimeters (SLA and SLB) and around April 7th for the higher SLs, which coincides with warmer air temperature (Figure 6.1). A rain-on-snow event on April 12th affects snowpack drainage output at all elevations, but re-freezing is obvious at SLD since the observed output is about half of the output at SLA, which indicates that some cold-content is still present in the snowpack at higher elevation in early April. The snowpack drainage response time to rain events during the early season is delayed by an hour at most at SLD despite the deep snowpack (237 ± 27 cm on April 19th at snow transect D), while no delays are observed at SLA. Snowmelt ceased later at SLC despite being at lower elevation than SLD, probably due to the difference in aspect between the two sites and a very dense forest cover at SLC blocking most of the short-wave radiations. The snowpack drainage-output from SLD shows more sensitivity to daily fluctuations compared to the other lysimeters due to its southwest facing aspect (longer exposure to short-wave radiation) and due to the absence of forest cover acting as a "greenhouse" by trapping long-wave radiation under the forest canopy overnight. In Stephen's Creek headwater catchment, 63% of the catchment area is characterized by a canopy closure inferior to 50%, so a similar snowmelt pattern as the one observed at SLD may be expected for most of the catchment area.

Figure 6.1 Daily precipitation (as throughfall), air temperature (average, max.-min. in gray) and hourly snowpack drainage output at four snow lysimeters

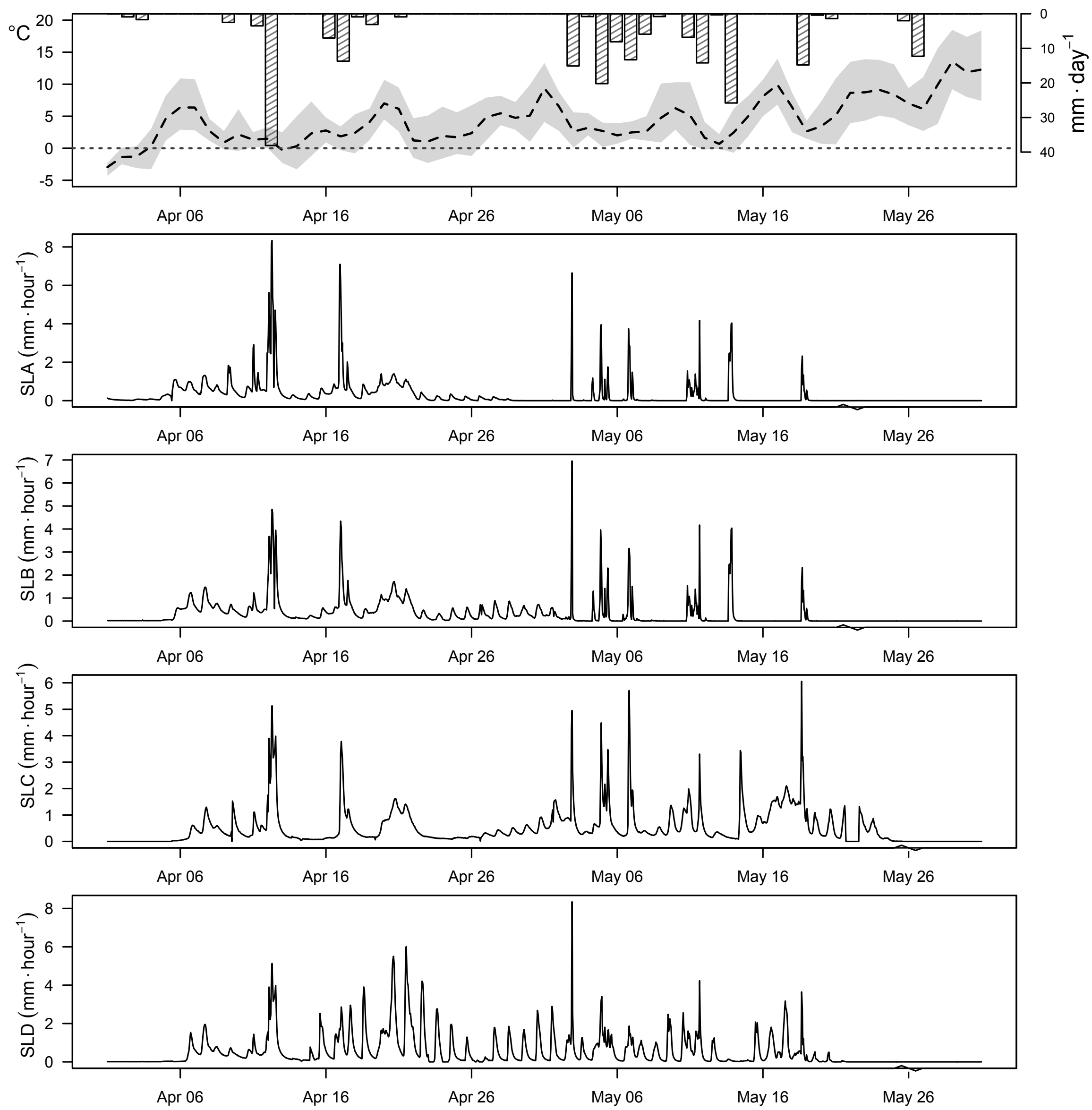

6.1.2 Snow-water-equivalent modelling (YAM)

The YAM model was calibrated using the weekly snow-water-equivalent measurements and the results presented in Figure 6.2 demonstrate a good overall performance of the simulation across the semi-distributed modelling grid. The daily-predicted values are well within the 70% limits of confidence expressed by the standard deviations of the SWE measurements for transects A to D. The recurring discrepancies between the predicted and observed SWE values for cell 14 (transect E – Figure 6.2, lower graph) can be partly due to the fact that YAM simulates SWE for the cell's center point, while the snow transect E is located about 20 m higher in elevation – falsely suggesting a systematic underestimation. The contrasting standard deviation's range between transects D and E is probably due to the more sampling-intensive design (snow wires) used for E.

Figure 6.2 Simulated and observed snowpack (SWE) and simulated daily SWE budget

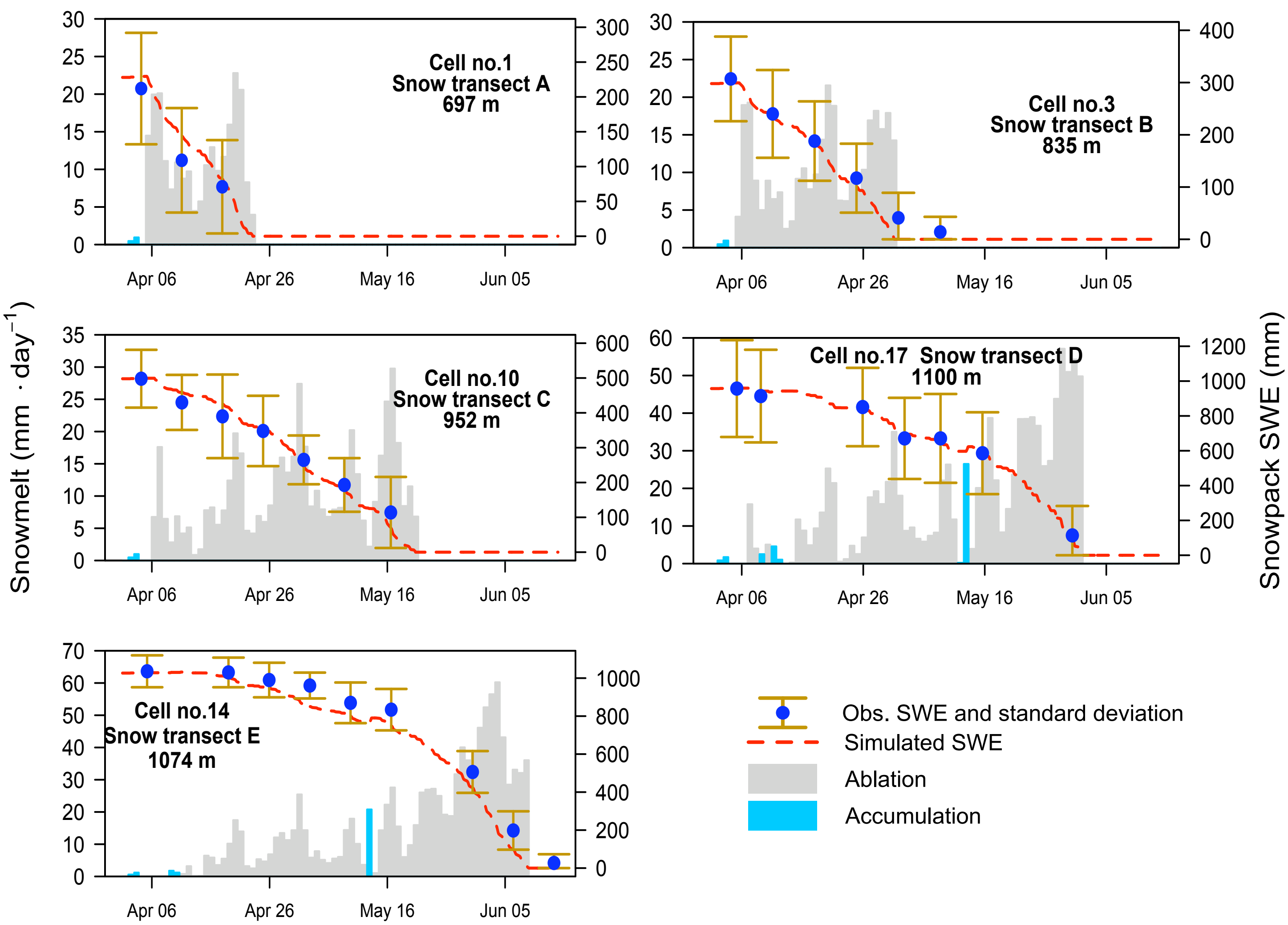

A quick ocular inspection of the daily snowpack budget from lower to higher elevation reveals just how decisive of a factor elevation is on snowmelt processes in this climate. Peaks in snowmelt intensity are observed at the end of April for the lower cells while they occur about 4 to 6 weeks later 300 m higher in elevation. Elevation has a double weight on SWE dynamics because it also favors an increase in snowfall precipitation during colder periods.

The snowpack drainage-output data as well as the SWE data confirm the influence of aspect on snowmelt. The early to mid-season snowmelt peaks in cell 17 (from April 1st to mid-May) are not nearly replicated with the same intensity in cell 14, despite being at a slightly lower elevation. Cell 17 is mainly south facing as opposed to cell 14, which is northwest facing.

6.1.3 Discharges and piezometer water-levels

The hydrological regime of Stephen's Creek headwater catchment is more snowmelt dominated compared to Roberts Creek. A total of 1,399 mm of runoff occurred from Oct. 1st, 2008, to Sept. 30th, 2009; more than half (51%) was discharged during the freshet (April 1st to June 30th) and 31% during the rainy season (October 1st to December 31st). In Roberts Creek, 924 mm of runoff occurred during the same period but only 36% was discharged during the spring and 31% discharged during the autumn (Figure 6.3).

Figure 6.3 Monthly discharge distributions at Stephen's Creek at the weir and Roberts Creek at the mouth from October 1st 2008 to October 31st 2009

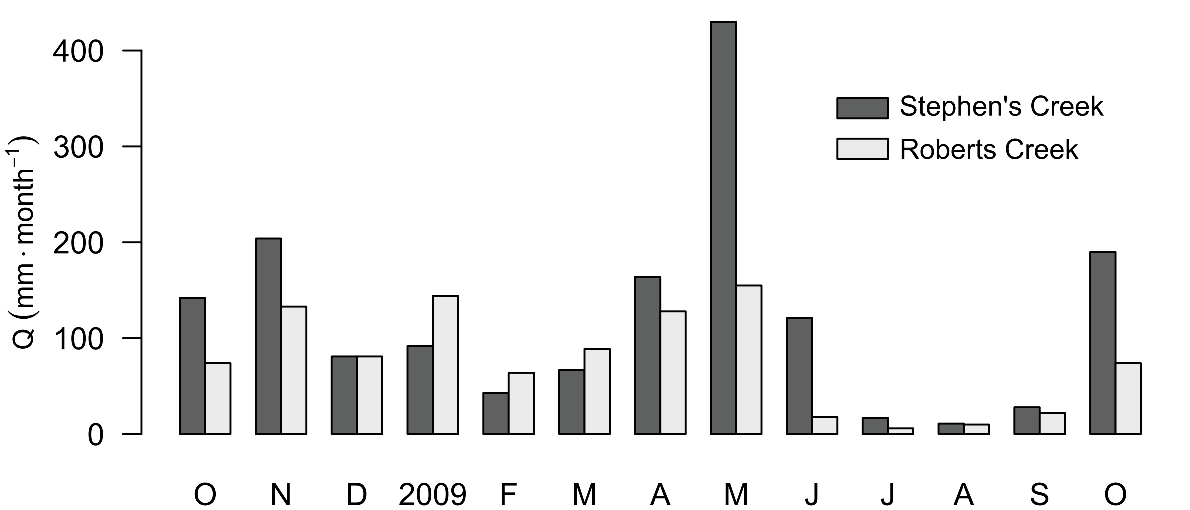

As is expected from a headwater catchment, the specific discharge is higher during the "wet" periods of the year since the subsurface storage capacity is less than at the watershed scale. This relationship does not hold during the winter because of increased snow accumulation at higher elevation in Stephen's Creek. Headwater catchments are expected to be more impacted by low flows during the summer because of their smaller storage capacity; however, this was not observed in the research area. The specific discharges during summer low flows were higher for Stephen's Creek at the weir than for Roberts Creek at the mouth – even after considering a 10% error due to watershed delineation and rating curves (not shown in Figures 6.4). Baseflow periods following rainfall events in September were also higher at the weir but within the 10% margins of error. The annual hydrographs for both rivers are presented in Figure 6.4 along with the simulated discharges for Stephen's Creek at the mouth as computed with equations 5.7 and 5.8.

Figure 6.4 Annual hydrographs for Stephen's Creek at the weir (Q_{weir}) , Roberts Creek at the mouth (Q_{RC}) and simulated discharges for Stephen's Creek at the mouth (Q_{St})

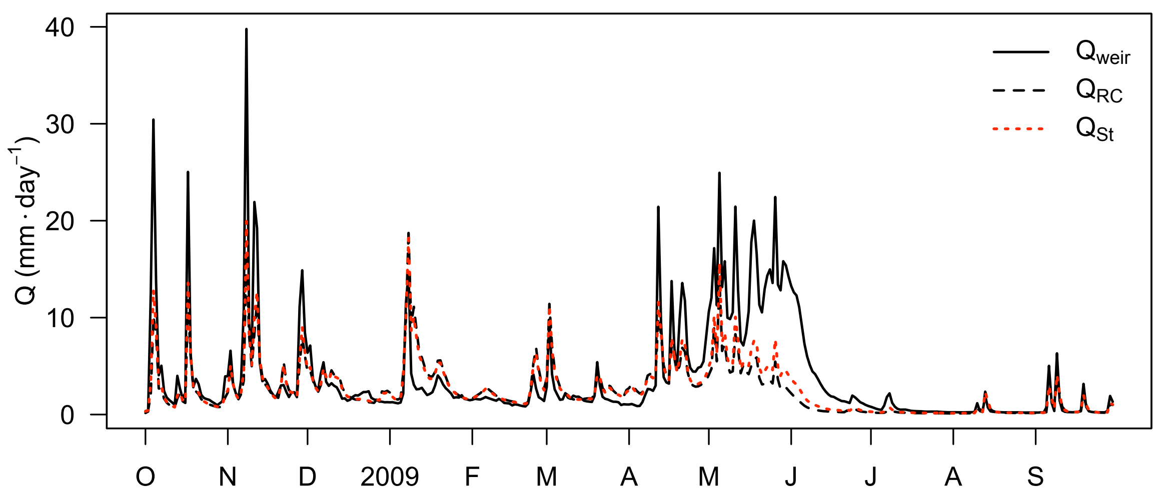

The daily water-level at the piezometer appears to follow a roughly logarithmic relationship when plotted against daily stream discharge. A closer look at the observations reveals a marked counter clock-wise hysteresis pattern, which implies a higher discharge on the rising limb than on the falling limb for a given water-level (Figure 6.5). It is especially discernable during the April 12th rain-on-snow event (see Figure 6.6 for precipitation and snowmelt data).

Figure 6.5 Stephen's Creek discharge at the weir plotted against shallow groundwater-level from April 1st to May 3rd 2009 (day 1 to 33 in lower graph). For ease of interpretation ease, the rising limb of the hydrograph is coloured brown while the falling limb is light blue.

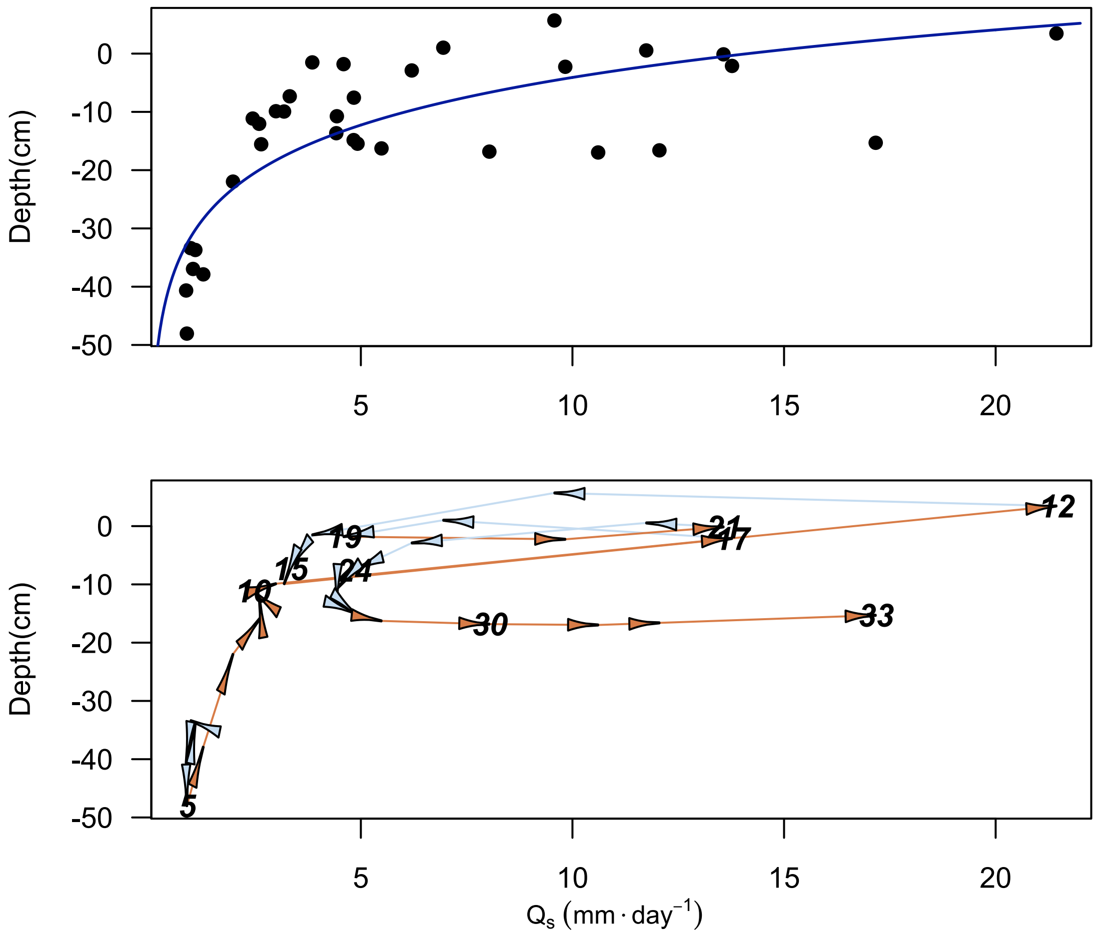

The piezometer is located in a vernal pool (a depression underlain by an impeding layer seasonally filling-up with water, Rains *et al.*, 2006) close to the catchment outlet in the footslope zone and acts as a transient storage for upslope areas. Water pooling over the ground surface was observed at a few occasions during the freshet. Hydraulic conductivity (K_{sat}) decreases exponentially with depth for most podzolic soil profile underlain by subglacial till (Hinton *et al.*, 1993; Hutchinson and Moore, 2000), but the piezometer was installed in a 1m deep coarse sand layer deposit, for which I assume K_{sat} values to be much higher than for compacted till, and homogeneous from the bottom to the top of the profile. No slug tests to determine hydraulic conductivity were performed.

Figure 6.6 Instantaneous discharges for Stephen's Creek at the weir (solid line), piezometer water-level fluctuations (dashed line). The upper bar plot represents the area-weighted average snowpack drainage-output for the whole catchment (solid bars are snowmelt as modelled by YAM and gradient bars are throughfall) while the lower bar plot shows only the modelling-cell where the piezometer is located.

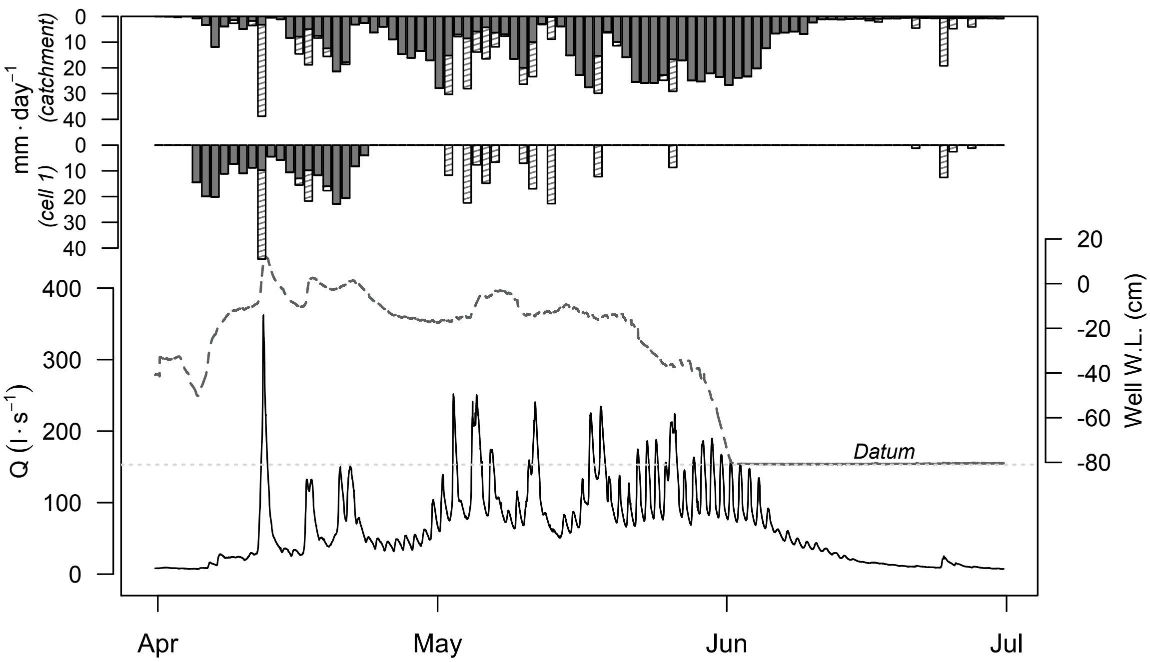

The piezometer shows a rather quick response to rainfall events and to local snowmelt input. However, the snowpack at lower elevation is completely melted by the 3rd week of April and the piezometer shows a relatively high water-level (> -40 cm) until May 29th, before dropping to the datum level (and below) in just 81 hours. Except for short-lived responses associated with rain events, the relatively stable shallow groundwater-level from the end of April to the end of May is not due to local control since the snow in a ~100 m radius around the piezometer was long gone by the end of that period. These high levels can be explained by "non-local" contribution from upslope area.

Figure 6.6 shows how responsive Stephen's Creek is to daily snowmelt – just as it was observed for the snowpack drainage output at SLD (Figure 6.1). These melting fluctuations are mostly caused by higher air temperature during the day but they are certainly exacerbated by the sparse forest cover composing most of the catchment area, which influences the snowpack's radiation budget.

6.1.4 Antecedent rainfall and melt index, Brook90 results and water balance assessment

The antecedent rainfall and melt index (ARMI) was used to estimate the antecedent soil-moisture conditions. ARMI gradually increased in April and May to peak on June 3rd, close to the end of the snowmelt season. Significant rainfall events over the summer caused the index to rise, but ARMI was limited to less than 40% of what was observed during the peak of June 3rd – except during the last rainfall event recorded on October 17th when ARMI rose to at least 46%.

Figure 6.7 Antecedent rainfall and melt index (ARMI). The upper bar plot represents the average rainfall and snowmelt for the catchment and the lower plot is the ARMI.

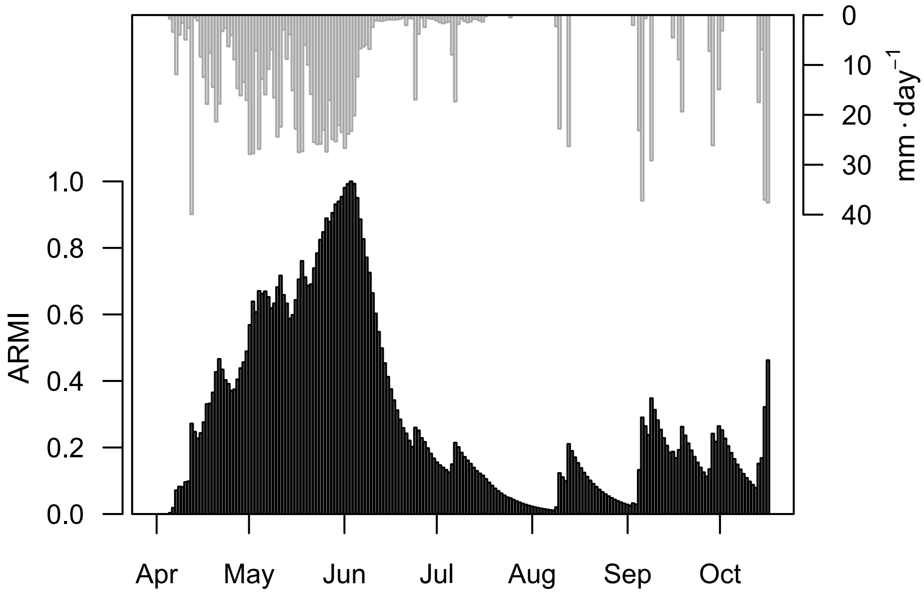

The lumped Brook90 model was used to model daily evapotranspiration necessary to the water-balance assessment. The parameter optimization was based on observed discharge data at Stephen's Creek at the weir; the efficiency function (R_{eff} – equation 5.11) was maximized at 0.8. The simulated evapotranspiration and simulated/observed discharges are displayed in Figure 6.8.

Figure 6.8 Simulated evapotranspiration and stream discharge by the Brook90 model

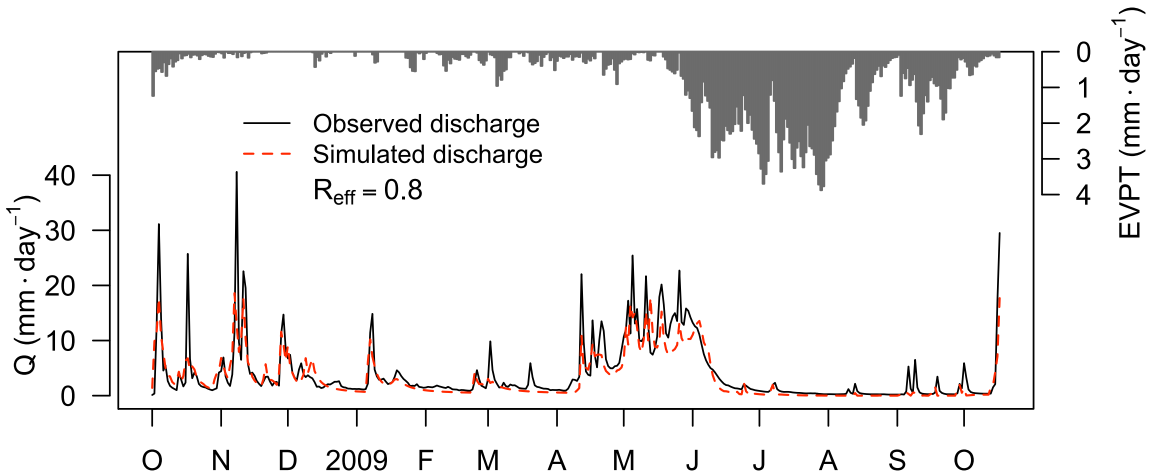

Based on the water-balance assessment, the soil and groundwater storage responses are consistent with ARMI – with a peak in recharge occurring at the end of May and in early June. As expected, discharge of stored water is occurring during most of the summer. It is interesting to note that the major rain-on-snow event on April 12th did not significantly contribute to subsurface recharge. The mass balance assessment from April 1st to September 1st indicates a net subsurface recharge of about 150 mm.

Figure 6.9 Weekly subsurface water balance assessment. The dates listed on the x-axis represent the storage balance for the preceding 7 days inclusively.

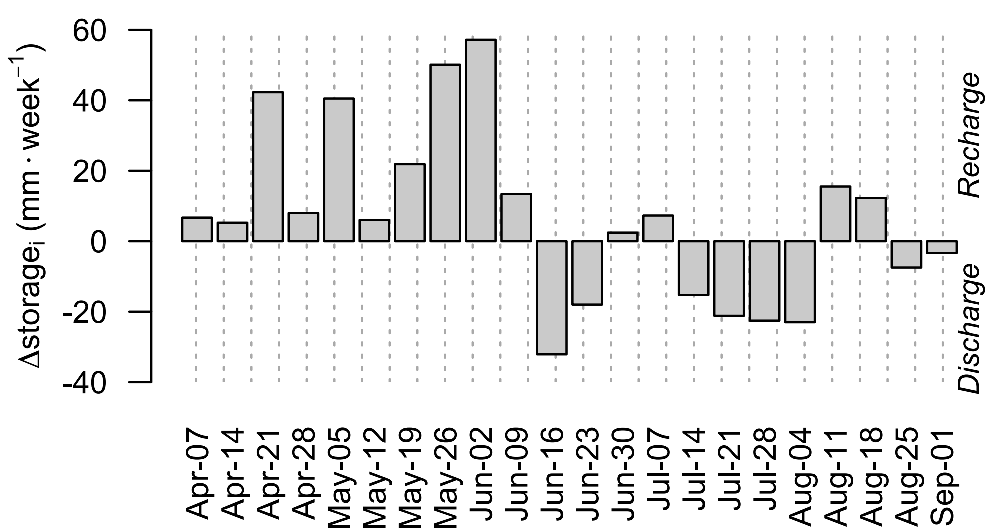

6.2 Isotopic Signature of the Snowpack – spatial and temporal variations

Snow core sampling on April 1st revealed an isotopically heterogeneous snowpack. An analysis of covariance (ANCOVA) on 14 samples using elevation as an explanatory variable and forest cover as a 2-level covariate factor (for forested or non-forested sampling sites) showed that elevation is weakly but significantly impacting the $\delta^{18}O$ and D isotopic concentration at the $\alpha = 0.05$ level (p-value = 0.03 and 0.04 respectively); while no significant differences were observed between forested and non forested sites ($p = 0.65$ and 0.56). A linear regression using only elevation as an explanatory variable was computed and the results produced a low coefficient of determination ($R^2 = 0.32$). Diagnostic plots for normality were questionable. A Student's t-test was computed and the results failed to reject the null hypothesis –that the sample distribution is not significantly different than a normal distribution ($p > 0.11$). The residuals and errors were interpreted as being normally distributed, although the lower-most sample has a much higher leverage than the rest of the distribution based on Cook's distance. This sample was taken out of the distribution and the regression model was computed again (Figure 6.10). The distribution is still considered non-significantly skewed, but to a lesser extent ($p > 0.09$) while the impact of elevation on the variance explained gained significance ($p < 0.01$) – so did the model's coefficient of determination ($R^2 = 0.42$).

Clearly, variables other than elevation are explaining the heterogeneity of the snowpack during the snow-accumulation phase, the most plausible speculations being intra-event variability during precipitation events over-riding altitudinal control on fractionation processes and/or rain-on-snow dynamics causing the isotopic signature of a given event to be stored as snow at higher elevation only.

Figure 6.10 Snowpack isotopic signature on April 1st at different elevations. The sample that was left out of the distribution is marked as an empty circle

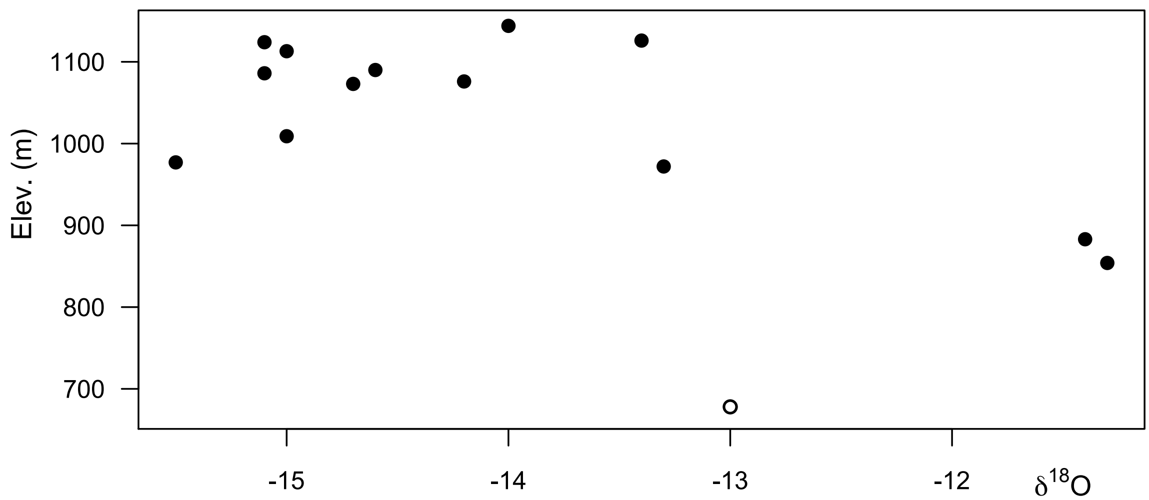

6.2.1 Isotopic signature of snowpack drainage output

The temporal variation between all snow lysimeters (SLs) looks consistent (Figure 6.11) and the spatial distribution seems to be influenced by elevation. These observations were tested through a multiple linear regression (MLR) using days and elevation as continuous variables and through a two-way analysis of variance (ANOVA) by transforming these variables as factors, as proposed by Moore (1989). The time-series was divided into two periods, from April 5th to April 29th when all SLs were snow-covered, and from May 3rd to May 19th when only the two upper-most SLs were yielding melt-water. All diagnostic plots showed normally distributed residuals and errors, and t-tests for normal distribution showed non-significant skews in the isotopic distribution at each SL ($p > 0.5$).

During early spring, both methods revealed that elevation and time are significantly related to $\delta^{18}O$ variations ($p < 0.001$). During the later period, the two-way ANOVA confirmed once again the significance of both predictors ($p < 0.001$) while the MLR showed that only elevation significantly impacts the difference in means between the two sites ($p < 0.008$), whereas time did not ($p > 0.32$). The information provided by both tests are not conflicting, but should be interpreted in accordance to the structure of their model. Because time is treated as a 20-level factor (for 20 days) in the two-way ANOVA, it confirms that the isotopic signal significantly varies across days, indifferently of their order of occurrence. Contrastingly, the proposed MLR model treats time as a continuous variable; no relationship with time simply means that no significant temporal linear trend was observed during the late spring – as opposed to early spring when a strong relationship was found. Snowmelt fractionation processes are influenced by a variety of factors, in particular snowmelt intensity and rain water input (Rodhe, 1998). These statistical results corroborates the hypothesis that the variance observed in the snowpack drainage-output during the ablation season can be well explained by elevation, which is in accordance with the weaker relationship found in the snow core samples. The "enrichment trend" of about 2-3‰ over the 25-day period in the early spring is significant and could be interpreted as a response to "non-local" fractionation processes operating at the catchment scale – such as a gradual increase in melt intensity due to latent heat. Similar snowmelt isotopic enrichment trends over time have been observed by Hooper and Shoemaker (1986), Laudon *et al.* (2002) and are well documented by Taylor *et al.* (2001). The apparent lack of temporal relationship during the later part of the season (i.e. neither enriched or depleted melt-water) is probably due to frequent rain-on-snow events (Figure 6.6) and distinct snowmelt dynamics between forested and non-forested sites (latent-heat dominated vs. radiative – Figure 6.1) – which possibly influences melt-water contact time with the ice grains and isotopic fractionation (Rodhe, 1998). Despite these variations during the later period, the spatial relationship between SLC and SLD still holds – which emphasizes the dominating control exerted by altitude over snowfall isotopic signature during the winter.

Figure 6.11 Snowpack drainage-water isotopic signature at four snowmelt lysimeters

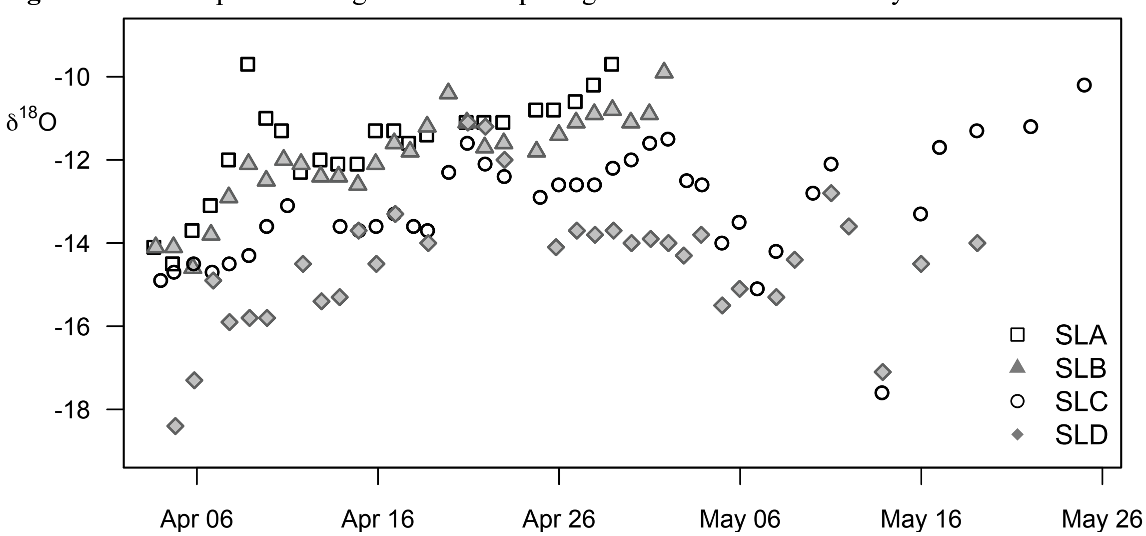

6.2.2 Daily regression models and isotopic mass balance assessment

The expected influence of elevation on snowmelt dynamic was confirmed, which gives statistical grounds for computing daily linear regressions between the SLs in order to estimate the isotopic signature of each cell based on their elevation. Due to the large amount of graphics, the daily regression plots from April 4th to May 19th are presented in appendix K, along with their coefficients of determination and their slope values. Note that day one refers to April 1st. The regression results were rejected when $R^2 < 0.75$ for days when 3 to 4 SLs were outputting melt-water, and when the slope was positive or null after day 33 when only 2 SLs could be compared. Based on those criteria, less than a third of the daily results were rejected (days 1 to 6, 12, 19, 20 to 23 and 42 to 44). For those 15 discarded days, averaged SLs isotopic signatures were given to the modelling cells as per an empirical method previously explained (section 5.4.2 – averaging protocol). The standard errors for the regression results that were retained average 0.44 ± 0.18 ‰.

The sampling of snowpack drainage water was initiated on April 4th; therefore, the values from the 1st to the 3rd of April are a repetition of the April 4th value. The snowmelt season starts around April 6th for the lower cells – therefore this extrapolation is not likely to have an impact on the isotopic mass balance assessment. The last modelled isotopic value was repeated until the total disappearance of the snowpack when the length of the isotopic record did not match the cell's SWE record as determined by YAM. A customized approach was necessary for cell #20 (north facing aspect) since its simulated snowmelt record extends twice the duration of the simulated $\delta^{18}O$ record. An enrichment trend was added to the extrapolated results at the end of the isotopic record in order to approximately match the closure errors observed in the neighbouring cells. The late spring snowpack drainage-water isotopic signature is likely to have an influence on the hydrograph separation since the melt-water output gets greater as the season proceeds, as observed at the SWE transects (Figure 6.2).

The mass balance closure errors (C.E.) at the SLs (Figure 6.12) are generally negative - suggesting a slight overall isotopic enrichment of the snowpack with time, which is consistent with the temporal fractionation trend as observed previously. It should be noted that the drainage-water samples were not depth integrated and that snow core samples might be affected by sub-local variability. It is hard to assess whether these relatively small errors are due to sampling, fractionation processes or both.

The closure errors for the modelling cells are comparable to the ones observed at the SLs, although some exceptions stand out (Figure 6.13), such as cell #7 (C.E.: -19.5%) – which might be due to snow core sampling in a sub-local anomaly since the closure errors of the neighbouring cells are about half that value. Cells at lower elevation show an enhanced isotopic enrichment than at higher elevation, which is probably due to the more pronounced impact of isotopically enriched rainwater on the shallower snowpack. The cells at upper elevation have closure errors close to what was observed at SLC and SLD, suggesting that the regression models and the averaging protocol captured most of the natural variations created by fractionation processes. A Student's *t*-test was performed to test whether any significant differences existed between the closure errors at the SLs and at the cells and none was found ($p > 0.4$).

Figure 6.12 Isotopic mass-balance assessments for the snow lysimeters

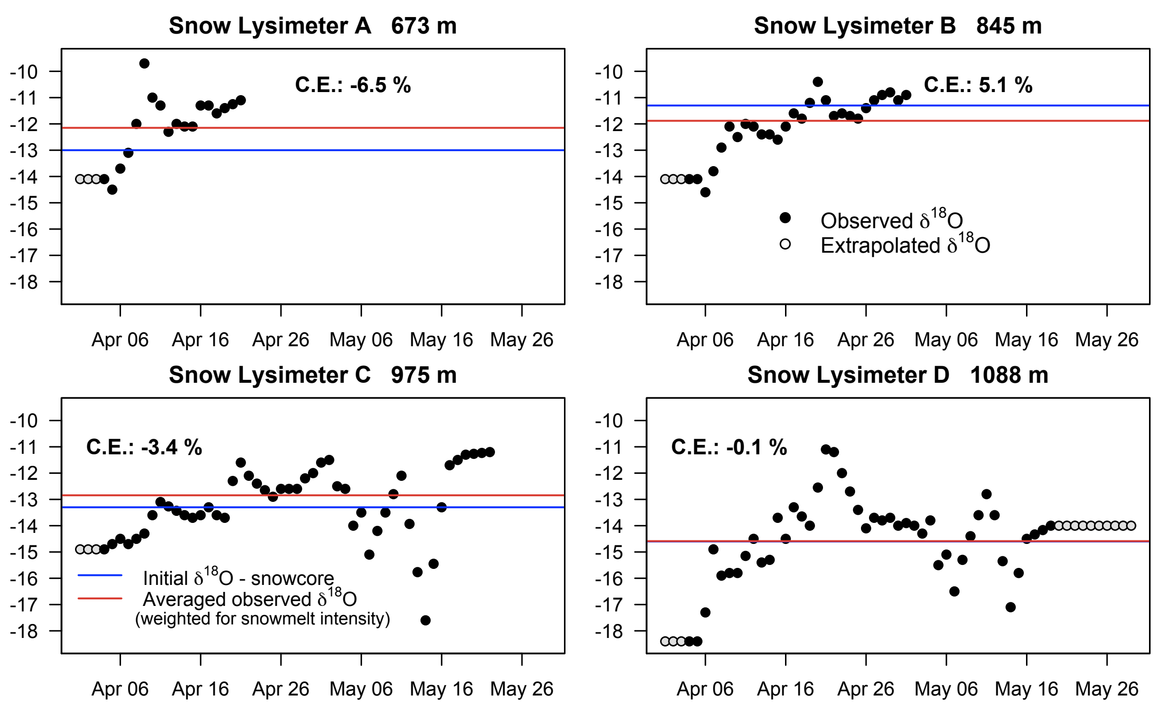

Figure 6.13 Isotopic mass-balance assessment for the modelling space

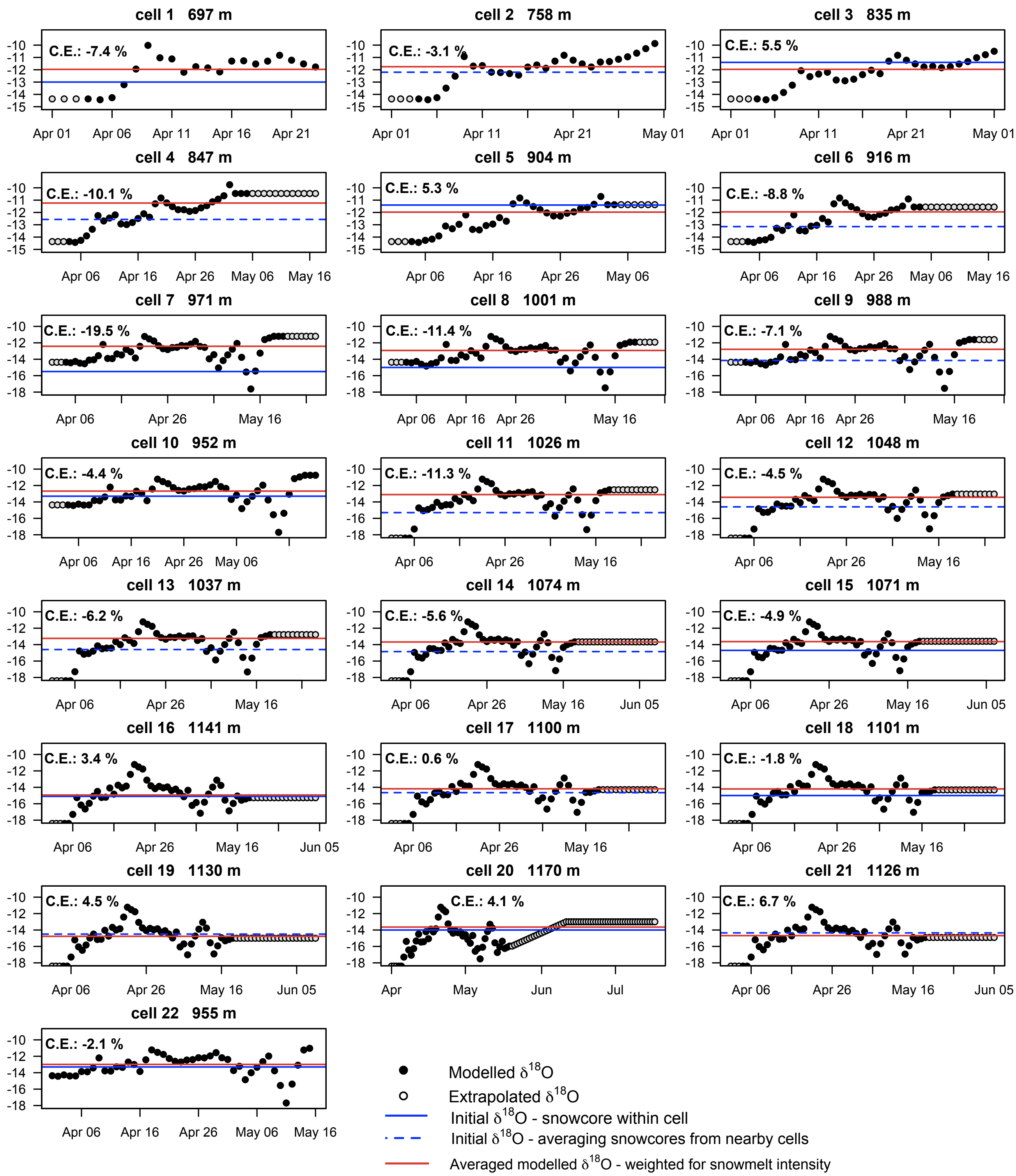

6.3 Two-component Hydrograph Separation Results

The daily results obtained for the YAM model and the isotopic regression models were multiplied together to obtain a daily $\delta^{18}O$ flux for each cell composing the modelling space. The runCE model provided a platform to account for event water transit time at the cell – and globally at the catchment scale. The uncertainty for the stream water and pre-event water was set to the analytical error (0.1‰) and the average standard error for the regression models was used to describe the uncertainty of event-water (0.44‰).

Figure 6.14 Two-component hydrograph separation results. Upper graph: isotopic signature of components and output from the runCE simulation. Lower graphs: hydrograph separation using the runCE and the volume-weighted average (VWA) methods.

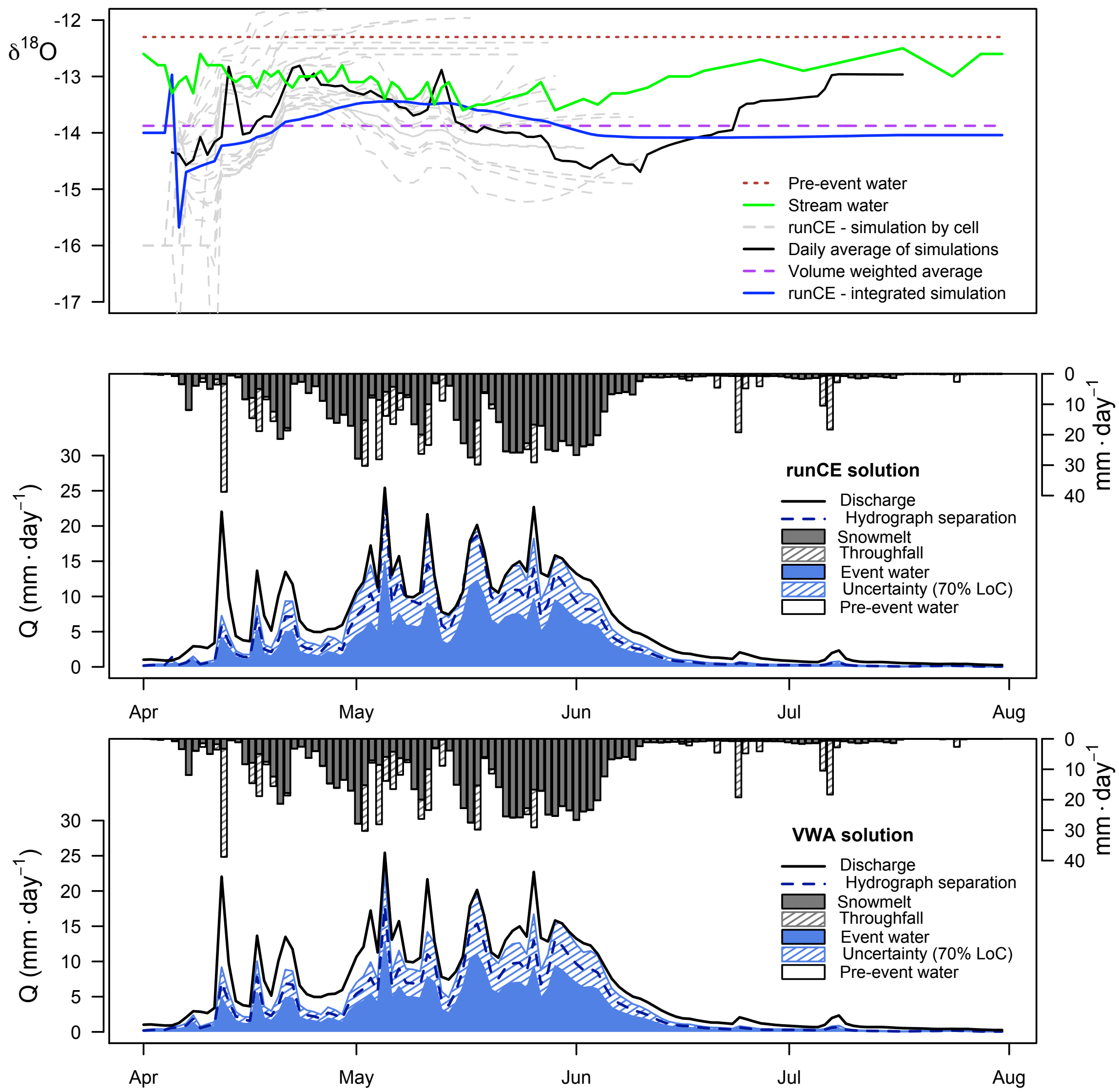

During the month of April, pre-event water is dominating the hydrograph, representing 62 ± 11% of the streamflow (the error term represents the mean uncertainty for the period as determined by equation 5.22). This is in accordance with most 2-IHS studies conducted during snowmelt (Moore, 1989, Rhode, 1998; Laudon *et al.*, 2002-2004-2007). However, the contribution of event water drastically increases as the snowmelt season progresses into the month of May. The average *event* water contribution to the streamflow from April 30th to June 5th is estimated to 78 ± 26%, then slowly decreases to 37 ± 10% for the remaining of June and down to 24 ± 8% in average for the month of July. Based on previous studies, it is unusual for event water to dominate streamflow composition. Out of the 993 mm of snowmelt/rain-on-snow input to the catchment, runCE estimated that 491 ± 121 mm contributed to streamflow from April 1st to July 31st, which means that close to half of the event water went into subsurface recharge. The results are summarized in Table 6.3. Snowpack drainage is the most uncertain component, which explains the large uncertainty values when streamflow is dominated by event water as explained in section 5.5.2. A better characterization of the spatial variability in isotopic signature of snowpack drainage (e.g., more sampling in time and space) would likely have reduced the uncertainty of the event water component.

It is obvious from inspection of Figure 6.13 that the runCE simulation dampened much of the isotopic variation in the event water signal. The area-weighted average of the individual runCE simulations (per cell) caused mathematical anomalies (event water > 100% of streamflow) when a first attempt was made to use those values as event water for the separation. Processing these averaged values with the runCE algorithms a second time greatly smothered the signal and solved the anomalies. It is debatable whether the second runCE application on already "processed" data truly represents a transit mechanism within the subsurface environment. However, this integrated simulation succeeded in modelling the dominant isotopic melt-water signal over time while semi-quantitatively accounting for transit time. The runCE and the VWA methods provided similar results at the lower limit of confidence (Table 6.3) suggesting that the "temporal resolution" gains realized by runCE are offset by the spatial uncertainty associated with melt-water. However, this is partly due to the structure of the first order uncertainty calculation used in this study because it gives a disproportional weight to the most uncertain component the more it dominates the hydrograph. A better-suited approach to calculate uncertainty would be to use a method that does not rely on normality assumptions such as the bootstrap Monte-Carlo model (Joerin *et al.* 2002) and should be considered for future studies.

6.3.1 Two-component hydrograph separation at Stephen's Creek at the mouth

A two-component separation was performed at the mouth to see if significant differences could be observed between the catchment and watershed scale. The fact the discharges were estimated for Stephen's Creek at the mouth does not affect the accuracy of the separation since IHS results yield fractions of streamflow as opposed to absolute values.
Initially, the snowmelt and isotopic values were modelled only for the area within the catchment's boundary and not for the whole of Stephen's Creek's headwater. The sub-alpine area contributing to streamflow and not included in the catchment was subdivided into 7 cells (Figure 6.15) that were attributed the snowpack drainage-water isotopic flux from modelled cells located at a similar elevation and aspect and under a similar forest cover (Table 6.2). Only the headwater area was assumed to deliver event water to the stream. The contribution of rainfall events at lower elevation was ignored since they were not sampled for snow-free area and during snow-free period. This may lead to an overestimation of pre-event water since rainfall during the spring is usually isotopically "heavier" than snowmelt. These risks were minimized in the summer by sampling baseflow at least 72 hours after any rainfall event had occurred. It is acknowledged that the event water characterization for the whole of Stephen's headwater is not as rigorous as the characterization done for the headwater catchment. However, half of the SLs and two SWE transects were deployed outside of the headwater catchment boundary (Figure 4.2), but within Stephen's headwater. Therefore, it is reasonable to assume that both the YAM model and the isotopic regression models are valid for the area of interest.

Table 6.2 Correspondence between modeling cells and Stephen's headwater subdivisions

Stephen's subdivision	Attributed the (average) isotopic flux of cell(s):
23	16 and 19
24	18
25	13
26	5,6,7 and 8
27	3
28	2
29	1

Figure 6.15 Stephen's Creek Headwater Subdivisions

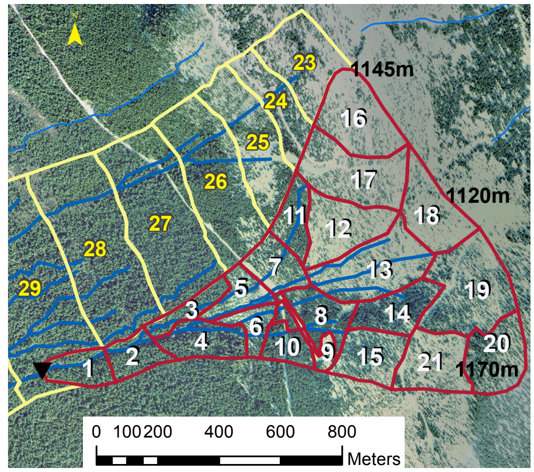

The pre-event water signature at Stephen's Creek at the mouth could not be determined with confidence since snowmelt at lower elevation was already contributing to streamflow when the pre-event baseflow was sampled at the weir (late March). The pre-event signature at the mouth was assumed to be the same as the signature at the weir, which was -12.3‰. The error values were not changed for the uncertainty analysis at the mouth. Only the volume-weighted approach was used for the separation at the mouth. Mathematical convergence could not be achieved with runCE, probably due to an insufficient difference between pre-event water and runCE event water.

Figure 6.16 Two-component hydrograph separation for Stephen's Creek at the mouth (stream discharges were estimated)

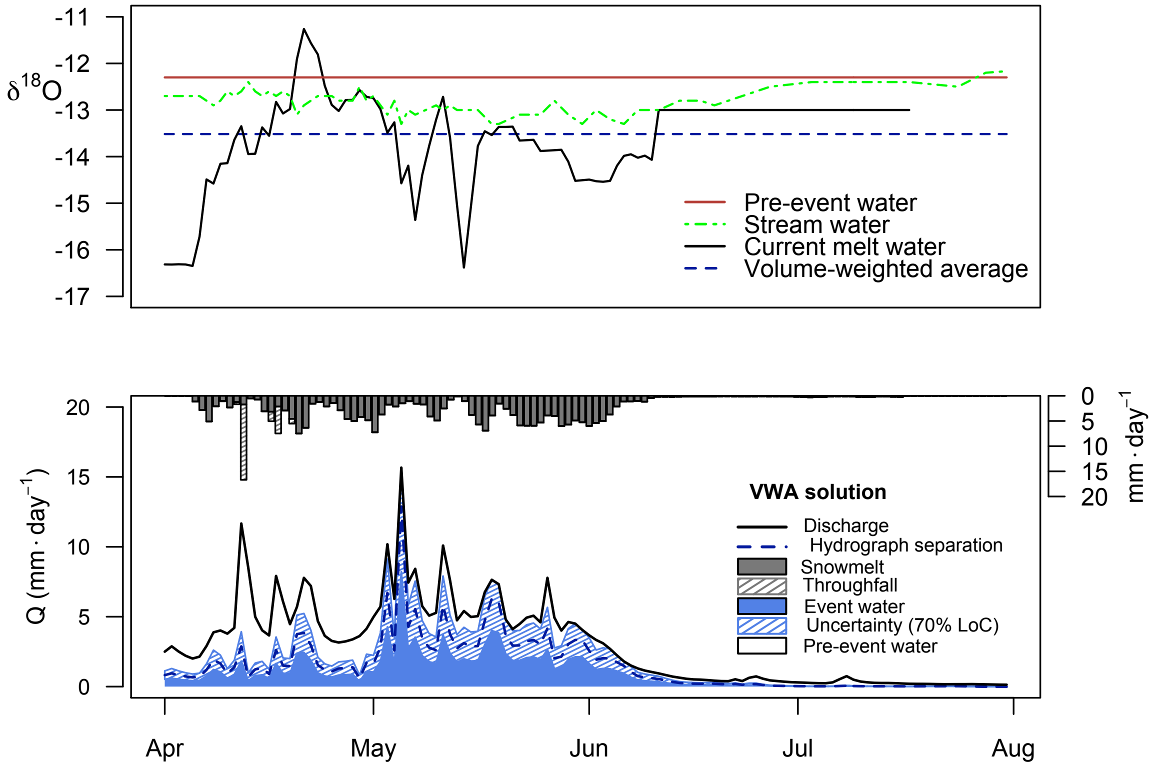

The two-component separation at the mouth provided very similar results to the VWA separation undertaken in the headwater catchment during the main hydrological period of the freshet. Based on a paired Student's *t* test, event water contribution to streamflow was significantly higher in the catchment in April and July and a very weak significance was also observed in May (Table 6.3). The test for significance was dismissed for April and May since the error terms overlap. In July, event water made-up 34 ± 11% of the streamflow in the catchment as opposed to only 7 ± 4% at the mouth. Only 30 mm of rainfall occurred in early July, which was likely not sufficient to bias the pre-event water estimate. Stream and subsurface isotopic signature and local water meteoric line for all samples can be found in appendix L. The silicon concentration for all samples is in appendix M.

Table 6.3 Summary of event water contribution (%) to the streamflow for Stephen's Creek at the weir (headwater catchment) and Stephen's Creek at the mouth based on two 2-IHS methods

Period	**runCE**	**Volume-weighted average (VWA)**		
	Headwater catchment (%)	Headwater catchment (%)	Stephen's Creek watershed (%)	Paired Student's *t* test (p-value)
April 1st to April 29th	37 ± 11	41 ± 12	34 ± 12	0.013
April 30th to June 5th	78 ± 26	66 ± 19	62 ± 23	0.044
June 6th to June 30th	38 ± 10	43 ± 13	41 ± 15	0.407
July 1st to July 31st	24 ± 8	34 ± 11	7 ± 4	**<0.001**

6.4 Three-Component Hydrograph Separation

A three-component hydrograph separation was attempted in the research catchment by characterizing soil water based on three ephemeral subsurface outflows. For GWB (Figure 4.2), the source of runoff could be visually identified at the contact between the mineral soil and the bedrock. The sources for GWC and GWL were interpreted as saturated throughflow over shallow hardpan horizons in the podzolic soil profile. Due to the extensive snowpack cover, the pre-event subsurface water could not be sampled. The first samples were collected long after the initiation of snowmelt on April 22nd, April 24th and May 2nd for GWB, GWC and GWL respectively.

The [Si] and $\delta^{18}O$ signatures for the three sources fall into three clearly separated clusters (Figure 6.17). The soil water signature was determined by averaging all samples for both tracers. The mixing diagram suggests that the three components are colinear, which violates one of the fundamental assumption of the 3-IHS method (Hinton *et al.*, 1993). It is worth emphasizing that the soil-water samples do not represent the pre-event soil-water conditions since they were not collected prior to snowmelt.

It is generally assumed that diluted silica concentrations in the soil (as ortho-silic acid – H_4SiO_4) originate from amorphous silica, a secondary mineral produced from mineral weathering, and that diluted concentrations are controlled by its abundance, by alkalinity and by Al^{3+} mobility (Wilson, 1986; Gunnarsson and Arnórsson, 1999 and Vesely *et al.*, 2005). However, research in the last two decades has revealed that organic matter (i.e. phyoliths) and biogenic imogolite complexes in podzoilic soils are important sources of silica in solution and vegetative uptake/decay cycle is believed to control diluted concentrations under constant pH values and soil moisture conditions (Wilson, 1986; Farmer, 2005; and Vesely *et al*. 2005). These studies suggest that silica does not behave as conservatively as it was once assumed. A previous study reported silica uptake by diatoms in the stream (Hooper and Shoemaker, 1986), but non-conservative behaviour in the soil itself should undoubtedly be a more significant concern for hydrologists undertaking tracer-based studies. The large scatter in silicon concentrations observed in soil-water samples may be an indication of a non-conservative behaviour.

For the purpose of the exercise, an assumed value of 3.5 ppm was given to the silicon concentration of the soil-water component in order to enable the separation. This value is within the range of diluted concentrations for Douglas fir forests at 15 cm depth (3.53 ± 0.65 ppm; reported by Cornelis *et al.*, 2010) and is likely the most representative scenario for the pre-snowmelt soil water conditions. The isotopic value found in soil water was left unchanged. Because this is a simulation, the procedure is subjective and based on literature values. The interpretation of these results should be done with caution.

Figure 6.17 Mixing diagram for [Si] and $\delta^{18}O$. The black dashed lines represent the theoretical mixing triangle and yellow lines are for the fictional separation

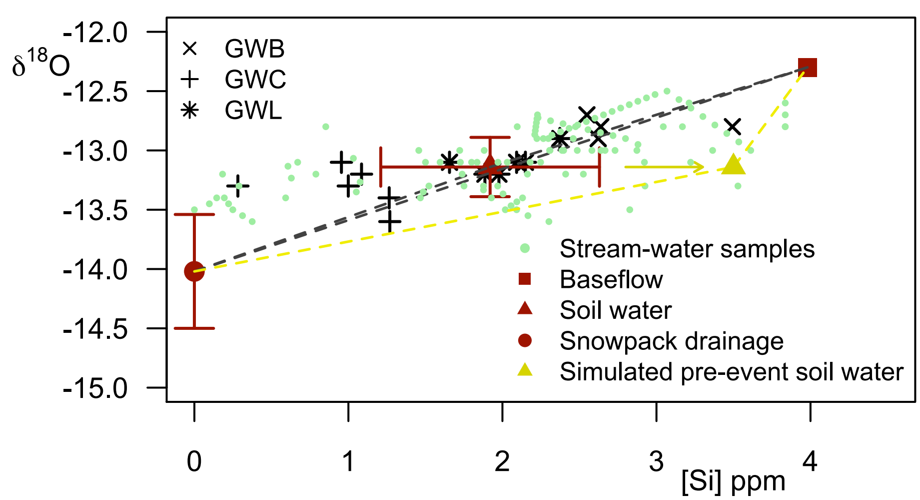

Figure 6.18 Three-component hydrograph separation using a fictional silicon concentration to define the soil-water component. Upper two graphs show component and stream concentrations for both tracers; the middle graph shows the hydrograph separation and the lower two graphs show the corrected fraction of groundwater, soil water and snowpack water composing the streamflow for smothered and raw stream concentrations

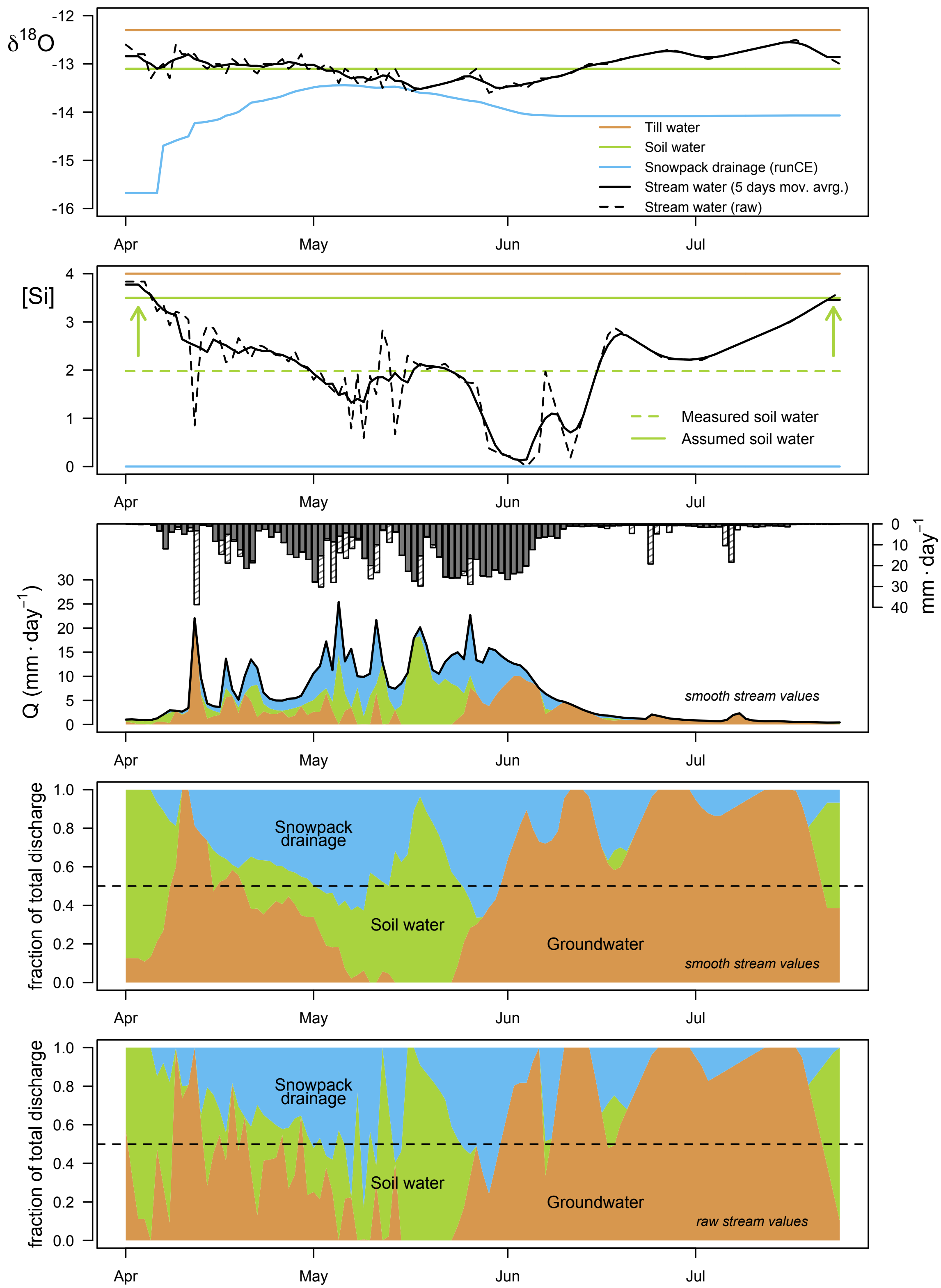

Stream-water samples falling outside of the fictional mixing triangle (yellow lines in Figure 6.17) indicate mathematical anomalies due to undefined heterogeneities or end-members; consequently the total contributions will exceed 100% of streamflow at these occasions. These errors were corrected by subtracting the excess-flow proportionally to the contribution of each component. Due to the large daily [Si] variations observed in the stream, the separation was "smothered" using a 5-day moving average on the stream's concentrations values (both tracers). Raw and smothered results are presented in Figure 6.18. Given its hypothetical nature, no uncertainty analyses were attempted for this separation.

The three-component separation shows little groundwater contribution to streamflow during the bulk of the freshet. The domination of the groundwater contribution during the April 12th rain-on-snow event and its decreasing influence thereafter seems to be in accordance with the results computed by both 2-IHS methods. The silicon content of pre-event soil-water exacerbates the sensitivity of soil-water vs. snowpack drainage-water fractions – therefore it is hard to confidently interpret the timing of each component's contribution. It can only be acknowledged that old soil-water likely plays an important role in snowmelt freshet, which cannot be appreciated with the two-component analysis since isotopic homogeneity is assumed between soil water and groundwater.

6.5 Nitrate Export Dynamics During Snowmelt

Streamwater was sampled for phosphate, ammonium and inorganic nitrate/nitrite at three different locations along Stephen's Creek during the freshet and over the summer: at the weir, at the mouth and halfway between the weir and the mouth. The concentrations in phosphate and ammonium were systematically below analytical detection limits; therefore, only nitrate/nitrite export to streamflow was addressed. The hydrograph was divided into 6 relatively homogeneous periods based on the results obtained from the hydrograph separation. The concentrations were very low throughout the study period. The highest value found was 1.76 ppm on April 7th and was observed at the mid-stream sampling location. Snowmelt started on April 6th with 3.4 mm released from the snowpack and increased by 350% on April 7th to 11.9 mm – however stream discharge only gained 60% of its previous day value. From April 6th to 11th, the antecedent rainfall melt index was only at 7% of its maximum value for the freshet period, suggesting drier antecedent moisture conditions, and pre-event water contribution to the streamflow was about 75%.

Figure 6.19 Nitrate/Nitrite values at three different locations on Stephen's Creek presented against 2-IHS and 3-IHS results, piezometer water levels and snowpack drainage output. Note the varying logarithmic scale between graphs for nitrate/nitrite concentrations (continuing next page).

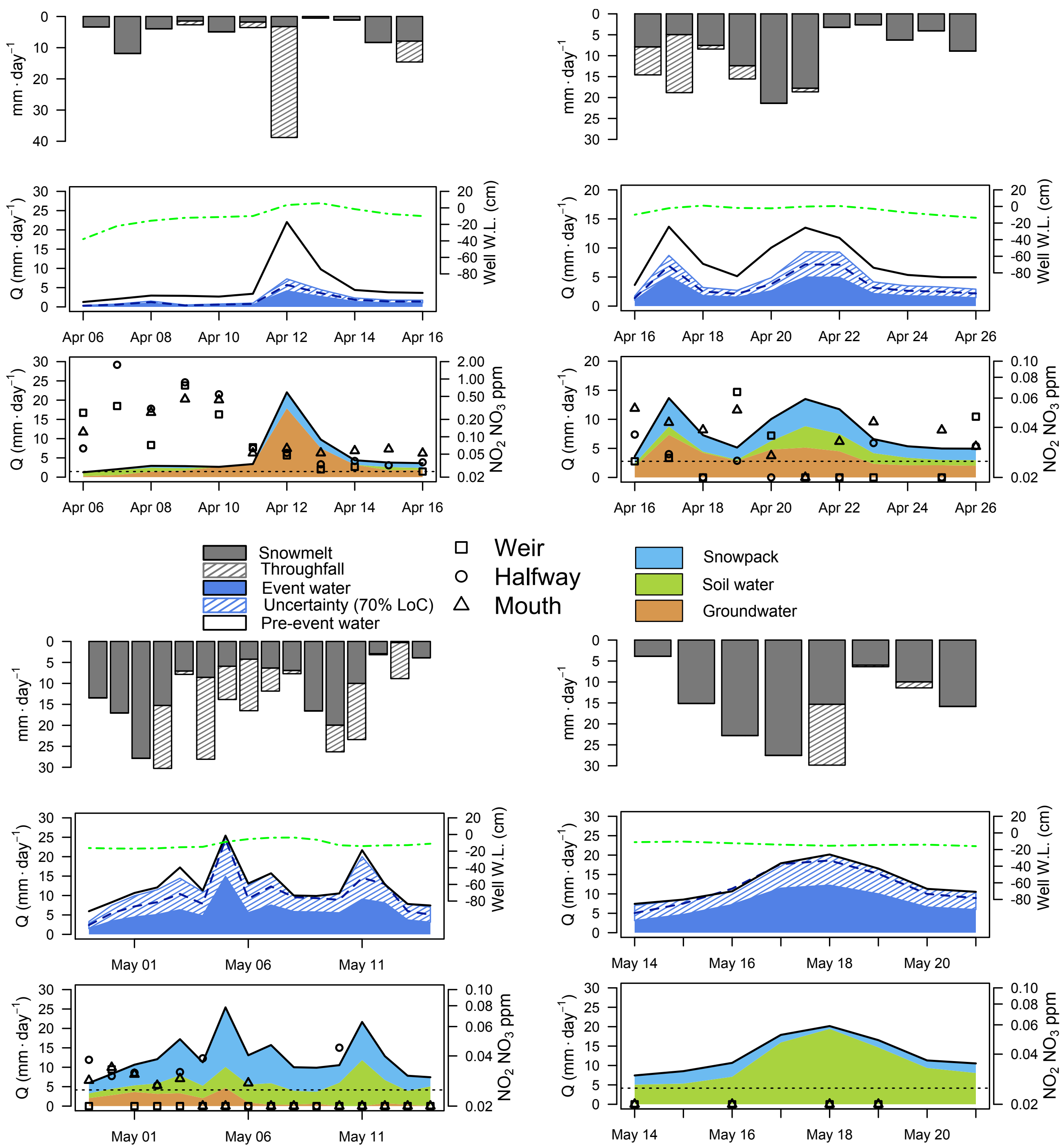

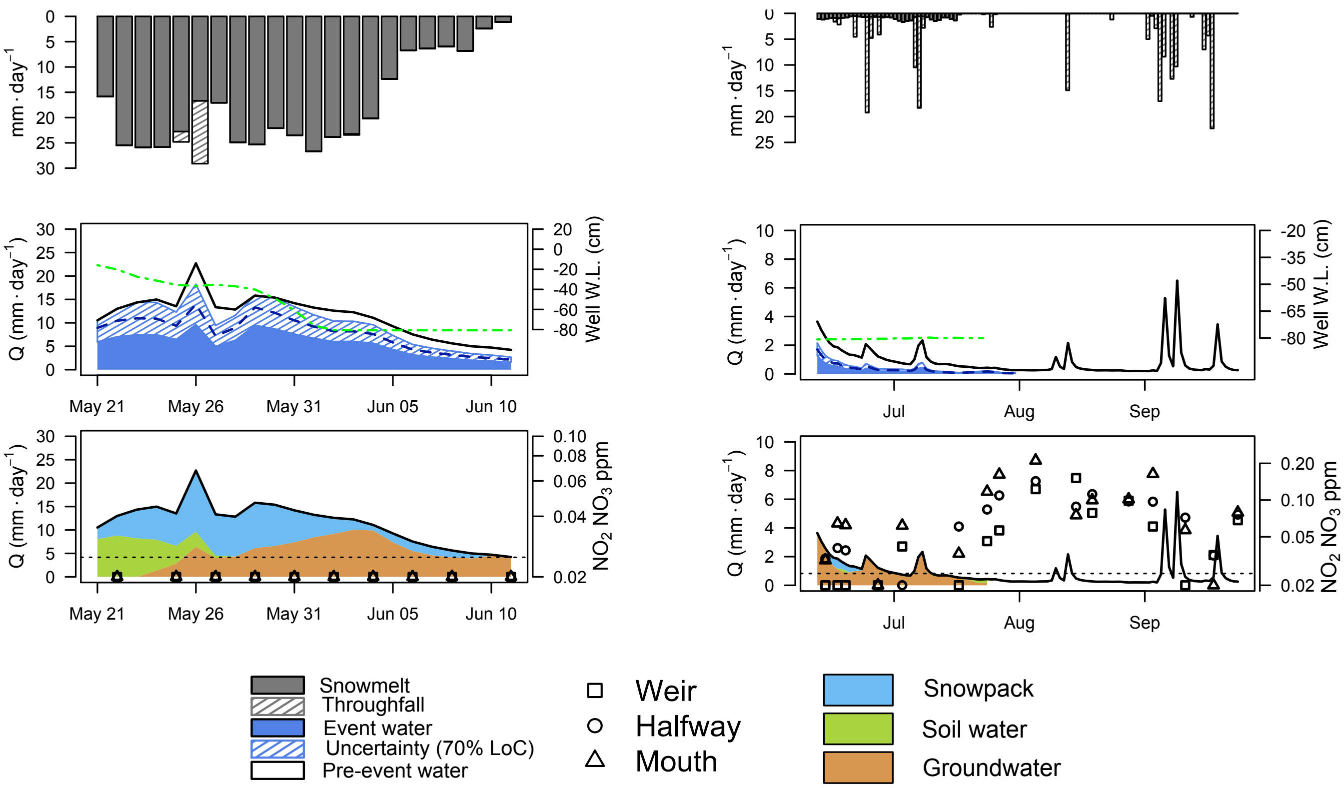

Nitrate/nitrite concentrations are below detection limits for most of May and early June; these periods are characterized by event water (and possibly soil water) dominating the hydrograph. The concentrations increase above detection limit from mid-June, but remain very low throughout the summer (generally < 0.2 ppm). A one-way ANOVA was computed during the early spring (April 4th to April 16th) and the summer (June 17th to September 24th) to see if the mean concentration between sampling sites were statistically different. The analysis could not be performed for the early spring period because the skewed distribution failed to meet normality. The summer distribution was not considered significantly different than normal ($p > 0.09$). The test revealed that the differences in concentrations in-between sites were considered highly significant for all sites ($p < 0.001$); thus nitrate/nitrite concentrations were at their highest at the mouth and at their lowest at the weir during the baseflow dominated period.

Concentrations higher than 0.1 ppm appear to occur during days of negative water-balance (subsurface discharge) and low ARMI index. Multiple linear regressions were used to see if these two indexes were related to nitrate/nitrite loadings. The distribution for the entire monitoring period failed to meet normality at all sites. Just like for the ANOVA, only the summer period could be investigated (June 17th to September 24th).

Diagnostic plots showed that the errors and residuals were abnormally distributed for the regression model at the weir. This sampling site will not be interpreted. Results from the mid-river and the mouth showed that nitrate/nitrite loadings were negatively related to the ARMI index ($p < 0.016$) but not to the subsurface mass balance index ($p > 0.38$). The later variable was taken out of the model and a single linear regression was performed using only ARMI as a predictor. The results gained significance ($p < 0.001$) and determination power ($R^2 = 0.44$).

6.6 Recession Analysis

Recession analysis was carried out for Stephen's Creek at the weir and Roberts Creek's at the mouth in order to see if their contrasting runoff regime could have an influence on late summer groundwater yield. A total of seven recession segments were picked for the analysis. The start and end days of the periods were defined based on discharge data and the ARMI index.

Figure 6.20 Antecedent rainfall and melt index (ARMI) for the headwater catchment and selected recession segments for Stephen's Creek at the weir and Roberts Creek at the mouth. Note the logarithmic scale for discharges.

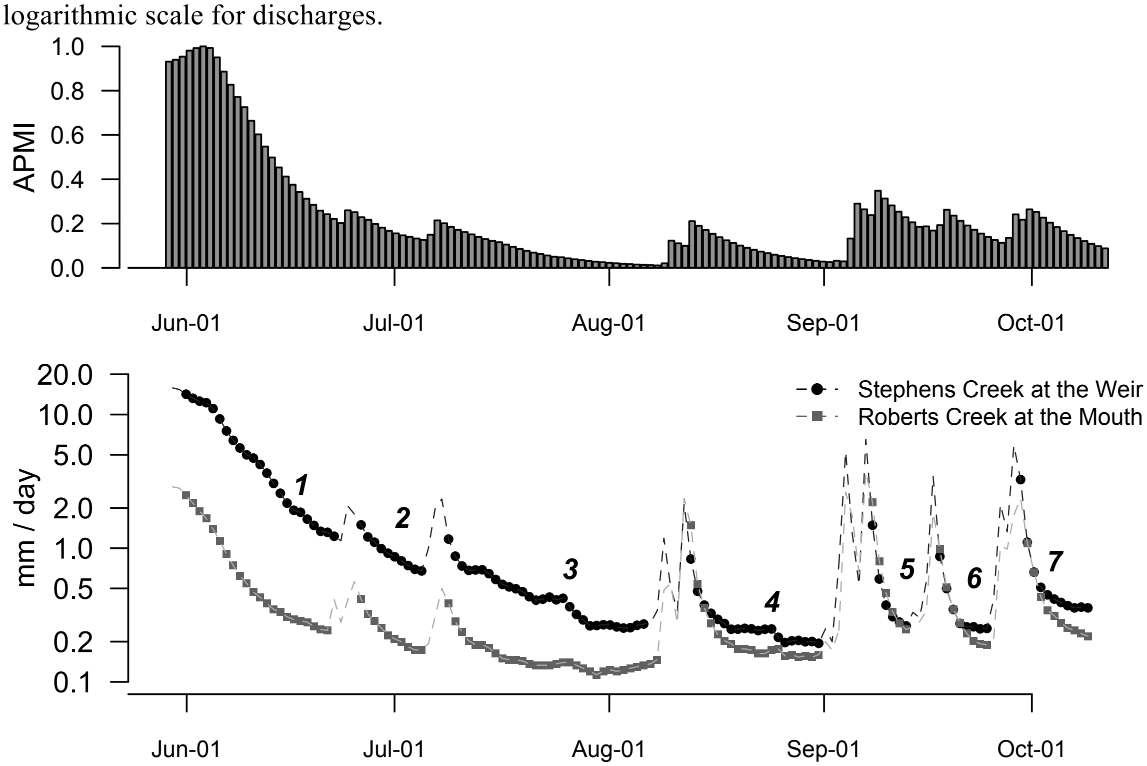

Based on the linear storage outflow model (Depuit – Boussinesq aquifer) given in Barnes (1939), the shape of the recession curves should be linear when plotted on a logarithmic scale – if the contribution of vertical flow components are negligible. The behaviour of the recession limbs in both creeks is clearly non-linear (Figure 6.20), as is the case for most natural drainage systems (Moore, 1997). Recharge and evapotranspiration (EVPT) are, by definition, vertical flows affecting the subsurface storage during most periods of the year, which can make the selection of recession limbs a subjective procedure. Given the short duration of stream discharge monitoring at Stephen's Creek, summer periods affected by substantial EVPT losses had to be included in the analysis. The streamflow anomalies observed in the July and August curves (#3-4) are likely due to EVPT, but the timing and magnitude of these effects seem consistent between the two creeks so it is assumed that EVPT will induce similar errors and won't impede the comparisons of the creeks' recession characteristics. Moreover, the remaining of the snowpack is still melting in the upper-most northwest facing catchment's cell during the first recession period – which will likely augment the scatter of the residuals for that specific period.

Master recession curves based on the single linear, single power-law and dual linear reservoirs were fitted to the streamflow data by calibrating the parameters of the models using the loss function as detailed in section 5.6. Segmented linear models for the complete periods were also fitted for comparison's sake. Furthermore, an attempt was made to fit logarithmic relationships to graphically delimited sub-periods when only deeper groundwater outflow was believed to contribute to discharge (referenced as segmented linear baseflow). The residuals from the model fits are presented in Figure 6.21 for Stephen's Creek at the weir, Figure 6.22 for Roberts Creek at the mouth and the results are summarized below in Table 6.4. All computational codes for the recession analysis can be found in appendix J.

Figure 6.21 Residual distribution from recession model fits for Stephen's Creek at the weir. The recession period #1 does not plot on the y-scale given for the master dual linear model (residual interval: [-4 : 0.5]), the master single power-law (residual interval: [-2.3:1.5]), the segmented single linear (residual interval: [-1.5:1.3]) and the segmented baseflow linear (residual interval: [-0.3:0.3]).

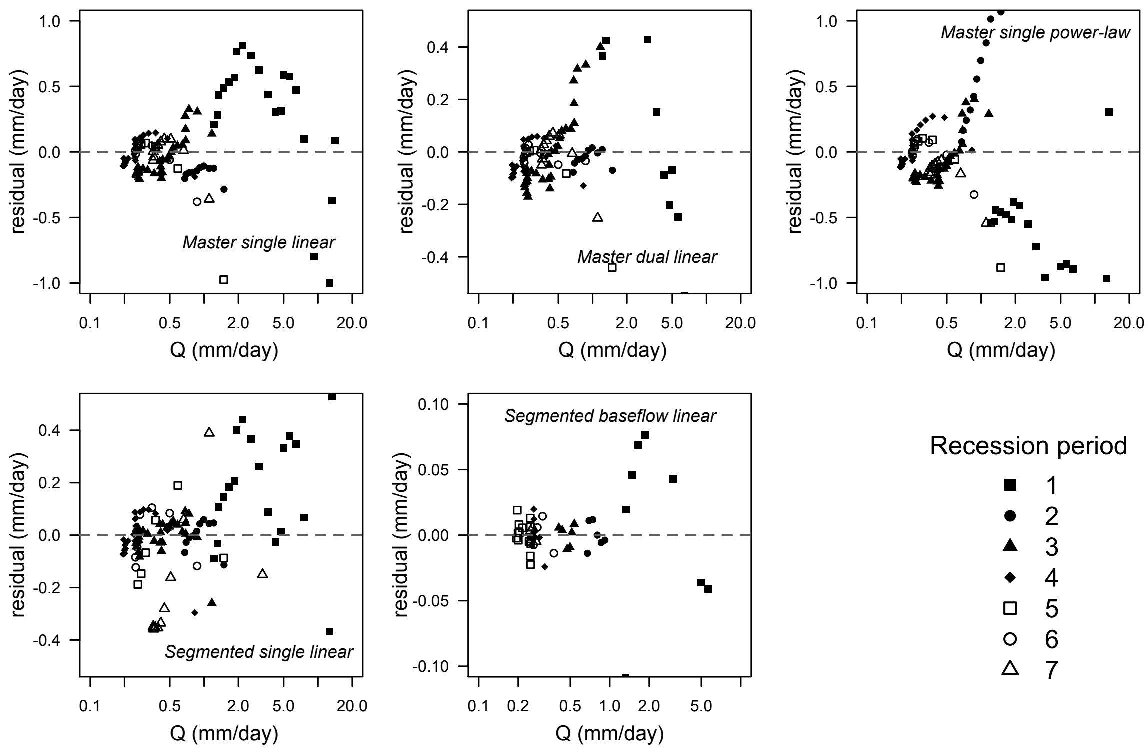

Figure 6.22 Residual distribution from recession model fits for Roberts Creek at the mouth

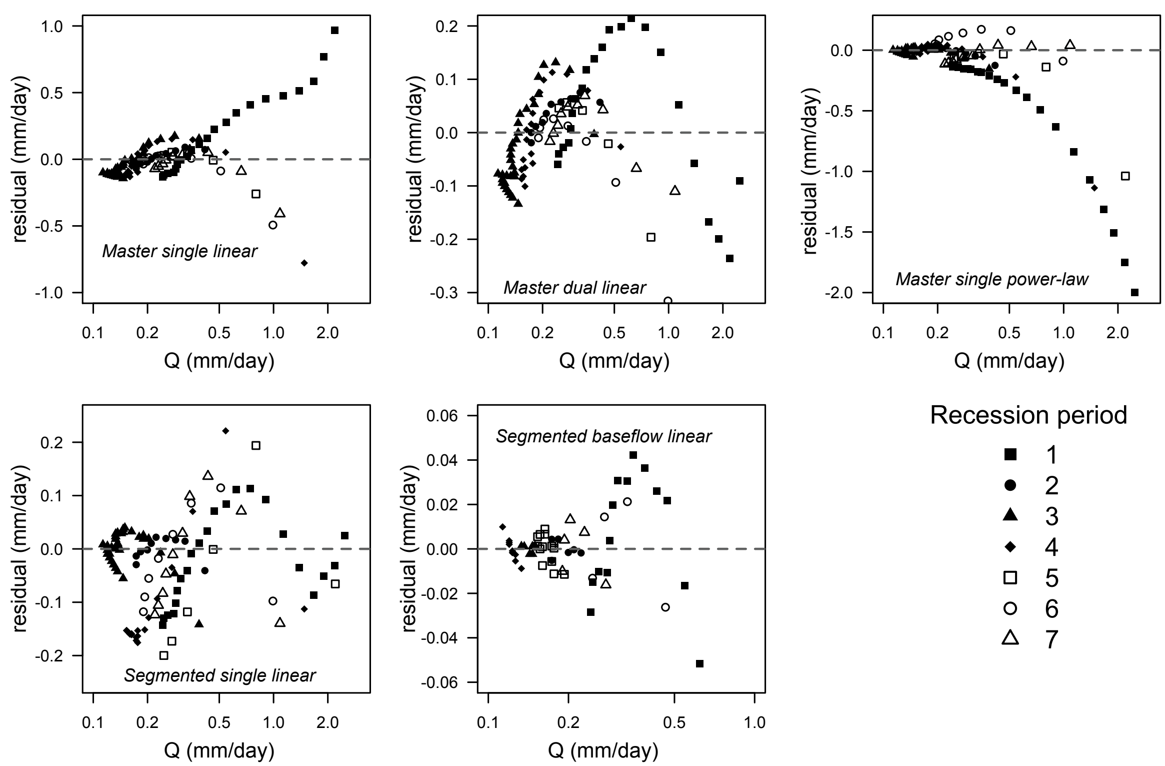

Table 6.4 Summary of recession constant and performances of the models from April to October 2009 (segmented linear models for complete recession periods are not included)

Master curves	**Stephen's Creek at the weir** Recession constant(s)		Loss function value (ε_r)	**Roberts Creek at the mouth** Recession constant(s)		Loss function value (ε_r)
Linear	0.90 (k)		0.293	0.85 (k)		0.408
Dual linear	**0.92 (k_1)** **0.22 (k_2)**		**0.211**	**0.89 (k_1)** **0.20 (k_2)**		**0.307**
Power-law	0.120 (α) 1.05 (β)		0.413	0.049 (α) 2.36 (β)		0.336
Graphical Baseflow *(periods)*	Recession constant (k)	R^2	Residual stand. err. (deg. freedom)	Recession constant (k)	R^2	Residual stand. err. (deg. freedom)
1	0.89	0.98	0.0741 (14)	0.93	0.93	0.094 (13)
2	0.94	0.98	0.0157 (4)	0.95	0.95	0.024 (4)
3a	0.95	0.97	0.0186 (4)	0.98	0.91	0.014 (4)
3b	0.98	0.63	0.0457 (7)	1.00	*NA*	*NA*
4	0.98	0.79	0.049 (12)	0.99	0.66	0.04 (12)
5	0.89	0.90	0.048 (2)	0.81	0.92	0.08 (2)
6	0.98	0.72	0.019 (3)	0.91	0.84	0.06 (3)
7	0.95	0.84	0.052 (6)	0.93	0.95	0.035 (5)

It can be seen from all residual plots that recession period #1 creates a high level of scatter, especially in Stephen's Creek at the weir. As mentioned before, this is likely attributable to snowmelt at higher elevation. Also, the discharge values during that period are about an order of magnitude higher than in the other recession segments.

The master recession analysis found that the dual-linear reservoir approach (serial) models streamflow recession the best based on performances evaluated by the loss function (ε_r = 0.211 and 0.307 for Stephen's and Roberts Creek respectively). This is in accordance with the results obtained by Moore (1997) in a very similar environment, although the loss function value found from calibration was much lower (ε_r = 0.067) – supporting the fact that the recession segments investigated in this study were likely more affected by vertical flows. Due to the large amount of recession constants, the segmented single linear reservoir results are not given in Table 6.4 since the dual-linear master curve seem to explain substantially better the recession characteristics of the watersheds based on the residual plots.

The k recession constant (or the recession slope) gets closer to one the more a river yields a sustained flow in time – which indicates good storage capacity. Based on the master dual-linear analysis, the recession characteristics of the upslope and footslope zones of the catchment vary similarly for both watersheds. The upslope contribution can be interpreted as draining hillslopes after an event – the *k* constant for the upslope zone is 0.22 and 0.20 for Stephen's Creek and Roberts Creek respectively. The footslope contribution is interpreted as the groundwater and riparian contributions (i.e. baseflow) and has a *k* constant of 0.92 and 0.89 for Stephen's Creek and Roberts Creek respectively. Both recession constants are higher for Stephen's Creek headwater, which means that the daily discharge differential is less accentuated than for Roberts Creek at the mouth. Although it is difficult to statistically assess the significance of these small differences in *k* values, if these are validated this would mean that Stephen's Creek headwater catchment generally supports a steadier baseflow than a larger basin such as Roberts Creek, which is an unexpected outcome.

The baseflow-only linear recession constants for the individual recession periods (Figure 6.23) show that Stephen's Creek streamflow is decreasing more rapidly than Roberts Creek during the summer, and the inverse relationship is observed for the autumn. These apparent relationships were tested separately with paired Student's *t*-tests (for segments 1 to 4; and 5 to 7) and the results were not considered statistically significant for neither season ($p > 0.09$ and $p > 0.24$). It should be said that these statistical tests perform better with a greater sample size (i.e. more recession segments).

Figure 6.23 Baseflow-only linear recession constants for Stephen's Creek and Roberts Creek per period investigated

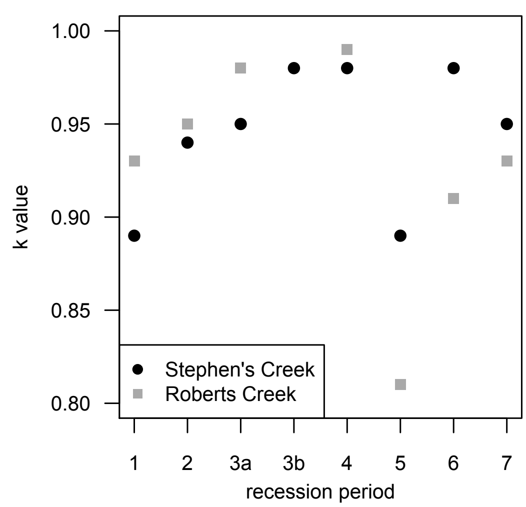

7 Discussion

7.1 Summary of Key Findings

(1) Snowmelt started on April 7th with an average intensity of 10 mm·day^{-1}, peaked in the beginning of June at ~30 mm·day^{-1} before drastically diminishing to less than 5 mm·day^{-1} by mid-June. Large diel fluctuations in snowmelt-output were observed under open forest-canopy and were also clearly identifiable in instantaneous stream discharge records. The antecedent rainfall and melt index suggested high soil-moisture conditions (ARMI > 0.5) from the beginning of May until the middle of June. Consistently high water-levels were monitored at the piezometer from April 12th to May 29th before a sharp drop occurred on May 31st. Distinct counter-clock wise hysteresis patterns were detected for stream discharge records when plotted against shallow groundwater –levels.

(2) The snowpack isotopic signature was negatively correlated with elevation on April 1st, suggesting significant altitudinal isotopic fractionation of snowfall during the accumulation period. This spatial pattern was also detected in snowpack drainage-water samples at all four SLs for the whole monitoring period. Furthermore, an “enrichment” trend was also detected at all SLs in April, suggesting consistent fractionation in space. Daily linear regressions were performed to model the $\delta^{18}O$ signature of snowpack drainage-output and a $\delta^{18}O$ mass-balance quality assessment using pre-melt snow core samples showed that the simulated closure errors for the cells were not significantly different than those computed for the sampling sites.

(3) The runCE two-component hydrograph separation at the weir revealed that event water clearly dominated streamflow (78 ± 26%) a month after the onset of snowmelt – during the peak period of the freshet. It was estimated that event water made up about 24 ± 8% of the streamflow during the July dominated baseflow period. Based on the volume-weighted average 2-IHS method, the contributions of event water to streamflow were indistinguishable between the headwater catchment and the whole watershed from April to June, but was significantly less at the mouth in July (34 ± 11% at the weir vs. 7 ± 7% at the mouth; $p < 0.001$). A major rain-on-snow event, which occurred at the onset of the snowmelt period (April 12th), mainly mobilized pre-event water. For the season, it was calculated that about half of meltwater and rain-on-snow (502 ± 123 mm) directly contributed to groundwater recharge, which is about twice as much as what was calculated with the traditional mass-balance approach (244 mm).

(4) The three-component hydrograph separation method was not successful because it failed to satisfy the condition of non-colinearity of components. Soil water was not sampled prior to the snowmelt season; the silicon concentrations determined from soil water sampled during the event created the most uncertainty. A simulated 3-IHS was performed by assuming a pre-event silicon concentration for soil water based on literature data for a Douglas fir forest. This procedure is not empirical, but the results showed that soil water might have been confounded with event water in the 2-IHS results due to their close isotopic signature. Either way, the outcomes of both methods suggest little groundwater contribution during the bulk part of the spring freshet.

(5) Phosphate and ammonium concentrations in streamflow were below detection limits for the whole study period and nitrate/nitrite remained very low – as expected of pristine forested environments in coastal B.C. Evidence of "flushing" export mechanism was found for nitrate/nitrite in early spring due to high concentrations measured at all sites on the very first day of snowmelt and prior to any significant stream discharge responses. Piezometer data showed a rapidly rising water-level during that period, suggesting fast subsurface mobilization. Pre-event water (probably as soil water) was dominating the hydrograph when the flushing occurred. The skewed distribution prevented parametric statistical analysis to be performed during early spring only. Concentrations were under detection limits for most of the month of May and the first half of June when it was determined that very small volume of pre-event water composed the streamflow.

(6) Nitrate/nitrite concentrations in the summer are significantly greater at downstream sites. No correlations were found with stream discharge or subsurface storage water-balance, but summer concentrations at the lower-elevation sampling sites were inversely and significantly related to the antecedent rainfall and melt index (ARMI), suggesting higher yield during drier soil moisture conditions. Due to insufficient ecosystemic and water quality data, it is hard to assess the mechanism causing their variance in time.

(7) Recession flow modelling was complicated by evapotranspiration and by isolated input from the remnant snowpack affecting the discharges of the first recession limb. The dual-linear reservoir master recession curve performed the best for Roberts Creek and Stephen's Creek. It was determined that upslope and footslope recession constants (k_1 and k_2) are higher for Stephen's Creek than for Roberts Creek, suggesting a more sustained baseflow for the snowfed headwater catchment. Segmented linear baseflow analysis showed the opposite relationship during the spring and summer period – however, the small differences in k values between watersheds were not considered statistically significant and these results are somewhat uncertain because only a few days were used to make up each segments.

7.2 Snowmelt Runoff Mechanisms in Stephen's Creek

Saturated throughflow (or interflow) is a common stormflow generating mechanism in forested catchment with shallow soil underlain by impervious basal till or bedrock (Weiler *et al.*, 2005) – which are very common in British Columbia. Hutchinson and Moore (2000) studied throughflow variability using an extensive piezometric network during rainfall events in the UBC Research Forest close to Vancouver. They found that the shallow water-levels were well correlated to surface topography during high flows only, which suggest a controlling effect of decreasing hydraulic conductivity with depth on stream discharge during rainfall events. Because storm events are short-lived and assumed more intense compared to snowmelt events, it is unclear if saturated throughflow has the same dominating role during the freshet, or if matrix-dominated diffuse processes in near-stream zones (i.e. piston-flow or translatory flow) are preponderant. This question was addressed by monitoring subsurface water-level and conducting hydrograph separations.

7.2.1 Piezometric interpretation: lateral or vertical flow?

The piezometer was not located in the riparian area (discharge zone) nor on a hillslope (recharge zone) but in a geomorphic hollow, which can be considered both a recharge or discharge zone depending on soil moisture conditions. Therefore, it is difficult to determine if rising water-levels are an indication of lateral saturated throughflow or rising water-table. The literature was consulted to see how similar piezometric results were interpreted. Kendall *et al.* (1999) have investigated runoff flow paths during snowmelt in a Vermont catchment underlain by glacial till using chemical tracers and a large number of wells (n = 18) distributed on hillslopes (recharge zone) and in the riparian area (discharge zone). They found opposing characteristics between both environments. The hillslope sites had very low water-levels (some were "dry") prior to snowmelt and a greater total rise at peak melt than for wells located in discharge zones. As opposed to riparian sites, diel fluctuations were not discernable at the hillslopes – the piezometric surface was continuously rising as snowmelt progressed, indicating that subsurface storage was filling-up. Water-levels remained above pre-melt levels well into the recession period, contrarily to riparian sites which receded prior to peak discharge. Counter clock-wise hysteresis patterns were observed at the hillslopes, but clock-wise behaviour was typical of riparian sites. Another investigation, but at a smaller scale, took place close to the research area on the Sunshine Coast (B.C.) in Gray Creek headwaters (Kim, 2001; Kim *et al.*, 2004). The authors reported clock-wise hysteresis loops and diel fluctuations between a riparian pit-outflow and shallow groundwater-level, which is consistent with the Kendall *et al.* study (1999) and the observations made in this present study. All these characteristics indicate that the piezometer in the research catchment was monitoring a perched water table fed by hillslope contributions from a large area as opposed to riparian groundwater-levels. Another supporting factor is that the pool sustained high water-levels long after the snow has melted in the vicinity of the instrument (despite the fact that it was installed in a highly conductive deposit) before pore-water suddenly drained at the end of May – probably due to an abrupt cessation of hillslopes hydrologic connectivity. This piezometeric "collapse" occurred when the snowline reached 1100 m on the southeast facing aspect. Evapotranspiration increased by 122% between the last two weeks of May (May 18th to 24th: 0.36 ± 0.24 mm; May 25th to May 31st: 0.8 ± 0.45 mm) based on the Brook90 model. This increase is significant but small in absolute terms and is not likely to explain on its own the fast water-level drop observed at the piezometer.

The asynchronous peak of the antecedent rainfall and melt index (AMRI) on June 3rd compared to the high piezometric levels (throughout April and May) is somewhat suspicious, but can be explained by the delayed occurrence of snowmelt at high elevation since ARMI is weighted by area.

7.2.2 Event water dominating the hydrograph? Methodological considerations

The two-component hydrograph separation showed that event water composed most of the hydrograph during the bulk part of the spring freshet. This is a very unusual outcome, most 2-IHS studies found that pre-event water makes up most of the streamflow; sometimes a larger fraction of event water is found during snowmelt, possibly due to overland-flow on soil frost (reviewed by Buttle, 1994; Laudon, 2004) – but this fraction rarely exceeds 50%. IHS methods are built on assumptions often hard to verify (e.g. well mixed pre-event reservoir), therefore methodological uncertainty may arise and explain the discrepancy observed in this study. Four issues are addressed: the clarity of the event water signal, the event water dynamics, the soil water contribution and the size of the pre-event water reservoir.

(1) Clarity of the signal: The sensitivity of the separation is exacerbated by the small difference in isotopic signature between the event and pre-event water – ranging by only 1.14‰ to 1.5‰ during peak melt. This comes as a surprise since the traditional asset of IHS during spring freshet is that the large volume of depleted water infiltrating the ground in a short period of time acts as an ideal tracer (Rodhe, 1998). One might think that the isotopic seasonal signal may not be as pronounced in coastal regions, but long-term precipitation data collected at Saturna Island (Figure 7.1) shows that the seasonal variation is about 5‰ on average.

However, a volume-weighted (VW) average of Saturna's precipitation reveals that fall and winter isotopic signature is more representative of the signal attached to groundwater recharge due to the seasonality of precipitation. The lighter signature found for the deep groundwater in Gibsons could be indicative of selective recharge during snowmelt as observed by Krabbenhoft *et al.* (1990) in a lake-dominated ecosystem, but this would be a preliminary inference to be verified since no comparative time-series data can support the fact that the mean and variance of the isotopic dataset on Saturna Island is representative of Gibsons' precipitation. Also, the recharge area for Gibsons' aquifer (300 m to 1100 m) lays at higher elevation than the Saturna rain gauge (178 m). Undoubtedly, a more successful separation would have been achieved during a summer storm event.

Figure 7.1 Isotopic signature of precipitation on Saturna Island, B.C. (located 85km south of the research catchment) from 1997 to 2006 inclusively. *Source: Canadian Network for Isotopes in Precipitation (CNIP), 2009*

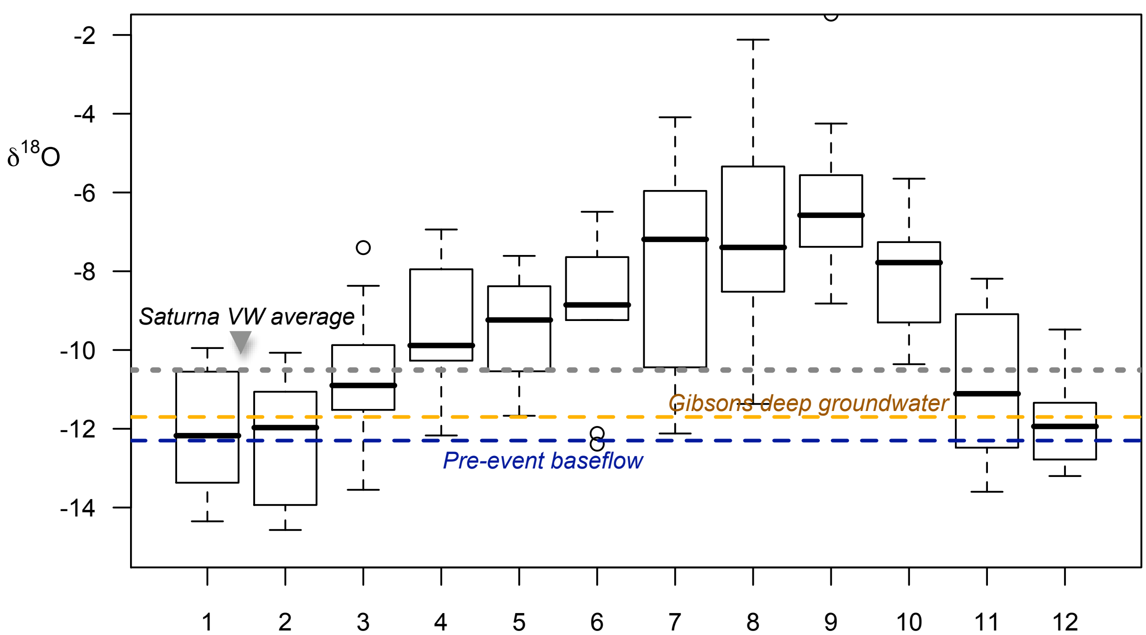

(2) Event water dynamics: Although it has been rarely observed in published studies, many authors argue that IHS during snowmelt is questionable because of spatial variability in the event water signal (see section 5.1.4). To the best of my knowledge, only one other study (Whyte, 2004) attempted a two-component hydrograph separation during snowmelt in B.C.'s mountainous landscape. The author was unsuccessful to characterize spatial variation, partly due to a lack of correlation with elevation at three out of eight 1.5 m^2 snowmelt lysimeters; consequently, the results could not be quantified. A similar sampling design for snowpack drainage water was used in the present study but the catchment area was up-scaled to 6 m^2, which likely contributed to buffer plot-scale anomalies in the snowpack isotopic release. Spatial variability was indeed detected, but all sampling sites were well correlated with elevation and the uncertainty calculation factored in the 0.44‰ error due to unexplained variance. The runCE model accounted for temporal variability and transfer time to streamflow, although it is admitted that a deterministic approach would be more desirable. Considering all those factors, it is concluded that the paired snowmelt modelling and isotopic regression approach captured most of the event water dynamicity. Therefore, snowmelt spatial variability was probably not a major issue in this study.

(3) Soil water contribution: The errors due to subsurface heterogeneities were not assessed before snowmelt started and these are likely a much bigger challenge for this hydrograph separation. Similarly to most studies, baseflow signature was used to characterize pre-event water and the analytical error to define its uncertainty. The colinearity between the subsurface samples taken during the event and the isotopic composition of baseflow and snowmelt insinuates that streamwater and soil water are well-mixed products of two major isotopic reservoirs. However, it is most plausible that pre-event soil water kept the memory of antecedent rainfall events in November (and winter melt events), which means that its signature could very well be close to the value that was sampled *during* the event. An argument supporting this thesis comes from the small variation observed in the soil water isotopic composition both in time and space compared to the variation of the snowmelt signature. If this turns out to be valid, the hydrograph separation would merge event water with an important fraction of soil water that was there long before the snow was deposited on the ground – resulting in an important overestimate of event water. This scenario suggests that the components partitioned in this 2-IHS study would in fact be snowmelt/shallow soil-water vs. deeper soil water/groundwater/riparian water, instead of the traditional event vs. pre-event water. Another possibility is to claim the “status quo” in respect to the assumptions of the 2-IHS – suggesting that soil water had the same isotopic signature as pre-event baseflow prior to the onset of snowmelt. In this case, the event water computed by the separation would be a sound estimate of the real hydrological conditions of the catchment. This scenario is considered unlikely since most IHS studies indicated an overwhelming presence of pre-event water in streamflow. It is concluded that the partitioned event water may also include a large fraction of soil water.

(4) Storage over-turn: The last issue addressed the total storage available in Stephen's Creek catchment. After a thorough literature review on the subject, it was found that only Sueker *et al.* (2000) conducted a 2-IHS and a 3-IHS study during a comparable snowmelt season in terms of magnitude (~3 to 4 months freshet) as opposed to ~1 month for most other studies (e.g. Dincer *et al.*, 1970; Buttle and Sami, 1990; Laudon *et al.*, 2002; Laudon *et al.,* 2004; Laudon *et al.,* 2007). Sueker *et al.* (2000) compared 6 adjacent subalpine/alpine watersheds in Colorado with different physiological characteristics but under similar elevation. Based on the study site's description, three catchments (Fern Creek, Spruce Creek and Fall river) were comparable to Stephen's Creek in terms of average slope, substrate and forest cover – although their area is considerably larger and the soil thickness is not quantitatively defined but presumed thin. Similar results were found in all three systems as the present study, with a large fraction of pre-event water during the initial period (~ 50%) and event water composing most of the streamflow during the peak melt in June (up to 76%). The authors interpreted those results as an initial migration of most pre-event/reacted subsurface water during the early season followed by a gradual replenishment of the subsurface storage by event/un-reacted snowmelt water. Pre-event water dominated the hydrograph only in the watershed with the shallowest flow-duration curve – indicative of a larger subsurface storage capacity. The study sites and results described in Sueker *et al.* (2000) are very similar to what is observed in Stephen's Creek, and the replication to several watersheds makes their interpretation stronger.

Similarly to what was found in Colorado, the virtual 3-IHS conducted in the present study showed that groundwater/riparian contribution is rapidly increasing during the recession limb after a month-long period when the hydrograph was clearly dominated by event/soil water contributions, despite the fact that the $\delta^{18}O$ signature has not receded to pre-event levels in June. This is likely due to the increase of silicon content in stream water caused by a long-enough transit time of melt-water in the subsurface (subsurface flow is getting increasingly vertical as the hillslopes drain) to allow it to react with resident minerals and phytoliths and gradually acquire the groundwater/riparian chemical signature. Therefore, if the results of the simulated 3-IHS are representative of the real conditions, they would not be in contradiction with the 2-IHS method that found a large fraction of event water (28 to 48%) still composing the streamflow during the recession period.

Figure 7.2 Mass-balance estimates of the principal reservoirs in Stephen's Creek headwater catchment. The simulation period is from April 1s to September 1st inclusively

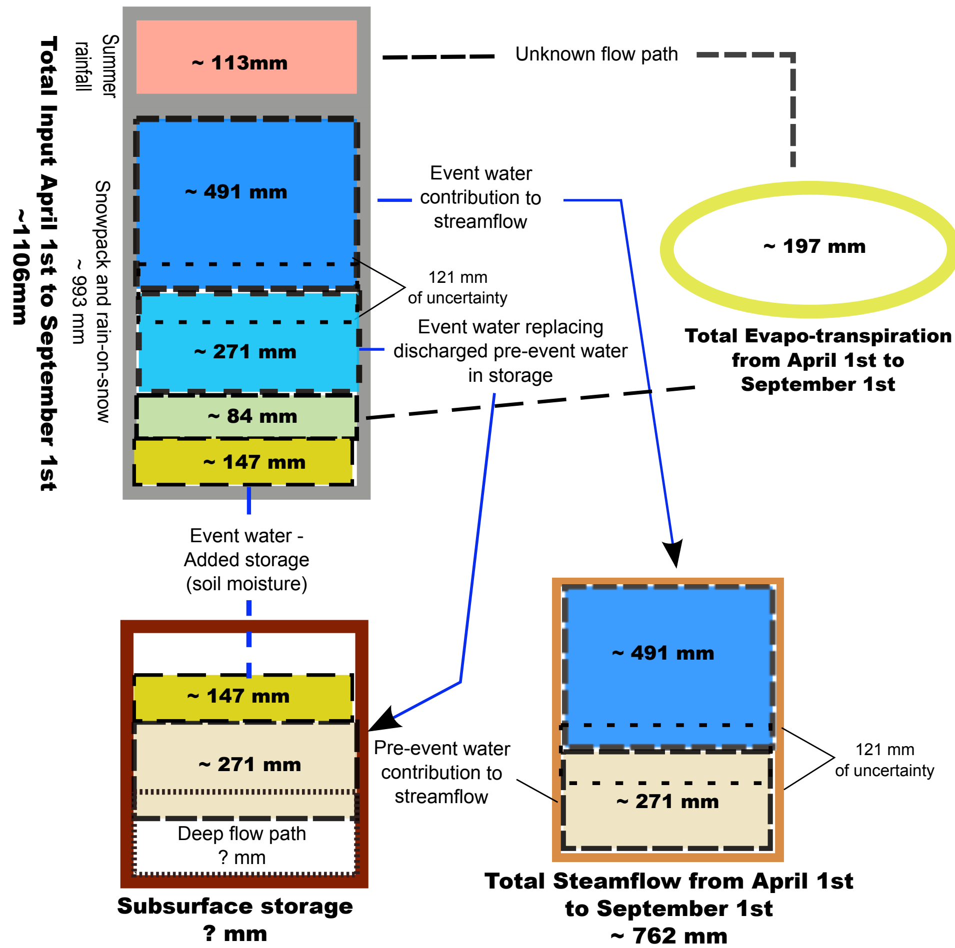

The mass-balance estimates are convincingly supporting a storage over-turn. The traditional water-balance approach revealed that out of 1106 mm of snowmelt/rain-on-snow and summer rainfall released in the catchment, 762 mm contributed to streamflow and 197 mm to evapotranspiration during the spring freshet and the summer season. It is estimated that snowmelt created a net subsurface gain (probably as soil moisture) of ~147 mm to be carried over after September 1st (Figure 7.2). However, this value may be overestimated since it is plausible that a fraction of soil water was confused for event water in the two-component separation, as explained above. Also, subsurface or surface trans-boundary runoff was assumed negligible.

These mass-balance estimates suggest that spring snowmelt had a net impact on recharge, even after summer ended. These figures were partly obtained by modelling the evapotranspiration flow using Brook90. The results were not calibrated to soil moisture or saturated groundwater-levels data. Therefore, a significant margin of error is to be considered and any interpretations should be kept qualitative, despite the figures.

Based on the study done by Sueker *et al.* (2000) and supported by the mass-balance estimates calculated above, it is proposed that shallow subsurface storages in Stephen's Creek were over-turned by the large volume of event water infiltrating the soil. The increasing pre-event fraction dominating the hydrograph again in July suggests that deeper flow-path did not undergo a similar "flushing", but were partially replenished with event water.

7.2.3 Hydrograph separation at the mouth: the influence of storage on low flows

The 2-IHS at the mouth added an un-quantifiable uncertainty in the event water signal compared to the separation at the weir since generalization had to be made regarding the snowmelt flux (some sectors were not modelled by YAM, but extrapolated) and the contributing area (limited to 670 m and higher). Also, the impact of rainfall below the snowline on stream isotopic signature was dismissed. It was argued that these sources of error would favour pre-event water, but statistical tests revealed that no significant differences in event water contributions between the downstream and the upstream sites existed during most of the snowmelt season. Significant differences in event water contributions were only found in July (34 ± 11% vs. 7 ± 4%). Rainfall is not believed to have affected stream signature since summer streamflow was sampled during baseflow periods only. These findings reinforce previous results by demonstrating that hillslopes and event water from headwater catchments are the main sources of water downstream during prolonged freshet. The large difference found in July can be explained by the fresh recharge that took place in the headwaters only, which likely affected deeper flow paths as opposed to the downstream site. Therefore, the event water measured at the mouth and at the weir are arguably the same in terms of absolute volume, but the contribution of older riparian water increasingly "dilutes" the headwater baseflow as it travels downstream. This would be in contradiction with isotopic evidences obtained by Laudon (2004) from a smaller freshet in a Swedish watershed, who reported that deep flow path (>90 cm deep) at a section located 4 m away from the stream was not affected by snowmelt input. It is argued that the much larger volume of snowmelt observed in B.C.'s coastal landscape makes the direct comparison between both sites irrelevant. However, it is acknowledged that subsurface sampling of hillslope and riparian water would have been a more desirable sampling scheme to address this topic with increased confidence.

7.2.4 The role of landscape characteristics on snowmelt runoff

Due to equipment failure, it was impossible to determine the role of peat bog's surface water or gleysols (hydrophilic soil with high organic content) on runoff generation. A small area of gleysols, which developed on a sloping surface (10-15°), was identified in the headwater and initially monitored for subsurface water level fluctuations. The two probes were unfortunately destroyed under the weight of the snowpack and all data were lost. Saturated overland-flow was observed at some locations during the late melt season; thus it is believed that these areas are potentially an important source of quick runoff. Kværner and Kløve (2006) found that small increases in peatland's slope angle could significantly reduce the ability of the soil to retain event water.

Ditches along roads can interrupt lateral flow and enhance rapid runoff during storm or snowmelt events (Wemple *et al.*, 1996). Important surface runoff was observed on the access trail (a decommissioned logging road) going up the catchment (close to SLC – Figure 3.1) – creating deep erosion gullies over time. In July 2009, the dimension of the largest was approximately 80 cm wide and 50 cm deep. The discharges observed in these gullies during peak melt were estimated to 5-10 liters per second at most. Unlike what was observed by Whyte (2004) in the Slocan Valley, the water joined the creek at a lower junction; therefore, no trans-boundary runoff was suspected. The impacts of landscape characteristics and ditches on streamflow are not the focus of this study, but they certainly played a role in the rapid delivery of event/soil water to the stream.

7.2.5 Lateral flow as a dominant flow path during snowmelt: a paired interpretation of isotopic and piezometric data

The data presented in this study have an undeniable level of uncertainty as repetitively mentioned before. However, the IHS results clearly indicate that spring runoff is dominated by a large contribution of snowmelt water and/or soil water, which is consistent with piezometric levels, suggesting active lateral flow. Saturated throughflow is known to be an important runoff mechanism during rainfall events in coastal B.C. (Gibson *et al.*, 2000; Hutchinson and Moore, 2000) and it was hypothesized in this study that a mechanism involving more vertical flow, such as translatory flow (Hewlett and Hibbert, 1967), would be preponderant during snowmelt. The findings I presented here cannot support such a proposal. Therefore, it is concluded that the runoff mechanisms at play during snowmelt are similar to the runoff mechanisms reported during rainfall events of comparable intensity and under similar antecedent soil-moisture conditions.

The interpretation of isotopic data indicates a shallow subsurface storage overturn during the freshet. Based on the July baseflow sampling, it was argued that deep subsurface flow paths (groundwater/riparian reservoirs) were significantly affected by spring recharge in the headwater catchment compared to the downstream environment. Nested subsurface sampling on hillslopes and in the riparian zone would be necessary to confirm or infirm these preliminary IHS results.

7.3 Nitrate Export to Streamflow and the Ecosystemic Approach

Many leading scientists in hydrology and ecology are calling for a more integrated "catchment science" pairing hydrometric, geochemical and isotopic tracer(s) methods with water quality monitoring and detailed ecological survey in order to enhance our understanding of the interactions between the water cycle and the environment (e.g., Bond, 2003; McDonnell *et al.*, 2007; Tetzlaff *et al.*, 2007). The nutrient sampling campain done in this study is supplementing the isotopic and hydrometric analyses: identifying dominant nutrient export mechanisms help better define the complexity of the system by giving a complementary perspective on runoff processes. Streamflow was sampled for nitrate/nitrite concentrations during the study period and different export mechanisms were observed in early spring compared to late summer. A typical "flushing" as defined by Hornberger *et al.* (1994) was detected in early April at the onset of snowmelt and prior to any significant increase in stream discharge. The distribution of nitrate concentrations between upstream and downstream sites was highly uneven spatially and temporally, supporting the flushing hypothesis. Creed *et al.* (1996) described this process as a NO_3^-/NO_2^- accumulation in soils characterized by a high saturation deficit being rapidly exported by a water table rising in conductive layers. The transiency of the high concentrations is explained by the supply being rapidly exhausted. In the present study, the flushing occurs when pre-event water is dominating the hydrograph – but probably as soil water, as suggested by the simulated 3-IHS results. The observation of this nutrient transport mechanism supports the predominance of rapid lateral flow paths early into the melt. It was hypothesized in section 2.5 that forested areas at high elevation were more prone to nutrient flushing during the onset of snowmelt because of a lesser vegetative demand over the winter. The hypothesis could not be tested with the chosen statistical methods due to non-normal distribution of the data. Also, qualitative interpretation cannot be achieved since no patterns are distinguishable between sampling sites. After the initial flushing occurred, nutrient concentrations are consistently under detection limits during most of the snowmelt period. Event water and shallow soil water were dominating the hydrograph during peak melt, which would dilute any concentrations possibly present in deeper flow paths.

Nitrate/nitrite concentrations gradually gained importance during the late summer but remained well under the peak values observed during the flushing event. The unequivocal spatial and temporal organization of the concentrations is an indication that a different nutrient export mechanism is at play. A clear relationship between sampling sites was statistically confirmed at a high level of significance and is consistent with previous results since it is presumed that a large fraction of water from deeper flow paths in the headwaters was replaced with melt water containing undetectable nitrate/nitrite concentrations. These results suggest that late summer nitrate concentrations are released by increasingly older water from deeper flow paths feeding the channel. The temporal variation is consistent between sampling sites, indicating that (a) regional control(s) of some sort explain(s) this variance. It is hard to rationalize these fluctuations since multiple colinear factors may be acting simultaneously. The advance of the growing season typically means more nutrient uptakes, but the nitrification of ammonium (NH_4+) in the soil may exceed the uptakes and accumulate in shallow horizons. This is not likely to have an immediate impact on stream's concentrations at low flows but short-lived and intense summer storms could transport the solutes to the riparian zones. Also, aquatic uptakes is non negligible during the summer, which also complicates that dynamics. Not to mention that nitrate is sensitive to reduction processes in anoxic environment. An integrated biogeochemical/ecosystemic approach would be better suited to model the nitrogen cycle and explain these temporal variations in streamflow by pairing it with the water cycle. For instance, soils were assumed similar across Stephen's Creek watershed since detailed soil surveys were not undertaken. This sort of information would be valuable since soil's depth and geochemical signature are factors affecting nutrient dynamics.

The evidence presented above of alternating nutrient export mechanisms during the spring and the summer are somewhat consistent with the results obtained by Creed *et al.* (1996) and Creed and Band (1998) in Ontario and by McHale *et al.* (2002) in an Appalachian catchment; however, both authors observed relatively high nitrate concentrations in deeper flow paths (glacial till) – which is not the reality for coastal environments. Also, those studies have identified translatory flow as the dominant runoff mechanism explaining flushing export, and McHale *et al.* (2002) found that groundwater was the main contributor to streamflow for the six storms monitored. Again, evidence presented before suggest a much different hydrological dynamic during snowmelt in coastal catchments. The flushing export was instead created by saturated throughflow, but the draining state was similarly controlled by old water contribution – at significantly lower concentrations.

7.4 Low Flows and Interpretation of Recession Constants

Summer low flows were lower for Roberts Creek at the mouth than for Stephen's Creek at the weir, even after considering a 10% margin of error due to rating curves and catchment area. This result alone comes as a surprise since it is usually considered that steep headwater catchments have a poor storage capacity, and as a result yield very little water during baseflow-dominated period. The rating curve standard error is estimated at 8% for Stephen's Creek at the weir, and at 5% for Roberts Creek at the mouth as per Water Survey of Canada standards. It was demonstrated that the accuracy of discharges measurements using the traditional velocity-area approach during low flows decrease with decreasing discharges (Moore *et al.*, 2007). However, the rating curve is assumed accurate at low flows for the summer of 2009, since a WSC hydrometric technician conducted discharge measurements in May, June, July and September; and the lowest measurement in 5 years was obtained during the July visit (Ferguson, 2010 – personal communication).

Lower specific discharges at Roberts Creek are echoed by the master recession constants modelled for both watersheds. The dual-linear reservoirs model proposed by Moore (1997) for steep coastal watersheds with shallow soil was the most appropriate for both systems. The differences in recession constants ($k_{1,2}$) representing upslope and footslope reservoirs between each watershed are very small, and could possibly be explained by rating curve errors or biased recession segments. However, these results are coherent with the positive net balance of snowmelt on recharge since it suggests that baseflow deceases slower in Stephen's Creek as opposed to Roberts Creek. It is difficult to imagine by which mechanism, under similar snow conditions, vegetation and climate, a headwater catchment could sustain a larger baseflow than a bigger basin with presumably more storage capacity. Two hypothesis are proposed.

First, the storage capacity of Roberts Creek is assumed larger because it drains a bigger gently-sloping area with enhanced sediment deposits downstream. This assumption is wrong, and in fact the storage capacity – weighted by area – is about the same (or even larger) for Stephen's Creek headwater catchment. Gravitational water has a shorter residence time in steep slopes, diminishing the amount of saturated water that can be stored in the footslope zone. Other landscape characteristics can positively influence storage in a headwater catchment, such as debris jams along the creek or geological complexities (e.g. fault line). Saturated gleysols or rainfed peat bogs can also have an influence on water yield during rainfall or snowmelt events, but it is believed that they contribute very little to baseflow since most of those landmarks are assumed disconnected from groundwater flow paths, and they are not prone to matrix flow due to their high organic content. Evidence supporting this claim comes from Gibson *et al.* (2000), who estimated that bog-groundwater accounted for less than 3% of streamflow during a summer rainfall event in a coastal bog-forested upland catchment close to Prince-Rupert, B.C., based on isotopic, biogeochemical and hydrometric evidences.

The second hypothesis addresses the actual volume of water stored in each watershed, as opposed to their capacity to store water. Because the recession analysis was carried out for a period of the year prior to which only the snowmelt-dominated catchment was subject to "deep" subsurface recharge, this hypothesis assumes that the storage in Roberts Creek is generally somewhat depleted during the early summer compared to Stephen's Creek catchment. When the summer begins, Roberts Creek baseflow mines into deeper and less conductive flow paths while Stephen's Creek can rely on "spilling" storages. Short-lived rainfall events would be less very effective at recharging deeper flow path, which would explain the steeper recession limbs observed at Roberts Creek following September rainfall events (Figure 6.19). It would be interesting to know if this recession pattern between Stephen's Creek and Roberts Creek is consistent for years with very shallow snowpack. An equally palpable difference between both systems would confirm that Stephen's Creek catchment has increased storage capacity compared to Roberts Creek – assuming negligible inter-annual storage memory. However, if higher recession constants would be discernable only during years with significant snow accumulation, this would indicate that snowmelt is unequivocally recharging deep flow paths at a level that cannot be matched by winter rainfall events – enhancing baseflow months after the snow has melted. This reflection lays ground to some interesting questions to be considered for future research.

The recession analysis presented in this study offers insights on what could be significant differences between the low flow hydrology of rainfed and snowfed dominated systems. The second hypothesis presented above, which suggests that snowmelt significantly impacts deep subsurface flow paths and baseflow yield far into the summer/early autumn, is consistent with isotopic results and judged more credible than the *a priori* hypothesis concerning the possible enhanced storage capacity of the headwater catchment. However, this finding remains ambiguis since the evapotranspiration demand between the headwaters and lower elevation areas were assumed similar – which is, in reality, hard to determine given the complexity of the environment. A warmer climate at lower elevation promotes an increased evaporative flux and a longer growing season, while the younger regrowth composing most of the forest in the headwater catchment typically consumes more soil-water than older growth.

8 Conclusion

The aim of this research was to enhance the understanding of snowmelt processes in coastal watersheds and create a more informed dialogue in the communities about how to adapt to the regional impacts of climate change on water resources. Three main aspects were covered during this project: snowmelt runoff generation processes, nutrient export to streamflow and recession analysis between two contrasting watersheds.

The impact of climate change on late summer low flows have been mentioned in many studies (e.g. Leith and Whitfield, 1998; McCarty *et al.*, 2001), but the hydrological processes by which those changes could be materialized – from a snowfed to a rainfed regime – have never been empirically demonstrated, as far as I am aware. Despite the isotopic methods being tainted with uncertainties, the results of the present study are clear and consistent with piezometric data, nutrient loadings and recession modelling. Snowmelt was monitored in the headwaters of Stephen's Creek watershed and isotopic data indicated that the main contributor to streamflow initially in April was pre-event water, mainly as groundwater. The snowmelt intensity greatly increased during the month of May and June and direct contributions from the snowpack and the soil clearly dominated the hydrograph. It was concluded that only saturated throughflow could explain such a rapid response from the hillslopes, which suggest that the main runoff mechanism operating during snowmelt events is the same as what is commonly observed during rainfall events in steep coastal environment. It was suggested that the large input of melt water was sufficient to over-turn the shallow subsurface reservoir and a fraction of the deeper groundwater/riparian reservoir since snowmelt could be traced late into the summer during baseflow dominated period at the headwater site. It was also proposed that the balance of snowmelt/rainfall inputs and stream discharge/evapotranspiration between April 1st and September 1st was positive in the headwater catchment – suggesting a net recharge to be carried over into the next hydrological year. Further isotopic and nutrient sampling at the mouth of Stephen's Creek revealed that headwater hillslopes are the main downstream source of water during the freshet, but downstream groundwater/riparian reservoirs dominate the streamflow from July and onwards.

A spatially disorganized flushing mechanism occurring prior to any significant increase in stream discharge controlled nitrate/nitrite exports to streamflow in early April. Nutrient concentrations were under detection limits for most of the spring freshet period, but gradually increased in July with drier soil moisture conditions. Late summer loadings were controlled by groundwater/riparian seepage and were significantly higher in downstream sites. A consistent temporal pattern was observed at all sites but could not be explained.

Finally, recession analysis between Stephen's Creek and Roberts Creek suggested that the small snowfed headwater catchment could sustain a given baseflow for a longer period of time than the larger rainfall-dominated watershed. It was proposed that their storage capacities were similar, but riparian reservoirs were saturated in Stephen's Creek at the onset of summer due to the extensive snowmelt season, as opposed to Roberts Creek, resulting in an enhanced capacitiy to support baseflow during late summer. The recession analysis results are consistent with isotopic evidence, suggesting that deep groundwater recharge occurred due to snowmelt inputs. However, the role of evapotranspiration between the headwaters and the lower areas of the watershed should be better characterized in order to dissipate the ambiguity of this surprising finding.

It was initially hypothesized in the first and second chapter of this thesis that groundwater recharge could be enhanced during snowmelt due to a runoff mechanism involving more vertical flow as opposed to lateral flow. It was found that the dominant runoff mechanism during snowmelt events was in fact rapid lateral flow. However, delayed runoff (i.e. vertical flow) undoubtedly occurred in large amount but did not dominate the hydrograph at any time due to the overwhelming importance of saturated throughflow. Vertical matrix flow is diffuse and travels at much slower velocities, but a constant input of water for about two months kept the soil moist and conductive and was successful to significantly recharge deeper flow paths – something that could presumably not be achieved at the same level if that water would have fallen as rain during discrete events.

Evidence presented in this study indicate that climate change has the potential to negatively impact late summer baseflow in watersheds that are currently considered "hybrid" such as Chapman Creek and Gray Creek. The absolute decrease in streamflow is unknown but could be significant, especially during years with high summer evapotranspiration. Water conservation programs have been proven successful to control water demand growth, but multiple approaches are suggested in order to secure a viable aquatic environment in exploited creeks.

Bibliography

Allan J. David (1995), Chapter 13 – Nutrient Dynamic in: *Stream Ecology: structure and function of running waters*, Springer, Drodrecht, The Netherland, 283-304

Allen D.M., J. Scibek, P. Whitfield and M. Wei (2004), Climate Change and Groundwater: Summary Report, *Final Report for Climate Change Action Fund, Natural Resources Canada*, Project A369, 404pp.

Anderson, A.E. (2008), Patterns of water table dynamics and runoff generation in a watershed with preferential flow networks, Ph.D. thesis, Faculty of Graduate Studies (Forestry), University of British Columbia, unpublished

Anderson, M.G. and T.P. Burt (1980), Interpretation of recession flow, *Journal of Hydrology*, **46**, 89-101

B.C. Ministry of Environment (2009), Summary of water licenses for Chapman Creek, Water License Web Query – Water Stewardship Division, available online: http://a100.gov.bc.ca/pub/wtrwhse/water_licences.input

B.C. Ministry of Environment (2009b), Historic snow survey data for British Columbia, Government of British-Columbia, consulted on October 10th 2009, available online: http://a100.gov.bc.ca/pub/mss/stationdata.do?station=3A26

B.C. Ministry of Forests & Range (2008), Biogeoclimatic ecosystem classification subzone/variant map for the Sunshine Coast forest district, Government of British Columbia, Victoria, BC

Baker T.E. and J.B. Nyberg (1974), Chapman Creek integrated resource management study, Experimental project 732, British Columbia Forest Service, Victoria, BC

Bako, M.D. and A. Owoade (1988), Field application of a numerical method for the derivation of baseflow recession constant, *Hydrological Processes*, **2**, 331-336

Barnes, B.S. (1939), The structure of discharge recession curves, *Transactions – American Geophysical Union*, **20**, 721-725

Barnett, T.P., J.C. Adam, D.P. Lettenmaier (2005), Potential impacts of a warming climate on water availability in snow-dominated regions, *Nature*, **438**, 303-309

Benda L., M.A. Hassan, M. Church, C.L. May (2005), Geomorphology of Steepland Headwaters: the transition from hillslopes to channels, *Journal of the American Water Resources Association*, **41**, 835-851

Bengtsson, L. (1985), Characteristics of snowmelt induces peakflows in a small northern basin, *Nordic Hydrology*, **16**, 137-156

Berka C., H. Schreier and K. Hall (2001), Linking water quality with agricultural intensification in a rural watershed, *Water, Air, and Soil Pollution*, **127**, 389-401

Beven K.J. (2006), Streamflow Generation Processes, *Benchmark Papers in Hydrology – International Association of Hydrological Sciences*, McDonnell J.J. [ed], 431p.

Bond, B. (2003), Hydrology and Ecology meet – and the meeting is good, invited commentary, *Hydrological Processes*, **17**, 2087-2089

Bonell, M. (1998), Selected challenges in runoff generation research in forests from the hillslope to headwater drainage basin scale, *Journal of the American Water Resources Association*, **34**(4), 765-785

Buttle, J.M. (1994), Isotopic hydrograph separations and rapid delivery of pre-event water from drainage basins, *Progress in Physical Geography*, **18**(1), 16-41

Buttle, J.M. (1998), Fundamentals of small catchment hydrology, in: Kendall, C. and J.J. McDonnell (Eds.), *Isotope Tracers in Catchment Hydrology*, Elsevier, Amsterdam, pp.1-49

Brantley S.L., Y. Chen (1995), Chemical weathering rates of pyroxenes and amphiboles, in: White A.F., S.L. Brantley (Eds), Chemical Weathering Rates of Silicate Minerals, *Reviews of Mineralogy*, Volume 31, Chelsea, Michigan, pp.119-172

Brodie, R.S. and J.J. Hostetler (2005), A review of techniques for analysing baseflow from stream hydrographs, *Australian Government Connected Water Project*, available online: http://www.connectedwater.gov.au/documents/IAH05_Baseflow.pdf (2010)

Brooks, R., H. Barnard, R. Coulombe and J. J. McDonnell (2010), Ecohydrologic separation of water between trees and streams in a Mediterranean climate. *Nature-Geoscience*, **3**, 100-104

Calder, I.R. (1992), Hydrologic effects of land-use change, In: Maidment D.R. [Ed], *Handbook of Hydrology*, McGraw-Hill, New-York, pp.13.1-13.5

Canadian Network for Isotopes in Precipitation (2009), University of Waterloo, Canada. Data provided by Jean Birks, Adjunct Professor, Department of Earth Sciences, University of Waterloo, Canada

Cayan D., R. Laprise (1999), A semi-implicit semi-lagrangian regional climate model: the Canadian RCM, *Monthly Weather Review*, **127**(3), 341-362

Carson, Brian (2008), Professional geoscientist (P.Geo) and local consultant (Carson Land Management Ltd.), Roberts Creek, BC

Chapman, A.R. and D.E. Reksten (1991), Chapman Creek hydrology data summary and analysis, Ministry of Environment Water Management Division, Victoria, BC

Cooper, L.W. (1998), Isotopic fractionation in snow cover, in: Kendall, C. and J.J. McDonnell(Eds.), *Isotope Tracers in Catchment Hydrology*, Elsevier, Amsterdam, pp.119-136

Corbett, D.M. *et al.* (1943), Stream-gaging procedure; a manual describing methods and practices of the Geological Survey, USGS Water Supply paper 888, *U.S. Gov. Printing Office*, Washington, pp.1-245, available online: http://pubs.er.usgs.gov/ - search:basic/query=stream gaging/page=6/page_size=25:5

Cornelis, J.-T., J. Ranger, A. Iserentant and B. Delvaux (2010), Tree species impact the terrestrial cycle of silicon through various uptakes, *Biogeochemistry*, **97**, 231-245

Creed, I.F., L.E. Band, N.W. Foster, I.K. Morrison, J.A. Nicolson, R.S. Semkin and D.S. Jeffries (1996), Regulation of nitrate-N release from temperate forests: A test of the N flushing hypothesis, *Water Resources Research*, **32**(11), 3337-3354

Creed, I.F. and L.E. Band (1998), Export of nitrogen from catchments within a temperate forest: Evidence for a unifying mechanism regulated by variable source area dynamics, *Water Resources Research*, **34**(11), 3105-3120

Danard, M. (1980), Mean annual precipitation (1941-70) over British Columbia, report No.24, Water Investigations Branch, Water Resources Service, Province of British Columbia

DeWalle, D.R., B.R. Swistock, W.E. Sharpe (1998), Three-component tracer model for storm flow on a small Appalachian forest catchment, *Journal of Hydrology*, **104**, 301-310

Dinçer T., B.R. Payne, T. Florkowski, J. Martinec and E. Tongiorgi (1970), Snowmelt runoff from measurements of Tritium and Oxygen-18, *Water Resources Research*, **6**(1), 110-124

Dingman, S.L. (2008), Physical Hydrology – 2nd edition, *Waveland Pr. Inc*, 656p.

Dooge, J.C.I. (1959), A general theory of the unit hydrograph, *Journal of Geophysical Research*, **64**, 241-256

Dooge, J. C. I. (1986), Looking for hydrologic laws, *Water Resources Research*, **22**(9), 46 – 58

Eaton B. and R.D. Moore (2010), Chapter 4 – Regional Hydrology in: Pike R.G., T.E. Redding, R.D. Moore, R.D. Winker and K.D. Bladon [Eds.], Compendium of Forest Hydrology and Geomorphology in British Columbia, B.C. Ministry of Forest and Range, Forest Science Program, Victoria, B.C. and FORREX Forum for Research and Extension in Natural Resources, Kamloops, B.C. Land Management Handbook, **66**, URL: http://www.for.gov.bc.ca/hfd/pubs/Docs/Lmh/Lmh66.htm

Environment Canada (2009a) AHCCD database*, Meteorological Service of Canada*, Ottawa, Canada, available online: http://www.cccma.bc.ec.gc.ca/hccd/index.shtml

Environment Canada (2009b) HYDAT database, *Water Survey of Canada*, Ottawa, Canada, available online: http://www.wsc.ec.gc.ca/hydat/H2O/

Federer, C.A. (1971), Solar radiation absorption by leafless hardwood forests, *Agricultural Meteorology*, **9**, 3-20

Federer, C.A., C. Vörösmarty and B. Fekete (2003), Sensitivity of annual evaporation to soil and root properties in two models of contrasting complexity, *Journal of Hydrometeorology*, **4**, 1276-1290

Ferguson, S. (2010), Hydrometric technician with the Water Survey of Canada conducting discharge measurements and maintaining equipment at the Roberts Creek hydrometric station (08GA047)

Fohrer, N., S. Haverkamp, K. Eckhardt and H.-G. Frede (2001), Hydrologic response to land-use changes on the catchment scale, *Phys. Chem. Earth*, **26**(7-8), 577-582

Friedman R., J. Monger and H. Tipper (1990), Age of the Bowen Island Group, southwestern Coast Mountains, British Columbia, *Canadian Journal of Earth Sciences* **27**, 1456-1461

Gallant, R.E. (1975), Nonlinear Regression, *The American Statistician*, **29**(2), 73-81

Genereux, D. (1998), Quantifying uncertainty in tracer-based hydrograph separation*,* *Water Resources Research*, **34**, 915-919

Gibson, J.J., J.S. Price, R. Aravena, D.F. Fitzgerald and D. Maloney (2000), Runoff generation in a hypermaritime bog-forest upland, *Hydrological Processes*, **14**, 2711-2730

Goodison, B.E., H.L. Ferguson and G.A. McKay (1981), Measurement and data analysis, in: Gray, D.M. and D.H. Male (eds), *Handbook of Snow: principles, processes, management and use*, Pergamon Press, Willowdale, pp.191-265

Gomi, T., R.C. Sidle and J.S. Richardson (2002), Understanding Processes and Downstream Linkages of Headwater Systems, *BioScience*, **52**(10), 905-916

Grayson, R.B., A.W. Western and F.H.S. Chiew (1997), Preferred states in spatial soil moisture patterns: Local and nonlocal controls, *Water Resources Research*, **33**(12), 2897-2908

Griffiths G.A. and B. Clausen (1997), Streamflow recession in basins with multiple water storages*, Journal of Hydrology*, **190**, 60-74

Halford, K. and G.C. Mayer (2000), Problems associated with estimating ground water discharge and recharge from stream-discharge records, *Ground Water*, **38**(3), 331-342

Hall, F.R. (1968), Base-flow recessions – a review, *Water Resources Research*, **4**(5), 973-983

Hamlet, A.F. and D.P. Lettenmaier (1999), Effects of climate change on hydrology and water resources in the Columbia river basin, *Journal of the American Water Resources Association*, **35**(6), 1597-1623

Hamlet, A.F., P.W. Mote, M.P. Clark, D.P. Lettenmaier (2005), Effects of temperature and precipitation variability on snowpack trends in the western United States, *Journal of Climate*, **18**, 4545 – 4561

Hewlett, J.D. and A.R. Hibbert (1967), Factors affecting the response of small watersheds to precipitation in humid areas. In: Sopper, W.E., H.W. Lull [Eds], *International Symposium on Forest Hydrology*, Pergamon Press, New-York, 275-290

Hewlett, J.D. (1982), Principles of Forest Hydrology, *University of Georgia Press*, Athens, GA, 183p.

Hinton, M.J., S.L. Schiff and M.C. English (1994), Examining the contributions of glacial till water to storm runoff using two- and three-component hydrograph separation, *Water Resources Research*, **30**(4), 983-993

Hock, R. (1999), A distributed temperature-index ice and snowmelt model including potential direct solar radiation, *Journal of Glaciology*, **45**(149), 101-111

Hoeg, S., S. Uhlenbrook and C. Leibundgut (2000), Hydrograph separation in a mountainous catchment – combining hydrochemical and isotopic tracers, *Hydrological Processes*, **14**, 1199-1216

Hooper R.P. and C.A. Shoemaker (1986), A comparison of chemical and isotopic hydrograph separation, *Water Resources Journal*, **22**, 1444-1454

Hornberger, G.M., K.E. Bencala and D.M. McKnight (1994), Hydrological controls on dissolved organic carbon during snowmelt in the Snake River near Montezuma, Colorado, *Biogeochemistry*, **25**, 147-165

Horton, R.E. (1936), Maximum ground-water levels, *Transactions, American Geophysical Union*, **17**(2), 344-357

Horton, R.E. (1945), Erosional development of streams and their drainage basins: hydro-physical approach to quantitative morphology, *Geological Society of America Bulletin,* **56** (3): 275–370

Huntington, T.G. (2003), Climate warming could reduce runoff significantly in New England, USA, *Agricultural and Forest Meteorology*, **117**, 193-201

Huntington, T.G. (2006), Evidence for intensification of the global water cycle: Review and synthesis, *Journal of Hydrology*, **319**, 83-95

Hutchinson, D.G. and R.D. Moore (2000), Throughflow variability on a forested hillslope underlain by compacted glacial till, *Hydrological Processes*, **14**, 1751-1766

Ineson, P., K. Taylor, A.F. Harrison, J. Poskitt, D.G. Benham, E. Tipping and C. Woof (1998), Effects of climate change on nitrogen dynamics in upland soils. 1. A transplant approach, *Global Change Biology*, **4**, 143-152

Iqbal, M. (1983), An Introduction to Solar Radiation, New-York, Academic Press

Jewitt, G. (2006), Integrating blue and green water flows for water resources management and planning, *Physics and Chemistry of the Earth*, **31**, 753-762

Joerin C., K.J. Beven, I. Iorgulescu and A. Musy (2002), Uncertainty in hydrograph separations based on geochemical mixing models, *Journal of Hydrology*, **255**, 90-106

Jost *et al*. In preparation. Distributed temperature index snow melt modelling for forested watersheds

Jugen J.R. and T. Lewis (2007), Part III: The Soils Landscapes of BC: section 3.3 – The Coast Mountains and the Island, in *Soil Landscapes of BC*, Government of British Columbia, Ministry of Environment - Environmental Stewardship Division, consulted on Septembre 10th 2009, available online: http://www.env.gov.bc.ca/soils/landscape/3.3coast.html

Kachroo, R.K. (1992), Storage required to augment low flows: a regional study, *Hydrological Science Journal*, **37**(3), 247-261

Kendall, C. and E.A. Caldwell (1998), Fundamentals of isotope geochemistry, in: Kendall, C. and J.J. McDonnell [Eds.], *Isotope Tracers in Catchment Hydrology*, Elsevier, Amsterdam, pp.51-86

Kendall, K.A., J.B. Shanley and J.J. McDonnell (1999), A hydrometric and geochemical approach to test the transmissivity feedback hypothesis during snowmelt, *Journal of Hydrology*, **219**, 188-205

Keppeler E.T. and R.R. Ziemer (1990), Logging effects on streamflow: Water yield and summer low flows at Caspar Creek in Northwestern California, *Water Resources Research*, **26**(7), 1669-1679

Kim, H.J. (2001), Hydrologic contributions of subsurface flow during snowmelt and rainfall in a forested catchment, coastal British Columbia, M.Sc. thesis, Department of Geography, University of British Columbia, unpublished

Kim, H.J., R.C. Sidle, R.D. Moore and R. Hudson (2004), Throughflow variability during snowmelt in a forested mountain catchment, coastal British Columbia, Canada, *Hydrological Processes*, **18**, 1219-1236

Knisel, W.G. Jr. (1963), Baseflow recession analysis for comparison of drainage basins and geology, *Journal of Geophysical Research*, **68**(12), 3649-3653

Knowles, N., M.D. Dettinger, D.R. Cayan (2006), Trends in snowfall versus rainfall in the western United States, *Journal of Climate*, **19**, 4545-4559

Krabbenhoft, D.P., C.J. Browser, M.P. Anderson and J.W. Valley (1990), Estimating groundwater exchange with lakes, 1, The stable isotope mass balance method*, Water Resources Research*, **26**, 2445-2453

Kværner J. and B. Kløve (2006), Tracing sources of summer streamflow in boreal headwater using isotopic signatures and water geochemical components, *Journal of Hydrology*, **331**, 186-204

Laudon, H. and O. Slaymaker (1997), Hydrograph separation using stable isotopes, silica and electrical conductivity: an alpine example, *Journal of Hydrology*, **201**, 82-101

Laudon, H., H.F. Hemond, R. Krouse and K.H. Bishop (2002), Oxygen 18 fractionation during snowmelt: Implications for spring flood hydrograph separation, *Water Resources Research*, **38**(11), 1258. doi:10.1029/2002WR00510

Laudon, H., S. Köhler, J. Seibert and K.H. Bishop (2004), Hydrological flow paths during the spring flood: Congruence between hydrometric measurements and oxygen-18 in snowmelt, soil water and runoff, *Water Resources Research*, **40**(3), W03102. doi:10.1029/2003WR002455

Laudon, H., V. Sjöblom, I. Buffam, J. Seibert and M. Mörth (2007), The role of catchment scale and landscape characteristics for runoff generation of boreal streams, Journal of Hydrology, 344, 198-209

Lavkulich, Les (2010), Professor Emeritus, Faculty of Land of Food Systems, University of British-Columbia

Leith, R.M. and P. Whitfield (1998), Evidence of climate change effects on the hydrology of streams in south-central B.C., Canadian Water Resources Journal, **23**(3), 219-230

Leslie, C.D. (2008), P.Geo., M.Sc., resource geologist with Rebelex Resources Corp., personal communication

Likens G., C.T. Driscoll and D. Buso (1996), Long-term effects of acid rain: Response and recovery of a forest ecosystem, Science, **272**, 244-245

Lis G., L.I. Wassenaar and M.J. Henry (2008), High precision laser spectroscopy D/H and $^{18}O/^{16}O$ measurements of microliter natural water samples, *Analytical Chemistry,* **80**, 287-293

Luo Y., B. Su, W.S. Currie, J.S. Dukes, A. Finzi, U. Hartwig, B. Hungate, R.E. McMurtrie, R. Oren, W.J. Parton, D.E. Pataki, M. Rebecca Shaw, D.R. Zak and C.B. Field (2004), Progressive nitrogen limitation of ecosystem responses to rising atmospheric carbon dioxide, *BioScience*, **54**(8), 731-739

Markoff M.S. and A.C. Cullen (2007), Impact of climate change on Pacific Northwest hydropower, *Climatic Change*, **87**, 451-469

McCabe, G.J., D.M. Wolock (1999), General-circulation-model simulations of future snowpack in the western United-States, *Journal of the American Water Resources Association*, **35**(6), 1473-1484

McCarty, J.J., O.F. Ganziani, N.A. Leary, D.J. Dokken, K.S. White [Eds] (2001), IPCC Climate Change 2001: Impacts, Adaptation and Vulnerability. The third assessment report of the working group II of the Intergovernmental Panel on Climate Change (IPCC), *Cambridge University Press*, Cambridge, U.K. and New-York, USA, 1000p.

McDonnell, J.J. and C.H. Taylor (1987), Surface and subsurface water contributions during snowmelt in a small Precambrian Shield watershed, Muskoka, Ontario, *Atmosphere – Ocean*, **25**, 251-266

McDonnell, J.J. (1990), A rationale for old water discharge through macropores in steep, humid catchment, *Water Resources Research*, **26**(11), 2821-2832

McDonnell, J.J., M. Sivapalan, K. Vaché S. Dunn, G. Grant, R. Haggerty, C. Hinz, R. Hooper, J. Kirchner, M. L. Roderick, J. Selker and M. Weiler (2007), Moving beyond heterogeneity and process complexity: A new vision for watershed hydrology, *Water Resources Research*, **43**, W07301, doi:10.1029/2006 WR005467

McGuire, K.J., J.J. McDonnell (2006), A review and evaluation of catchment transit time modelling , *Journal of Hydrology*, **330**, 543-563

McGuire, K. J., M. Weiler, and J. J. McDonnell (2007), Integrating tracer experiments with modelling to assess runoff processes and water transit times, *Advances in Water Resources*, **30**, 824 – 837

McHale, M.R. J.J. McDonnell, M.J. Mitchell and C.P. Cirmo (2002), A field-based study of soil water and groundwater nitrate release in an Adirondack forested watershed, *Water Resources Research*, **38**(4), 1031, doi:10.1029/2000WR000102

Mielko C. and M.-K. Woo (2006), Snowmelt runoff processes in a headwater lake and its catchment, subarctic Canadian Shield, *Hydrological Processes*, **20**, 987-1000

Moore, R.D. (1989), Tracing runoff sources with deuterium and oxygen-18 during spring melt in a headwater catchment, southern Laurentians, Québec, *Journal of Hydrology*, **112**, 135-148

Moore, R.D. (1997), Storage-outflow modelling of streamflow recessions, with application to a shallow-soil forested catchment, *Journal of Hydrology*, **198**, 260-270

Moore, R.D. (2005), Slug injection using salt in solution, *Streamline Watershed Management Bulletin* **8**(2), 1-6

Moore, R.D., D.M. Allen and K. Stahl (2007), Climate Change an Low Flows: Influence of Groundwater and Glaciers, *Final Report for Climate Change Action Fund, Natural Resources Canada*, Project A875, 201pp.

Moore, R.D., G. Richards and A. Story (2008), Electrical Conductivity as an Indicator of Water Chemistry and Hydrologic Process, *Streamline Watershed Management Bulletin* **11**(2), 25-29

Mote, Philip W. (2003), Trends in snow water equivalent in the Pacific Northwest and their climatic causes, *Geophysical Research Letters*, **30**(12), (3), 1-4

Mote P.W., A.F. Hamlet, M.P. Clark and D. Lettenmaier (2005), Declining mountain snowpack in western North-America, *Bulletin of the American Meteorological Society*, **86**(1), 39-49

Murray C.D. and J.M. Buttle (2003), Impacts of clearcut harvesting on snow accumulation and melt in a northern hardwood forest, *Journal of Hydrology,* **271**, 197–212

Neal, T. L. (2005), Impacts of climate change and population growth on residential water demand in the Okanagan Basin - British Columbia, *M.A. thesis*, Univ. B.C., Vancouver, B.C., Unpublished, 103p.

Nijssen B., G.M. O'Donnell, A. Hamlet and D.P. Lettenmaier (2001), Hydrologic sensitivity of global rivers to climate change, *Climatic change*, **50**, 143-175

Peel, M.C., B.L. Finlayson and T.A. McMahon (2007), Updated world map of the Köppen-Geiger climate classification, *Hydrology and Earth System Sciences*, **11**, 1633-1644

Peterson B.J., W.M.Wollheim, P.J. Mulholland, J.R. Webster, J.D. Meyer, J.L. Tank, E. Marti, W.B. Bowden, H.M. Valett, A.E. Hershey, W.H. McDowell, W.K. Dodds, S.K. Hamilton, S. Gregory, D.D. Morrall (2001), Control of Nitrogen Export from Watersheds by Headwater Streams, *Science*, **292**(86), DOI: 10.1126/science.1056874

Press, W.H., B.P. Flannery, S.A. Teukolsky and W.T. Vetterling (1986), Numerical Recipes: The Art of Scientific Computing, *Cambridge University Press*, Cambridge, 818p.

Rains, M.C., G.E. Fogg, T. Harter, R.A. Dahlgren and R.J. Williamson (2006), The role of perched aquifers in hydrological connectivity and biogeochemical processes in vernal pool landscapes, Central Valley, Californiam *Hydrological Processes*, **20**(5), 1157-1175

Rantz S.E. *et al.* (1982), Measurement and Computation of Streamflow Volume II: computation of discharge, USGS Water-Supply paper 2175, *U.S. Gov. Printing Office*, Washington, pp.285-631, available online: http://pubs.usgs.gov/wsp/wsp2175/

Reckhow, D.A., P.C. Singer (1990), Chlorination by-products in drinking waters: from formation potentials to finished water concentrations, *Journal of the American Water Works Association*, **82**(4), 173-180

Regonda, S.K., B. Rajagopalan, M. Clark and J. Pitlick (2005), Seasonal cycle shifts in hydroclimatology over the western United-States, *Journal of Climate*, **18**, 372-384

Reynolds, B. and A. Edwards (1995), Factors influencing dissolved nitrogen concentrations and loadings in upland streams on the UK, *Agricultural Water Management*, **27**, 181-202

Rodenhuis, D., K.E. Bennett, A.T. Werner, T.Q. Murdock and D. Bronaugh (2007), Climate Overview 2007: Hydro-climatology and future climate impacts in British Columbia, *Pacific Climate Impacts Consortium 2007 report*, Victoria, Canada, available online: http://pacificclimate.org/docs/publications/PCIC.ClimateOverview.pdf

Rodhe, A (1998), Snowmelt-Dominated Systems, in: Kendall, C. and J.J. McDonnell [Eds.], *Isotope Tracers in Catchment Hydrology*, Elsevier, Amsterdam, pp.391-433

Rowland J.D. and R.D. Moore (1992), Modelling solar irradiance on sloping surfaces under leafless deciduous forests, *Agriculture and Forest Meteorology*, **60**(1-2), 111-132

Savenije H.H.G. (2004), The importance of interception and why we should delete the term evapotranspiration from our vocabulary. Invited commentary, *Hydrological Processes,* **18**, 1507-1511

Schelker, J. (2008), Interactions of streamflow dynamics and mercury variations in a small mountainous catchment in the Adirondak Mountains, NY State – Process understanding and modelling, Diploma Thesis, *Albert Ludwig University of Freiburg, Germany*, unpublished

Scibek J. and D.M. Allen (2006), Modelled impacts of predicted climate change on recharge and groundwater levels, *Water Resources Research*, **42**, W11405, doi:10,1029/2005WR004742

Scibek J., D.M. Allen, A.J. Cannon and P.H. Whitfield (2007), Groundwater-surface water interaction under scenarios of climate change using a high-resolution transient groundwater model, *Journal of Hydrology*, **333**(2-4), 165-181

Shaver, G.R., J. Canadell, F.S. Chapin III, J. Gurevitch, J. Harte, G. Henry, P. Ineson, S. Jonasson, J. Melillo, L. Pitelka and L. Rustad (2000), Global Warming and Terrestrial Ecosystems: A Conceptual Framework for Analysis, *BioScience*, **50**(10), 871-882

Shuttleworth, W.J. and J.S. Wallace (2002), Evaporation from sparse crops – An energy combination theory, *Quarterly Journal of the Royal Meteorological Society*, **111**, 839-855

Sivapalan, M. (2003), Process complexity at hillslope scale, process simplicity at the watershed scale: is there a connection? Invited commentary, *Hydrological Processes*, **17**, 1037-1041

Sklash, M.G. (1990), Environmental isotope studies of storm and snowmelt generation, in: Anderson, M.G. and T.P. Burt [Eds.], *Process Studies in Hillslope Hydrology*, Wiley, Chichester, pp.401-405

Snover, A.K., A.F. Hamlet and D.P. Lettenmaier (2003), Climate change scenarios for water planning studies – pilot applications in the Pacific Northwest, *Bulletin of the American Meteorological Society*, **84**(11), 1513-1518

Soil Classification Working Group (1998), The Canadian System of Soil Classification, 3rd edition, Agriculture and Agri-food Canada publication 1646, 187p.

Solomon, S., D. Qin, M. Manning, Z. Chen, M. Marquis, K.B. Averyt, M. Tignor and H.L. Miller [Eds.] (2007), IPCC Climate change 2007: the physical science basis – Contribution of the working group I to the fourth assessment report of the international panel on climate change, Cambridge University Press, Cambridge, U.K. and New-York, USA, 996pp.

Soon, Maureen (2009) Scientist and manager of analytical facilities, Department of Earth and Ocean Sciences, University of British Columbia, BC

Stewart I.T., D.R. Cayan, M.D. Dettinger (2005), Changes toward earlier streamflow timing across western North-America, *Journal of Climate*, **18**, 1136-1155

Stichler, W. (1987), Snowcover and snowmelt processes studied by means of environmental isotopes, in: Jones, H.G., OrvilleThomas, W.J. [Eds]. *Seasonal snowcovers: Physics, Chemistry, Hydrology*. NATO ASI Ser., Ser. C: Math. Phys. Sci., vol. 211, Reidel, Dordrecht, The Netherlands, pp.673-726

Sunshine Coast Regional District (SCRD – 2008), Regional Growth Strategy: Updated data and trends related to regional growth issues, SCRD Planning and Development Department, Sechelt, B.C., available online: http://www.scrd.ca/files/File/Planning/RGS/SCRD_update_report.pdf

Sunshine Coast Regional District (SCRD – 2009), Unpublished Data, Waterworks Department, Sechelt, B.C.

Tallaksen, L.M. (1989), Analysis of time variability in recessions, in: Roald, L., K. Nordseth and K.A. Hassel [Eds], FRIENDS in Hydrology, *International Association of Hydrological Sciences Publications*, **187**, 85-96

Tallaksen, L.M. (1995), A review of baseflow recession analysis, *Journal of Hydrology*, **165**, 349-370

Taylor S., X.H. Feng, J.W. Kirchner, R. Osterhuber, B. Klaue and C.E. Renshaw (2001), Isotopic evolution of a seasonal snowpack and its melt, *Water Resources Research* **37**, 759-769

Tetzlaff, D., C. Soulsby, P.J. Bacon, A.F. Youngson, C. Gibbins and I.A. Malcolm (2007), Connectivity between landscapes and riverscapes – a unifying theme in integrating hydrology and ecology in catchment science?, Invited commentary, *Hyrological Processes*, **21**, 1385-1389

Toews, D.A.A. and E. Hetherington (2010), Chapter 1 – Forest hydrology in British Columbia: context and history in: Pike R.G., T.E. Redding, R.D. Moore, R.D. Winker and K.D. Bladon [Eds.], Compendium of Forest Hydrology and Geomorphology in British Columbia, B.C. Ministry of Forest and Range, Forest Science Program, Victoria, B.C. and FORREX Forum for Research and Extension in Natural Resources, Kamloops, B.C. Land Management Handbook, **66**, URL: http://www.for.gov.bc.ca/hfd/pubs/Docs/Lmh/Lmh66.htm

Thompson, J. (2007), Running dry: Where will the West get its water?, Science Findings, **97**, Portland, OR: U.S. Department of Agriculture, Forest Service, Pacific Northwest Research Station, 5p.

Thompson, M., M.H. Ramsey and B. Pahlavanpour (1982), Water analysis by inductively coupled plasma atomic-emission spectrometry after a rapid pre-concentration, *The Analyst* **107**, 1330-1334

Triton Environmental Consultants (2006), Chapman Creek Watershed Drinking Water Source Assessment: Final Report no. 3661/WP2366, prepared for the Sunshine Coast Regional District, B.C., 106p.

Unnikrishna P.V., J.J. McDonnell, C. Kendall (2002), Isotope variations in a Sierra Nevada snowpack and their relation to meltwater, *Journal of Hydrology* **260**, 38-57

Viessman, W.Jr., G.L. Lewis and J.W. Knapp (1989), Introduction to Hydrology, *Harper Collins*, New-York, 780pp.

Wang T., A. Hamann, D.L. Spittlehouse and S.N. Aitken (2006), Development of scale-free climate data for western Canada for use in resource management, *International Journal of Climatology*, **26**, 383-397

Wang X.L., K. Klinka, H.Y.H. Chen and L. de Montigny (2002), Root structure of western hemlock and western redcedar in single- and mixed-species stands, *Can. J. For. Res.*, **32**, 997-1004

Weiler, M., B.L. McGlynn, K.J. McGuire and J.J. McDonnell (2003), How does rainfall becomes runoff? A combined tracer and runoff transfer function approach, *Water Resources Research*, **(39)**11, 1315. doi: 10.1029/2003WR00233.

Weiler, M., J.J. McDonnell, I. Tromp-Van Meerveld and T. Uchida (2005), Subsurface Stormflow. In: Anderson, M.G. [Ed], *Encyclopedia of Hydrological Sciences*, John Wiley and Sons, Chichester, U.K., pp.1719 - 1732

Wels, C., J. Cornett and B. LaZerte (1991), Hydrograph separation: A comparison of geochemical and isotopic tracers, *Journal of Hydrology*, **122**, 253-274

Wemple, B.C., J.A. Jones and G.E. Grant (1996), Channel network extension by logging roads in two basins, Western Cascades, Oregon, *Water Resources Bulletin*, **32**, 1195-1207

Whitfield, P.H. (2001), Linked hydrologic and climate variations in British Columbia and the Yukon, *Environmental Monitoring and Assessment*, **67**, 217-238

Whyte, D.M. (2004), Hydrologic response during snowmelt in three steep headwater catchments: Ringrose Slope, Slocan Valley, British Columbia, *M.Sc. thesis – geography*, Department of Geography, University of British-Columbia, unpublished

Zentner M., S.T. Nelson, A.L. Mayo (2000), The timing of groundwater recharge in mountainous aquifers : a preliminary study form the Wasatch Plateau of Utah, *Eos Trans. AGU*, **81**(48), Fall Meet. Suppl., Abstract H61D-1

Zhang, X., K. David Harvey, W.D. Hogg and T.R. Yuzyk (2001), Trends in Canadian streamflow, *Water Resources Research*, **37**(4), 987-998

Appendices

Appendix A – Concentrates vs Raw Samples Concentration

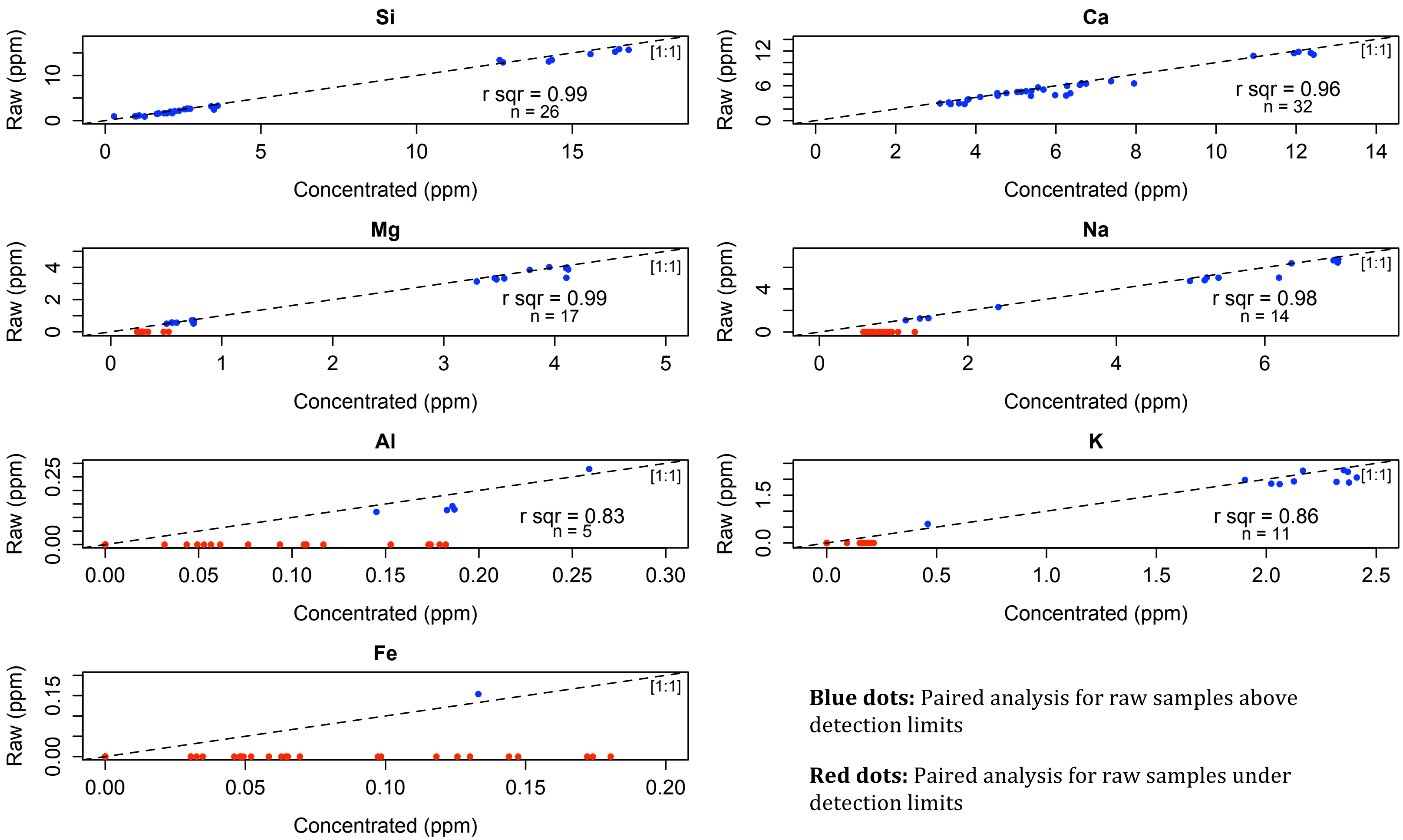

Blue dots: Paired analysis for raw samples above detection limits

Red dots: Paired analysis for raw samples under detection limits

Appendix B – ICP-AES Analytical Procedures

ICP-AES uses nitrogen plasma to break the chemical bonds of a very small volume of solution. Once the sample is ionized, the intense heat excites metal impurities present in the water. These emit photons at different wavelengths specific to their elemental structure (atomic spectral line) when they return to lower energy levels. The spectrum is measured by a multiple detectors polychromator and elemental concentrations are derived from those readings. The values were averaged when more than one spectral line was used per element. The full suite of calibration standards was run every 40 samples and an internal quality control (QC) standard (*n=22*) was used to compute the accuracy of the method.

Europium (Eu - 1 ppm) was added to the calibration standards and to the samples in order to correct for analytical errors induced by differences in density caused by variations in their HNO_3 concentrations. A partial recovery of Eu in a sample (i.e. 0.92 ppm) indicates that only 92% of the chemical constituents are detected. To correct for this density factor affecting the measurements, metal concentration values were divided by the recovered europium concentrations for every observation. Europium values read by the ICP-AES are considered more accurate because this element does not occur in nature and is therefore very unlikely to be present in solution, even in trace amounts. Also, europium's distinct atomic spectral line reduces the risk of spectral interferences with other metals (Soon, personal communication 2009).

Appendix C – Lachat Analytical Procedures

For NH_4^+ analysis, the method requires heating samples with salicyalate and hypochlorite in an alkaline phosphate buffer, resulting in the production of an emerald green dye that is in proportion to HN_3^+ concentration. The colour is then intensified by the addition of sodium nitroprusside. Results are expressed as NH_4^+-N.

The NO_x determination method involves reducing NO_3^- to NO_2^- by passing the sample through a column containing copper-coated cadmium, diazotizing it with sulphanilamide dihydrochloride and measuring absorption of the resulting magenta dye at 520 nm. Values are expressed as NO_3^-/NO_2-N.

The PO_4^{3-} concentrations are measured by digesting the samples with sulphuric acid and persulphate to hydrolize polyphosphates and organic P to PO_4^{3-}. The reaction with ammonium molybdate and antimony potassium tartrate under acidic conditions produces ascorbic acid which absorbs at 880nm. Values are expressed as PO_4^{3-} - P.

Analysis for Cl^- involves measuring the absorption of ferric thiocyanate at 480 nm. This compound is produced as a result of the liberation of thiocyanate from mercuric thiocyanate through the formation of soluble mercuric chloride. Absorption at 480 nm is proportional to Cl^- concentration.

Appendix D – Instantaneous Discharge Hydrograph with Q Measurements

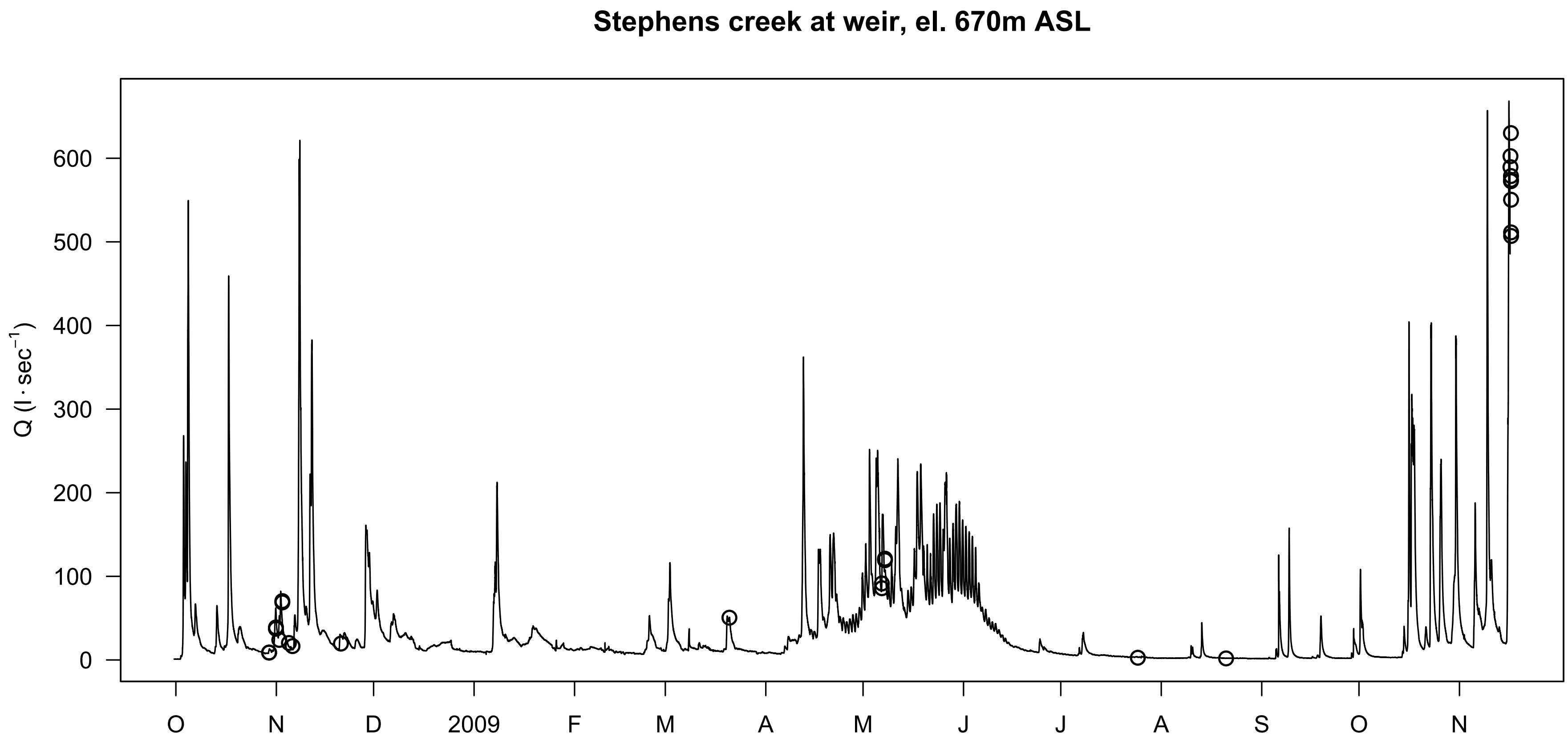

Appendix E – Computation of Stream Discharges from the Stage Discharge Rating Equations, Stephens Creek at the weir (plateform = *R*)

#Importing rating curve from the Water Survey of Canada's HQfit software
#Creating <u>linear regression models</u> between the 669 stage points making up the curve

```
# H = stage
# Q = discharge

xx = length(HQfit.smo$H)

curve.S1 = matrix(0,xx,1)
curve.Q1 = matrix(0,xx,1)
curve.S = rep(list(matrix(0,2,1)),xx)
curve.Q = rep(list(matrix(0,2,1)),xx)
curve.lm = rep(list(matrix(0,1,1)),xx)
curve.inter = matrix(0,xx,1)
curve.slope = matrix(0,xx,1)

for(i in 1:xx){     curve.S1[i] = HQfit.smo$H[i+1]
                    curve.Q1[i] = HQfit.smo$Q[i+1]
                    curve.S[[i]] = rbind(HQfit.smo$H[i],curve.S1[i])
                    curve.Q[[i]] = rbind(HQfit.smo$Q[i],curve.Q1[i])
               }

for(i in 1:xx) {    curve.lm[[i]] = lm(curve.Q[[i]] ~ curve.S[[i]])
                    curve.inter[i] = coefficients(curve.lm[[i]])[1]
                    curve.slope[i] = coefficients(curve.lm[[i]])[2]
               }

HQfit.curve = cbind(HQfit.smo,curve.inter,curve.slope)
```

#Corrected gauge height values at the weir

```
obs = coredata(vn1.PST.z)
```

#Dataframe defining the slopes and intercepts in-between 669 gauge height values

```
curve = data.frame(cbind(HQfit.curve[,c(-3,-4)],intercept=c(0,curve.inter[-xx,]),slope=c(0,curve.slope[-xx,])))
curve = curve [-1,]
```

#Computing discharge from slopes and intercepts in previous dataframe

```
Q = mapply(function(o,i) curve$intercept[i] + curve$slope[i] * o, obs, cut(obs,c(curve.test$H),labels=FALSE)
+ 1)
rm(curve,curve.lm,curve.inter,curve.slope,curve.S,curve.S1,curve.Q,curve.Q1,xx,obs)
```

#Attaching time stamps to instantaneous discharges (liters per second)

```
Q.ls = zoo(Q,time(vn1.PST.z))
```

#HOURLY Q: Forecast computing (observation at 13:00 = 13:00 to 13:59)

#15 min time series - L/15min

```
Q.l.15min = 900*coredata(Q.ls)
Q.l.15min = zoo(Q.l.15min, as.chron(format(time(Q.ls)),tz="PST"))
```

#60min. aggregated time series - L/60min

```
Q.l.60min = aggregate(coredata(Q.l.15min), list(trunc(time(Q.l.15min),"hours")), FUN = sum)
Q.l.60min = Q.l.60min[1:9892,]
Q.l.60min = zoo(Q.l.60min$x, as.chron(Q.l.60min$Group.1,tz="PST"))
```

#60min. aggregated time series - mm/hr (based on watershed area = 0.715225 sq km)

```
mm = coredata(Q.l.60min)
mmm = mm/715225
Q.mm.60min = zoo(mmm, index(new.Q.l.60min))
```

#Change area = +/- 5% err for catchment area (l = lower confidence, u = upper confidence)

```
mm = coredata(Q.l.60min)
mmm = mm/679464 #lower end
l.Q.mm.60min = zoo(mmm, index(Q.l.60min))
rm(mm,mmm)

mm = coredata(Q.l.60min)
mmm = mm/750986 #upper end
u.Q.mm.60min = zoo(mmm, index(Q.l.60min))
rm(mm,mmm)
```

#Daily aggregated time series for the whole monitoring period - in mm

```
Q.mm.z1 = Q.mm.60min[14:9877]
Q.day.mm = aggregate(coredata(Q.mm.z1), list(trunc(time(Q.mm.z1),"days")), FUN = sum)
Q.day.mm = zoo(Q.day.mm$x, Q.day.mm$Group.1)
rm(new.Q.mm.z1)
```

#Daily Aggregated time series for +-5% err due to catchment area

```
u.Q.mm.60min = u.Q.mm.60min[14:9877]
l.Q.mm.60min = l.Q.mm.60min[14:9877]
u.Q.mm.day = aggregate(coredata(u.Q.mm.60min), list(trunc(time(u.Q.mm.60min),"days")), FUN = sum)
l.Q.mm.day = aggregate(coredata(l.Q.mm.60min), list(trunc(time(l.Q.mm.60min),"days")), FUN = sum)
u.Q.mm.day = zoo(u.Q.mm.day$x, u.Q.mm.day$Group.1)
l.Q.mm.day = zoo(l.Q.mm.day$x, l.Q.mm.day$Group.1)
```

#Plot HQ curve with equations form HQfit

```
quartz(h=4,w=6)
plot(HQfit.curve$Q,HQfit.curve$H,main="",ylab="",xaxp = c(0,800,8),xlab="",
type="l",las=1,lty=2,col="gray25");mtext("Stage (cm)",2,2.5);mtext(expression("Discharge (L "%.%" sec"^{-
1}*")"),1,2.1)
points(salt.points$Q,salt.points$VN1,pch=19,cex=0.8)
ablinepiece(a=14.3,b=0,from=0,to=100,lty=3,col="gray50")
ablinepiece(a=29.545,b=0,from=90,to=190,lty=3,col="gray50")
text(170,6,expression(Q[t] == -7.124 %.% (Stage[t] + 7.523)^{5.846}),cex=0.75,font=3)
text(250,21,expression(Q[t] == -2.523 %.% (Stage[t] + 3.326)^{3.077}),cex=0.75,font=3)
text(400,37,expression(Q[t] == -0.041 %.% (Stage[t] + 16.419)^{1.688}),cex=0.75,font=3)
```

Appendix F – Physical Characteristics of the Sub-Modelling Space

Cell no.	Elev. (m)	Area (ha)	Aspect (deg)	Slope (deg)	DBH (cm)	Tree height (m)	Crown dom.[1] (%)	Crown closu. (ratio)	Density (trees per ha)
1	697	2.2	255	13	43	31	45	0.8	2462
2	759	2.1	260	19	40	31	39	0.7	4365
3	835	1.6	238	23	47.5	26	62	0.8	3183
4	847	3.0	270	23	82	37	45	0.5	1952
5	904	2.1	243	25	20	14.5	59	0.9	3867
6	916	1.6	270	22	20	13	65	0.7	3867
7	971	2.6	230	21	24	17.5	89	0.6	4138
8	1001	2.8	270	16	27	14	50	0.9	10584
9	988	0.9	275	21	Open	Open	Open	Open	Open
10	952	1.7	265	21	32.5	19	53	0.7	3422
11	1026	2.2	210	23	27	14	50	0.7	10584
12	1048	4.5	200	20	33	10	80	0.3	955
13	1037	6.2	250	13	33	9	89	0.3	955
14	1074	3.2	300	21	39	11	91	0.5	1910
15	1071	3.4	295	22	39	11	91	0.5	1910
16	1141	5.3	230	8	33	9	89	0.3	955
17	1100	6.0	190	12	33	9	89	0.3	955
18	1101	4.3	230	12	33	9	89	0.3	955
19	1130	7.2	305	14	39	11	91	0.7	1910
20	1170	4.0	305	7	72	34	46	0.5	1363
21	1126	4.1	285	14	33	9	89	0.4	955
22	955	0.4	260	22	27	16	63	0.3	6366
SLA	673	NA	229	8	43	31	45	0.7	2462
SLB	845	NA	230	24	30	25	56	0.7	3629
SLC	975	NA	266	20	32.5	19	53	0.7	3422
SLD	1088	NA	226	28	Open	Open	Open	Open	Open

1 – (Crown's height / Tree height) ratio

Appendix G – Canopy Interception Codes (plateform = *R*) and Snowpack Drainage Output

***# 1st step:* Creating air temperature time series for every cell based on lapse rate**

#Importing data from existing R objects, set period and Δ Elevation

```
Ta = zoo(climate$Temp, time(precip))              #Ta time series file
days=122                                          #Number of days from April 1st to July 31st
hours = 2928                                      #Number of hours from April 1st to July 31st
tlr = zoo(climate$T_lapse,time(Ta))               #Ta lapse rate imported from spread sheet (hourly)
tlr.m = matrix(coredata(tlr),hours,1)             #Hourly Ta lapse rate as a matrix
temp.m = matrix(coredata(Ta),hours,1)             #Hourly Ta as a matrix
delta.grid.elev = grid.elev - 975                 #Δ Elevation between weather station and cells
delta.SLs.elev = SLs.elev – 975                   #Δ Elevation between weather station and SLs
grid=22                                           #Number of cells to simulate
```

#Creating empty matrices to be filled-in by loop structures

```
cells.temp.list = rep(list(matrix(0,hours,1)),grid)     #List for cells' Ta
SLs.temp.list = rep(list(matrix(0,hours,1)),SLs)        #List for Snow lysimeters' Ta
```

#Calculating Ta at each cell composing the list (grid = 22 cells) and at each SLs (4)

```
for(j in 1:grid) {
        for(i in 1:hours) cells.temp.list[[j]][i] = temp.m[i] + (tlr.m[i] * delta.grid.elev[j])
                                }

for(j in 1:SLs) {
        for(i in 1:hours)       SLs.temp.list[[j]][i] = temp.m[i] + (tlr.m[i] * delta.SLs.elev[j])
                                }
```

***#2nd step:* Creating precipitation time series for each cell based on precipitation lapse rate**

#Importing data from existing R objects and set period

```
days.a=21                                         #Time period for all SLs
days.b=31
days.c = 52
days.d = 59
plr = zoo(climate$P_lapse,time(precip))           #Precip lapse rate (hourly)
plr.m = matrix(coredata(plr),hours,1)             #Precip lapse rate as a matrix (hourly)
precip.m = matrix(coredata(precip),hours,1)       #Rainfall data at 975m el. (see chapter 5)
```

#Creating empty matrices to be filled-in by loop structures

```
cells.precip.list = rep(list(matrix(0,hours,1)),grid)
SLs.precip.list = rep(list(matrix(0,hours,1)),SLs)
cells.precip.list.z = rep(list(matrix(0,hours,1)),grid)
SLs.precip.list.z = rep(list(matrix(0,hours,1)),SLs)
cells.precip.list.days = rep(list(matrix(0,hours,1)),grid)
SLs.precip.list.days = rep(list(matrix(0,hours,1)),grid)
cells.precip.list.agg = rep(list(matrix(0,days,1)),grid)
SLs.precip.list.agg = rep(list(matrix(0,days,1)),grid)
```

#Calculating Ta at each cell composing the list (grid = 22 cells) and at each SLs (4) and correcting #mathematical errors due to negative lapse rate (precip. < 0mm)

```
for(j in 1:grid) {
	for(i in 1:hours) cells.precip.list[[j]][i] = precip.m[i] + (precip.m[i] * plr.m[i] * delta.grid.elev[j])
				}
for(j in 1:grid) {
	for(i in 1:hours) cells.precip.list[[j]][i] = replace(cells.precip.list[[j]][i], cells.precip.list[[j]][i] < 0, 0)
				}
for(j in 1:SLs) {
	for(i in 1:hours)	SLs.precip.list[[j]][i] = precip.m[i] + (precip.m[i] * plr.m[i] * delta.SLs.elev[j])
				}
for(j in 1:SLs) {
	for(i in 1:hours)	SLs.precip.list[[j]][i] = replace(SLs.precip.list[[j]][i], SLs.precip.list[[j]][i] < 0, 0)
				}
```

#Re-attaching time stamp to lapsed rainfall data and aggregating to daily values

```
for(j in 1:grid) cells.precip.list.z[[j]] = zoo(cells.precip.list[[j]], time(precip))
for(j in 1:SLs) SLs.precip.list.z[[j]] = zoo(SLs.precip.list[[j]], time(precip))
for(j in 1:grid) cells.precip.list.days[[j]] = zoo(cells.precip.list[[j]], as.Date(time(precip)))
for(j in 1:grid) cells.precip.list.agg[[j]] = aggregate(cells.precip.list.days[[j]],force,sum)
for(j in 1:SLs) SLs.precip.list.days[[j]] = zoo(SLs.precip.list[[j]], as.Date(time(precip)))
for(j in 1:SLs) SLs.precip.list.agg[[j]] = aggregate(SLs.precip.list.days[[j]],force,sum)
```

<u>#3rd step:</u> Creating rainfall time series for each cells based on lapse rate for Ta and precipitation

#Creating empty matrices (rainfall objects) to be filled-in by loop structures

```
cells.rain.list = rep(list(matrix(0,hours,1)),grid)
SLs.rain.list = rep(list(matrix(0,hours,1)),grid)
cells.rain.list.z = rep(list(matrix(0,hours,1)),grid)
SLs.rain.list.z = rep(list(matrix(0,hours,1)),SLs)
cells.rain.list.days = rep(list(matrix(0,hours,1)),grid)
SLs.rain.list.days = rep(list(matrix(0,hours,1)),grid)
cells.rain.list.agg = rep(list(matrix(0,days,1)),grid)
SLs.rain.list.agg = rep(list(matrix(0,days,1)),grid)
```

#Substracting rainfall values when Ta < snowmelt temperature (set to -0.3ºC) – SWE accumulation #and melt is already accounted by the YAM model

```
for(j in 1:grid) {
	for(i in 1:hours)	cells.rain.list[[j]][i] = replace(cells.precip.list[[j]][i], cells.temp.list[[j]][i] < -0.3, 0)
				}

for(j in 1:SLs) {
	for(i in 1:hours)	SLs.rain.list[[j]][i] = replace(SLs.precip.list[[j]][i], SLs.temp.list[[j]][i] < -0.3, 0)
				}
```

#Attaching time stamps to hourly throughfall data and aggregating to daily values

```
for(j in 1:grid) cells.rain.list.z[[j]] = zoo(cells.rain.list[[j]], time(precip))
for(j in 1:SLs) SLs.rain.list.z[[j]] = zoo(SLs.rain.list[[j]], time(precip))
for(j in 1:grid) cells.rain.list.days[[j]] = zoo(cells.rain.list[[j]], as.Date(time(precip)))
for(j in 1:grid) cells.rain.list.agg[[j]] = aggregate(cells.rain.list.days[[j]],force,sum)
for(j in 1:SLs) SLs.rain.list.days[[j]] = zoo(SLs.rain.list[[j]], as.Date(time(precip)))
for(j in 1:SLs) SLs.rain.list.agg[[j]] = aggregate(SLs.rain.list.days[[j]],force,sum)
```

***#4th step*: Computing canopy interception storage and throughfall based on YAM equations (Chp. 5)**

#Object describing forest cover for each cell and SLs

```
frac.fc = c(0.8,0.7,0.8,0.5,0.9,0.7,0.6,0.9,0.7,0.7,0.7,0.3,0.3,0.5,0.5,0.3,0.3,0.3,0.7,0.4,0.4,0.3)
frac.fc.SLs = c(0.7,0.7,0.7,0.3)
```

#Set maximum rainfall interception storage for each cell based on YAM input file

```
imax.grid = 5 * frac.fc                    #Maximum storage = 5mm for 100% forest cover
imax.SLs = 5 * frac.fc.SLs
E = 1                                      #Daily evaporation from the canopy
```

#Empty matrices representing throughfall and time series objects for canopy storage calculation
#(a,b) to be filled-in by loop structure

```
throughfall = rep(list(matrix(0,days,1)),grid)
a = rep(list(matrix(0,days,1)),grid)
b = rep(list(matrix(0,days,1)),grid)
```

#Computing interception storage for the cells

```
for(j in 1:grid) {
        for(i in 1:days) {      if(i==0){a[[j]][i] = 0 + cells.rain.list.agg[[j]][i]
                                        if(a[[j]][i] < imax.grid[j]) b[[j]][i] = a[[j]][i]
                                        if(a[[j]][i] >= imax.grid[j]) b[[j]][i] = imax.grid[j]
                                        }
                                if(i > 1){if(b[[j]][i-1] >= 0 && b[[j]][i-1] < E)
                                                {a[[j]][i] = 0 + cells.rain.list.agg[[j]][i]
                                                if(a[[j]][i] >= imax.grid[j]) b[[j]][i] = imax.grid[j]
                                                if(a[[j]][i] < imax.grid[j]) b[[j]][i] = a[[j]][i]
                                                }
                                        if(b[[j]][i-1] >= E && b[[j]][i-1] <= imax.grid[j])
                                                {a[[j]][i] = b[[j]][i-1] - E + cells.rain.list.agg[[j]][i]
                                                if(a[[j]][i] >= imax.grid[j]) b[[j]][i] = imax.grid[j]
                                                if(a[[j]][i] < imax.grid[j]) b[[j]][i] = a[[j]][i]
                                                }
                                        }
                        }
                }
rm(a)
```

#Computing throughfall for the cells

```
for(j in 1:grid) {
        for(i in 1:days) { if(i==1) throughfall[[j]][i] = cells.rain.list.agg[[j]][i] - b[[j]][i]
                        if(i > 1){
                                if(b[[j]][i-1] >= 0 && b[[j]][i-1] <= E) throughfall[[j]][i] = cells.rain.list.agg[[j]][i] -
b[[j]][i]
                                if(b[[j]][i-1] > E && b[[j]][i-1] <= imax.grid[j]) throughfall[[j]][i] =
cells.rain.list.agg[[j]][i] - (imax.grid[j] - (b[[j]][i-1] - E))
                                }
                        }
                }

inter.storage = b                          #Canopy storage reservoir
rm(b)
```

#Repeating the 4th step with Snow Lysimeter values

```
a = rep(list(matrix(0,days,1)),SLs)
b = rep(list(matrix(0,days,1)),SLs)
throughfall.SLs = rep(list(matrix(0,days,1)),SLs)

for(j in 1:SLs) {
        for(i in 1:days) { if(i==0) {     a[[j]][i] = 0 + SLs.rain.list.agg[[j]][i]
                                          if(a[[j]][i] < imax.SLs[j]) b[[j]][i] = a[[j]][i]
                                          if(a[[j]][i] >= imax.SLs[j]) b[[j]][i] = imax.SLs[j]
                                        }
                              if(i > 1) {     if(b[[j]][i-1] >= 0 && b[[j]][i-1] < E)
                                                {
                                                 a[[j]][i] = 0 + SLs.rain.list.agg[[j]][i]
                                                 if(a[[j]][i] >= imax.SLs[j]) b[[j]][i] = imax.SLs[j]
                                                 if(a[[j]][i] < imax.SLs[j]) b[[j]][i] = a[[j]][i]
                                                }
                                          if(b[[j]][i-1] >= E && b[[j]][i-1] <= imax.SLs[j])
                                                {
                                                a[[j]][i] = b[[j]][i-1] - E + SLs.rain.list.agg[[j]][i]
                                                if(a[[j]][i] >= imax.SLs[j]) b[[j]][i] = imax.SLs[j]
                                                if(a[[j]][i] < imax.SLs[j]) b[[j]][i] = a[[j]][i]
                                                }
                                        }
                              }
                }
rm(a)

for(j in 1:SLs) {
        for(i in 1:days) { if(i==1) throughfall.SLs[[j]][i] = SLs.rain.list.agg[[j]][i] - b[[j]][i]
                              if(i > 1) { if(b[[j]][i-1] >= 0 && b[[j]][i-1] <= E) throughfall.SLs[[j]][i] =
SLs.rain.list.agg[[j]][i] - b[[j]][i]
                                        if(b[[j]][i-1] > E && b[[j]][i-1] <= imax.SLs[j]) throughfall.SLs[[j]][i] =
SLs.rain.list.agg[[j]][i] - (imax.SLs[j] - (b[[j]][i-1] - E))
                                        }
                              }
                }

inter.storage.SLs = b
rm(b)
```

***#5th step: Adding thoughfall values to daily ΔSWE values as modelled by YAM* in order to obtained #daily snowpack drainage output**

#Creating empty matrices to be filled-in by loop structures

```
grid.swe =  rep(list(matrix(0,days,1)),grid)
grid.precip =  rep(list(matrix(0,days,1)),grid)
grid.total.output = rep(list(matrix(0,days,1)),grid)
SLs.swe =  rep(list(matrix(0,days.a,1)),SLs)
SLs.precip =  rep(list(matrix(0,days.a,1)),SLs)
SLs.total.output = rep(list(matrix(0,days.a,1)),SLs)
daily.wa.output2 = matrix(0,days,1)
daily.wa.output = rep(list(matrix(0,22,1)),days)
daily.wa.precip = rep(list(matrix(0,22,1)),days)
daily.wa.precip2 = matrix(0,days,1)
daily.wa.swe = rep(list(matrix(0,22,1)),days)
daily.wa.swe2 = matrix(0,days,1)
```

#Substracting SWE accumulation from the YAM output

```
for(j in 1:grid)  {
        for(i in 1:days) grid.swe[[j]][i] = replace(cells.swe.list[[j]][i,2],cells.swe.list[[j]][i,2] < 0, 0)
                                }
for(j in 1:SLs)  {
        if(j == 1) for(i in 1:days.a) SLs.swe[[j]][i] = replace(SLs.M[[j]][i],SLs.M[[j]][i] < 0, 0)
        if(j == 2) for(i in 1:days.b) SLs.swe[[j]][i] = replace(SLs.M[[j]][i],SLs.M[[j]][i] < 0, 0)
        if(j == 3) for(i in 1:days.c) SLs.swe[[j]][i] = replace(SLs.M[[j]][i],SLs.M[[j]][i] < 0, 0)
        if(j == 4) for(i in 1:days.d) SLs.swe[[j]][i] = replace(SLs.M[[j]][i],SLs.M[[j]][i] < 0, 0)
                }
```

#Adding throughfall values to snowmelt

```
for(j in 1:grid)  grid.precip[[j]] = throughfall[[j]]
for(j in 1:grid) { for(i in 1:days) grid.total.output[[j]][i] = grid.precip[[j]][i] + grid.swe[[j]][i] }
for(j in 1:SLs)  SLs.precip[[j]] = throughfall.SLs[[j]]
for(j in 1:SLs)  SLs.total.output[[j]] = SLs.precip[[j]][1:length(SLs.swe[[j]])] + SLs.swe[[j]]
```

#Calculating an area weighted average for throughfall (called precip), d.swe and total drainage
#output

#Output

```
for(i in 1:days)  {
        for(j in 1:grid) {daily.wa.output[[i]][j] = grid.total.output[[j]][i]*grid.area[j,2] }
}
for(i in 1:days) daily.wa.output2[i] = sum(daily.wa.output[[i]])/catchment.area

daily.wa.output = daily.wa.output2
rm(daily.wa.output2)
```

#Throughfall

```
for(i in 1:days)  {
        for(j in 1:grid) {daily.wa.precip[[i]][j] = grid.precip[[j]][i]*grid.area[j,2]        }
}
for(i in 1:days) daily.wa.precip2[i] = sum(daily.wa.precip[[i]])/catchment.area

daily.wa.precip = daily.wa.precip2
rm(daily.wa.precip2)

#SWE WA

for(i in 1:days)  {
        for(j in 1:grid) {daily.wa.swe[[i]][j] = grid.swe[[j]][i]*grid.area[j,2]    }
}
for(i in 1:days) daily.wa.swe2[i] = sum(daily.wa.swe[[i]])/catchment.area

daily.wa.swe = daily.wa.swe2
rm(daily.wa.swe2)
```

Appendix H – runCE 2-IHS (plateform = *R*)

***#1st step**: Calculate isotopic flux from each cell*

#Creating empty matrices to be filled-in by loop structures

```
oxy.grid.conc = rep(list(matrix(0,23,3)),grid)
daily.wa.oxy = rep(list(matrix(0,22,1)),days)
oxy.days.conc.A2 = rep(list(matrix(0,grid,1)),days)
daily.wa.oxy2 = matrix(0,days,1)
#oxy.grid.cells = isotopic signature for each cells computed with the regression models (chp. 5) – codes not
#presented here
```

#Calculating concentrations – listed by cells

```
for(j in 1:grid) oxy.grid.conc[[j]] = oxy.grid.cells[[j]] * grid.total.output[[j]][1:length(oxy.grid.cells[[j]])]
```

#Cells concentration – listed by days

```
for(i in 1:days)
        for(j in 1:grid)  {
        if(is.na(oxy.grid.conc.A2[[j]][i]))        oxy.days.conc.A2[[i]][j] = 0
        else     oxy.days.conc.A2[[i]][j] = oxy.grid.conc.A2[[j]][i]
                                        }
```

#Calculate daily area weighted average for concentrations

```
for(i in 1:days)  {
        for(j in 1:grid) {daily.wa.oxy[[i]][j] = oxy.days.conc.A2[[i]][j]*grid.area[j,2] }
}
for(i in 1:days) daily.wa.oxy2[i] = sum(daily.wa.oxy[[i]])/catchment.area

daily.wa.oxy = daily.wa.oxy2
rm(daily.wa.oxy2)
```

***#2nd step:** Initiate runCE modelling for every cell*

```
runCE.flag = 1          #Flag to start simulation
```

#Simulation period

```
start.sim = as.Date("2009-04-01")                    #Start day of simulation
end.sim = as.Date("2009-09-24")                      #End day of simulation
dates = seq(start.sim,end.sim,"days")                #Time vector for plotting results

#Simulation period per individual cell in days (corresponds to the length of their SWE record form April 1st)
dt = c(23,30,31,47,40,47,58,54,54,51,59,58,59,70,68,65,62,63,71,108,66,46)

#Simulation period for integrated runCE model
dt1 = as.numeric(end.sim) - as.numeric(start.sim) +1
```

#Pre-event concentration

```
Cp = rep(-12.3, 22)
```

#Importing stream discharge (Q) and 18O stream isotopic signature (Cs), daily snowmelt (M) and #daily 18O flux (M.by.Cm) – Here I create 22 identical Q and Cs matrices subset for the SWE records' #length of each cell

```
Q = rep(list(matrix(0,1,1)),grid)
Cs= rep(list(matrix(0,1,1)),grid)

for(j in 1:grid) {
Q[[j]]=matrix(coredata(Q.mm.day[183:(183+dt[j]-1)]),length(coredata(Q.mm.day[183:(183+dt[j]-1)])),1)
Cs[[j]]=matrix(daily.sth[1:dt[j]],dt[j],1)
}
```

#Building empty matrices for every parameters to resolve

```
M=rep(list(matrix(0,1,1)),grid)
M.by.Cm = rep(list(matrix(0,1,1)),grid)
runCE = rep(list(matrix(0,1,1)),grid)
E = rep(list(matrix(0,1,1)),grid)
f.runCE = rep(list(matrix(0,1,1)),grid)
sumE = rep(list(matrix(0,1,1)),grid)
sumE.by.Ce = rep(list(matrix(0,1,1)),grid)
sumM = rep(list(matrix(0,1,1)),grid)
sumM.by.Cm = rep(list(matrix(0,1,1)),grid)
f = rep(list(matrix(0,1,1)),grid)
g = rep(list(matrix(0,1,1)),grid)
counter = matrix(0,grid,1)
```

#Adjust the empty matrices to the length of SWE record at every cell

```
for(j in 1:grid) {
        M[[j]] = matrix(0,dt[j],1)
        M.by.Cm[[j]] = matrix(0,dt[j],1)
        runCE[[j]] = matrix(0,dt[j],1)
        E[[j]] = matrix(0,dt[j],1)
        f.runCE[[j]] = matrix(0,dt[j],1)
        sumE[[j]] = matrix(0,dt[j],1)
        sumE.by.Ce[[j]] = matrix(0,dt[j],1)
        sumM[[j]] = matrix(0,dt[j],1)
        sumM.by.Cm[[j]] = matrix(0,dt[j],1)
        f[[j]] = matrix(0,dt[j],1)
        g[[j]] = matrix(0,dt[j],1)
        }
```

#Extract the current melt water concentration

```
Cm = M.by.Cm/M
```

#Fill-in M and M.by.Cm for each cell.

```
for(j in 1:grid) {

M[[j]] = matrix(c(grid.total.output[[j]][1:dt[j]],rep(0,(dt[j] - length(grid.total.output[[j]][1:dt[j]])))),dt[j],1)
M.by.Cm[[j]]= matrix(c(oxy.grid.conc[[j]][1:dt[j]],rep(0,(dt[j] - length(oxy.grid.conc[[j]][1:dt[j]])))),dt[j],1)
```

#Calculate Melt (given) sum variables

```
for (i in 1:dt[j]){
        if(i==1){
```

```
		sumM.by.Cm[[j]][i] = M.by.Cm[[j]][i]
		sumM[[j]][i] = M[[j]][i]
	} else {
		sumM.by.Cm[[j]][i] = (sumM.by.Cm[[j]][i-1] + M.by.Cm[[j]][i])
		sumM[[j]][i] = sumM[[j]][i-1] + M[[j]][i]
		}
}
```

#Starting value for runCE iteration

```
z = -16
```

#Start of simulation

```
if(runCE.flag ==1){

for(i in 1:dt[j]) {					#Loop computing a runCE value per cell

	Diff.runCE=1
	runCE.Old=0
	RMS = 0

	#Initial values for runCE (value of z)

	if(i==1)runCE[[j]][i] = z  else runCE[[j]][i] = runCE[[j]][i-1]


	#Iteration optimisation loop

	while(Diff.runCE > 0.00000001) {
		#difference in runCE between the two last runs will be less then the given value

	#count total number of iterations
	counter[j] = counter[j] +1

	#store old runCE in variable
	runCE.Old = runCE[[j]][i]

	#Calculate event water fraction f and event water amount E
	f.runCE[[j]][i] = (Cs[[j]][i] - Cp[j]) / (runCE.Old-Cp[j])
	E[[j]][i] = Q[[j]][i] * f.runCE[[j]][i]

	#Calculate sum variables

	if(i==1){
		sumE[[j]][i] = E[[j]][i]
		sumE.by.Ce[[j]][i] = E[[j]][i]*runCE.Old
		} else {
		sumE.by.Ce[[j]][i] = sumE.by.Ce[[j]][i-1] + E[[j]][i]*runCE.Old
		sumE[[j]][i] = sumE[[j]][i-1]+E[[j]][i]
		}


	#Calculate new (fitted) runCE
	f[[j]][i] = sumM.by.Cm[[j]][i] - sumE.by.Ce[[j]][i]
	g[[j]][i] = sumM[[j]][i] - sumE[[j]][i]
	runCE[[j]][i] = f[[j]][i] / g[[j]][i]
```

```
#Calculate the difference between the old and the new runCE value
        RMS = sqrt((runCE[[j]][i]^2 + runCE.Old^2)/2)
        Diff.runCE = abs(RMS - abs(runCE[[j]][i]))
        }
}
}
}
```

 # plot runCE results (by cell)

```
b=c(1:22)
quartz(w=8,h=10)
plot(c(1:dt[1]),runCE[[1]], col = b[1],type="o",ylim = c(-16.5,-9),xlim=c(0,65))
for(k in 2:11)  { lines(c(1:dt[k]),runCE[[k]], col=b[k], type="o") }
legend("bottomright",as.character(c(1:11)),lty = rep(1,11),col = c(1:11))
lines(c(1:dt[20]),Cs[[20]],col="green",lwd=2)

quartz(w=8,h=10)
plot(c(1:dt[12]),runCE[[12]], col = b[12],type="o",ylim = c(-20,-12),xlim=c(0,108))
for(k in 13:22)  { lines(c(1:dt[k]),runCE[[k]], col=b[k], type="o") }
legend("bottomright",as.character(c(12:22)),lty = rep(1,11),col = c(12:22))
lines(c(1:dt[20]),Cs[[20]],col="green",lwd=2)
```

#number of iterations that was needed to resolve E

```
print(counter)
```

#new concentration values per cell

```
runCE.grid.conc = rep(list(matrix(0,1,1)),grid)
runCE.days.conc = rep(list(matrix(0,grid,1)),dt[20])
daily.wa.runCE = rep(list(matrix(0,grid,1)),dt[20])

for(j in 1:grid)  runCE.grid.conc[[j]] = matrix(0,dt[j],1)
for(j in 1:grid)  runCE.grid.conc[[j]] = runCE[[j]] * grid.total.output[[j]][1:dt[j]]
for(i in 1:dt[20]) { for(j in 1:grid) {      if(is.na(runCE.grid.conc[[j]][i])) runCE.days.conc[[i]][j] = 0
                                              else      runCE.days.conc[[i]][j] = runCE.grid.conc[[j]][i]
                                        }
                   }

for(i in 1:dt[20])  {
        for(j in 1:grid) daily.wa.runCE[[i]][j] = runCE.days.conc[[i]][j]*grid.area[j,2]
                   }

daily.wa.runCE2 = matrix(0,fourth.25[20],1)

        for(i in 1:fourth.25[20]) daily.wa.runCE2[i] = sum(daily.wa.runCE[[i]])/catchment.area

daily.wa.runCE = daily.wa.runCE2
rm(daily.wa.runCE2)
```

#volume average (daily area weighted average concentration / daily area weighted average output)

```
daily.vwa.runCE = matrix(0,fourth.25[20],1)

for(i in 1:fourth.25[20])        daily.vwa.runCE[i] = daily.wa.runCE[i] / daily.wa.output.runCE[i]

quartz()
plot(daily.vwa.runCE,type="o")
```

```
lines(c(1:dt[20]),Cs[[20]],col="green",lwd=2)
```

#<u>3rd step:</u> use the runCE output (per cell) as the current melt water signature for an integretad runCE #simulation for the whole catchment

```
#Store old runCE by grid
runCE.grid = runCE
dt.grid = dt
```

#Set single pre-event concentration

```
Cp = -12.3
```

#Import stream discharge (Q) and 18O isotopic signature (Cs), daily area weighted average snowmelt (M) and daily 18O flux (M.by.Cm) – catchment time series

```
Q=matrix(coredata(Q.mm.day[183:(183+dt-1)]),length(coredata(Q.mm.day[183:(183+dt-1)])),1)
Cs=matrix(daily.sth,dt,1)
M=matrix(c(daily.wa.output,rep(0,(dt - length(daily.wa.output)))),dt,1)
M.by.Cm=matrix(c(daily.wa.oxy,rep(0,(dt - length(daily.wa.oxy)))),dt,1)
if(Cm.flag == 1) Cm = matrix(c(replace(test2,test2=="NaN",0),rep(0,(dt - length(daily.wa.M)))),dt,1)
if(Cm.flag ==2 ) Cm = M.by.Cm/M
```

#Building empty matrices for every parameters to resolve

```
runCE = matrix(0,dt,1)
E = matrix(0,dt,1)
f.runCE = matrix(0,dt,1)
sumE = matrix(0,dt,1)
sumE.by.Ce = matrix(0,dt,1)
sumM = matrix(0,dt,1)
sumM.by.Cm = matrix(0,dt,1)
f = matrix(0,dt,1)
g = matrix(0,dt,1)
```

#Calculate Melt (given) sum variables

```
for (i in 1:dt){
	if(i==1){
		sumM.by.Cm[i] = M.by.Cm[i]
		sumM[i] = M[i]
	} else {
		sumM.by.Cm[i] = (sumM.by.Cm[i-1] + M.by.Cm[i])
		sumM[i] = sumM[i-1] + M[i]
		}
		}
```

#Starting value for runCE iteration

```
z = -16
```

#Start of runCE catchment simulation

```
if(runCE.flag ==1){

	counter = 0
```

```
for(i in 1:dt) {

        Diff.runCE=1
        runCE.Old=0
        RMS = 0

        #Initial values for runCE (value of z)
        if(i==1)runCE[i] = z  else runCE[i] = runCE[i-1]


        #Iteration optimisation loop
        while(Diff.runCE > 0.00000001) {
                #difference in runCE between the two last runs will be less then the given value

        #count total number of iterations
        counter = counter +1

        #store old runCE in variable
        runCE.Old = runCE[i]

        #Calculate event water fraction f and event water amount E
        f.runCE[i] = (Cs[i] - Cp) / (runCE.Old-Cp)
        E[i] = Q[i] * f.runCE[i]

        #Calculate sum variables

        if(i==1){
                sumE[i] = E[i]
                sumE.by.Ce[i] = E[i]*runCE.Old
                } else {
                sumE.by.Ce[i] = sumE.by.Ce[i-1] + E[i]*runCE.Old
                sumE[i] = sumE[i-1]+E[i]
                }


        #Calculate new (fitted) runCE
        f[i] = sumM.by.Cm[i] - sumE.by.Ce[i]
        g[i] = sumM[i] - sumE[i]
        runCE[i] = f[i] / g[i]

        #Calculate the difference between the old and the new runCE value
        RMS = sqrt((runCE[i]^2 + runCE.Old^2)/2)
        Diff.runCE = abs(RMS - abs(runCE[i]))
        }
}
}

#number of iterations that was needed to resolve E

print(counter)
```

#Weighted average – for graph

```
WA = sumM.by.Cm [dt,1]/ sum(M)
WA = rep(WA,dt)
```

***#4th step*: Uncertainty analysis (by Genereux, 1998) at 70% level of confidence**

```
Wp = matrix(0,dt,1)   #Uncertainty value to be computed
W18Op = 0.1  #analytical error (0.1)
W18Oe = 0.44  #standard residual error for relationship > 0.75 Rsqr - 70% level of confidence
W18Os = 0.1  #analytical error (0.1)

for(i in 1:dt) Wp[i] = sqrt(((((runCE[i] - Cs[i]) / (Cp - runCE[i])^2)*W18Op)^2)+((((Cs[i] - Cp) / (Cp - runCE[i])^2)*W18Oe)^2)+(((1 / (Cp - runCE[i]))*W18Os)^2))
```

***#5th step*: Plotting the results**

```
require(TTR)

quartz(width=8, height = 6)
par(mfrow = c(3,1), mar = c(1.8,4,0.3,4)+0.3)
```

#Creating upper and lower limits set by uncertainty analysis

```
lower.E = matrix(0,dt,1)
upper.E = matrix(0,dt,1)

for(i in 1:dt){   lower.E[i] = Q[i] * (f.runCE[i] - Wp[i])
                  upper.E[i] = Q[i] * (f.runCE[i] + Wp[i])
               }
```

#Maximise upper limit for E (uncertainty) - so it does not exceed Q

```
upper.E2 = matrix(0,dt,1)

for(i in 1:dt) upper.E2[i] = replace(upper.E[i], upper.E[i] > Q[i], Q[i])
```

#Maximise upper limit for E (Event water) - so it does not exceed Q

```
lower.E2 = matrix(0,dt,1)

for(i in 1:dt) lower.E2[i] = replace(lower.E[i], lower.E[i] > Q[i], Q[i])
```

#Plotting isotopic signature for the stream, pre-event and event water (runCE, current melt water #and volume weighted average)

```
plot( 1:dt, WA, type = "l", lwd = 1.3, lty = 2, col = "darkblue", main = "",
      ylab = " ",
      xlab = " ",
      xaxt = "n",
      yaxt = "n",
      ylim = c(-17,-12),
      cex.lab = 1,
      cex.axis = 1
      )
lines(1:108, Cm[1:108], lty = 1, col = "black", lwd = 1.3)
lines(1:dt, runCE, lty = 3, col = "darkred", lwd = 1.5)
lines(1:dt, rep(Cp,dt), col = "brown",lwd = 1.3)
lines(1:dt, Cs, col = "green",lty = 4, lwd = 1.3)
legend(129,-15, c("Pre-event water","Stream water","Current melt water","Weighted average", "runCE"), col = c("brown","green","black","darkblue", "darkred"),lwd= c(rep(1.5,5)),text.col = "273", lty = c(1,4,1,2,3), cex =
```

```
0.9, merge = TRUE, bg = "219", bty = "n")
axis(2,yaxp = c(-17,-12, 5),line = 0.25, las = 1, cex.axis=1)
mtext(side=2, line =2.3, at = -12.5, las=2, expression(delta^18*O))
```

#Plotting IHS using runCE as event water signature

```
plot(dates, rep(15,177),type = "n", lwd = 1.3, col = "black", main = "",
        ylab = "",
        xlab = " ",
        yaxt = "n",
        ylim = c(0,40)
        )
xvals = seq(dates[1],dates[160],"days")
polygon(c(xvals,rev(xvals)), c(rep(0,160),rev(replace(lower.E2[1:160],lower.E2[1:160]<0,0))),col="royalblue",
border = NA)
polygon(c(xvals,rev(xvals)),
c(replace(lower.E2[1:160],lower.E2[1:160]<0,0),rev(upper.E2[1:160])),col="royalblue", density = 30, angle =
30)
lines(dates[1:160],E[1:160], lty = 2 , col = "darkblue", lwd = 1.5)
lines(dates, Q, lwd = 1.5, col = "black")
axis(2,yaxp = c(0,30,6),line = 0.25, las = 1, cex.axis=1)
mtext(side = 2, line =3, at = 15, expression("Q (mm"%.%"day"^{-1}*")"),cex = 1.1)
rect(as.numeric(dates[1])+130,17.5,as.numeric(dates[1])+140,19.5,
col="gray40");text(as.numeric(dates[1])+150,18.5,"Snowmelt",cex=0.9)
rect(as.numeric(dates[1])+130,15,as.numeric(dates[1])+140,17, col="gray40", density = 30, angle =
30);text(as.numeric(dates[1])+148.25,16,"Rainfall",cex=0.9)
rect(as.numeric(dates[1])+130,12.5,as.numeric(dates[1])+140,14.5,col =
"royalblue");text(as.numeric(dates[1])+151.5,13.5,"Event water",cex=0.9)
rect(as.numeric(dates[1])+130,10,as.numeric(dates[1])+140,12, col="royalblue",density = 30, angle =
30);text(as.numeric(dates[1])+161.5,10.9,"Uncertainty (75% L.of C.)",cex=0.9)
rect(as.numeric(dates[1])+130,7.5,as.numeric(dates[1])+140,9.5,col =
"white");text(as.numeric(dates[1])+154.5,8.5,"Pre-event water",cex=0.9)
lines(c(as.numeric(dates[1])+130,as.numeric(dates[1])+140),rep(21,2),col = "darkblue", lty = 2, lwd =
1.5);text(as.numeric(dates[1])+159.5,21,"Hydrograph separation",cex=0.9)
lines(c(as.numeric(dates[1])+130,as.numeric(dates[1])+140),rep(23.5,2),col = "black", lty = 1, lwd =
1.5);text(as.numeric(dates[1])+150.2,23.5,"Discharge",cex=0.9)
```

#Adding snowpack drainage output barplot to graph

```
M0 = matrix(c(daily.wa.M[1:122],rep(0,55)),1,dt)
M1 = matrix(c(daily.wa.output.copy-daily.wa.M,rep(0,55)),1,dt) #precip.d obj - see format runCE codes
M2 = rbind(M0,M1)

require(plotrix)
par(new="T")
barplot(M2, beside=F,ylab="",axes=F,ylim = c(100,0), col = c("gray40", "gray40"), density = c(NA,30), angle
= c(NA,30),cex.axis=1.3,cex.lab=1.2)
axis(4,yaxp = c(0,40,4),line = 0.25, las=1,cex.axis=1)
axis.break(3,149,style = "slash")
mtext(side=4,line=2.3,at = 20,expression("mm"%.%"day"^{-1}),cex = 1.1)
```

#Computing IHS using the volume-weighted average (VWA) approach as event water signature

```
f.wa = matrix(0,dt,1)
E.wa = matrix(0,dt,1)
Wp.wa = matrix(0,dt,1)
```

#VWA Calculation

```
for(i in 1:dt) {  f.wa[i] = (Cs[i] - Cp) / (WA[i] - Cp)
                                E.wa[i] = Q[i] * f.wa[i]
                        }
```

#Uncertainty analysis

```
for(i in 1:dt) Wp.wa[i] = sqrt(((((WA[i] - Cs[i]) / (Cp - WA[i])^2)*W18Op)^2)+((((Cs[i] - Cp) / (Cp -
WA[i])^2)*W18Oe)^2)+(((1 / (Cp - WA[i]))*W18Os)^2))

lower.E.wa = matrix(0,dt,1)
upper.E.wa = matrix(0,dt,1)

for(i in 1:dt){   lower.E.wa[i] = Q[i] * (f.wa[i] - Wp.wa[i])
                                upper.E.wa[i] = Q[i] * (f.wa[i] + Wp.wa[i])
                        }
```

#Maximise upper limit for E (uncertainty) - so it does not exceed Q

```
upper.E2.wa = matrix(0,dt,1)

for(i in 1:dt) upper.E2.wa[i] = replace(upper.E.wa[i], upper.E.wa[i] > Q[i], Q[i])
```

#Maximise upper limit for E (Event water) - so it does not exceed Q

```
lower.E2.wa = matrix(0,dt,1)

for(i in 1:dt) lower.E2.wa[i] = replace(lower.E.wa[i], lower.E.wa[i] > Q[i], Q[i])
```

#Graphing IHS - VWA approach

```
plot(dates, rep(15,177),type = "n", lwd = 1.3, col = "black", main = "",
        ylab = "",
        xlab = " ",
        yaxt = "n",
        ylim = c(0,40)
        )
xvals = seq(dates[1],dates[160],"days")
polygon(c(xvals,rev(xvals)),
c(rep(0,160),rev(replace(lower.E2.wa[1:160],lower.E2.wa[1:160]<0,0))),col="royalblue", border = NA)
polygon(c(xvals,rev(xvals)),
c(replace(lower.E2.wa[1:160],lower.E2.wa[1:160]<0,0),rev(upper.E2.wa[1:160])),col="royalblue", density =
30, angle = 30)
lines(dates[1:160],E.wa[1:160], lty = 2 , col = "darkblue", lwd = 1.5)
lines(dates, Q, lwd = 1.5, col = "black")
axis(2,yaxp = c(0,30,6),line = 0.25, las = 1, cex.axis=1)
mtext(side = 2, line =3, at = 15, expression("Q (mm"%.%"day"^{-1}*")"),cex = 1.1)
rect(as.numeric(dates[1])+130,17.5,as.numeric(dates[1])+140,19.5,
col="gray40");text(as.numeric(dates[1])+150,18.5,"Snowmelt",cex=0.9)
rect(as.numeric(dates[1])+130,15,as.numeric(dates[1])+140,17, col="gray40", density = 30, angle =
30);text(as.numeric(dates[1])+148.25,16,"Rainfall",cex=0.9)
rect(as.numeric(dates[1])+130,12.5,as.numeric(dates[1])+140,14.5,col =
"royalblue");text(as.numeric(dates[1])+151.5,13.5,"Event water",cex=0.9)
rect(as.numeric(dates[1])+130,10,as.numeric(dates[1])+140,12, col="royalblue",density = 30, angle =
30);text(as.numeric(dates[1])+161.5,10.9,"Uncertainty (75% L.of C.)",cex=0.9)
rect(as.numeric(dates[1])+130,7.5,as.numeric(dates[1])+140,9.5,col =
```

```
"white");text(as.numeric(dates[1])+154.5,8.5,"Pre-event water",cex=0.9)
lines(c(as.numeric(dates[1])+130,as.numeric(dates[1])+140),rep(21,2),col = "darkblue", lty = 2, lwd =
1.5);text(as.numeric(dates[1])+159.5,21,"Hydrograph separation",cex=0.9)
lines(c(as.numeric(dates[1])+130,as.numeric(dates[1])+140),rep(23.5,2),col = "black", lty = 1, lwd =
1.5);text(as.numeric(dates[1])+150.2,23.5,"Discharge",cex=0.9)
```

#Adding snowpack drainage output barplot to graph

```
#Create matrix with precip column for barplot
M0 = matrix(c(daily.wa.M[1:122],rep(0,55)),1,dt)
M1 = matrix(c(daily.wa.output.copy-daily.wa.M,rep(0,55)),1,dt) #precip.d obj - see format runCE codes
M2 = rbind(M0,M1)

require(plotrix)
par(new="T")
barplot(M2, beside=F,ylab="",axes=F,ylim = c(100,0), col = c("gray40", "gray40"), density = c(NA,30), angle
= c(NA,30),cex.axis=1.3,cex.lab=1.2)
axis(4,yaxp = c(0,40,4),line = 0.25, las=1,cex.axis=1)
axis.break(3,149,style = "slash")
mtext(side=4,line=2.3,at = 20,expression("mm"%.%"day"^{-1}),cex = 1.1)
```

Appendix I – runCE 3-IHS (plateform = *R*)

```
#Set the components' concentration

Csth.Si = coredata(approx.STH.Si)        #[Si] in streamwater (variable)
runCE = runCE[1:115]                     #Snowpack drainage event isotopic sign. from runCE (variable)
Cp.Si = 4                                #Groundwater pre-event [Si] (constant)
Cp = -12.3                               #Groundwater pre-event isotopic signature (constant)
Cs = Cs.copy[1:115]                      #Streamwater isotopic signature (variable)
SW.Si = 3.5                              #Soil water pre-event [Si] (constant)
SW.oxy = -13                             #Soil water isotopic signature (constant)

#Compute fraction of event water, soil water and groundwater composing the streamflow

fe.3 = matrix(0,115,1)                   #Fraction of event water
fe.soil = matrix(0,115,1)                #Fraction of soil water
fe.gw = matrix(0,115,1)                  #Fraction of groundwater

#Three-component IHS model

for(i in 1:115)  fe.3[i] = (((Csth.Si[i] - SW.Si)*(Cp - SW.oxy)) - ((Cs[i]-SW.oxy)*(Cp.Si - SW.Si)))/(((0 -
SW.Si)*(Cp - SW.oxy)) - ((runCE[i]-SW.oxy)*(Cp.Si - SW.Si)))

for(i in 1:115) fe.soil[i] = ((Cs[i] - Cp)/(SW.oxy - Cp)) - fe.3[i]*((runCE[i] - Cp)/(SW.oxy - Cp))
for(i in 1:115) fe.gw[i] = ((Cs[i] - SW.oxy)/(Cp - SW.oxy)) - fe.3[i]*((runCE[i] - SW.oxy)/(Cp - SW.oxy))

#Deleting mathematical incongruences (0% > fraction of a component > 100%) by limiting the
#fractions between 0 and 100%

fe.soil.norm = matrix(0,115,1)
fe.gw.norm = matrix(0,115,1)
fe.event.norm = matrix(0,115,1)

for(i in 1:115) { fe.soil.norm[i] = replace(fe.soil[i],fe.soil[i]<0,0)
                  fe.soil.norm[i] = replace(fe.soil.norm[i], fe.soil.norm[i] > 1, 1)
                  fe.gw.norm[i] = replace(fe.gw[i],fe.gw[i]<0,0)
                  fe.gw.norm[i] = replace(fe.gw.norm[i], fe.gw.norm[i] > 1, 1)
                }

for(i in 1:115) {  fe.event.norm[i] = 1 - (fe.soil.norm[i] + fe.gw.norm[i])
                  fe.event.norm[i] = replace(fe.event.norm[i],fe.event.norm[i] <0 , 0)
                }

cbind(fe.soil.norm,fe.gw.norm,fe.event.norm)

#Deleting mathematical incongruences: distributing evenly the errors of the components when they
add up to more than 100% of the stream discharge

fe.incon = matrix(0,115,1)
fe.soil.corr = matrix(0,115,1)
fe.gw.corr = matrix(0,115,1)

for(i in 1:115) fe.incon[i] = (fe.event.norm[i] + fe.soil.norm[i] + fe.gw.norm[i]) - 1
```

```
for(i in 1:115) { if(fe.incon[i] == 0) {  fe.soil.corr[i] = fe.soil.norm[i]
                                          fe.gw.corr[i] = fe.gw.norm[i]
                                          }
                  if(fe.incon[i] !=0) {   fe.soil.corr[i] = fe.soil.norm[i] - ((fe.soil.norm[i] / (fe.incon[i] + 1)) *
fe.incon[i])
                                          fe.gw.corr[i] = fe.gw.norm[i] - ((fe.gw.norm[i] / (fe.incon[i] + 1)) *
fe.incon[i])
                                          }
                  }

cbind(fe.soil.corr,fe.gw.corr,fe.event.norm)
```

#Computing 3-IHS with smoothen stream concentration values (5 days standard moving average)

```
require(TTR)
smth.Cs= SMA(Cs,n=5)
smth.Cs = c(rep(smth.Cs[5],2),smth.Cs[5:115],rep(smth.Cs[115],2))
smth.Csth.Si= SMA(Csth.Si,n=5)
smth.Csth.Si = c(rep(smth.Csth.Si[5],2),smth.Csth.Si[5:115],rep(smth.Csth.Si[115],2))

Cs.sm = smth.Cs
Csth.Si.sm = smth.Csth.Si
fe.3.sm = matrix(0,115,1)
fe.soil.sm = matrix(0,115,1)
fe.gw.sm = matrix(0,115,1)

for(i in 1:115)  fe.3.sm[i] = (((Csth.Si.sm[i] - SW.Si)*(Cp - SW.oxy)) - ((Cs.sm[i]-SW.oxy)*(Cp.Si -
SW.Si)))/(((0 - SW.Si)*(Cp - SW.oxy)) - ((runCE[i]-SW.oxy)*(Cp.Si - SW.Si)))

for(i in 1:115) fe.soil.sm[i] = ((Cs.sm[i] - Cp)/(SW.oxy - Cp)) - fe.3.sm[i]*((runCE[i] - Cp)/(SW.oxy - Cp))
for(i in 1:115) fe.gw.sm[i] = ((Cs.sm[i] - SW.oxy)/(Cp - SW.oxy)) - fe.3.sm[i]*((runCE[i] - SW.oxy)/(Cp -
SW.oxy))

fe.soil.norm.sm = matrix(0,115,1)
fe.gw.norm.sm = matrix(0,115,1)

for(i in 1:115) { fe.soil.norm.sm[i] = replace(fe.soil.sm[i],fe.soil.sm[i]<0,0)
                  fe.soil.norm.sm[i] = replace(fe.soil.norm.sm[i], fe.soil.norm.sm[i] > 1, 1)
                  fe.gw.norm.sm[i] = replace(fe.gw.sm[i],fe.gw.sm[i]<0,0)
                  fe.gw.norm.sm[i] = replace(fe.gw.norm.sm[i], fe.gw.norm.sm[i] > 1, 1)
                }

fe.event.norm.sm = matrix(0,115,1)

for(i in 1:115) {   fe.event.norm.sm[i] = 1 - (fe.soil.norm.sm[i] + fe.gw.norm.sm[i])
                    fe.event.norm.sm[i] = replace(fe.event.norm.sm[i],fe.event.norm.sm[i] <0 , 0)
                }

cbind(fe.soil.norm.sm,fe.gw.norm.sm,fe.event.norm.sm)

fe.incon.sm = matrix(0,115,1)

for(i in 1:115) fe.incon.sm[i] = (fe.event.norm.sm[i] + fe.soil.norm.sm[i] + fe.gw.norm.sm[i]) - 1

fe.soil.corr.sm = matrix(0,115,1)
fe.gw.corr.sm = matrix(0,115,1)
```

```
for(i in 1:115) { if(fe.incon.sm[i] == 0) {       fe.soil.corr.sm[i] = fe.soil.norm.sm[i]
                                                    fe.gw.corr.sm[i] = fe.gw.norm.sm[i]
                                                 }
                  if(fe.incon.sm[i] !=0) {        fe.soil.corr.sm[i] = fe.soil.norm.sm[i] - ((fe.soil.norm.sm[i] /
(fe.incon.sm[i] + 1)) * fe.incon.sm[i])
                                                  fe.gw.corr.sm[i] = fe.gw.norm.sm[i] - ((fe.gw.norm.sm[i] /
(fe.incon.sm[i] + 1)) * fe.incon.sm[i])
                                                }
        }

cbind(fe.soil.corr.sm,fe.gw.corr.sm,fe.event.norm.sm)
```

#Plot results 3-IHS

```
quartz(width=6, height = 8)
par(mfrow = c(5,1), mar = c(1.8,5,0.3,5)+0.3)
```

#Isotopic signature

```
plot( daily[1:115], runCE, type = "l", lwd = 1.5, lty = 1, col = "steelblue2", main = "",
        ylab = " ",
        xlab = " ",
        yaxt = "n",
        ylim = c(-16,-12),
        cex.lab = 1,
        cex.axis = 1
        )
lines(daily[1:115], rep(Cp,115), lty = 1, col = "tan3", lwd = 1.5)
lines(daily[1:115], rep(SW.oxy,115), lty = 1, col = "yellowgreen", lwd = 1.5)
lines(daily[1:115], Cs.sm, col = "black",lwd = 1.5)
lines(daily[1:115], Cs.copy, lty=2, lwd = 1.3)
legend(daily[1]+75,-13.9, c("Till water","Soil water","Snowpack drainage (runCE)","Stream water (5 days
mov. avrg.)","Stream water (raw)"), col = c("tan3","yellowgreen","steelblue2","black","black"),lwd=
c(rep(1.5,4),1.3),text.col = "273", lty = c(rep(1,4),2), cex = 0.9, merge = TRUE, bg = "219", bty = "n")
axis(2,yaxp = c(-16,-12, 4),line = 0.25, las = 1, cex.axis=1)
mtext(side=2, line =2.3, at = -12.5, las=2, expression(delta^18*O))
```

#Silicon concentrations

```
require(fields)
plot( daily[1:115], rep(0,115), type = "l", lwd = 1.5, lty = 1, col = "steelblue2", main = "",
ylab = " ",
xlab = " ",
yaxt = "n",
ylim = c(0,4),
cex.lab = 1,
cex.axis = 1
        )
lines(daily[1:115], rep(Cp.Si,115), lty = 1, col = "tan3", lwd = 1.5)
lines(daily[1:115], rep(mean.GWL.Si,115), lty = 2, col = "yellowgreen", lwd = 1.5)
lines(daily[1:115],rep(SW.Si,115),lty = 1, col = "yellowgreen",lwd=1.5)
lines(daily[1:115], Csth.Si.sm, col = "black",lwd = 1.5)
lines(daily[1:115],Csth.Si.copy,lty=2,lwd=1.3)
arrows(daily[1]+2,2.3,daily[1]+2,3.3,col="yellowgreen",length=0.1,lwd=2);arrows(daily[1]+113,2.3,daily[1]+11
3,3.3,col="yellowgreen",lwd=2,length=0.1)
```

```
legend(daily[1]+80,1.5, c("Measured soil water","Assumed soil water" ), col =
c("yellowgreen","yellowgreen"),lwd= c(rep(1.5,2)),text.col = "273", lty = c(2,1), cex = 1, merge = TRUE, bg =
"219", bty = "n")
axis(2,yaxp = c(0,4, 4),line = 0.25, las = 1, cex.axis=1)
mtext(side=2, line =2.3, at = 3.5, las=2, expression("[Si]"))
```

#Calculating stream discharge for each component

```
Q.soil = matrix(0,115,1)
Q.snow = matrix(0,115,1)
Q.till = matrix(0,115,1)

for(i in 1:115) { Q.soil[i] = Q[i] * fe.soil.corr[i]
                  Q.snow[i] = Q[i] * fe.event.norm[i]
                  Q.till[i] = Q[i] * fe.gw.corr[i]
                }
```

#Plotting Hydrograph Separation – based on smooth version

```
plot(daily[1:115], rep(15,115),type = "n", lwd = 1.3, col = "black", main = "",
        ylab = "",
        xlab = " ",
        yaxt = "n",
        ylim = c(0,40)
        )
xvals = seq(daily[1],daily[115],"days")
polygon(c(xvals,rev(xvals)), c(rep(0,115),rev(Q.till)),col="tan3", border = NA)
polygon(c(xvals,rev(xvals)), c(Q.till,rev(Q.till+Q.soil)),col="yellowgreen", border = NA)
polygon(c(xvals,rev(xvals)), c(Q.till+Q.soil,rev(Q.till+Q.soil+Q.snow)),col="steelblue2", border = NA)
lines(daily[1:115], Q[1:115], lwd = 1.5, col = "black")
axis(2,yaxp = c(0,30,6),line = 0.25, las = 1, cex.axis=1)
mtext(side = 2, line =3, at = 15, expression("Q (mm"%.%"day"^{-1}*")"),cex = 0.9)
text(as.numeric(daily[1])+100,6,"smooth stream values",cex=0.9,font=3)

#Create matrix with precip column for barplot
M0 = matrix(daily.wa.M[1:115],1,115)
M1 = matrix(daily.wa.output.copy[1:115]-daily.wa.M[1:115],1,115)
M2 = rbind(M0,M1)

require(plotrix)
par(new="T")
barplot(M2, beside=F,ylab="",axes=F,ylim = c(100,0), col = c("gray40", "gray40"), density = c(NA,30), angle
= c(NA,30),cex.axis=1.3,cex.lab=1.2)
axis(4,yaxp = c(0,40,4),line = 0.25, las=1,cex.axis=1)
mtext(side=4,line=2.8,at = 20,expression("mm"%.%"day"^{-1}),cex = 0.9)
```

#Plotting mixing diagram – smooth version

```
xvals = seq(daily[1],daily[115],"days")
plot(xvals,fe.gw.corr, type="n", col="black",yaxt = "n",ylim = c(0,1),ylab="",xlab="")
polygon(c(xvals,rev(xvals)), c(rep(0,115),rev(fe.gw.corr.sm)), col="tan3",border = NA)
polygon(c(xvals,rev(xvals)), c(fe.gw.corr.sm,rev(fe.gw.corr.sm+fe.soil.corr.sm)), col="yellowgreen",border =
NA)
polygon(c(xvals,rev(xvals)), c(fe.gw.corr.sm+fe.soil.corr.sm,rev(rep(1,115))), col="steelblue2",border = NA)
axis(2,yaxp = c(0,1,5),line=0.25,las=1)
mtext(side=2,line=2.8, at = 0.5, expression("fraction of total discharge"),cex=0.8)
abline(h=0.5, lty=2)
text(as.numeric(daily[1])+75,0.2,"Groundwater",cex=1.1)
```

```
text(as.numeric(daily[1])+45,0.3,"Soil water",cex=1.1)
text(as.numeric(daily[1])+30,0.8,"Snowpack",cex=1.1)
text(as.numeric(daily[1])+30,0.73,"drainage",cex=1.1)
text(as.numeric(daily[1])+100,0.1,"smooth stream values",cex=0.9,font=3)
```

#Plotting mixing diagram – raw values

```
xvals = seq(daily[1],daily[115],"days")
plot(xvals,fe.gw.corr, type="n", col="black",yaxt = "n",ylim = c(0,1),ylab="",xlab="")
polygon(c(xvals,rev(xvals)), c(rep(0,115),rev(fe.gw.corr)), col="tan3",border = NA)
polygon(c(xvals,rev(xvals)), c(fe.gw.corr,rev(fe.gw.corr+fe.soil.corr)), col="yellowgreen",border = NA)
polygon(c(xvals,rev(xvals)), c(fe.gw.corr+fe.soil.corr,rev(rep(1,115))), col="steelblue2",border = NA)
axis(2,yaxp = c(0,1,5),line=0.25,las=1)
mtext(side=2,line=2.8, at = 0.5, expression("fraction of total discharge"),cex=0.8)
abline(h=0.5, lty=2)
text(as.numeric(daily[1])+75,0.2,"Groundwater",cex=1.1)
text(as.numeric(daily[1])+45,0.3,"Soil water",cex=1.1)
text(as.numeric(daily[1])+30,0.8,"Snowpack",cex=1.1)
text(as.numeric(daily[1])+30,0.73,"drainage",cex=1.1)
text(as.numeric(daily[1])+100,0.1,"raw stream values",cex=0.9,font=3)
```

Appendix J – Recession Analysis (plateform = *R*)

***#1st step*: Define the recession segments to model**

```
obs = list(ste.lst[[1]],ste.lst[[2]],ste.lst[[3]],ste.lst[[4]],ste.lst[[5]],ste.lst[[6]],ste.lst[[7]])     #Observed Q
t = list(c(1:length(ste.days[[1]])),c(1:length(ste.days[[2]])),                                            #Time stamp
    c(1:length(ste.days[[3]])),c(1:length(ste.days[[4]])),c(1:length(ste.days[[5]])),
    c(1:length(ste.days[[6]])),c(1:length(ste.days[[7]])) )
nr = 7                                                                              #number of recession segments
```

***#2nd step*: Master single linear reservoir model**

```
#Object to fill-in by loop structure

sum.r = matrix(0,nr,1)                          #Loss function object
r.2 = rep(list(matrix(0,1,1)),nr)               #Loss function object
pred = rep(list(matrix(0,1,1)),nr)              #Predicted Q values

#Master linear model function

lin.loss.func = function(Q0) {
        Q01 = Q0[1]
        Q02 = Q0[2]
        Q03 = Q0[3]
        Q04 = Q0[4]
        Q05 = Q0[5]
        Q06 = Q0[6]
        Q07 = Q0[7]
        k = Q0[8]
for(j in 1:nr) { if(j==1) for(i in 1:length(obs[[j]])) pred[[j]][i] = Q01*exp(-k*t[[j]][i])
                 if(j==2) for(i in 1:length(obs[[j]])) pred[[j]][i] = Q02*exp(-k*t[[j]][i])
                 if(j==3) for(i in 1:length(obs[[j]])) pred[[j]][i] = Q03*exp(-k*t[[j]][i])
                 if(j==4) for(i in 1:length(obs[[j]])) pred[[j]][i] = Q04*exp(-k*t[[j]][i])
                 if(j==5) for(i in 1:length(obs[[j]])) pred[[j]][i] = Q05*exp(-k*t[[j]][i])
                 if(j==6) for(i in 1:length(obs[[j]])) pred[[j]][i] = Q06*exp(-k*t[[j]][i])
                 if(j==7) for(i in 1:length(obs[[j]])) pred[[j]][i] = Q07*exp(-k*t[[j]][i])
                 }

#Loss function

for(j in 1:nr)
        for(i in 1:length(obs[[j]]))      r.2[[j]][i] = ((pred[[j]][i] - obs[[j]][i])/obs[[j]][i])^2
for(j in 1:nr)    sum.r[j] = sum(r.2[[j]]) / length(r.2[[j]])
sqrt(sum(sum.r) / nr )
}

#Optimization of loss function with starting values (here one Q0 by recession segment and one common k
value)

op.ln = optim(c(17,1.5,1.5,1,2,1.2,3, 0.40), lin.loss.func)
master.lin.k = op.ln$par[8]
master.lin.er = op.ln$value
master.lin.Q0 = op.ln$par[1:7]
```

***#3rd step:* #dual-linear reservoir serial model**

#Master dual-linear function

```
dual.loss.func = function(x) {
	Q01 = x[1]
	Q02 = x[2]
	Q03 = x[3]
	Q04 = x[4]
	Q05 = x[5]
	Q06 = x[6]
	Q07 = x[7]
	Q11 = x[8]
	Q12 = x[9]
	Q13 = x[10]
	Q14 = x[11]
	Q15 = x[12]
	Q16 = x[13]
	Q17 = x[14]
	k1 = x[15]
	k2 = x[16]
	for(j in 1:nr) { if(j==1) for(i in 1:length(obs[[j]])) pred[[j]][i] = Q01*exp(-k2*t[[j]][i]) + ((k2*Q11)/(k2-
k1))*(exp(-k1*t[[j]][i]) - exp(-k2*t[[j]][i]))
			 if(j==2) for(i in 1:length(obs[[j]])) pred[[j]][i] = Q02*exp(-k2*t[[j]][i]) + ((k2*Q12)/(k2-
k1))*(exp(-k1*t[[j]][i]) - exp(-k2*t[[j]][i]))
			if(j==3) for(i in 1:length(obs[[j]])) pred[[j]][i] = Q03*exp(-k2*t[[j]][i]) + ((k2*Q13)/(k2-
k1))*(exp(-k1*t[[j]][i]) - exp(-k2*t[[j]][i]))
			if(j==4) for(i in 1:length(obs[[j]])) pred[[j]][i] = Q04*exp(-k2*t[[j]][i]) + ((k2*Q14)/(k2-
k1))*(exp(-k1*t[[j]][i]) - exp(-k2*t[[j]][i]))
			if(j==5) for(i in 1:length(obs[[j]])) pred[[j]][i] = Q05*exp(-k2*t[[j]][i]) + ((k2*Q15)/(k2-
k1))*(exp(-k1*t[[j]][i]) - exp(-k2*t[[j]][i]))
			if(j==6) for(i in 1:length(obs[[j]])) pred[[j]][i] = Q06*exp(-k2*t[[j]][i]) + ((k2*Q16)/(k2-
k1))*(exp(-k1*t[[j]][i]) - exp(-k2*t[[j]][i]))
			if(j==7) for(i in 1:length(obs[[j]])) pred[[j]][i] = Q07*exp(-k2*t[[j]][i]) + ((k2*Q17)/(k2-
k1))*(exp(-k1*t[[j]][i]) - exp(-k2*t[[j]][i]))
			}

#Loss function

for(j in 1:nr)
	for(i in 1:length(obs[[j]]))	r.2[[j]][i] = ((pred[[j]][i] - obs[[j]][i])/obs[[j]][i])^2
for(j in 1:nr)	sum.r[j] = sum(r.2[[j]]) / length(r.2[[j]])
sqrt(sum(sum.r) / nr )
}
```

#Optimization of loss function with starting values (here one Q0 and Q1 value by recession segment and one common k1 and k2 value)

```
op.dual = optim(c(18,2,2,1.5,2.5,2,3.5,12,1,1,1,1,1,2,0.01,0.1), dual.loss.func)
master.dual.ks = c(op.dual$par[15],op.dual$par[16])
master.dual.er = op.dual$value
master.dual.Q0 = op.dual$par[1:7]
master.dual.Q1 = op.dual$par[8:14]
```

***#4th step:* #power-law reservoir serial model**

#Object to fill-in through loop structure

```
u = rep(list(matrix(0,1,1)),nr)
```

```
p = rep(list(matrix(0,1,1)),nr)

#Master power-law function

pl.loss.func = function(x) {
        Q01 = x[1]
        Q02 = x[2]
        Q03 = x[3]
        Q04 = x[4]
        Q05 = x[5]
        Q06 = x[6]
        Q07 = x[7]
        a = x[8]
        b = x[9]
        for(j in 1:nr) { if(j==1) for(i in 1:length(obs[[j]])) { u[[j]][i] = (a^(1/b))*(b-1)*Q01^(b-1)/b
                                                        p[[j]][i] = b / (1-b)
                                                        pred[[j]][i] = Q01*(1+u[[j]][i] * t[[j]][i])^p[[j]][i]
                                                        }
                    if(j==2) for(i in 1:length(obs[[j]])) { u[[j]][i] = (a^(1/b))*(b-1)*Q02^(b-1)/b
                                                        p[[j]][i] = b / (1-b)
                                                        pred[[j]][i] = Q02*(1+u[[j]][i] * t[[j]][i])^p[[j]][i]
                                                        }
                    if(j==3) for(i in 1:length(obs[[j]])) { u[[j]][i] = (a^(1/b))*(b-1)*Q03^(b-1)/b
                                                        p[[j]][i] = b / (1-b)
                                                        pred[[j]][i] = Q03*(1+u[[j]][i] * t[[j]][i])^p[[j]][i]
                                                        }
                    if(j==4) for(i in 1:length(obs[[j]])) { u[[j]][i] = (a^(1/b))*(b-1)*Q04^(b-1)/b
                                                        p[[j]][i] = b / (1-b)
                                                        pred[[j]][i] = Q04*(1+u[[j]][i] * t[[j]][i])^p[[j]][i]
                                                        }
                    if(j==5) for(i in 1:length(obs[[j]])) { u[[j]][i] = (a^(1/b))*(b-1)*Q05^(b-1)/b
                                                        p[[j]][i] = b / (1-b)
                                                        pred[[j]][i] = Q05*(1+u[[j]][i] * t[[j]][i])^p[[j]][i]
                                                        }
                    if(j==6) for(i in 1:length(obs[[j]])) { u[[j]][i] = (a^(1/b))*(b-1)*Q06^(b-1)/b
                                                        p[[j]][i] = b / (1-b)
                                                        pred[[j]][i] = Q06*(1+u[[j]][i] * t[[j]][i])^p[[j]][i]
                                                        }
                    if(j==7) for(i in 1:length(obs[[j]])) { u[[j]][i] = (a^(1/b))*(b-1)*Q07^(b-1)/b
                                                        p[[j]][i] = b / (1-b)
                                                        pred[[j]][i] = Q07*(1+u[[j]][i] * t[[j]][i])^p[[j]][i]
                                                        }
                    }

#Loss function

for(j in 1:nr)
        for(i in 1:length(obs[[j]]))     r.2[[j]][i] = ((pred[[j]][i] - obs[[j]][i])/obs[[j]][i])^2
for(j in 1:nr)   sum.r[j] = sum(r.2[[j]]) / length(r.2[[j]])
sqrt(sum(sum.r) / nr )
}
```

#Optimization of loss function with starting values (here one Q0 value by recession segment and one common *a* and *b* value)

```
op.pl = optim(c(15,3,3,1,1,1,2,0.00003,2), pl.loss.func) #a=0.00003  b=2
master.pl.coeff = c(op.pl$par[8],op.pl$par[9])
master.pl.er = op.pl$value
master.pl.Q0 = op.pl$par[1:7]
```

Appendix K – Daily Isotope Regression Models

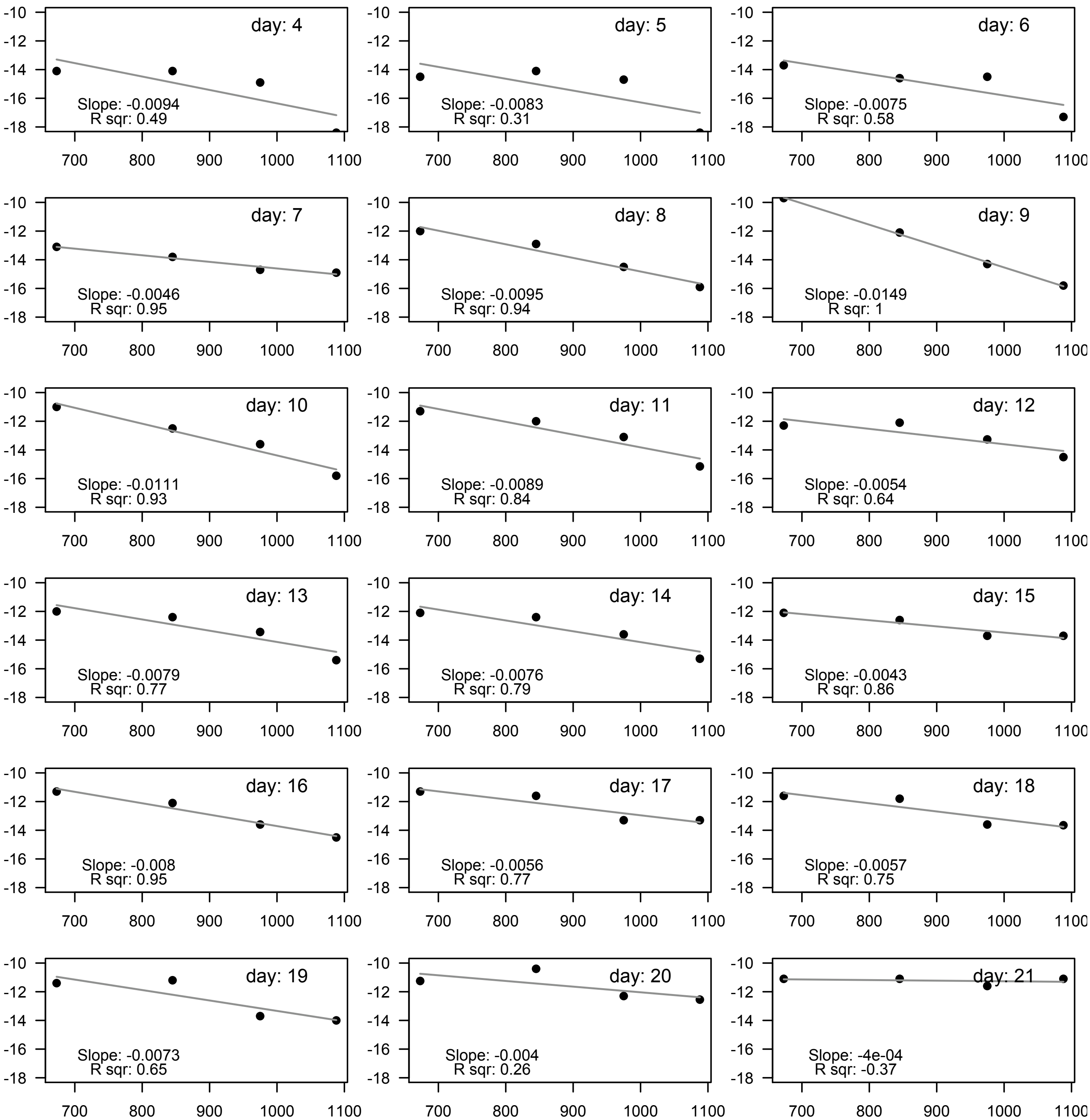

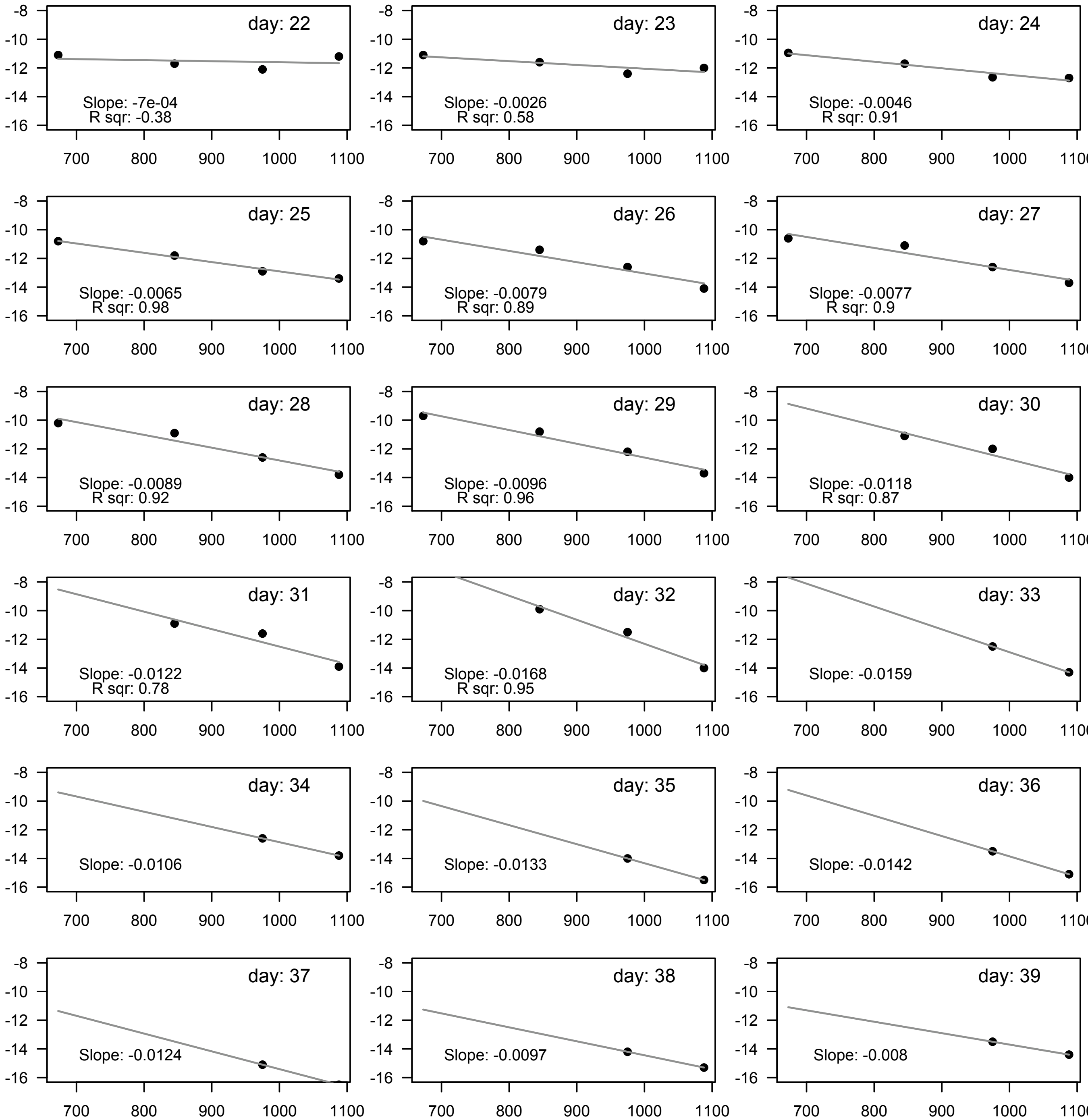
day: 22
Slope: -7e-04
R sqr: -0.38
day: 23
Slope: -0.0026
R sqr: 0.58
day: 24
Slope: -0.0046
R sqr: 0.91
day: 25
Slope: -0.0065
R sqr: 0.98
day: 26
Slope: -0.0079
R sqr: 0.89
day: 27
Slope: -0.0077
R sqr: 0.9
day: 28
Slope: -0.0089
R sqr: 0.92
day: 29
Slope: -0.0096
R sqr: 0.96
day: 30
Slope: -0.0118
R sqr: 0.87
day: 31
Slope: -0.0122
R sqr: 0.78
day: 32
Slope: -0.0168
R sqr: 0.95
day: 33
Slope: -0.0159
day: 34
Slope: -0.0106
day: 35
Slope: -0.0133
day: 36
Slope: -0.0142
day: 37
Slope: -0.0124
day: 38
Slope: -0.0097
day: 39
Slope: -0.008
-8
-10
-12
-14
-16
700
800
900
1000
1100

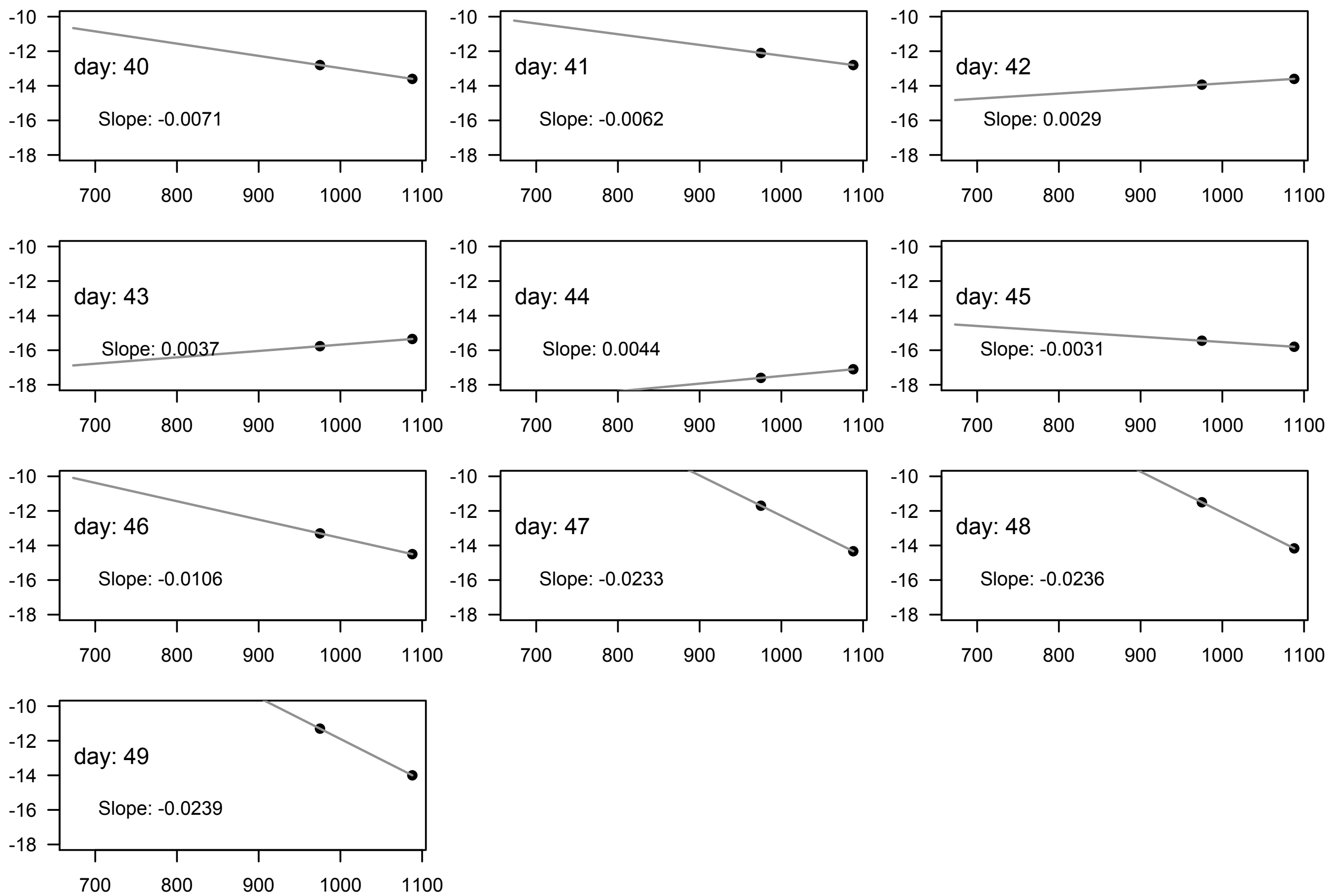
day: 40
Slope: -0.0071
day: 41
Slope: -0.0062
day: 42
Slope: 0.0029
day: 43
Slope: 0.0037
day: 44
Slope: 0.0044
day: 45
Slope: -0.0031
day: 46
Slope: -0.0106
day: 47
Slope: -0.0233
day: 48
Slope: -0.0236
day: 49
Slope: -0.0239
-10
-12
-14
-16
-18
700
800
900
1000
1100

Appendix L – Isotopic Signature of Stream and Subsurface Samples

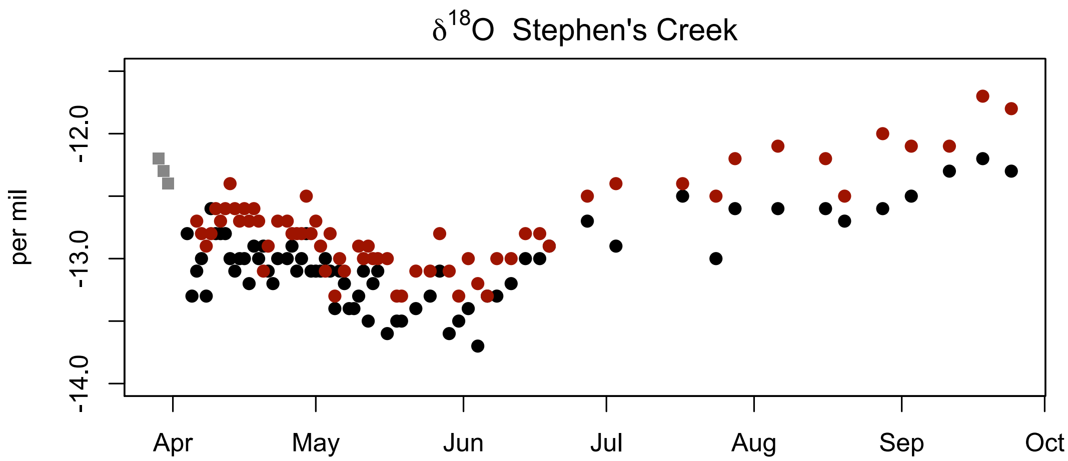

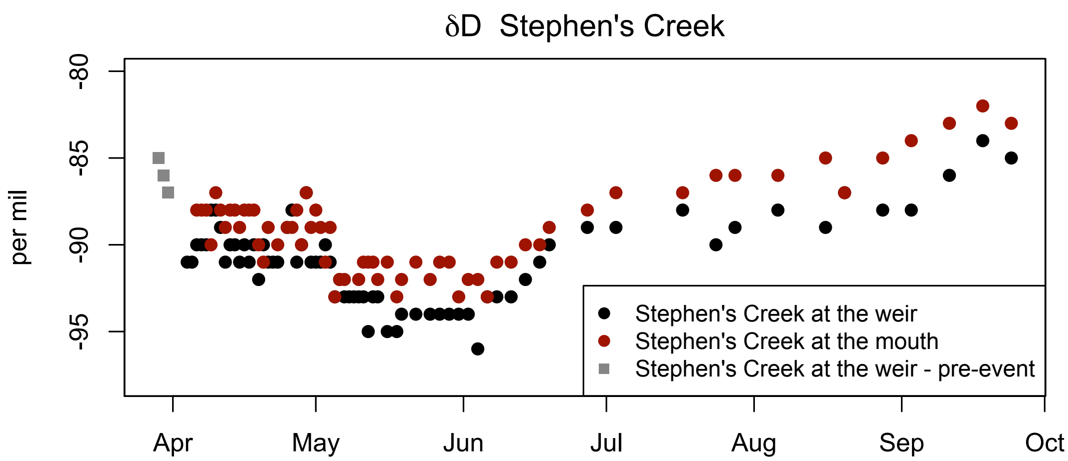

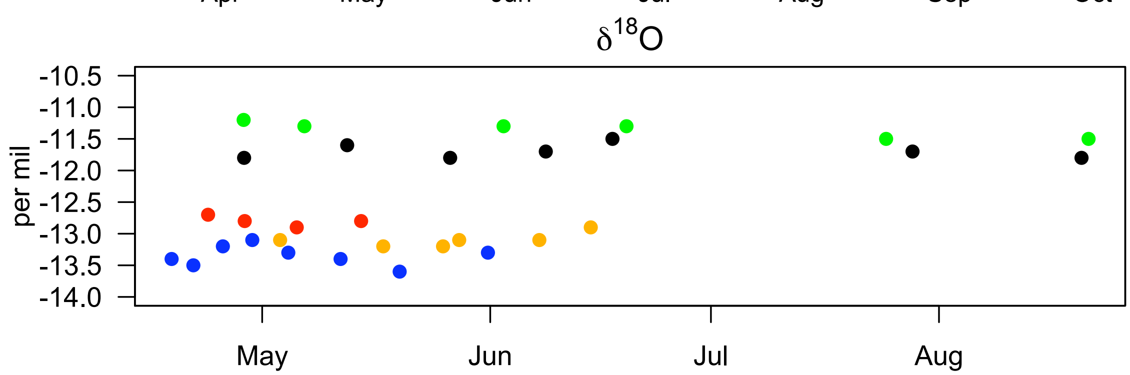

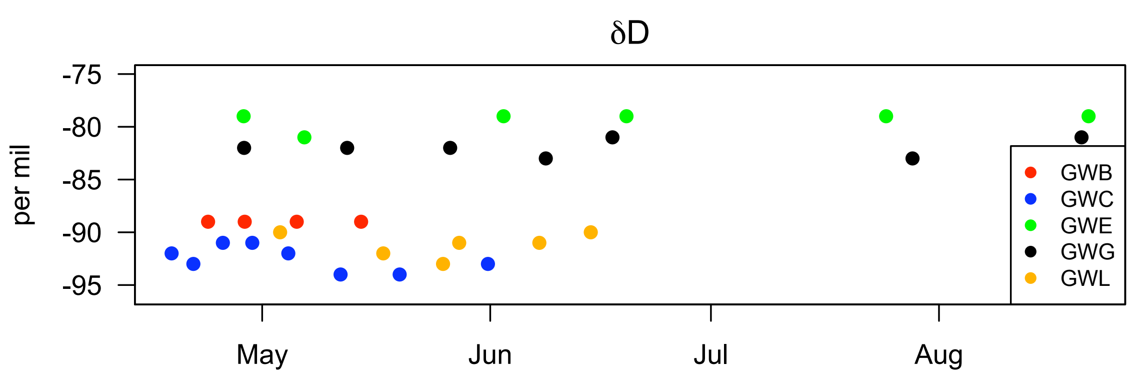

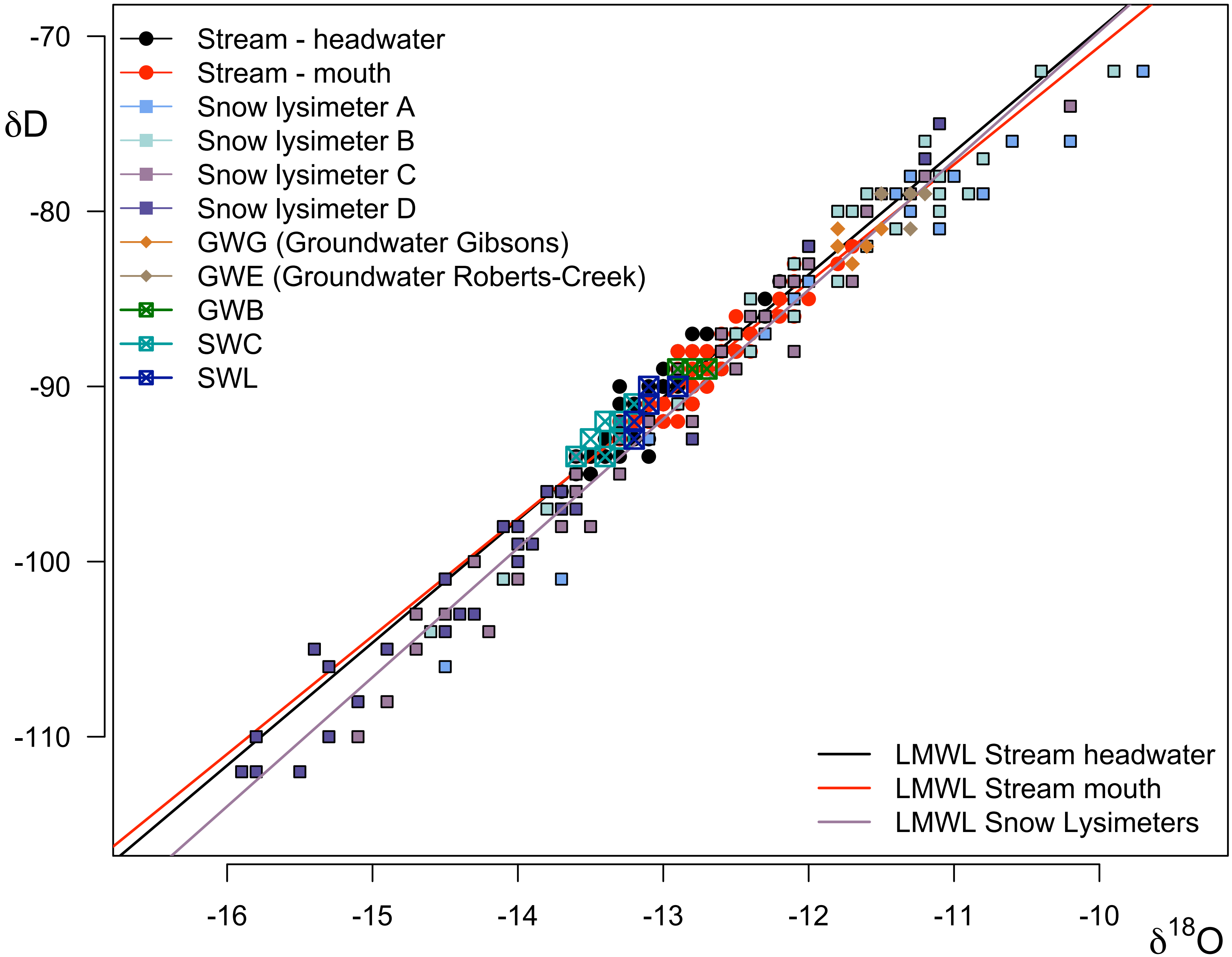

δD
-70
-80
-90
-100
-110
Stream - headwater
Stream - mouth
Snow lysimeter A
Snow lysimeter B
Snow lysimeter C
Snow lysimeter D
GWG (Groundwater Gibsons)
GWE (Groundwater Roberts-Creek)
GWB
SWC
SWL
LMWL Stream headwater
LMWL Stream mouth
LMWL Snow Lysimeters
-16
-15
-14
-13
-12
-11
-10
δ18O

Appendix M – Silicon Concentration of Stream Samples and Subsurface Concentrations of Multiple Solutes